University of Southampton

FACULTY OF MEDICINE

School of Cancer Sciences

Volume 1 of 1

Characterisation of novel human CD27-specific monoclonal antibodies for cancer therapy

DOI: 10.5258/SOTON/D2337

by

Franziska Heckel

ORCID ID 0000-0002-7564-1932

Thesis for the degree of Doctor of Philosophy

August 2022

University of Southampton

ABSTRACT

Faculty of Medicine
School of Cancer Sciences

Doctor of Philosophy

Characterisation of novel human CD27-specific monoclonal antibodies for cancer therapy

Franziska Heckel

Monoclonal antibodies (mAbs) are employed in the frontline treatment of cancer. These mAbs are known to work through a variety of mechanisms, for example by directly targeting tumour cells to mediate their clearance, or to augment immune responses against cancers. The majority of agonistic mAbs target members of the tumour necrosis factor receptor superfamily (TNFRSF), which provide T-cell costimulatory signalling. Cluster of differentiation (CD) 27 is a member of the TNFRSF and pre-clinical studies investigating mAbs targeting CD27 have demonstrated substantial anti-tumour activity in murine tumour models. In particular, durable cures were observed when anti-CD27 mAb was combined with a direct tumour targeting anti-CD20 mAb. The stimulation of CD27 on T cells promoted myeloid cell activation, leading to enhanced antibody-dependent cellular phagocytosis (ADCP), mediated by the anti-CD20 mAb, which contributed to tumour clearance. Similarly, anti-human CD27 (hCD27) mAb, varlilumab, induced *in vitro* activation of peripheral blood monocytes, indicated by CD14 downregulation. Despite these promising data, the therapeutic efficacy of anti-hCD27 mAbs in the clinic has been less impressive, potentially due to a lack of understanding of the ideal mAb format. Identifying the key determinants that govern hCD27 agonism might help to achieve better therapeutic outcomes.

Four novel and two clinically relevant anti-hCD27 mAbs were characterised with regards to epitope specificity, and the influence of both epitope and isotype on agonism. A range of affinities and avidities via cell-surface binding and surface plasmon resonance (SPR) were identified. Alanine scanning mutagenesis showed that the mAbs bound across the three cysteine-rich domains (CRDs) of the receptor with membrane-distally binding mAbs being more agonistic than membrane-proximal binding ones in an in vitro reporter cell assay. Further, mAbs binding to the external surface of a hCD27 homodimer were stronger agonists than mAbs binding internally-facing residues. When the agonistic activity of anti-hCD27 mAbs of different isotypes was compared, human immunoglobulin 2 (hIgG2, h2) mAb outperformed hIgG1 (h1) counterparts by inducing stronger transcriptional activation and increased $CD8^+$ T-cell proliferation. Increased agonism was also observed by inhibitory Fcγ receptor (FcγR) IIb-mediated hCD27 cross-linking, through co-culture with FcγRIIb-expressing cells or the use of Fc-engineered h1 mAbs with enhanced affinity to FcγRIIb.

The therapeutic efficacy of hCD27.15 (the best agonist *in vitro*) in combination with the clinically relevant direct targeting mAb (daratumumab, anti-hCD38) was investigated *in vivo*. However, no survival benefit was observed in hCD27 transgenic hCD38 A20-tumour-bearing mice. Treatment of Daudi lymphoma bearing, human PBMC-injected mice with hCD27.15 monotherapy resulted in some slowing of tumour growth.

Finally, the bystander effects of anti-hCD27 mAbs in PBMCs were explored. Only stimulation of PBMCs with varlilumab (but no other anti-hCD27 mAb) resulted in indirect effects on monocytes, causing downregulation of CD14 and upregulation of CD16 and CD86, suggesting differentiation of monocytes. The CD14 downregulation might partially be mediated by hCD27- or T-cell receptor signalling. Further work into the underlying mechanism is required.

Together this work highlights the importance of mAb-engineering and the selection of the optimal mAb format in order to generate more clinically efficacious anti-CD27 mAb agonists with better therapeutic outcomes.

Table of Contents

List of Tables

List of Figures

List of Accompanying Materials

DOI: 10.5258/SOTON/D2337 (https://doi.org/10.5258/SOTON/D2337)

Declaration of Authorship

I, Franziska Heckel, declare that this thesis, titled Characterisation of novel human CD27-specific monoclonal antibodies for cancer therapy, and the work presented in it is my own and has been generated by me as the result of my own original research.

I confirm that:

1. This work was done wholly or mainly while in candidature for a research degree at this University;
2. Where any part of this thesis has previously been submitted for a degree or any other qualification at this University or any other institution, this has been clearly stated;
3. Where I have consulted the published work of others, this is always clearly attributed;
4. Where I have quoted from the work of others, the source is always given. With the exception of such quotations, this thesis is entirely my own work;
5. I have acknowledged all main sources of help;
6. Where the thesis is based on work done by myself jointly with others, I have made clear exactly what was done by others and what I have contributed myself;
7. Parts of this work have been published as:

   Heckel F, Turaj AH, Fisher H, Chan H, Marshall MJ, Dadas O, et al. Agonistic CD27 antibody potency is determined by epitope-dependent receptor clustering augmented through Fc-engineering. *Commun. Biol*. 2022;5(1):1-15.

Signature: _____ Date: _____

Acknowledgements

First, I would like to thank my supervisors, Sean and Steve, for their support and guidance during my PhD. Thank you for giving me opportunities that paved the way for a promising career in science. I would also like to thank Diego and Tibor, my supervisors at Celldex Therapeutics, for their advice towards my work. I would also like to extend my thanks to the Lim group and the whole Antibody and Vaccine Group who have been supportive and encouraging during my time at Southampton.

I want to express a very special thanks to the Antibody production team, specifically Claude, Chris, Tanya, Ian and Jinny. Thank you for always striving to provide me with whatever I needed whenever I needed it! My project would have been at a stand-still without you.

I would also like to thank the PCU staff, particularly Lisa and Vikki, for training and making me proficient in animal work; thank you for always being patient. I would like to thank Sonya for her support with the microscopy aspect of my project (particularly those “fun” long imaging sessions); and running through and testing protocols with me. I also cannot forget to thank Steve and Jackie, both of whom were dedicated to the smooth running of the lab; I am forever grateful that you could supply me with horrendous amounts of transfection flasks when needed.

I give the most heartfelt thanks to Anna. From the beginning, you have always been there for me, regardless of whether it was for professional or personal matters. I will always treasure our “lab sporting” in-between incubation times and music sessions when we were processing tumours. Even now, I can still remember the first cone we isolated together (AF1). I wouldn’t have finished this journey without you! I would also like to say a special thanks to Heng Sheng, Michael and Kirstie who always lent a listening ear for my PhD related problems, however trivial they may be. I also want to thank Richard and Josie for reviewing my work willingly.

I want to convey my most heartfelt thanks to the friends that I have made throughout my time in Southampton: Lara, Charys, Julia, Shaun, Josie and Maryia. There are no words that could describe how much you guys have helped me through the ups and downs of the last few years. Whether it be long chats in your cars, movie nights, dinners … ALL the fun things we did together. I will always cherish these moments.

To my German friends, Kathi and Lena: Thank you for always keeping me company, no matter how many miles apart we were! Phone calls with you and meeting up on holiday were always a welcome distraction, and the care packages you sent always helped me through the most stressful times. I want to express my biggest and most whole-hearted thanks to my parents, my sister, Steffi, and my brother in law, Markus. Thank you ever so much for supporting me through this journey where I was away from all of you. I have never felt alone because I always knew you were there rooting for me and cheering me on from the side lines. Thank you for picking up the phone, night and day, whenever I needed comfort, giggles and to celebrate my successes. Above all, thank you for believing in me when I didn’t.

Finally to my funders, Cancer Research UK, MRC and Celldex therapeutics: thank you for funding this project; I have been able to learn so much and will complete my PhD enriched with many experiences that you helped to facilitate.

Definitions and Abbreviations

A:I	activating to inhibitory ratio
acc	acceleration
ADAP	adhesion and degranulation-promoting adaptor protein
ADCC	antibody-dependent cellular cytotoxicity
ADCP	antibody-dependent cellular phagocytosis
ADPR	adenosine diphosphate-ribose
AML	acute myeloid leukaemia
APC	antigen presenting cell
ASCT	autologous stem cell transplantation
AVE	avelumab
AVG	Antibody and Vaccine Group
Bcl	B cell lymphoma
BCR	B-cell receptor
BID	BH3-interacting domain death agonist
BM	bone marrow
Bmax	maximal specific binding
BMSC	bone marrow stromal cell
BSA	bovine serum albumin
BsAb	bispecific antibody
BTK	Bruton's tyrosine kinase
cAMP	cyclic adenosine monophosphate
CAR	chimeric antigen receptor
CCL	CC-chemokine ligand
CCR	CC-chemokine receptor
CD	cluster of differentiation
CDC	complement dependent cytotoxicity
CDR	complementarity-determining region
CFSE	carboxyfluorescein succinimidyl ester
CHO cells	Chinese ovarian hamster cells
CHOP	cyclophosphamide, hydroxydaunorubicin, Oncovin, prednisone
cIAP	cellular inhibitor of apoptosis

CITE-seq	cellular indexing of transcriptomes and epitopes by sequencing
CML	chronic myeloid leukaemia
CR	complete response
CRC	colorectal cancer
CRD	cysteine-rich domain
cRPMI	complete Roswell Park Memorial Institute 1640 medium
CRS	cytokine release syndrome
CSA	cyclosporine A
CTL	cytotoxic T lymphocyte
CTLA	cytotoxic T lymphocyte antigen
CXCR	CXC-chemokine receptor
DAG	diacylglycerol
dara	daratumumab
DC	dendritic cell
dcc	deceleration
DMSO	dimethylsulfoxide
DN	double negative
DP	double positive
EBV	Epstein-Barr virus
EDTA	ethyleneadiaminetetraacetic acid
ELISA	enzyme-linked immunosorbent assay
Ep-CAM	epithelial cell adhesion molecule
ER	endoplasmic reticulum
ERAP	endoplasmic reticulum aminopeptidase
$F(ab')_2$	fragment antigen binding
FACS	fluorescence activated cell sorting
Fc	fragment crystallisable
FCS	foetal calf serum
FcγR	Fc gamma receptor
FDA	Food and Drug Administration
FGFR	fibroblast growth factor receptor
FoxP3	forkhead-box protein P3
GADS	GRB2-related adapter downstream of Shc
GC	gastric cancer
GFP	green fluorescent protein
GITR	glucocorticoid-induced TNFR-related protein
GM-CSF	granulocyte-macrophage colony-stimulating factor

GPI	glycophosphatidylinositiol
GRB	growth factor receptor-bound protein
GvHD	graft versus host disease
h	human
h1/2/4	human immunoglobulin G1/2/4
HNSCC	head and neck squamous cell carcinoma
HPK	hematopoietic progenitor kinase
HPV	human papilloma virus
HSC	haematopoietic stem cell
i.p.	intraperitoneal
i.v.	intravenous
IC	immunocomplex
ICAM	intercellular adhesion molecule
ICD	intracellular domain
ICOS	inducible T-cell co-stimulator
IFN	interferon
Ig	immunoglobulin
IgSF	immunoglobulin superfamily
IKK	IκB kinase
IL	interleukin
IL-12R	interleukin 12 receptor
IP_3	inositol-1,4,5-trisphosphate
ITAM	immunoreceptor tyrosine based activation motif
ITIM	immunoreceptor tyrosine-based inhibitory motif
ITK	IL-2 induced tyrosine kinase
iTreg	induced regulatory T cell
IκB	inhibitor of κB
JAK	Janus kinase
JNK	Jun N-terminal Kinase
k_a	association rate constant
k_d	dissociation constant
K_D	equilibrium dissociation constant
LAMP	lysosomal-associated membrane protein
LAT	linker protein of activated T cells
LFA	lymphocyte functional antigen
LN	lymph node
LPS	lipopolysaccharide

LSC	leukaemic stem cell
m	mouse
m1/m2a	mouse immunoglobulin G1/2a
mAb	monoclonal antibody
MAC	membrane attack complex
MAPK	mitogen-activated protein kinase
mCD27	mouse CD27
mCD70	mCD70
mCMV	minimal cytomegalovirus
MFI	median fluorescence intensity
MGUS	monoclonal gammopathy of undetermined significance
MHC	major histocompatibility complex
MIF	macrophage migration inhibitory factor
min	minutes
MM	multiple myeloma
MRP	myeloid related protein
NAADP	nicotinic acid adenine dinucleotide phosphate
NAD/NADP	nicotinamide adenine dinucleotide/phosphate
NFAT	nuclear factor of activated T cells
NF-κB	nuclear factor kappa-light-chain-enhancer of activated B cells
NHSBT	National Health Service Blood and Transplant
NIK	NF-κB-inducing kinase
NK cell	natural killer cell
NOD	non-obese diabetic
NT	not treated
nTreg	natural regulatory T cell
ORF	open reading frame
ORR	overall response rate
OS	overall survival
OVA	ovalbumin
p:MHC	peptide:major histocompatibility complex
PAP	prostatic acid phosphatase
PBMC	peripheral blood mononuclear cell
PBS	phosphate buffered saline
PCD	programmed cell death
PCR	polymerase chain reaction
PD	progressive disease

PD-1	programmed cell death protein 1
PDK1	phosphoinositide-dependent kinase 1
PD-L1	programmed cell death protein 1 ligand
PFA	paraformaldehyde
PFS	progression-free survival
PHA	phytohemagglutinin
PI	propidium iodide
PI3K	phsphoinositide 3-kinase
PIP_2	phosphatidylinositol-4,5-bisphosphate
PIP_3	phosphatidylinositol (3,4,5)-trisphosphate
p-IκBα	phosphorylated IκBα
PKC	protein kinase C
PLAD	pre-ligand assembly domain
PLCγ	phosphatidylinositol 4,5-bisphosphate phosphodiesterase γ
PLO	peripheral lymphoid organ
PMA	phrbol `12-myuristate 13-acetate
PR	partial response
PS	phosphatidylserine
pt	patient
r	rat
r2a	rat immunoglobulin G2a
RAG	recombination activating gene
rb	rabbit
RCC	renal cell carcinoma
RING	really interesting new gene
RNA	ribonucleic acid
ROS	reactive oxygen species
RPMI	Roswell Park Memorial Institute 1640 medium
RT	room temperature
RU	response units
s.c.	subcutaneous
S1PR1	sphingosine-1-phosphate receptor 1
SAPK	stress-activated phosphor-kinase
sCD27	soluble human CD27
scFv	single chain variable fragment
SCID	severe combined immunodeficiency
SD	stable disease

SDS PAGE	sodium dodecyl sulfate polyacrylamide gel electrophoresis
SH2	Src homology domain
SHIP	SRC-homology-2-domain-containing 5’ inositol phosphatase
SLE	systemic lupus erythromatosis
SLO	secondary lymphoid organ
SLP	SH2 domain-containing leukocyte phosphoprotein
SMM	smoldering multiple myeloma
SOS	son of sevenless
SP	single positive
SPP	secreted phosphoprotein
SPR	surface plasmon resonance
SRF	serum response factor
SRK	SRC family protein tyrosine kinase
STAT	signal transducers and activators of transcription
STORM	stochastic optical reconstruction microscopy
STP	serine/threonine/proline-rich domain
TAK	transforming growth factor β-activated kinase
TAP	transporter associated with antigen processing
TBS-T	Tris-buffered saline with Tween 20
T_{CM}	central memory T cell
TCR	T cell receptor
T_{EM}	effector memory T cell
tg	transgenic
TGF	transforming growth factor
Th	T-helper cell
TIM	TRAF interaction motif
TLR	toll-like receptor
TMD	transmembrane domain
TME	tumour microenvironment
TNBC	triple negative breast cancer
TNF	tumour necrosis factor
TNFR	tumour necrosis factor receptor
TNFRSF	tumour necrosis factor receptor superfamily
TNIK	NCK-interacting protein kinase
TRAF	TNF receptor associated factor
Treg	regulatory T cell
T_{RM}	tissue resident memory T cell

UTR	untranslated region
varli	varlilumab
VEGF	vascular endothelial growth factor
VLP	virus-like particle
WT	wild type
ZAP70	zeta chain of T-cell receptor associated protein kinase 70

Chapter 1 Literature review

1.1 Cancer Immunology

Cancer is a complex disease wherein cells accumulate genetic and epigenetic mutations, which lead to dysfunctional cell behaviour. Carcinogenesis is a multistep process: initiation of carcinogenesis is mediated by driver mutations that give the cell a selective survival advantage. During the progression phase, the transformed cells acquire additional mutations, termed passenger mutations that facilitate tumour growth and increase malignancy and disease progression. The mutations occurring during carcinogenesis commonly involve genes that are regulators of cell growth and the cell cycle, such as tumour suppressor genes or oncogenes. Associated gene aberrations in cancer include, among others, translocation, deletion and amplification of gene loci as well as other genetic abnormalities such as aneuploidy. The result is the transformation of a "normal" cell into a malignant cell, which evades the control of the cell cycle machinery and undergoes uncontrolled division. Proliferating malignant cells eventually acquire the capability to invade surrounding tissues and systemically metastasise and compromise organ functions throughout the body.[1]

The accumulation of mutations during carcinogenesis gives tumour cells the ability to further drive tumour development. These capabilities, as outlined by Hanahan and Weinberg, are referred to as "The Hallmarks of Cancer"[2,3] and are summarised in the following: 1) Sustained proliferative signalling: Cancer cells are able to take over the machinery controlling cell growth and mitosis for example through stimulation of their growth in an autocrine manner or alteration and overexpression of growth factor receptors. Furthermore, they also acquire the ability to constitutively activate downstream signalling pathways involved in cell growth in a growth factor-independent manner. 2) Evade growth suppressors: This involves the mutation of tumour-suppressor genes such as p53, controlling cell cycle progression and the genetic alteration of genes involved in apoptosis and cell death. 3) Activate invasion and metastasis: Cancer cells gain the ability to metastasise by up- or downregulation of adhesion molecules leading to increased motility and migration. However, it was also demonstrated, that cells of the tumour microenvironment (TME) can also promote metastasis by activation of specific proteins or the secretion of growth factors and cytokines. 4) Induce angiogenesis: Neo-vascularisation appears during the early or mid-stage

of human cancer and sustains the tumour's metabolism. Its induction is thereby mediated by the activation of an "angiogenic switch" within the tumour cells, leading to a shift in the balance of activating angiogenic factors and their inhibitory counterparts. Concomitant alterations in gene transcription result in increased expression of angiogenic vascular endothelial growth factor (VEGF) or downregulation of anti-angiogenic β-interferon (IFN). 5) Resist cell death: Under normal conditions, cells can only undergo a distinct number of cell cycles and continuous proliferation eventually leads to cell death. Tumour cells circumvent the induction of cell death by downregulation of pro-apoptotic factors (e.g. Bax, Bim) or upregulation of anti-apoptotic factors (e.g. B-cell lymphoma (Bcl) 2, Bcl-x_L). 6) Enable replicative immortality: Cell growth and division of most healthy human cells are limited by a distinct amount of cell cycles. After about 40-60 cell cycles the cells irreversibly transition into a state known as senescence (non-proliferative but viable), and then crisis (cell death). When a cancer cell develops, it is able to breach this limitation and acquire unlimited replicative potential. Hence it is suggested that tumour cells have longer telomeres and higher expression of telomerase allowing them to divide uncontrollably. 7) Reprogramming of energy metabolism: For uncontrolled cell proliferation and growth, provision of adequate nutrition and energy is essential. Therefore, tumour cells have the ability to adjust their energy metabolisms to support uncontrolled cell division and tumour growth. 8) Evading immune destruction: Normally tumour cells are detected via immune surveillance (where immune cells detect and clear tumour cells); however, tumour cells can acquire mechanisms to evade the immune surveillance and become malignant.[2,3]

1.1.1 Cancer immunoediting

Tumour cells can be detected and eliminated by the immune system in a process called immunosurveillance.[4] However, it has been proposed that whilst the immune system mainly acts to protect the body from tumours, it also can behave in a tumour-promoting way. This concept, termed "cancer immunoediting", is a multistep process and includes three phases ("3 E's"). The elimination phase corresponds to cancer immunosurveillance and is mediated by various immune cells. Secreted cytokines and chemokines facilitate the control and elimination of evolving tumour cells. The elimination phase is initiated by cells of the innate immune response (natural killer (NK) cells, NK-T cells, γδ T cells). These cells can recognise tumour cells and, in response, secrete IFN-γ. IFN-γ does not only have anti-tumour properties but also mediates the recruitment and activation of tumour-destructing immune cells such as NK cells, macrophages and dendritic cells (DCs). Additionally, IFN-γ secretion leads to the production of anti-angiogenic cytokines. T cells resident in tumour draining lymph nodes (LNs) encounter tumour specific antigen, become activated and differentiate into tumour-specific cluster of differentiation (CD) 4^+ and $CD8^+$ T cells. These highly

specific cells migrate to the tumour and destroy transformed cells through antigen recognition. However, it appears, that tumour cells are able to survive the elimination stage. In this case, the immune system and tumour cells enter an equilibrium stage whereby highly immunogenic tumour cell variants are still eliminated but newly arising, less immunogenic variants are not detected by immune cells such as the T cells. Thus, these transformed cells survive the selection process and escape the control of the immune system, which, as a consequence, manifests in malignant disease. (reviewed in[5]). As described above, T cells are key players in anti-tumour responses. It has been shown in colorectal cancer (CRC)[6] and multiple other cancers (e.g. ovarian, lung, renal cancer)[7] that infiltration of T cell subsets, such as T helper (Th) 1 cells and cytotoxic memory $CD8^+$ T cells is associated with a beneficial clinical outcome.[6]

1.2 T cells

1.2.1 T-cell development

T cells emerge from pluripotent haematopoietic stem cells (HSC) resident in the bone marrow (BM). T-cell progenitor cells (thymocytes) migrate from the BM to the thymus and enter it through the cortico-medullary junction where their differentiation is initiated.[8] Thymocytes undergo several developmental stages, defined by the expression of cell surface markers such as CD4, CD8, the adhesion molecule CD44, the α-chain of the interleukin (IL) 2 receptor CD25, as well as the expression of the T-cell receptor (TCR). The first stage is the double-negative (DN) stage, where thymocytes neither express CD4, CD8 or the TCR on their cell surface. The DN stage can further be divided into four developmental sub-stages based on the surface expression of CD25 and CD44 (Figure 1.1).[9] Thymocytes in the DN1 stage express CD44 but not CD25 and the genes encoding the TCR are still in the germline configuration. Upon maturation, DN1 thymocytes start to express CD25 alongside CD44 and the cells transit into the DN2 stage. During this stage, rearrangement of the TCRβ-chain, known as VDJ recombination, begins. This process continues in the DN3 stage, which can be characterised by the loss of CD44 expression. DN3 thymocytes that undergo successful gene rearrangement express the TCRβ-chain together with a surrogate pre-TCR α-chain on their cell surface, forming the pre-TCR, which associates with the CD3 complex. Cells in this stage undergo a process termed β-selection. Successful formation and signalling through the pre-TCR:CD3 complex results in the phosphorylation and degradation of the recombination activating gene 2 (RAG2) protein to prevent further TCRβ-chain rearrangement and allow cell proliferation and survival (DN4 stage). Furthermore, the co-receptors CD4 and CD8 are upregulated and expressed on the surface and cells become CD4 CD8 double-positive (DP) T cells. Thymocytes that have not undergone successful TCRβ-chain rearrangement remain in the DN3 stage and will die. During cell proliferation

in the DN4 stage, *RAG1* and *RAG2* gene transcription is repressed to prevent gene rearrangement of the TCRα-chain until the proliferative stage is ended. Successful rearrangement of the α-chain locus of DP thymocytes results in the assembly and expression of the TCR and subsequent selection processes within the thymus.[9,10] (see Figure 1.1). The first step of this selection process is the positive selection, which takes place in the cortex. DP thymocytes interact with self-peptides presented in a major histocompatibility complex (MHC) class I or class II-dependent manner. Those that are unable to recognise the self-peptide:MHC (p:MHC) complex undergo apoptosis, whereas those showing a strong interaction survive. Upon positive selection, DP thymocytes highly express the TCR and further mature by becoming single-positive (SP) thymocytes expressing either CD4 or CD8 on their cell surface. SP thymocytes migrate to the medulla, where they undergo selection processes to receive self-tolerance. Self-peptides are presented to the SP thymocytes on MHC class I or II by professional antigen-presenting cells (APCs) such as thymic DCs or specialised medullary epithelial cells. Cells that strongly react to the self-peptide are negatively selected (clonal deletion). Thymocytes that only weakly interact with self-p:MHC die by neglect, and thymocytes, who's TCR have the appropriate affinity to the self-peptides survive and are selected to enter the periphery to encounter foreign antigens.[10]

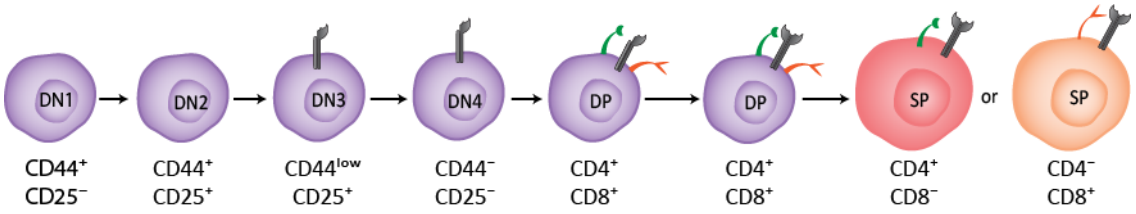

Figure 1.1| T-cell development in the thymus. Cells enter the thymus via the cortico-medullary junction and migrate through the outer and inner cortex while progressing through various stages of differentiation. Finally, the lymphocytes reach the medulla, where they develop into fully differentiated T cells and leave the thymus to function as effector cells in the periphery.

After completing the thymic maturation processes, naïve T cells enter the periphery via the blood stream. Here, they circulate from the blood into peripheral lymphoid organs (PLOs; such as LNs) and back into the blood. While in circulation, naïve T cells come in contact with DCs presenting foreign antigens on either MHC class I or MHC class II (section 1.2.2.1). Upon encounter with such an antigen in PLOs, naïve T cells remain in the T-cell zone where they undergo a process referred to as clonal expansion. Entry of the naïve T cell into the LN is mediated by selectins, integrins and chemokines. The chemokine ligand (CCL) 7, secreted by vascular high endothelial cells and stromal cells in the LN, is an especially strong chemoattractant to naïve T cells. It interacts with the chemokine receptor (CCR) 7, expressed on the surface of naïve T cells. After the naïve T cells have entered the LN, a CCL7 and CCL19 (also a ligand for CCR7) gradient guides the T cells into the T-cell zone of the LN, where T-cell activation is initiated through antigen-presenting DCs. Immature DCs become activated upon engulfment of a pathogen and the accompanied signalling through specific

surface receptors. Maturation of DCs is associated with phenotypic changes. As such, MHC class I and class II molecules and co-stimulatory molecules, necessary for T-cell activation, become highly expressed on the cell surface. Furthermore, maturing DCs also begin to express CCR7 which induces the recruitment of the DCs to PLOs along the CCL21 gradient produced by stromal cells in the LNs. Once the DCs enters the lymphoid tissue, they no longer possess phagocytic activity and are ready to initiate the adaptive immune response by activating naïve T cells in the LNs.[10]

1.2.2 T-cell activation and differentiation

Activation of naïve T cells generally requires three distinct signals (Figure 1.2). The first signal is provided by the interaction of the TCR with an antigen presented on a MHC by an APC (signal 1, section 1.2.2.1). The TCR signal alone is not sufficient to fully activate the T cell. Ligation of co-stimulatory receptors with their cognate ligands is essential (signal 2, section 1.2.2.2). Signals 1 and 2 together lead to the activation of naïve T cells and the production of cytokines (signal 3) resulting in T-cell differentiation, proliferation and effector functions (section 1.2.2.3).[11]

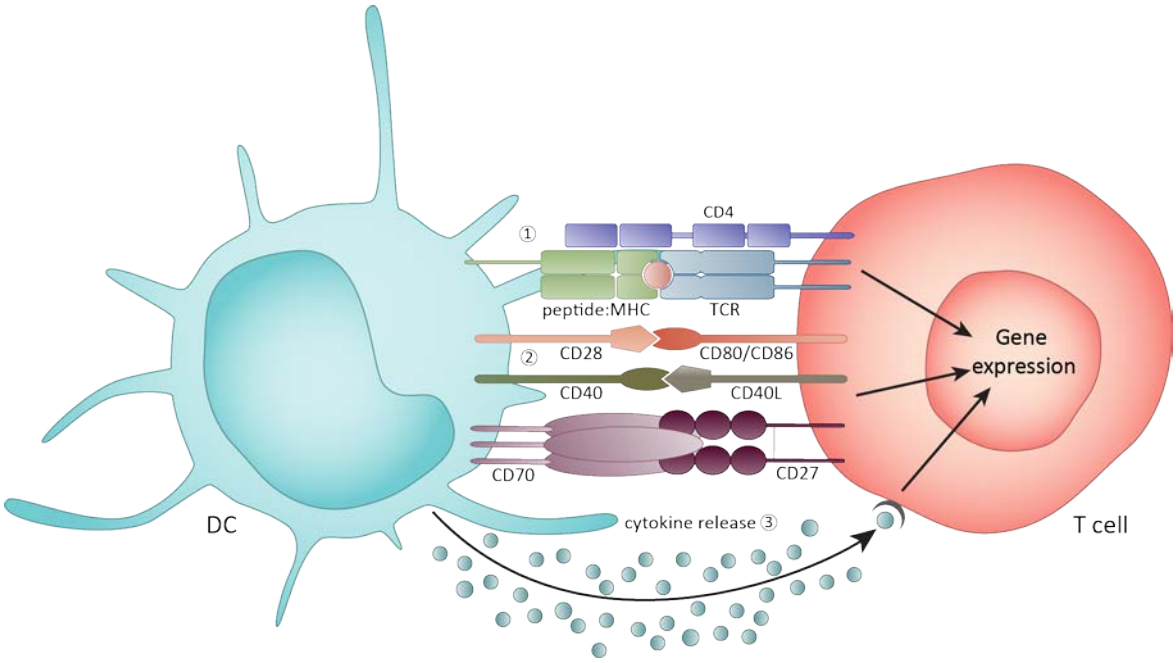

Figure 1.2| T-cell activation. Ligation of the TCR with p:MHC on APCs provides the initial signal ① for the T-cell activation. Additional interaction of co-stimulatory molecules (here CD28 and CD40) with their respective ligands (CD80/CD86 and CD40-ligand (CD40L)) provides signal ②; signal ② is essential to trigger cytokine release (signal ③) and the subsequent activation, differentiation and proliferation of the naïve T cell into distinct T-cell subsets.

1.2.2.1 Signal 1: TCR activation through antigen recognition

The first signal required for T-cell activation is provided by the interaction of the TCR with a p:MHC complex. MHC molecules are highly polymorphic allowing them to bind a huge variety of different peptides. Those peptides can be presented on two types of MHC complexes: MHC class I and MHC class II, which both have similar functions but differ in their origin, composition, source of antigen they present and cells they interact with.

MHC class I is composed of a single α-chain (α_1, α_2, α_3), which associates with β_2-microglobulin, forming a highly polymorphic binding groove (by α_1 and α_2 domains).[12] MHC I molecules are synthesised and assembled in the endoplasmic reticulum (ER).[13] The peptides MHC class I is loaded with are endogenous, of cytosolic origin, and are processed within the cytosol by ubiquitylation and proteasomal degradation. These peptides are translocated into the ER, facilitated by the transporter associated with antigen processing (TAP) complex.[14] MHC class I can carry peptides of 8-11 amino acids in length and longer peptides are further processed by ER aminopeptidase-1 (ERAP1) after translocation into the ER.[13,15] Peptides of the appropriate length are then loaded onto the binding groove and the stable p:MHC class I complex is transported through the Golgi apparatus to be presented on the cell membrane, where it is recognised by $CD8^+$ T cells.[13] MHC class II, in contrast, is only expressed on professional APCs such as macrophages, DCs or B cells. It is composed of an α-(α_1, α_2) and β-(β_1, β_2) chain, forming the antigen binding groove. Similar to MHC class I, MHC class II is synthesised in the ER and trafficked through the Golgi apparatus, where it acquires antigens from the endocytic pathway. In the phagolysosome MHC class II is loaded with peptides of 13-25 amino acid length[16,17] derived from the extracellular space through processes such as phagocytosis, endocytosis or micropinocytosis. Eventually, p:MHC class II is expressed on the cell surface, where it facilitates activation of $CD4^+$ T cells for T-cell activation.[12,13]

Moreover, it has been described that DCs are also able to present exogenous-derived antigens on MHC class I. [18] This process, named “cross-presentation”, entails antigen processing either via the cytosolic (proteasomal) or vacuolar (endosomal) pathway.[19] Cross-presentation is reported to be involved in immune responses against viral and bacterial infections as well as to contribute to $CD8^+$ T-cell tolerance to self-antigens.[20] Furthermore, cross-presentation of tumour antigens on MHC class I by DC subsets might also contribute to effective anti-tumour responses.[20,21]

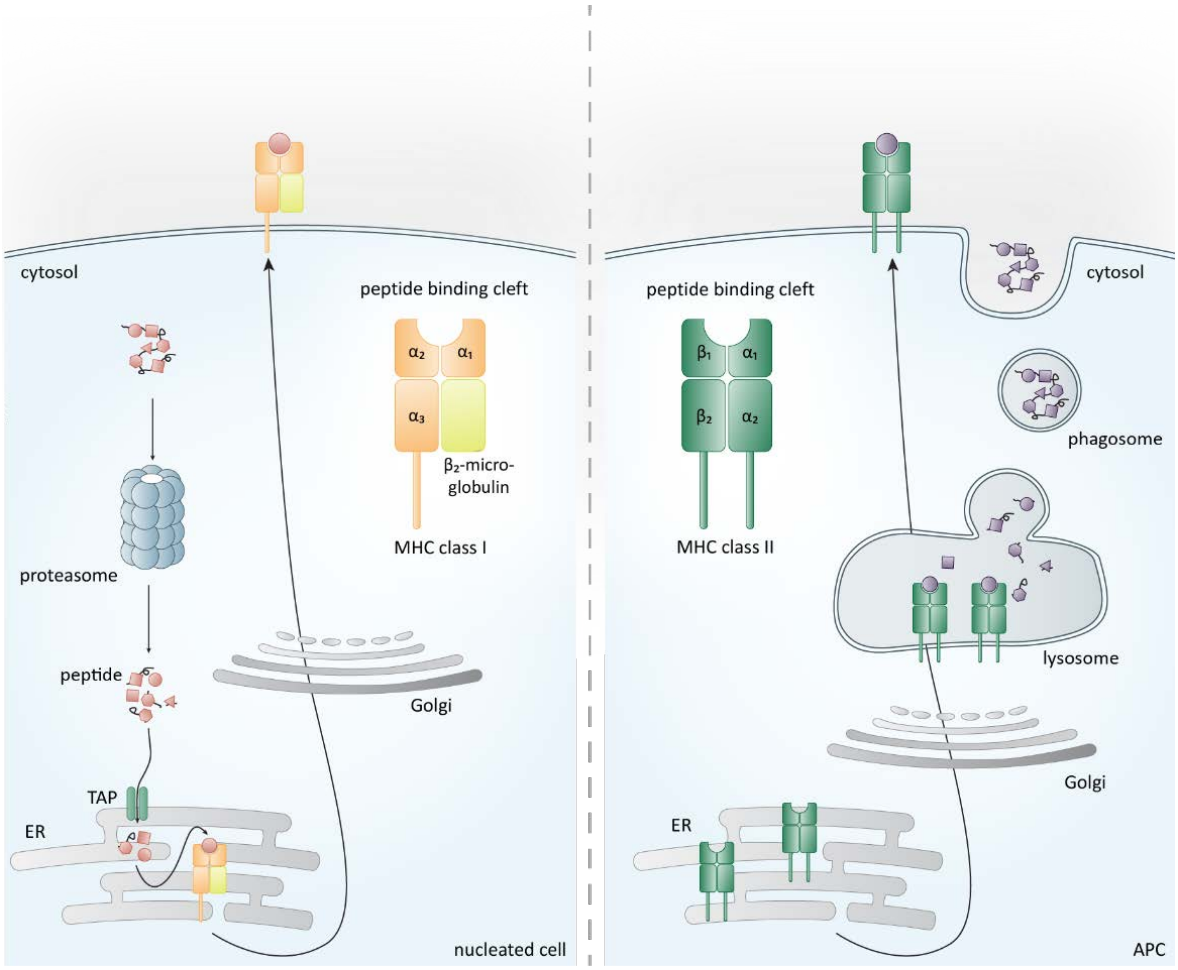

Figure 1.3| Antigen processing and MHC-presentation. A: Cytosolic antigens (e.g. misfolded proteins) that have been processed into peptides by ubiquitylation and proteasomal degradation enter the ER through the TAP complex. Peptides are loaded onto MHC class I molecules, comprised of a polymorphic heavy chain (α-chain) and an invariant light chain (β_2-microglobulin, mediated by the protein-loading complex (including tapasin, calreticulin, ERp57). p:MHC class I complexes are trafficked via the Golgi apparatus to the cell surface to present the antigen to $CD8^+$ T cells in the cytoplasm. **B:** Extracellular antigens (such as bacteria or viruses) enter the APC via pattern recognition receptors (e.g. Toll-like receptors (TLRs)) and enter the phagocytic pathway. The matured phagosome eventually fuses with lysosomes containing pre-assembled MHC class II molecules (assembled with an invariant light chain). Proteolytically processed peptides are loaded onto the binding groove of MHC class II and are transported via the Golgi complex to the cell surface to be presented to $CD4^+$ T cells.

Successful ligation of p:MHC with the TCR induces signalling. The TCR consist of an α- and β-chain building the TCRα:β-heterodimer, which forms the antigen-binding site (Figure 1.4). For stable expression of the heterodimer on the T-cell surface, association with CD3γ, CD3ε and CD3δ extracellular Ig-like containing domain protein chains as well as a disulphide-linked CD3ζ homodimer is essential. The TCR itself does not possess intrinsic signalling capabilities. Hence, signalling is mediated by immunoreceptor tyrosine-based activation motifs (ITAMs) present in the CD3 complex, with one each in the CD3γ, ε and δ chain and three ITAMs in each domain of the CD3ζ homodimer.[10]

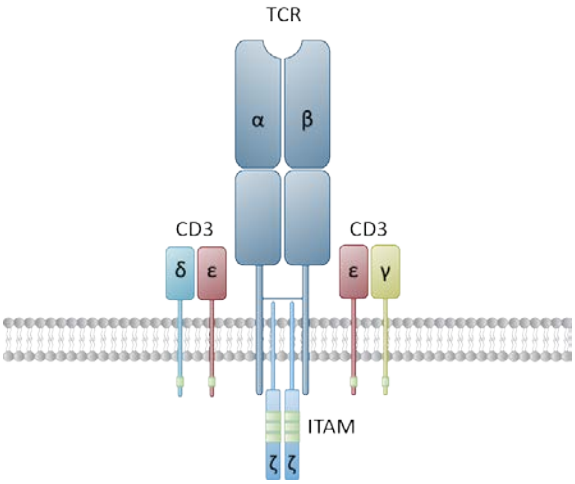

Figure 1.4| The TCR:CD3 complex. The TCR:CD3 complex is composed of the α- and β-chain of the TCR. For signalling, the TCR associates with the CD3 complex, which contains CD3γ, CD3ε and a CD3δ extracellular Ig-like containing domain protein chains as well as a disulphide-linked homodimer of CD3ζ. Chains of the CD3 complex contain ITAMs (one each in CD3γ, CD3ε and CD3δ; two in CD3ζ), which are crucial for downstream signal transduction.

Once TCR signalling is initiated, CD4 or CD8 co-receptors are recruited to conserved regions of the MHC and cluster with the TCR:CD3 complex (Figure 1.5). CD4 and CD8 co-receptors serve as a binding site for the SRC family protein tyrosine kinases (SRK) Lck and Fyn, which in turn phosphorylate the ITAMs contained in the CD3 complex. Lck activation and inactivation is thereby tightly regulated by phosphorylation and dephosphorylation of its tyrosine residues, mediated by tyrosine phosphatases such as CD45.[22] Upon Lck activation, the tyrosine kinase ζ-chain associated protein kinase of 70 kDa (ZAP70) is recruited and binds with its Src homology 2 (SH2) domain to the phosphorylated ITAMs in the CDζ chains of the CD3 complex. Lck-mediated phosphorylation of ZAP70 results in conformational changes, which enable its phosphorylating activity.[23] The first molecules to become phosphorylated by ZAP70 are the linker protein of activated T cells (LAT) and the SH2 domain-containing leukocyte phosphoprotein of 76 kDa (SLP-76). Phosphorylated tyrosine residues of LAT provide docking sites for downstream adaptor and signalling molecules involved in various signalling pathways associated with cell survival, proliferation and differentiation (Figure 1.5).[23,24] Binding of these adaptor molecules to LAT forms the LAT signalosome.

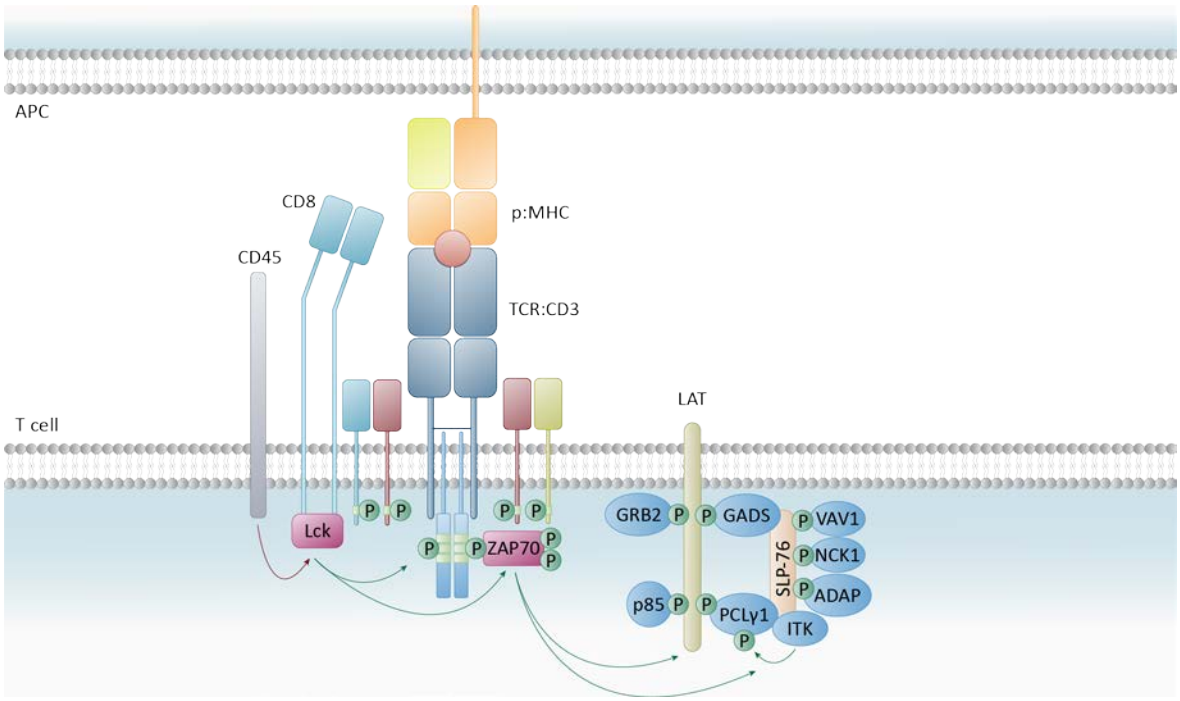

Figure 1.5| Initial steps of the TCR activation and formation of the LAT signalosome. Activation of Lck, bound to the cytoplasmic domains of CD4 or CD8, is regulated by CD45. Upon activation, Lck phosphorylates the ITAMs of the TCR:CD3 complex. Subsequently, ZAP70 is recruited and phosphorylated by Lck. ZAP70 in turn phosphorylates LAT and SLP-76. Next, LAT binds the C-terminal SH2-domain of phospholipase C γ1 (PLCγ1) as well as the growth factor receptor-bound protein 2 (GRB2) and GRB2-related adapter downstream of Shc (GADS) and the p85 subunit of the phosphoinositide 3-kinase (PI3K). Upon binding of these adaptor molecules, SLP-76 is recruited to the phosphorylated docking sites of LAT and associates with further adapter molecules such as VAV1, NCK1, IL-2-induced tyrosine kinase (ITK), GADS, PLCγ and the adhesion and degranulation-promoting adaptor protein (ADAP). Red arrows indicate de-phosphorylation, green arrows indicate phosphorylation.[22]

Successful formation of the LAT signalosome leads to the activation of PLCγ1-induced pathways or the canonical and non-canonical nuclear factor kappa-light-chain enhancer of activated B cells (NF-κB) pathway, leading to the translocation of nuclear factor of activated T cells (NFAT) into the nucleus. Further signalling is triggered, which results in Ca^{2+}-mobilisation, actin rearrangements and integrin activation (Figure 1.6).

PLCγ1 is activated through ITK-mediated phosphorylation and facilitates the hydrolysis of phosphatidylinositol-4,5-bisphosphate (PIP_2) into the secondary messengers inositol-1,4,5-trisphosphate (IP_3) and diacylglycerol (DAG). IP_3 subsequently binds the IP_3-receptor expressed on the ER, which causes Ca^{2+}-release from the ER into the cytoplasm. Depletion of Ca^{2+}-stores from the ER in turn triggers an influx of extracellular Ca^{2+} through Ca^{2+} release-activated Ca^{2+}-channels in a process termed store-operated Ca^{2+}-entry.[25] Ca^{2+} ions bind to calmodulin, which in turn activates calcineurin, a calmodulin-dependent phosphatase. Subsequently, NFAT is dephosphorylated and translocated into the nucleus, where it is involved in the transcription of genes associated with proliferation, differentiation and apoptosis.[26]

The second product resulting from the PCLγ-mediated hydrolysis of IP_2 is DAG. DAG binds Ras-GRB, which in turn is activated by protein kinase C (PKC) θ. This leads to the recruitment of son of sevenless (SOS), facilitating the phosphorylation of Raf. Via a phosphorylation cascade MEK and Erk become phosphorylated resulting in the nuclear translocation of Erk. In the nucleus, Erk phosphorylates the transcription factor Elk1, which in conjunction with the serum response factor (SRF), mediates the transcription of *fos*. Subsequently, Fos is phosphorylated by Erk and forms together with phosphorylated Jun the transcription factor AP-1, which regulates IL-2 gene transcription.[11,24]

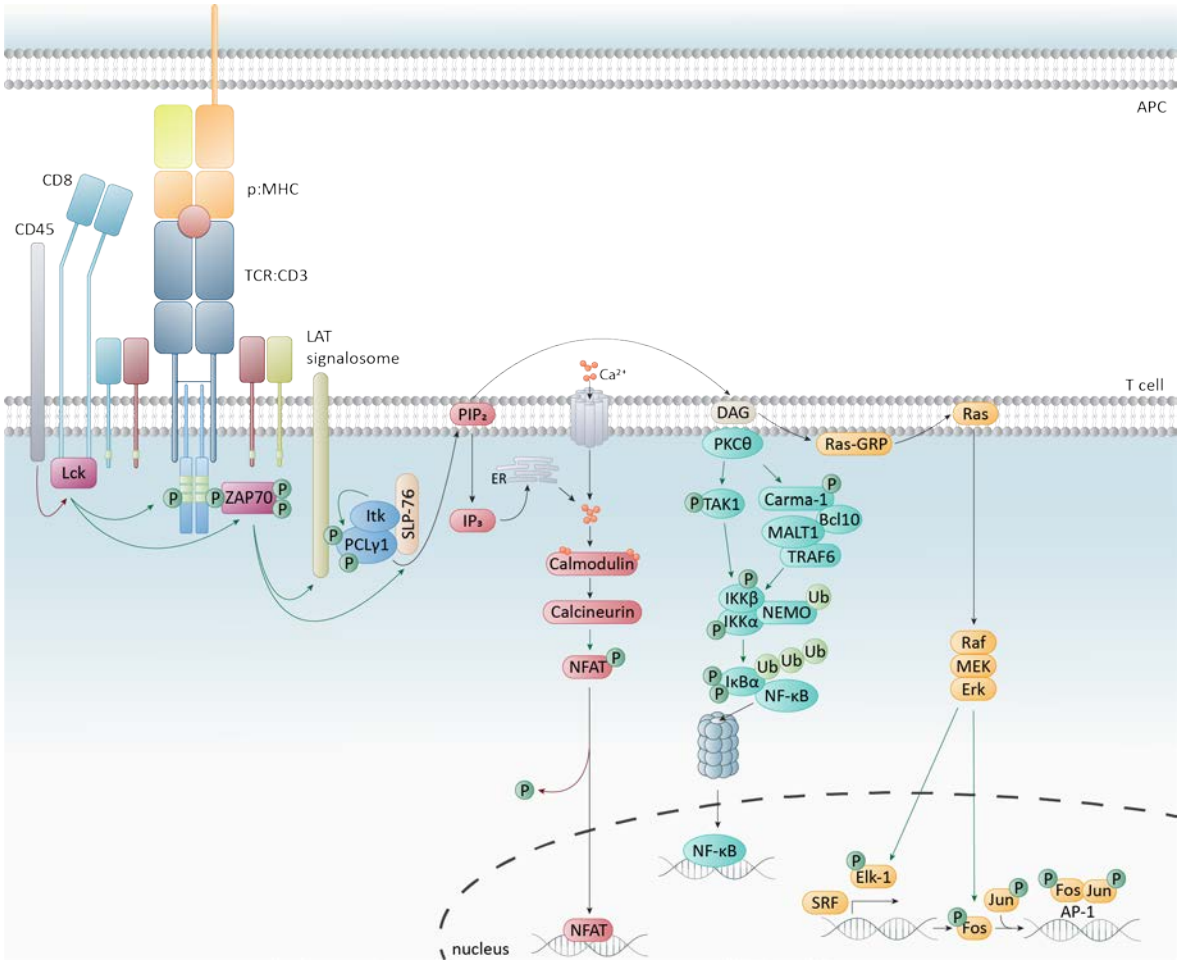

Figure 1.6| Signalling pathways induced upon TCR activation. Once the TCR engages p:MHC, the LAT signalosome is formed (here displayed simplified; for more detail see Figure 1.5). Phosphorylation of PLCγ leads to the initiation of signalling pathways resulting in NFAT and NF-κB translocation as well as the induction of the Raf-MEK-Erk pathway.

DAG not only induces the activation of the Ras/mitogen-activated protein kinase (MAPK) pathway, but also the canonical and non-canonical NF-κB pathway. Figure 1.6 details the canonical NF-κB pathway. The non-canonical NF-κB pathway as part of tumour necrosis factor receptor (TNFR)-signalling will be elucidated in section 1.3.4.

To initiate the canonical NF-κB pathway, DAG mediates the recruitment and activation of PKCθ. PKCθ in turn phosphorylates Carma-1, a member of a complex composed of Carma-1, Bcl10 and

MALT1. This leads to the recruitment of the TNFR associated factor (TRAF) 6, facilitating the ubiquitination of NEMO (IκB kinase (IKK) γ), which together with IKKα and IKKβ forms the IKK complex. To fully activate the IKK complex, activation of the transforming growth factor (TGF) β-activated kinase 1 (TAK1) complex is necessary. In turn, the activated IKK complex mediates phosphorylation and ubiquitination of the inhibitor of κB (IκB) α, which sequesters NF-κB, tagging it for proteasomal degradation. Degradation of IκBα subsequently leads to the release of NF-κB, its translocation into the nucleus and transcription of genes contributing to cell survival, growth and proliferation.[11,24,27]

1.2.2.2 Signal 2: T-cell co-stimulation

As elucidated above, T-cell activation is not solely reliant on the TCR interaction with a p:MHC complex but also on the interaction of co-stimulatory molecules, expressed on T cells, with their according ligands, presented on APCs (Figure 1.2). However, besides the co-stimulatory receptors, there are also co-inhibitory receptors contributing to immune homeostasis. They are involved in the negative regulation of immune responses and are represented by molecules such as the cytotoxic T-lymphocytes antigen (CTLA) 4 or programmed death protein 1 (PD-1).

Co-stimulatory and co-inhibitory molecules can be divided into two groups: members of the immunoglobulin superfamily (IgSF), and members of the tumour necrosis factor receptor superfamily (TNFRSF) (Figure 1.7). Co-stimulation by IgSF receptors is mainly mediated through the interaction of CD28, expressed on resting and activated T cells[24], and CD80/CD86, expressed on professional APCs. Ligation leads to signalling, facilitating the entry of the T cell into the G1 phase of the cell cycle, cell proliferation, differentiation and survival as well as production of cytokines such as IL-2 and the expression of the α-chain of the IL-2 receptor.[28] Another member of the IgSF is inducible T-cell co-stimulator (ICOS). It shares similar features with CD28, but unlike CD28 it is not constitutively expressed on T cells but upregulated upon TCR:p:MHC ligation and CD28 engagement on almost all subsets of the T-cell lineage. Downstream signalling via ICOS is initiated upon binding to its respective ligand ICOSL, expressed on APCs such as B cells, macrophages and DCs. Its activation results for example in the secretion of cytokines such as IL-4, which in turn mediates T_h2 cell differentiation.[28,29] Also a member of the IgSF, but not a co-stimulatory molecule, is the co-inhibitory molecule CTLA-4. The negative regulatory function of CTLA-4 is based on its homology to the co-stimulatory molecule CD28 expressed on T cells. CD28 binds to CD80/CD86 and provides the essential second signal for T-cell activation. CTLA-4 is upregulated upon T-cell activation and binds CD80/CD86 with a higher affinity than CD28. Mediating intrinsic and extrinsic effects, ligation of CTLA-4 with CD80/86 leads to cell cycle arrest and inhibition of T-cell proliferation and cytokine

release by APCs.[30] An immune response is not only regulated by CTLA-4 but also through PD-1. PD-1 is largely expressed on activated T cells, populations of antigen-specific exhausted T cells and tumour infiltrating lymphocytes. Its ligands programmed cell death protein ligand (PD-L) 1 and PD-L2 are expressed on various cell types. Pro-inflammatory cytokines, such as IFN-γ, lead to the upregulation of PD-L1 on haematological cells, and PD-L2 on DCs and macrophages. Under inflammatory conditions, the interaction of PD-1 (on T cells) and PD-L1 normally dampens the immune reaction of T cells to prevent autoimmunity and tissue destruction at the inflammatory site.[31]

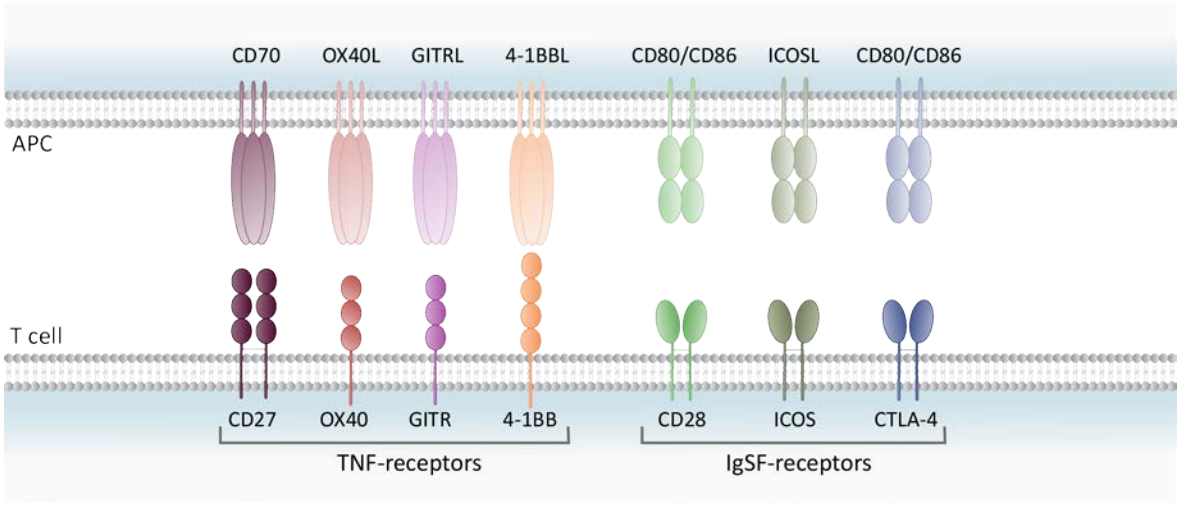

Figure 1.7| Selected T-cell co-stimulatory and co-inhibitory molecules and their respective ligands. Depicted are molecules of the TNFRSF or the IgSF, which contribute to immune homeostasis by mediating stimulatory and inhibitory signalling. For TNFRs, the number of cysteine-rich domains (CRDs) is indicated and their respective ligands are displayed as homotrimers. The receptors of the IgSF and their ligands are depicted as homodimers and the immunoglobulin (Ig) domains are indicated.

The other group of co-stimulatory molecules is formed by TNFRs, which mainly contribute to T-cell activation.[32-34] They can be distinguished into three sub-groups: death receptors (containing a death domain), decoy receptors (no intracellular adaptor molecules), and receptors containing TRAF-interacting motifs (TIMs).[35] Members of these TIM-containing TNFRs are molecules such as 4-1BB, OX40, CD27, CD40, GITR and CD30. They are type-I transmembrane proteins and their main characteristic is an extracellular domain composed of cysteine-rich domains (CRDs), which typically contain six cysteines forming three disulphide bonds.[36] The number of CRDs in TNFRs varies, with CD27[37,38], CD40[39] and GITR[40] possessing three, OX40[41] and 4-1BB[42,43] possessing four and CD30 possessing six CRDs in their extracellular domain[36] (Figure 1.7).

Signalling of co-stimulatory TNFRs is mediated through TRAFs. To date, six TRAF members (TRAF1-6) have been identified. They serve as adaptor molecules by binding to TIM-containing TNFRs and display a dual function; through an N-terminal really interesting new gene (RING)/zinc-finger domain, TRAFs (except TRAF1) have E3 ligase-like activity and ubiquitinate proteins involved in signalling cascades such as the NF-κB pathway or pathways associated with MAPK. The second

domain contained in TRAFs is a C-terminal coiled-coil (TRAF-N)/TRAF-C domain through which TRAFs can form homo- or heterodimers as well as sequence-specific interactions with cytoplasmic tails or other adaptor proteins.[44] Through the ability to link receptor signalling events to cytoplasmic proteins, which in turn mediate intracellular signalling, TRAFs play a role in T-cell development, differentiation and haemostasis.

The work described herein investigates the targeting of the co-stimulatory CD27 receptor with agonistic mAbs. A detailed review of the function of this receptor follows in section 1.3.

1.2.2.3 Signal 3: Cytokines and subsequent T-cell polarisation

The differentiation of naïve T cells into distinct T-cell subsets is depending on the cytokine milieu present after TCR:p:MHC interaction and the engagement of co-stimulatory molecules. Cytokines secreted by APCs bind to the according receptors expressed on T cells and trigger signalling pathways such as Janus kinase (JAK)/signal transducers and activators of transcription(STAT), leading to the translocation of master transcription regulators into the nucleus, which dictate lineage commitment (Figure 1.8). Therefore, $CD4^+$ T cells can develop into Th1 and Th2 cells [45] as well as into Th17, follicular Tfh or regulatory T cells (Tregs) (Figure 1.8). IL-12 and IFN-γ secretion from APCs evokes the upregulation of Tbet and drives the differentiation of IFN-γ-secreting $CD4^+T_h1$ cells. In contrast, in the presence of IL-4, $CD4^+$ T cells preferentially differentiate into Th2 cells via upregulation of the gene regulator GATA3. In response, Th2 cells secrete IL-4, IL-5 and IL-13. Th17 cells also derive from $CD4^+$ T cells and commit to the Th17 lineage by upregulation of RORγt in response to IL-6, TGF-β and IL-23. In turn, Th17 secrete IL-22 and cytokines of the IL-17 family: IL17-A and IL-17F.[11] Differentiation of Tfh cells is initiated by IL-6 and IL-21 and the translocation of Bcl6 into the nucleus. In turn, Tfh cells secrete IL-4 and IL-21 (Figure 1.8).

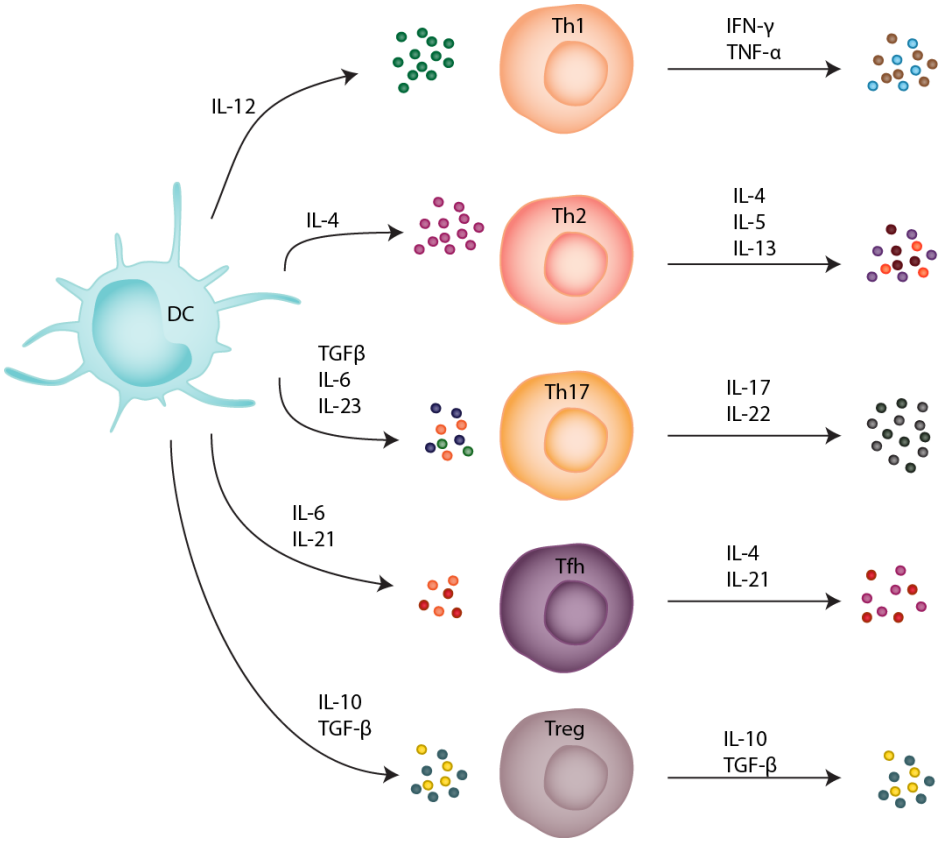

Figure 1.8| Polarisation of naive CD4⁺ T cells into effector subsets. Upon TCR engagement and ligation of co-stimulatory molecules with their cognate receptor and cytokine release by the APC, CD4⁺ T cells differentiate into effector T-cell subsets. Depending on the cytokine composition, CD4⁺ T cells can differentiate into Th1, Th2, Th17, Tfh cells and Tregs. Each T-cell subset can be characterised by a distinct cytokine profile that they secrete, and the resulting effector functions they elicit.

The T cells described above can have multiple functions in the immune system; Th1 cells provide help to B cells in terms of antibody production and mediate differentiation and activation of macrophages. Moreover, they are involved in the activation of cytotoxic CD8⁺ T cells and therefore contribute mainly to a cytotoxic T-cell response against tumours and intracellular pathogens such as viruses. Th2 cells provide help to B cells for class switching and antibody production. Furthermore, the cytokines secreted by Th2 cells are involved in the activation of B cells and eosinophils and in the control of the Th1 response. Th2 cells mainly mediate immune responses against extracellular pathogens such as parasites.[10,11] Th17 cells show pro-inflammatory properties and are involved in the clearance of extracellular pathogens such as bacteria and fungi. They promote survival and facilitate the recruitment of macrophages and neutrophils to infection sites and trigger the production of pro-inflammatory cytokines by surrounding immune and non-immune cells. Additionally, secretion of IL-17 enhances the production of IL-2 in Th1 cells and the proliferation of T cells and Tregs. Th17 cells are also thought to be the main mediators in inflammation-associated autoimmune disease[46]. Tfh cells provide B cell help in B cell follicles and therefore are involved in B-cell differentiation.[11] Another T-cell subset emerging from naïve CD4⁺ T

cells are Tregs which can be divided into two groups: naturally occurring Tregs (nTregs) and antigen-induced Tregs (iTregs). Development of nTregs is thymus-dependent and the fully matured cells mainly occur in secondary lymphoid organs (SLOs) where they are supposedly involved in the recognition of self-p:MHC complexes. Their differentiation is facilitated in response to TGF-β, resulting in the expression of the Treg-specific transcription factor forkhead-box-Protein P3 (FoxP3). nTregs can also be characterised by the expression of various surface markers such as CD25 and CTLA-4, and they mediate immunosuppression mainly through cell-cell contact and the inhibition of IL-2 gene transcription. iTregs, in contrast, emerge from peripheral $CD4^+CD25^-$ T cells and can be divided into Tr1 and Th3 cells. Differentiation of Tr1 cells is dependent on IL-10 and tumour necrosis factor (TNF)-α. Once activated in the periphery, Tr1 cells can be characterised by the production of IL-10 and TGF-β. Differentiation of Th3 cells, in contrast, depends on TGF-β and IL-4 and the cells in turn produce TGF-β. Tr1 and Th3 cells have immunosuppressive functions as they can dampen Th1 and Th2-mediated immune responses through secretion of IL-10 and TGF-β, as well as through direct cell-cell contact by binding of CTLA-4.[47]

Cytotoxic $CD8^+$ T cells (cytotoxic T lymphocytes; CTLs) represent another T-cell effector subset. Based on their secreted cytokines, they can be divided into two subsets: Type 1 CTLs and type 2 CTLs. Type 1 CTLs secrete IFN-γ as well as TNF-α. In contrast, type 2 CTLs, produce IL-4, IL-5, IL-10 and IL-13 in response to antigen recognition. Type 2 CTLs are only transiently induced and are thought to have regulatory functions[48], whereas conventional type 1 CTLs typically mediate cytotoxic target cell killing. Cell destruction can be mediated through Fas:FasL interactions, which are linked to caspase cascades, or the release of cytotoxic substances such as perforins or granzymes from intracellular cytolytic granules. Upon interaction of the CTL with its target cell, an immunological synapse is built which initiates the release of perforins and granzymes into the synaptic cleft via exocytosis of cytolytic granules. The activity of perforin is pH and Ca^{2+} dependent. Within cytotoxic granules, which have an acidic pH, perforins remain in an inactive state. However, upon formation of an immunological synapse perforins are released into the synaptic cleft and the neutral pH and high Ca^{2+} concentration of this region results in perforin activation.[49] The mechanism of how perforins enable granzyme entry into the cytosol of the target cell is still not fully clarified. One proposed mechanism is endosomolysis, which describes a two-step process: first, perforins bind to the plasma membrane in a Ca^{2+}-dependent manner and form small pores on the target cell, which allows an influx of Ca^{2+} (but not granzymes). Subsequently, the increased cytosolic concentration of Ca^{2+} triggers a membrane repair response. This results in the endocytosis of damaged membrane components and simultaneously the co-internalisation of granzymes and perforins from the synaptic cleft. Within the endosomes, perforins are thought to form larger and more stable pores through which granzymes can be secreted into the cytosol of the target cell to

initiate apoptosis.[50] Another study proposes that endocytosis might not be required for the induction of apoptosis; rather, that rapid cell killing is mediated through direct influx of granzymes via large perforin pores within the plasma membrane of the target cell.[51] Granzymes are serine proteases, secreted by CTLs that destroy target cells. In humans, five different granzymes are known, the most studied and well known of which are granzymes A and B.[52] Granzyme A induces cell death independently of caspases. Upon diffusion into the target cell, granzyme A prompts the production of ROS from the mitochondria and the disruption of the mitochondrial transmembrane potential. In response to ROS, the SET complex, a key substrate of granzyme A, is translocated into the nucleus. This complex contains the granzyme A activated DNase NM23-H and its inhibitor SET. Cleavage of SET by granzyme A activates NM23-H, which facilitates DNA damage, ultimately leading to cell death.[53] In contrast, granzyme B mediates cell death in a caspase-dependent manner and has over 300 known substrates. One main substrate is pro-caspase 3 which, when cleaved by granzyme B, can form homodimers. This results in the activation of caspase 3 and the initiation of downstream caspase cascades. Another mechanism of cell death induction by granzyme B is facilitated through the cleavage of the BH3-interacting domain death agonist (BID) and the subsequent activation of the Bcl2-family members Bax and Bak. Activation of Bax and Bak leads to the disruption of the mitochondrial transmembrane potential and eventually results in mitochondrial outer membrane permeabilisation. Because of this, apoptogenic factors such as cytochrome c, endonuclease G and the serine protease HtrA2/OMI are released from mitochondria into the cytosol These apoptogenic factors can then mediate the formation of the apoptotic protease-activating factor 1 complex, assembly of the apoptosome and activation of caspase cascades via caspase 9.[54]

Cytolysis can also be facilitated through cytokines such as IFN-γ, TNF-α or IL-2.[11] The encounter of CTLs with an antigen entails the induction of different activation phases; during the effector phase, priming of naïve $CD8^+$ T cells (described in more detail in section 1.3.5) takes place, followed by clonal expansion, the gain of effector functions, the migration to infection sites and the clearance of target cells. The final contraction phase represents the termination of an immune response, where the majority of effector CTLs die and only a minority differentiate into long-lived memory T cells. In the following phase (maintenance), memory T cells are maintained to be rapidly reactivated upon re-exposure with the antigen they have encountered before.[55]

Memory T cells can further be distinguished into three subsets: Effector memory T cells (T_{EM}), central memory T cells (T_{CM}) and tissue-resident memory T cells (T_{RM}). T_{EM} are $CD62L^{low}CCR7^-$ and can be found in non-lymphoid tissues where they display lytic activity. In contrast, T_{CM} are $CD62^{hi}CCR7^+$, reside in lymphoid organs and do not possess lytic capabilities.[55] The third type of

memory T cells are T_{RM}, which are long-term memory cells, residing in tissues such as intestines, skin, lungs and kidneys. T_{RM} are $CCR7^-$ and highly express homing molecules such as CD103 and CD69, and this CD69 expression leads to a decrease of sphingosine-1-phosphate receptor 1 (S1PR1), a molecule promoting tissue egression.[56] Their primary function is to provide a rapid immune response against re-infection with pathogens at the site of infection. Moreover, they are believed to contribute to anti-tumour immunity and improved clinical outcomes.[56-58]

1.3 The co-stimulatory molecule CD27

1.3.1 Structure of the CD27 gene

The co-stimulatory molecule CD27 belongs to the TNFRSF.[59] The gene encoding human CD27 (hCD27) was mapped to chromosome 12, band 12p3, and is comprised of six exons, each encoding distinct regions of the CD27 molecule (Figure 1.9).[60]

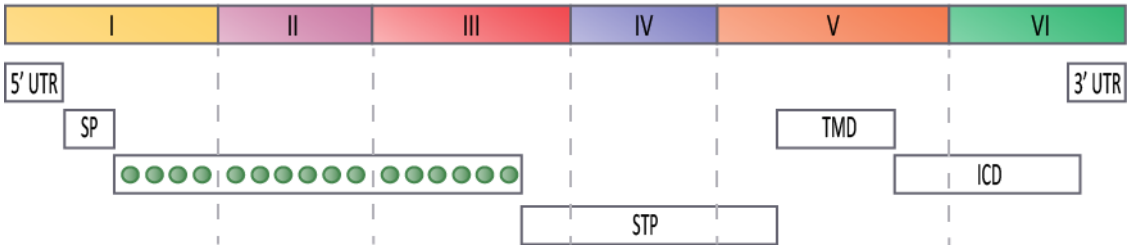

Figure 1.9| Schematic illustration of the hCD27 gene structure. Exon one encodes the 5' un-translated region (5' UTR) as well as the signal peptide (SP, 20 amino acids) and parts of the mature CD27 receptor (26 amino acids) with the first four of 16 cysteine residues (green circles). The second exon contains six cysteines (44 amino acids) and the third contains the six remaining cysteines (30 amino acids). The CD27 gene also contains a serine/threonine/proline-rich domain (STP), which is comprised of exons three and four (30 amino acids each) and exon five (11 amino acids). The transmembrane domain (TMD) of hCD27 is encoded by exon 5, and the intracellular domain (ICD) is encoded in parts by exon five (9 amino acids) and six (40 amino acids). Exon six encodes the 3' UTR and an AATAAA poly(A) sequence. Dashed lines represent splice sites (image adapted with permission from Loenen *et al.*[60]).

Human and mouse CD27 (mCD27) are 65% homologous with evolutionarily conserved regions.[61] The Cys-domain of mCD27 is 78% homologous to hCD27, with all 16 cysteines contained in this region being conserved. The STP region of mCD27, in contrast, is 9 amino acids shorter and shares 44% homology with hCD27. The cytoplasmic region and the C-terminal region are of 80% homology. However, mCD27 does not possess any known functional motifs in the C-terminal region and lacks the consensus sequence for PKC phosphorylation, which is present in hCD27 at residue 199.[61]

1.3.2 Expression of CD27 in humans and mice

In humans, CD27 appears as a 55 kDa disulphide-linked homodimer exclusively on the surface of immune cells of the lymphoid lineage and their immediate precursors.[59,62] Constitutive expression of hCD27 is reported on all subtypes of naïve ($CD45RA^+$) T cells. However, it is downregulated with progressive differentiation into effector $CD8^+$ T cells.[63,64] Thus, hCD27 is also only weakly expressed or absent on T_{EM} ($CD45RO^+$)[65], but it can be found on T_{CM}.[66] Further, hCD27 expression on peripheral blood mononuclear cell (PBMC)-derived Tregs is reported, and increased levels are detected on Tregs upon activation (after 3-5 days of stimulation), which decreases upon prolonged expansion (after 2-4 weeks of stimulation).[67] Additionally, hCD27 is also detectable on germinal centre B cells, memory B cells and plasma cells[68,69] as well as on a subset of human tonsillar B cells.[70] Further, hCD27 is expressed on NK cells. Similar to T cells, hCD27 loss on NK cells is associated with a more effector-like phenotype. Highly cytotoxic $CD56^{dim}$ NK cells weakly express hCD27, whereas the less cytolytic $CD56^{bright}$ NK cells are $hCD27^+$.[71]

Constitutive hCD27 expression has been evident in various haematological malignancies, such as chronic myeloid leukaemia (CML)[72] and acute myeloid leukaemia (AML)[73,74], and the role of hCD27 in these malignancies will be discussed in section 1.3.7. To date, hCD27 expression in solid tumours has not been reported.

In mice, CD27 was reported to be expressed on HSC and progenitor cells.[75,76] As in humans, mCD27 is equally detectable on mature $CD4^+$ and $CD8^+$ T cells. Additionally, it is also found on immature $CD3^-CD4^+CD8^+$ thymocytes as well as on $CD3^+CD4^+CD8^-$ and $CD3^+CD4^-CD8^+$ thymocytes.[77] In concordance with the CD27 expression in humans, mCD27 is only weakly expressed on effector $CD8^+$ T cells[78], but can be found on long-lived T_{CM} resident in SLOs.[79] Murine NK cells also express CD27 and here it can be used to distinguish between the Mac-1^{high} $CD27^{high}$ and Mac-1^{high} $CD27^{low}$ subset. In contrast to human NK cells, mCD27-expressing NK cells display cytotoxic activity and responsiveness to cytokines, whereas NK cells lacking mCD27 are rather unresponsive.[80] Murine B cells acquire CD27 expression at the centroblast stage and it peaks on germinal centre B cells. However, mCD27 expression is lost after B cell expansion and absent on memory B cells.[81]

Alongside the membrane-expressed hCD27, van Lier *et al.* detected a 32 kDa molecule that could be precipitated with anti-hCD27 mAb from the membrane of PHA- or CD3-stimulated T cells. The molecule was not derived from the 55 kDa hCD27 but metabolically synthesised during T-cell activation.[59] Hintzen *et al.* were also able to detect a soluble form of hCD27 (sCD27) and demonstrated that it was structurally related to the 55kDa hCD27 and that it also shared epitopes with the molecule expressed on the cell surface. After stimulation of PBMCs with coated anti-CD3,

sCD27 was detected by enzyme-linked immunosorbent assay (ELISA) in cell lysates and supernatant respectively. The concentration of sCD27 in the supernatant was 10-times higher than in cell lysates, and no sCD27 was detectable in unstimulated PBMCs. Upon stimulation with anti-CD3 mAb, sCD27 was strongly upregulated and its membrane expression peaked 3 days post-stimulation, decreased over time, and reached levels of resting T cells 7 days after stimulation. In the supernatant, sCD27 could be detected after 2 days of stimulation with anti-CD3 and its concentration constantly increased over the time course experiment.[82] sCD27 was also measured in high concentrations in the sera of 59 healthy donors (165 (±49) units/ml) and 24 hour urine samples of 11 healthy donors (mean output of $2.5\pm1.1x10^6$ units), showing the presence of sCD27 not only in cells and supernatant but also in body fluids. [82] To date, the function of sCD27 is not yet fully clarified. However, studies have shown that in a variety of haematological malignancies elevated sCD27 correlates with progressive disease stages and poor outcomes.[83,84]

1.3.3 Expression of CD70 in humans and mice

The ligand of CD27 is CD70 and its expression is tightly regulated and only induced upon activation of the respective cell. Human CD70 (hCD70) is absent on peripheral and immature DCs but its expression can be induced in the presence of certain agents, such as anti-CD40 mAb and prostaglandin E2[85,86] or upon irradiation[87]. In addition to its expression on DCs, it can also be found on other immune cell subsets such as NK cells[71], T cells[86] and activated B cells[88]. The expression of hCD70 is also described on haematological malignancies (see section 1.3.7), but can, in contrast to hCD27, also be present on malignant cells of solid tumours.

Tesselaar *et al*. characterised the expression of murine CD70 (mCD70) *in vitro* and *in vivo*. They stimulated purified T and B cells with a combination of lipopolysaccharide (LPS) and anti-CD3 or anti-CD40. Activated B cells demonstrated high levels of mCD70 mRNA whereas activated T cells showed upregulation of mCD70 mRNA to a lesser extent, and unstimulated T and B cells did not show any mRNA expression. The mCD70 mRNA expression was also reflected in the surface expression of mCD70. On B cells it was highly detectable, whereas T cells only displayed low levels and the expression could also not be enhanced by the addition of stimulants such as IL-2 or anti-CD28. Furthermore, the mCD70 expression was characterised on *in vitro* generated DCs and on the DC line D1. Immature, unstimulated DCs did not express mCD70. However, upon stimulation with anti-CD40 mAb and LPS, mCD70 expression was induced and highly detectable. *In vivo*, mCD70 is not expressed on lymphocytes of the spleen or LNs in non-immunised mice. However, upon intranasal infection with the influenza virus, mCD70 was detectable at high levels on

lung-infiltrating T cells, as well as in immune cells (B cells, T cells, DCs) of lung-draining LNs. However, in the latter, expression was restricted to the cytoplasm.[89]

1.3.4 Signalling by CD27

Depending on the cell type on which CD27 is expressed, different modes of action and signalling pathways are triggered upon simultaneous TCR engagement and CD27-CD70 ligation.[59,90] Signalling of CD27 is mediated by a cytoplasmic 13 amino acid motif (REEEGSTIPIQED), which is essential for the interaction with TRAFs.[91] Binding of TRAF2 and 5 to this motif results in the activation of stress-activated protein kinase (SAPK)/c-Jun N-terminal kinase (JNK) as well as the canonical and non-canonical NF-κB pathway (Figure 1.10).[90-93] Both the canonical and non-canonical NF-κB pathways are characterised by distinct transcription factors. NF-κB1 (p50), RelA (p65) and c-Rel belong to the canonical NF-κB pathway, whereas NF-κB2 (p52) and RelB are non-canonical. The transcription factors p50, as well as p52, are produced as precursor proteins (p105 and p100, respectively), and mature upon proteasomal degradation of their C-terminal region. Nuclear translocation of these transcription factors induces the expression of genes associated with anti-apoptotic pathways, cell survival and proliferation. Accordingly, the pathways induced upon CD27-CD70 ligation result in co-stimulatory signalling and eventually contribute to T-cell activation and expansion as well as to effector cell differentiation and formation of memory T-cell populations.

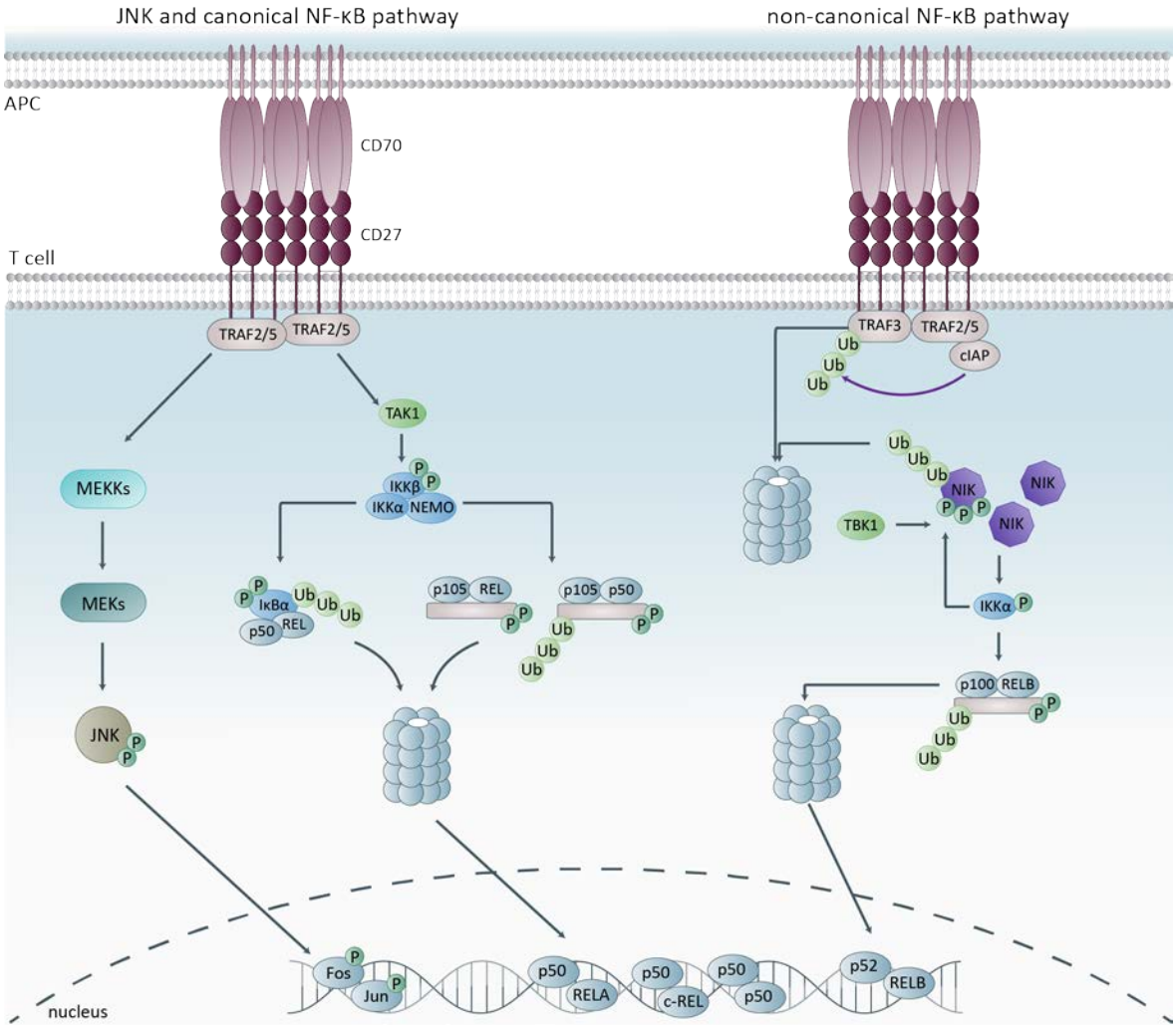

Figure 1.10| The canonical and non-canonical NF-κB pathway. Ligation of CD27 (on T cells) with CD70 (on APCs) results in the recruitment of TRAF 2/5, leading to downstream signalling through the JNK and canonical NF-κB pathway. The latter is initiated through the TAK1-mediated phosphorylation of IKKβ. This in turn leads to the activation of the IKK complex (IKKα, IKKβ, NEMO) and facilitates ubiquitination and phosphorylation of IκB, resulting in the proteasomal degradation of p50/REL, p105/REL or p105/p50 and their translocation into the nucleus. Activation of the non-canonical NF-κB pathway results in the recruitment of TRAF5 followed by TRAF2. One of the key players of the non-canonical NF-κB pathway is the NF-κB inducible kinase (NIK), directly phosphorylating IKKα, which in turn directly phosphorylates p100 resulting in its proteasomal degradation and the nuclear translocation of p52 and RelB. NIK-activation is thereby tightly regulated; under unstimulated conditions, TRAF3 mediates the negative regulation of the non-canonical NF-κB pathway by binding NIK. Additionally, TRAF3 forms a complex with cellular inhibitor of apoptosis (cIAP) and TRAF2. cIAP, possessing E3 ligase activity, ubiquitinates NIK, inducing its proteasomal degradation. In turn, to activate NIK, the TRAF3-TRAF2-cIAP complex has to be disrupted. Upon TNFR stimulation, this complex is recruited to the TIM of the TNFR and degradation of TRAF3 is induced through ubiquitination by cIAP, which triggers the release and accumulation of NIK and associated downstream signalling[27,94] (Figure adapted with permission from Sun *et al.* [27]).

1.3.5 Function of CD27

1.3.5.1 Co-stimulatory capacity of CD27

Multiple research groups have identified CD27 as a co-stimulatory molecule. Treatment of human naïve T cells with compounds mimicking antigen-stimulation such as anti-CD3 mAbs or phytohemagglutinin (PHA) led to a five-fold transient upregulation of hCD27 on T cells. The expression peaked three days post-stimulation and after seven days returned to levels found on naïve T cells.[59,62] The upregulation of hCD27 seemed to be dependent on TCR/CD3 triggered pathways leading to Ca^{2+} mobilisation and cyclic adenosine monophosphate (cAMP).[95] Moreover, the addition of hCD27-targeting mAbs to anti-CD3 mAb or PHA-treated PBMCs induced enhanced T-cell proliferation.[59] Similar results were observed with the hCD27-targeting mAb 1F5.[96] T-cell activation and proliferation were also crucially dependent on simultaneous TCR engagement, which then resulted in proliferation and production of IFN-γ and TNF-α by both $CD4^+$ and $CD8^+$ T cells. Of note, proliferation and cytokine production in this *in vitro* assay only occurred with plate-bound mAbs, suggesting a dependence on cross-linking of relevant receptors.[96] The role of the CD27-CD70 interaction in co-stimulation was further confirmed by Goodwin and co-workers, where hCD70-expressing CV-1/EBNA cells were co-cultured with purified human peripheral blood T cells and suboptimally stimulated with PHA. The ligation of hCD70 with hCD27 led to an increase in proliferation of $CD4^+$ and $CD8^+$ T cells, respectively.[97]

The function of CD27 as a co-stimulatory molecule was also demonstrated in the murine context. *In vitro* stimulation of mCD27 with mCD70, fused to a modified human IgG1 (hIgG1) Fc region[98], resulted in the proliferation of $CD8^+$ T cells obtained from OT-I TCR transgenic (tg) mice, as well as in the production of IFN-γ and IL-2. Of note, the augmenting effect of mCD27 on the T-cell proliferation was not affected when the interaction of CD28 with its ligands CD80/CD86 was blocked, suggesting that the CD27 signal is different from CD28.[98] Based on these findings Rowley *et al.* performed an adoptive transfer of carboxyfluorescein succinimidyl ester (CFSE)-labelled ovalbumin (OVA)-specific OT-I T cells to C57BL/6 mice to examine the role of CD27 *in vivo*. Administration of OVA in combination with the mCD70 hIgG1 Fc fusion protein led to a 17-fold increase of OT-I $CD8^+$ T cells compared to mice treated with OVA and hIgG. Moreover, co-administration of OVA and mCD70 hIgG1 Fc fusion protein resulted in the accumulation of OT-I $CD8^+$ T cells 68 hours post-stimulation, whereas control mice did not show such accumulation, suggesting that CD27 also mediates increased survival of activated antigen-specific $CD8^+$ T cells.[98] Further *in vivo* studies confirmed the role of CD27 as a co-stimulatory molecule. Hendriks *et al.* established a CD27 deficient mouse model ($CD27^{-/-}$) to study the role of CD27 in T-cell activation

and cell cycle. Comparison of the division of T-cell subsets of wild-type (WT) and CD27 deficient mice showed no differences, indicating that CD27 is not crucial for the generation and development of naïve T cells.[99] The research group further examined the effect of the CD27-deficiency on T-cell proliferation using a [^{3}H]thymidine incorporation assay. T cells were purified from the LNs of CD27$^{-/-}$ mice as well as from the respective WT mice and cultured for 3 days in the presence of coated anti-CD3 mAb. Deficiency of CD27 led to a 1.8-fold decrease in [^{3}H]thymidine incorporation compared to cells from WT mice, implying reduced T-cell proliferation. The addition of recombinant IL-2 or anti-CD28 mAb enhanced the expansion of T cells from CD27$^{-/-}$ mice, but could not overcome the difference in proliferation between CD27$^{-/-}$ and WT mice. This is in accordance with Rowley *et al.*, who also suggested the CD27 signal to be different from the co-stimulatory CD28 signal. Moreover, using CFSE-labelled T cells from WT and CD27$^{-/-}$ deficient mice, it was demonstrated that CD27 is not required for T cells to enter the cell cycle nor does it affect T-cell division.[99]

1.3.5.2 The role of CD27 in T-cell survival

These *in vitro* and *in vivo* data confirm the role of CD27 in T-cell activation, proliferation and expansion. Unlike CD28, the signal mediated by CD27 does not affect cell cycle entry or cell division. However, it contributes to CD4$^+$ and CD8$^+$ T-cell expansion and effector T-cell generation by accumulating and mediating survival signalling.[100] In fact, CD27 signalling results in the desensitisation of CD8$^+$ T cells to FasL-mediated apoptosis and the reduction of FasL on CD4$^+$ T cells.[101] Moreover, studies demonstrated the upregulation of the anti-apoptotic Bcl-2 member Bcl-x_L in primed CD8$^+$ T-cells, both at mRNA and protein level in response to CD27 stimulation.[102,103] However, it was also suggested that the pro-survival capacities of CD27 do not solely rely on Bcl-x_L. Genome-wide mRNA sequencing of primed CD8$^+$ OT-I T cells demonstrated *Pim-1* and the according Pim-1 kinase pathway (which is also involved in anti-apoptotic signalling) to be an early target of the CD27-CD70 axis after TCR/CD3 induced CD8$^+$ T-cell priming. Further investigation showed that this occurs independently of IL-2.[102] Lastly, T cell-APC communication is promoted through CD27-mediated expression of CXCL10 and XCL1 in CD8$^+$ T cells during T-cell priming, contributing to effector cell generation.[104]

1.3.5.3 The role of CD27 in T-cell priming and memory cell generation

The CD27-CD70 axis is also involved in the formation of T-cell immunity, especially in T-cell priming and the generation of memory T-cell populations. Naïve CD8$^+$ T cells undergo distinct developmental stages upon antigen-encounter. These include a clonal expansion phase, where large amounts of antigen-specific cytotoxic lymphocytes are generated, a contraction phase, where

the majority of the cells undergo apoptosis, and a memory phase, where the remaining antigen-specific cells build the memory $CD8^+$ T-cell pool that can rapidly be activated upon a secondary antigen encounter. Janssen and co-workers demonstrated that for the generation of a memory T-cell population, cross-priming of $CD8^+$ T cells by $CD4^+$ T cells during the priming phase is essential.[105] The proposed underlying mechanism is that $CD4^+$ T cells interact with APCs (mostly DCs) in a MHC class II dependent manner. This leads to the transient upregulation of CD40L on $CD4^+$ T cells and its ligation with CD40 expressed on APCs. In turn, APCs become activated, mature and licenced to activate naïve $CD8^+$ T cells in a MHC class I restricted manner.[105]

However, research demonstrated that not only $CD4^+$ T-cell help but also the CD27-CD70 axis plays a crucial role in T-cell priming and the formation of $CD8^+$ T-cell memory. Mice deficient for CD27 that were infected with influenza virus displayed, in comparison to WT mice, a decrease in lung-infiltrating $CD8^+$ and $CD4^+$ T cells as well as virus-specific $CD8^+$ T cells in the lungs during the primary immune response.[99] In turn, reinfection of the deficient mice resulted in a delayed recall response with decreased $CD4^+$ and $CD8^+$ T-cell numbers in the lungs compared to control mice. Of note, the effector cell differentiation of $CD4^+$ and $CD8^+$ T cells was not affected by the lack of CD27 signalling. Splenic $CD4^+$ and $CD8^+$ T cells of immunised WT and $CD27^{-/-}$ mice had comparable cytolytic activity and IFN-γ production.[99] These results indicate that CD27 signalling is essential for the generation of T-cell immunity in the primary and secondary response (in the context of the influenza mouse model), but not for effector cell differentiation. The role of the CD27-CD70 interaction in the priming of $CD8^+$ T cells in the primary response was demonstrated in further infection and immunisation mouse models. Administration of a blocking anti-CD70 mAb to mice infected with vaccinia virus, vesicular stomatitis virus or *Listeria monocytogenes* led to a reduction of antigen-specific $CD8^+$ T cells, and highlights the crucial role of CD70 in the priming of naïve $CD8^+$ T cells.[106] The involvement of CD27-CD70 signalling in the generation of a memory T-cell response was further evident in the context of CD40-mediated priming of $CD8^+$ T cells.[85] Priming of $CD8^+$ T cells is mediated by mature DCs, which mature upon ligation of CD40 with CD40L.[107] Taraban *et al.* demonstrated *in vivo* that DCs upregulate the surface expression of CD70 in response to CD40-CD40L interaction.[85] As CD27 is not only expressed on $CD4^+$ but also on $CD8^+$ T cells, DCs are subsequently able to interact with $CD8^+$ T cells for priming. To investigate the effect of the CD27-CD70 axis on T-cell memory formation, the research group adoptively transferred OVA-specific OT-I T cells into mice, immunised them with OVA, and treated them with agonistic anti-CD40 mAb as well as anti-CD70 mAb to block the CD27-CD70 interaction. This resulted in reduced numbers of OT-I $CD8^+$ T cells accompanied by impaired survival of the respective cells in the primary response. Re-challenge of the OT-I mice, which received anti-CD70 mAb during the priming phase, showed poor $CD8^+$ T-cell memory as reflected in decreased numbers and impaired expansion of $CD8^+$ OT-I

T cells. However, and in accordance with Hendriks *et al*.[99], the differentiation of naïve CD8$^+$ T cells into cytotoxic effector cells was not affected by the blockade of the CD27-CD70 interaction.[85] Similar results were obtained by Dolfi *et al.*, where CD27/CD70 signalling was only crucial during the priming phase and not the secondary recall phase for the generation of effective memory T cells.[101]

In addition to the relevance of CD27 signalling during CD8$^+$ T-cell priming and the formation of CD8$^+$ T-cell memory, it was also shown to be involved in the priming of CD4$^+$ T cells. In *in vitro* studies, CD4$^+$ T cells obtained from CD27$^{-/-}$ mice only poorly responded to primary and secondary influenza virus infection, which was reflected in reduced numbers of virus-specific lung-infiltrating CD4$^+$ T cells. However, the differentiation of activated CD4$^+$ T cells into IFN-γ producing effector cells seemed to be CD27-independent.[99] Involvement of CD27-CD70 was also demonstrated for human CD4$^+$ T cells.[103] Human PBMC-derived naïve CD4$^+$ T cells were co-cultured with mock- or CD70 transfected mouse 3T3 fibroblast cells and stimulated with anti-CD3 mAb for one day.[103] Subsequent culturing of the primed T cells in the presence of the Th1 and Th2 polarising cytokines (IL-12 and IL-4 respectively) showed TCR induced T-cell proliferation, which was greatly enhanced upon CD27-CD70 co-stimulation. However, only the addition of IL-12 resulted in an IFN-γ-producing Th1 CD4$^+$ T-cell population, and this was crucially dependent on CD70-mediated co-stimulation. In contrast, the addition of IL-4 did not lead to the differentiation of Th2 cells, suggesting that engagement of CD27 selectively contributes to the formation of CD4$^+$ Th1 cells during T-cell priming. The differentiation is thereby mediated through the upregulation of the Th1 master transcription factor Tbet, accompanied by the enhanced expression of the IL-12 receptor (IL-12R) γ2.[103]

These studies highlight the importance of the CD27-CD70 interaction in the generation of a potent T-cell immune response as well as the formation of a T-cell memory. Due to its co-stimulatory features, CD27 became a target of interest for cancer immunotherapy, where one aim is to stimulate the patient's own immune system by targeting effector cells, such as T cells, to elicit an anti-tumour response and generate anti-tumour memory. The role of CD27 in cancer immunotherapy will be elaborated in section 1.5.3.

1.3.6 Deficiency of CD27 and CD70

The functions of CD27 described above (section 1.3.5) underline the crucial role of the CD27-CD70 axis in an anti-viral immune response.[99,108] However, individuals have been identified where mutations of *CD27* or *CD70* led to CD27 or CD70 deficiency and associated immunodeficiency.

Studies show that individuals lacking CD27 expression are highly susceptible to Epstein-Barr virus (EBV) infections. Where this infection is mostly asymptomatic in immunocompetent individuals, immunocompromised patients frequently develop EBV-driven lymphoproliferative disorders and associated B-cell malignancies, such as Hodgkin's and non-Hodgkin's lymphoma with severe disease progression and often fatal outcomes.

To date, 18 patients have been described as showing a CD27-deficiency.[109-112] The index cases were two patients with a homozygous mutation in *CD27*. Both presented with persistent symptomatic EBV-viremia (individual 1: with lethal aplastic anaemia; individual 2: hypogammaglobulinemia with compromised mAb function). Detailed analysis of the immune phenotype of the surviving individual revealed that despite having fully differentiated $CD8^+$ and $CD4^+$ memory T-cell subsets, the proportion of IL-2 producing EBV-specific $CD8^+$ memory subsets was reduced. Moreover, the patient displayed diminished specific-antibody functions resulting from impaired T-cell dependent B-cell responses. [112] Analysis of a further 16 patients with CD27-deficiency also presented with EBV-driven lymphoproliferative disorders, which included, among others, B-cell lymphoma and Hodgkin's lymphoma.[109-111] The genetic profile of *CD27* was determined in 17 of the 18 patients, and the mutations leading to CD27-deficiency are summarised in Table 1.1.

Table 1.1| Genetic analysis of *CD27* in patients with CD27-deficiency. Listed are homozygous and heterozygous mutations of *CD27* that have been identified to date. Data adapted from Alkhairy *et al*.[109]

Homozygous mutations:		
Number of patients	**Mutation**	**Mutation outcome**
2	c.G24A/p.W8X (Exon 1)	nonsense
8	c.G158A/p.C53Y (Exon 2)	missense
4	c.G287A/p.C96Y (Exon 3)	missense
1	c.C232T/p.R78W (Exon 3)	missense
Heterozygous mutations:		
1	c.C30A/p.C10X (Exon 1) no other found	nonsense
1	cG24A/p.W8X (Exon 1) c.C139T/p.R107C (Exon 3)	not reported

Deficiency of CD70 has also been reported and largely mirrors the pathology observed in CD27-deficient patients. These patients (six patients identified) are also prone to EBV infections, EBV-driven lymphoproliferative disorders, development of B-cell malignancies and dysgammaglobulinemia. Immunophenotypic investigations revealed that the lack of CD70 expression on B cells results in decreased cytotoxic activity of EBV-specific $CD8^+$ T cells and impaired protection against EBV infections and associated disease.[113-115]

1.3.7 Role of CD27/CD70 in AML and CLL

As mentioned previously in sections 1.3.2 and 1.3.3, CD27-CD70 signalling plays a role in haematological malignancies such as AML and CML.[72,73] Under normal physiological conditions, CD27-CD70 expression is tightly regulated and crucially contributes to immune homeostasis. However, constitutive expression of CD27 on leukaemic stem cells (LSCs) and progenitor cells in CML promoted disease progression in a CML-disease-like mouse model.[72] Signalling through CD27 increased nuclear translocation of β-catenin and the transcription activator NCK-interacting kinase (TNIK; associates with TRAF2, an adaptor molecule of the CD27 signalling pathway), which both are known to drive Wnt signalling. This pathway, constitutively activated in LSCs and further enhanced through CD27 signalling, eventually leads to cell cycle progression, differentiation and proliferation. Interruption of the CD27-CD70 axis with a CD70 blocking mAb prolonged survival, but might also be associated with diminished T-cell activation.[72] Expression of CD27 was also evident on $CD34^+$ cells in the BM of newly diagnosed CML patients and BCR/ABL^+ leukaemia cell line SD-1. Detailed investigations confirmed the results observed in the mouse model. Wnt signalling was increased in leukaemia cells and cell proliferation was reduced upon blocking of the CD27-CD70 interaction.[72] In contrast to CML, co-expression of CD27 and CD70 was detected on AML LSCs, progenitor cells and blasts of AML patients. Signalling via CD70/CD27 induces, similar to CML, enhanced Wnt signalling promoted by TNIK and TRAF2. However, additional pathways, such as the JNK or NF-κB pathway are also initiated, which contribute to stemness. Targeting the CD27-CD70 axis can induce asymmetric cell division and decrease growth and colony formation of AML blasts.[73] The function of the CD27-CD70 axis makes it a good target for cancer immunotherapy e.g. CD70 targeting mAb.[116]

1.4 Cancer immunotherapy

Cancer therapy is versatile and includes various kinds of treatment options nowadays. The conventional approaches include surgical intervention, radiotherapy and chemotherapy. Depending on the type of cancer, the disease stage and severity, these approaches are likely to be combined to achieve the best possible prognosis for the patient. However, the efficacy of these treatments comes with limitations due to the nature of the disease, its location and accessibility, and disease severity. Surgical intervention, where the bulk tumour mass is excised, is only suitable for solid tumours and not haematological malignancies. Furthermore, in some cases, there is insecurity about the accuracy of the tumour excision and the reassurance of whether the whole tumour mass has been successfully removed without harming surrounding tissue. As with surgical removal of the tumour, radiotherapy, where ionising energy is applied to induce DNA damage and

subsequent cell death in the cancer tissue, can damage adjacent tissue. Chemotherapy, on the other hand, is suitable for systemic applications such as in haematological malignancies. Utilised therapeutics include alkylating agents to inhibit DNA synthesis (e.g. cyclophosphamide), cell cycle arresting compounds (e.g. etoposide), and antibiotics (e.g. doxorubicin). To achieve the best efficacy, chemotherapeutic compounds are mostly administered in combination regimens. For example, for diffuse large B-cell lymphoma the most commonly used treatment regimen is a combination of cyclophosphamide, doxorubicin, vincristine (Oncovin) and prednisone (CHOP) or a combination of CHOP with the immunotherapeutic mAb rituximab.[117] However, chemotherapy also comes with limitations. Its broad specificity hampers the specific and exclusive targeting of malignant cells and thus can be accompanied by severe systemic toxicities.

Therefore, over the last three decades, huge efforts have been made to invent new forms of targeted therapeutic approaches to increase specificity and minimise toxicities. One field emerging from this research is cancer immunotherapy. This type of cancer treatment utilises the host's innate and adaptive immune system to target and eliminate malignant cells. Different treatments are available, which can broadly be divided into active and passive therapeutic approaches.

1.4.1 Active cancer immunotherapy

Active cancer immunotherapy aims to induce endogenous cell-mediated and humoral immunity to initiate an anti-tumour response.[31] Therapeutics in this branch of therapy comprise primarily cancer vaccines, which can broadly be categorised into therapeutic and preventive vaccines.

Preventive vaccines comprise of vaccines that protect against infections; for example, the human papillomavirus (HPV), which has been shown to be associated with a higher risk of cervical cancer.[118] To date, there are two food and drug administration (FDA) approved HPV vaccines: Cervarix® and Gardasil®. Both vaccines are composed of non-infectious, non-oncogenic virus-like particles (VLPs) that assemble to resemble a HPV virion, which, upon immunisation, eventually leads to the induction of high antibody titres against HPV. Cervarix® is a bivalent vaccine, protecting against HPV 16 and 18, whereas Gardasil® is a quadrivalent vaccine, not only protecting against HPV 16 and 18 but also HPV 6 and 11. Two clinical phase III trials for each compound (FUTURE I/FUTURE II for Gardasil® and PATRICIA/Costa Rica HPV Vaccine Trial for Cervarix®) have investigated the safety and efficacy over a four-year time period. The vaccines were rated as generally safe with minor injection-related side effects. Both vaccines are highly immunogenic and able to induce antibody titres against the different HPV types (reviewed in[119]).

Administration of therapeutic cancer vaccines, in contrast to preventive vaccines, induces the priming of the immune system against tumour specific components to evoke an immune response against a pre-existing tumour. There are different types of therapeutic cancer vaccines, which include protein and DNA vaccines or DC-based vaccines. Protein-based vaccines are used for the immunisation against tumour-specific antigens (such as mutated oncogenes), tumour suppressor genes or overexpressed proteins. An idiotype-vaccine used for the treatment of lymphoma patients is an example of a protein-based vaccine and contains the tumour-specific B-cell lymphoma idiotype which is usually coupled to a carrier protein (keyhole limpet hemocyanin) and administered in combination with immunologic granulocyte-macrophage colony-stimulating factor (GM-CSF) to induce a stronger immune response.[120] Although the clinical phase I/II studies did show induction of a humoral and cell-mediated immune response, subsequent phase III clinical trials could not confirm the clinical efficacy of the idiotype-vaccination.[121,122] DNA vaccines are composed of plasmids containing genes encoding tumour antigens. Upon injection, the plasmids are taken up by APCs such as DCs. These cells subsequently process and present the antigen in an MHC dependent manner to stimulate and augment a T cell response against cells bearing the encoded tumour antigen. Furthermore, due to its double-strand nature DNA vaccines are also able to induce an innate immune response through cytosolic receptors such as TLRs.[123-125] Another form of therapeutic vaccine are DC-based vaccines. One such vaccine, known as sipuleucel-T, was approved in 2010 by the FDA for the treatment of asymptomatic or minimally symptomatic metastatic castrate-resistant prostate cancer. The underlying principle of this cell-based vaccine is to isolate autologous PBMCs from cancer patients and stimulate the APCs with a recombinant fusion protein (PA2024) comprised of recombinant prostate acid phosphate (PAP), an antigen present in the prostate, fused to GM-CFS. The aim is to generate PAP-specific T cells through the stimulation and activation of APCs by the administration of GM-CSF. Once the PBMCs have been stimulated *ex vivo*, the cells are re-infused into the patient.[126] The double–blind, placebo-controlled, multicentre phase III trial that eventually led to the FDA approval of the vaccine demonstrated a median survival benefit of 4.1 months and an increase of 38% in overall survival of 3 years.[127]

1.4.2 Passive cancer immunotherapy

Passive cancer immunotherapy includes cellular therapies such as adoptive cell transfer or chimeric antigen receptor (CAR) T cells (reviewed in[31]). For adoptive cell transfer, autologous T cells are primed *ex vivo* against a tumour specific antigen and subsequently re-infused into the patient to elicit a T-cell dependent anti-tumour specific response.[128] Recently, adoptive cell transfer has been refined by the development of CAR T-cell therapy.[129] CAR T cells are created by linking single-chain variable fragments (scFv) of the variable domain of a mAb to a transmembrane domain and

intracellular co-stimulatory and CD3ζ domain. This facilitates the targeting of T cells directly against specific antigens and accordingly causes an anti-tumour response in a MHC-independent manner, widening the number of potential target molecules.[130,131]

Cytokines, such as IL-2 or IFN-α, are also part of passive cancer immunotherapy. Treatment with both agents resulted to some degree in the activation of various immune cells or direct anti-tumour capacities.[132]

Besides these approaches, mAbs become more commonly utilised in the field of cancer treatment.[133] The mAbs used can be categorised into mAbs that directly target tumour cells and subsequently mediate their destruction (section 1.5.1) or immunomodulatory mAbs which engage with immune cells to enhance an anti-tumour immune responses (section 1.5.2).

1.5 Monoclonal antibodies for cancer immunotherapy

Humoral immunity is primarily mediated by mAbs, a soluble form of the B-cell receptor (BCR), secreted by terminally differentiated plasma cells.[134,135] mAb-secreting terminally differentiated plasma cells originate from HSCs that have undergone several B-cell developmental stages. The overview of the B-cell development is displayed in Figure 1.11 and includes six differentiation stages.

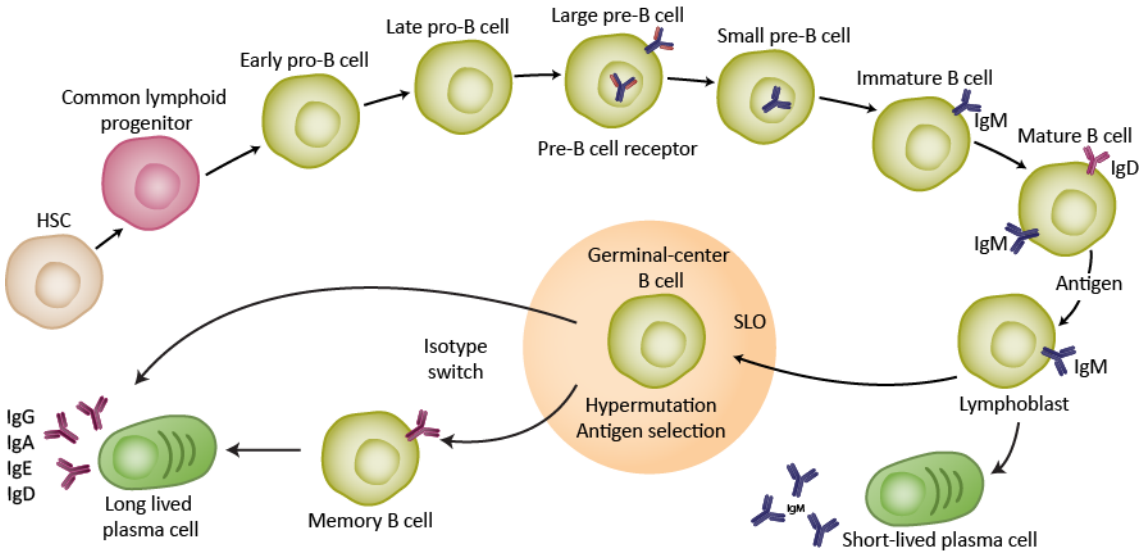

Figure 1.11| B cell development. B cells develop from a common lymphoid progenitor which evolved from a HSC. Progenitor cells progress through various stages including the early and late pre-B cell stage and the large and small B cell stage before they eventually become IgM expressing immature B cells. After additional rearrangement of the light chain, the immature B cells transition to the mature B cell stage expressing IgD and IgM and leave the BM. Once the B cells encounter an antigen, they migrate to the germinal centre in SLOs where they undergo somatic hypermutation and antigen selection. Once positively selected, the B cells leave the germinal centre as memory B cells, which eventually differentiate into antibody-secreting long-lived plasma cells (adapted from Kuehl *et al.*[136]).

The first stage is the early pro-B cell stage. It includes a process termed VDJ recombination, where the gene rearrangement of the heavy chain locus of the BCR is facilitated (Figure 1.12). Upon initial gene rearrangement, the early pro-B cell transitions into the late pro-B cell stage where the VDJ recombination is completed. Subsequently, the fully functional heavy chain, also termed the pre-B cell receptor, is transiently expressed on the cell surface and in the cytoplasm, marking the transition from a late pro-B cell to a large pre-B cell. Signalling through the pre-BCR results in allelic exclusion, which prevents further rearrangements of the heavy chain locus and in turn the expression of only one type of BCR with one antigen-specificity. Moreover, the expression of the pre-BCR evokes proliferation and drives the differentiation of the large into the small pre-B cell. In this stage, the pre-BCR is no longer expressed on the cell surface. Light chain VJ rearrangement takes place and the surrogate light chains associate with the heavy chain (Figure 1.12). The small pre-B cell becomes an immature B cell, which expresses the fully functional IgM on its surface. After alternative splicing of the heavy-chain locus, the immature B cell additionally expresses IgD and becomes a mature naïve B cell. It is at this stage that it leaves the BM and can either differentiate into a short-lived IgM-secreting plasma cell or migrate to SLOs such as the LN or the spleen. Once a mature naïve B cell has encountered an antigen in the B cell follicles, it can differentiate into a memory B cell or an antibody-secreting plasma cell.

The B-cell development stages are tightly regulated in order to maintain self-tolerance whilst creating a BCR repertoire able to recognise a vast diversity of antigens. The process to eliminate self-reactive B cells takes place in the immature B-cell stage (central tolerance). B cells that recognise self-antigen can undergo different fates; those that weakly bind the antigen are positively selected and receive signals to undergo further differentiation. B cells that do not interact with the antigen and cells that strongly bind self-antigen undergo apoptosis (negative selection). However, B cells strongly binding self-antigen are able to induce light-chain rearrangement (receptor editing) and can express a new BCR. In addition to the central tolerance acquired in the BM, B cells also have to acquire peripheral tolerance once they migrate to the SLOs. In the SLOs, upon antigen encounter, processes are initiated including clonal expansion, somatic hypermutation and class switch recombination, which all contribute to the generation of high-affinity, class-switched memory B cells and long-lived mAb-secreting plasma cells. [10,11]

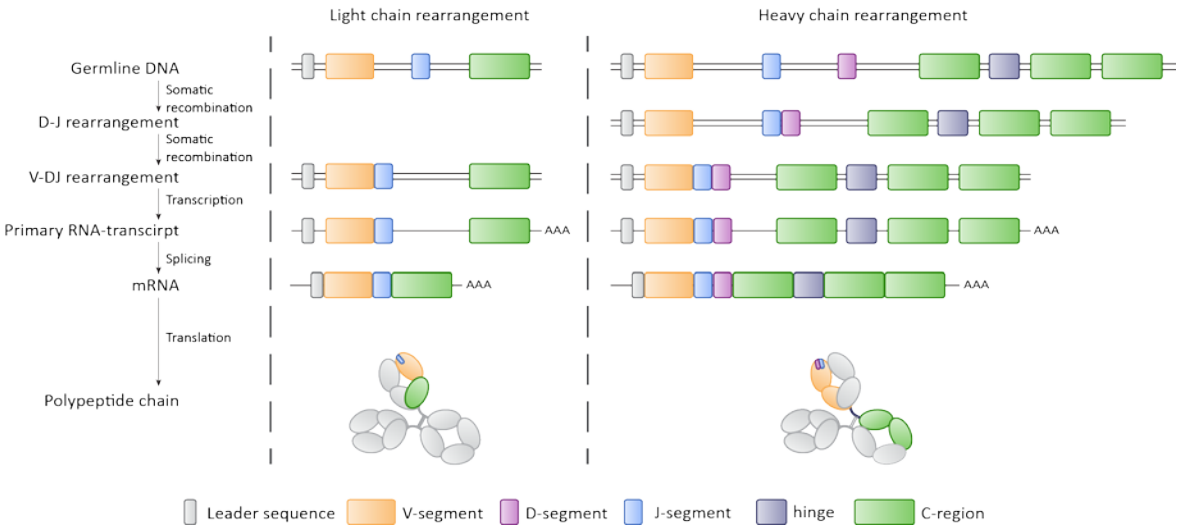

Figure 1.12| V(D)J recombination of the light and heavy chain of mAbs. Gene rearrangement of the light and heavy chain locus contributes to the generation of mAb diversity. At first, a variable (V) gene segment and diversity (D) segment are joined (VD) and subsequently are combined with a diversity (D) segment (VDJ). The leader sequence, C-region and hinge are spliced onto the VDJ segment. mRNA translation results in a complete Ig and disulphide bonds are formed. Similar gene rearrangements take place for the light chain locus. However, the variable domain is only formed from two segments (VJ) (Figure adapted from Murphy *et al.*[10]).

mAbs are Igs and therefore belong to the IgSF. There are five mAb isotypes: IgA, IgD, IgE, IgG and IgM. The most abundant Ig in human blood is IgG. It consists of two identical heavy (each 55 kDa) and two identical light (each 25 kDa) chains connected by disulphide bonds. The light chains contain both a constant (C_L) and variable (V_L) region, whereas the heavy chains are built of three constant regions (C_H1-3) and one variable (V_L) region (Figure 1.13). Both arms of the antibody are connected by disulphide bonds in the hinge region. The Ig molecule consists of two fragments: the fragment antigen binding ($F(ab')_2$) and fragment crystallisable (Fc). The $F(ab')_2$ contains two binding sites, also referred to as complementarity determining regions (CDRs), which are three regions of high sequence variability that form loops, able to recognise target epitopes with high specificity. Thus, the $F(ab')_2$ determines the mAb's specificity and the Fc the mAb's isotype, through which effector mechanisms such as neutralisation, opsonisation and complement activation are facilitated.[10]

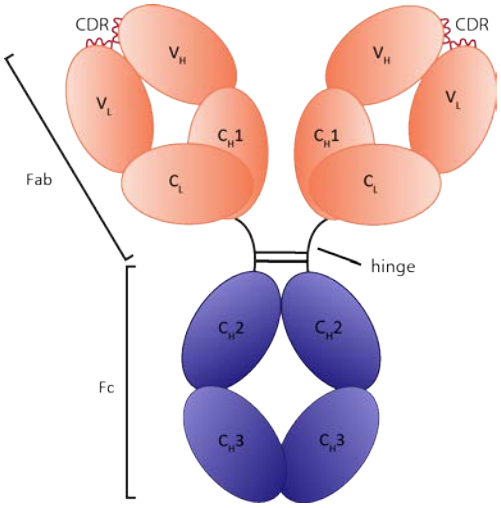

Figure 1.13| Schematic structure of a human IgG mAb. Human IgG mAbs are composed of two identical heavy chains (C_H1-3 + V_H) and two identical light chains (C_L+V_L), both linked together by disulphide bonds. The heavy and the light chains each, contain a variable domain, which builds the high specific CDRs. The mAb's isotype is defined by the heavy chains.

Current therapeutic mAbs are mostly IgG[137], however IgA[138] and IgE[139] mAbs are also under investigation. According to the serum level in the blood, IgG can be further divided into four subclasses, with IgG1 being the most abundant, followed by IgG2, IgG3 and IgG4.[140] The IgG subclasses share more than 90% homology. However, due to differences within the hinge region and N-terminal C_H2 domain, mAbs of different isotypes differ in their functionality and ability to bind to receptors and target molecules. hIgG1 mAbs possess a flexible hinge region; in comparison, the hinge region of hIgG2 mAbs is the shortest among all IgG subclasses. Moreover, hIgG2 is characterised by a rigid confirmation due to a poly-proline helix and inter-heavy chain disulphide bonds. hIgG3 contains the longest hinge region, which can be up to four times as long as the hinge region of hIgG1. Thus, due to the spatial distance of the Fab-arms to the Fc region, hIgG3 mAbs demonstrate high flexibility within the hinge region. The hinge structure of hIgG4 is similar to hIgG2 but its flexibility lies between a hIgG1 and hIgG2 hinge. (Figure 1.14).[141]

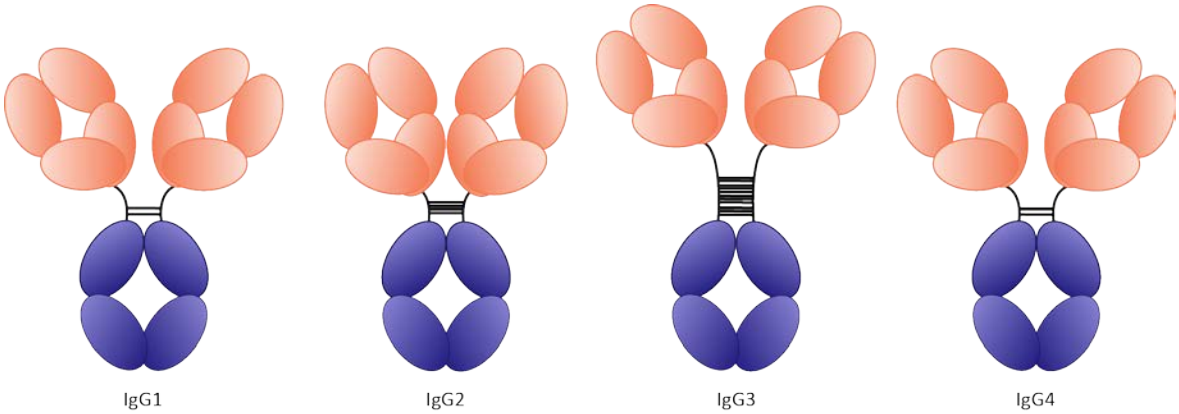

Figure 1.14| Schematic display of human IgG1-4 mAb structures. hIgG1 mAbs are characterised by a flexible hinge region, whereas hIgG2 displays a shorter hinge region and a more rigid conformation. hIgG3, in contrast, possesses the longest hinge region with high flexibility. The hinge region structure of hIgG4 is similar to hIgG2. However, its flexibility is between hIgG1 and hIgG2 (adapted from Vidarsson *et al.*[141]).

As mentioned previously, mAbs build humoral immunity and are able to bind target molecules with high specificity. Their effector functions, however, result from the interaction of the Fc-domain with Fc gamma receptors (FcγRs) expressed on innate immune cells. Thus, mAbs are an important linker of the adaptive and innate immune system.

FcγRs are type-1 transmembrane glycoproteins (except FcγRIIIB, which is attached to a glycosyl phosphatidyl inositol (GPI) anchor) and, as mAbs, belong to the IgSF. Human FcγRs (hFcγRs) can be divided into three classes: FcγRI, FcγRII and FcγRIII. FcγRII can be further divided into the isoforms A, B and C and FcγRIII into the isoforms A and B (Figure 1.15).[142] Some of the FcγRs are polymorphic; FcγRIIA exists either as FcγRIIA with a histidine ($FcγRIIA_{H131}$) or with an arginine at position 131 ($FcγRIIA_{R131}$)[143], FcγRIIIA has a polymorphism at residue 158 and can either be a phenylalanine ($FcγRIIIA_{F158}$) or a valine ($FcγRIIIA_{V158}$).[144] FcγRIIIB is also polymorphic. The two existing variants NA-1 and NA-2 differ in their amino acid sequence at four different positions.[145]

FcγRs possess an IgG-binding α-subunit, which for FcγRI and IIIA, is associated with a Fcγ-chain dimer. The α-domain itself is comprised of two (FcγRII/III) or, in the case of FcγRI, three extracellular Ig-domains, which serve as the binding site for Fc-domains of mAbs (Figure 1.15).

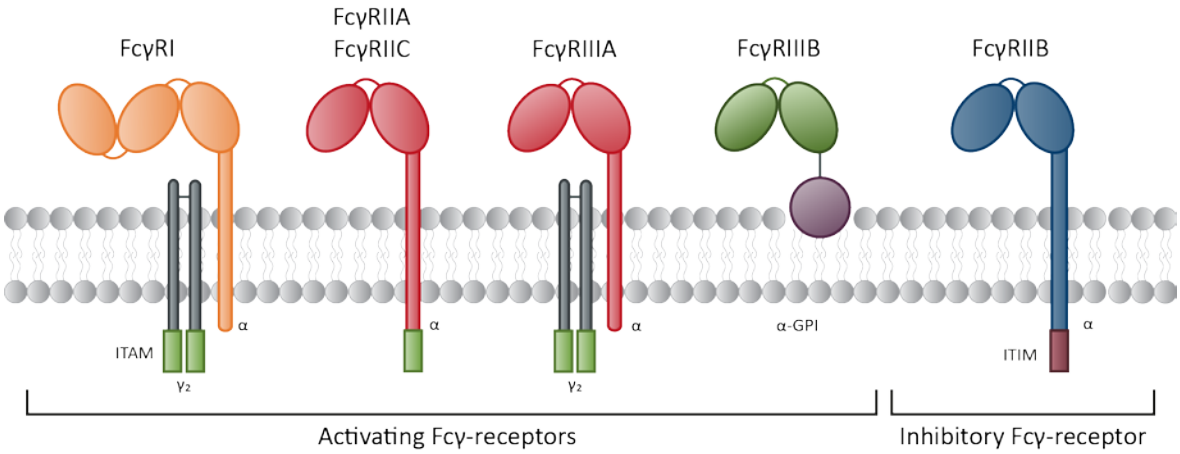

Figure 1.15| Schematic structure of human FcγRs. FcγRI is composed of three extracellular IgG domains, whereas FcγRII A/B/C and FcγRIIIA/B are composed of two extracellular IgG domains. Human FcγRs can be grouped into activating and inhibitory FcγRs. The activating receptors FcγRI, IIA, IIC and IIIA possess an ITAM, whereas FcγIIIB is incorporated into the membrane by a GPI-anchor. Furthermore, FcγRI and IIIA are associated with an Fcγ-chain dimer ($γ_2$). The inhibitory FcγRIIB in contrast is composed of an immunoreceptor tyrosine-based inhibition motif (ITIM).

Furthermore, FcγRs can be classified regarding their associated signalling domains. FcγRIIIB, exclusively expressed on neutrophils, is tethered via a GPI-anchor and does not possess a signal transduction subunit.[146,147] In contrast, FcγRI and IIIA contain a ligand-binding α-domain that associates with a signal-transducing Fcγ-chain dimer, possessing an ITAM in its intracellular domain. The FcγRIIA and IIC are not linked to an Fcγ-chain dimer. Instead, the ITAM motif is integrated into the α-subunit cytoplasmic tail (Figure 1.15).[146-148]

Activation of activating FcγRs by binding of mAb Fc-regions induces a complex signalling cascade, beginning with the phosphorylation of the ITAM and recruitment of SYK family kinases. Subsequent activation of downstream molecules such as LAT results in the production of PIP_3 through the PI3K, leading to the recruitment of Bruton's tyrosine kinase (BTK) and PLCγ and eventually to the increase of intracellular Ca^{2+} levels and further downstream signalling. In addition, the RAS-RAF-MAPK pathway plays a crucial role in cell activation upon FcγR crosslinking (reviewed in[149]). Depending on the FcγR-expressing cell type, different effector functions such as antibody-dependent cellular cytotoxicity (ADCC) or phagocytosis (ADCP) as well as the release of immunoregulatory molecules are triggered (Figure 1.16).

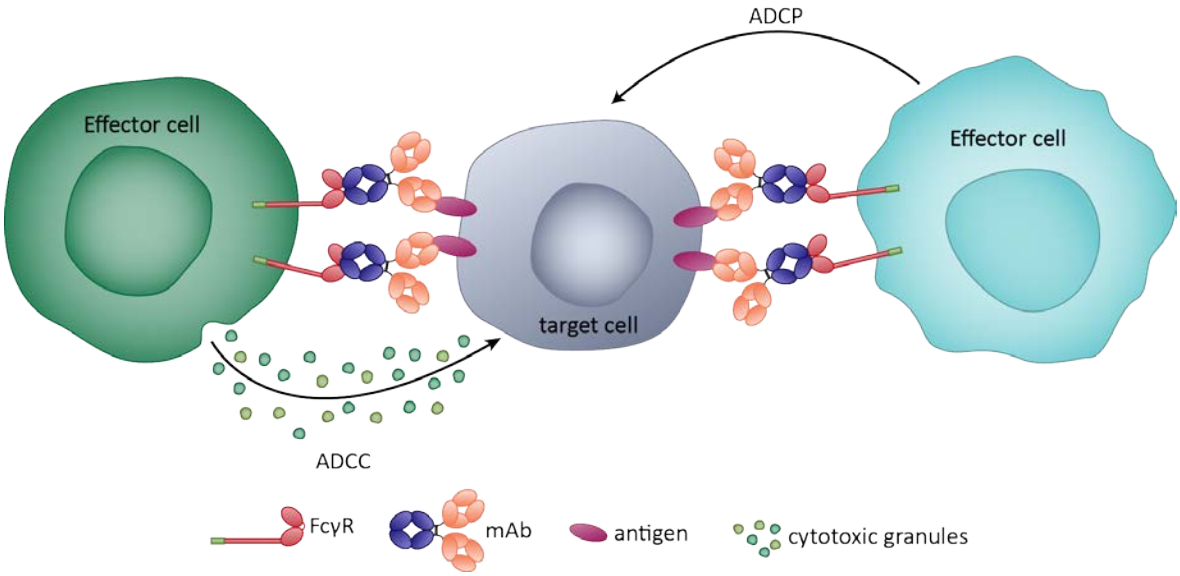

Figure 1.16| Fc-dependent mAb effector function. The binding of mAbs to their cognate target molecule and simultaneous engagement of activating FcγRs leads to the initiation of mAb effector functions. ADCC (mainly carried out by NK cells) results in the secretion of cytotoxic granules and the rapid lysis of the target cell. ADCP is mediated by professional APCs (such as macrophages). Upon FcγR activation, engulfment of the target cell and formation of the phagosome takes place. Once the phagosome has travelled inside the cell, it fuses with lysosomes (which contain cell digestive compounds), which eventually leads to the destruction of the target.

NK cells have been identified as the predominant immune cell subset to mediate ADCC in PBMCs. Beum *et al.* opsonised $CD20^+$ Daudi cells with rituximab and investigated ADCC by ^{51}Cr release assays and demonstrated that isolated NK cells, as well as PBMCs, were able to mediate ADCC. However, upon depletion of the NK cells from the PBMCs, ADCC was abrogated, indicating that NK cells play a crucial role in ADCC.[150] Clustering and activation of FcγRIIIA on NK cells results in the phosphorylation of ITAMs and induces signalling cascades (as previously described), eventually leading to intracellular Ca^{2+} increase and induction of the granule-exocytosis pathway. Secretion of cytotoxic granules containing perforin and granzymes evokes rapid lysis and death of target cells.[151]

ADCP is the other effector function mediated by the interaction of IgG-Fc with FcγRs. ADCP describes the engulfment of an opsonised target by professional phagocytes (such as

macrophages), mediated by the activation of their surface FcγRs. Macrophages express multiple FcγRs and it has been shown that the ratio of activating to inhibitory FcγRs on the cell surface is a crucial determinant for the efficacy of phagocytosis. Upon clustering and activation of FcγRs, phosphorylation of ITAMs takes place and phagocytic signalling pathways are initiated. However, this does not result in the mobilisation of intracellular Ca^{2+}, but instead the rearrangement of actin, leading to the formation of target-containing phagosomes. Once the phagosomes are in the cytoplasm, fusion with lysosomes takes place to form the phagolysosome. Due to the digestive enzymes contained in the lysosome, the fusion eventually leads to the degradation of the target. Macrophages additionally have the ability to present the processed peptides on their cell surface to trigger a T-cell mediated immune response. Furthermore, they are also able to secrete cytokines to help maintain ongoing immune responses.[152]

The FcγRIIb is the sole inhibitory FcγR and contains an immunoreceptor tyrosine-based inhibition motif (ITIM) in its cytoplasmic α-domain (Figure 1.15). Amongst other immune cells such as macrophages, it is predominantly expressed on B cells and plays a crucial role in the negative regulation of immune responses.[149] Concomitant, engagement of FcγRIIb with ITAM-containing receptors such as the BCR results in ITIM-phosphorylation followed by the recruitment of SRC-homology-2-domain-containing 5'-inositol phosphatase (SHIP) and SHIP-1. These phosphatases mediate the hydrolysis of PIP_3, thus leading to the inhibition of the recruitment of BTK and PCLγ and eventually Ca^{2+} release and proliferation.[149]

Further, FcγRs can be divided into high- and low-affinity receptors, according to their affinity to IgGs. Bruhns *et al*. have determined the binding and affinity of IgG isotypes to FcγRs by surface plasmon resonance (SPR) (Figure 1.17). The FcγRI is a high-affinity receptor for monomeric IgG1, IgG3 and IgG4, and the only FcγR containing a third extracellular Ig-domain. Thus, it is likely that this domain contributes to the enhanced affinity to IgG. However, studies suggest that IgG-Fc is not directly interacting with the third Ig domain and rather has a stabilising function.[153,154] Apart from FcγRIIIa, which binds to monomeric IgG3, the remaining low-affinity FcγRs are not able to bind monomeric IgG. Bruhns *et al*. also determined the binding of FcγRs to IgG immunocomplexes (IC) in a cell-based assay, where binding of FcγRs to aggregated IgG was generally stronger (strongest binding to IgG1 and IgG3 IC, weaker binding to IgG2 and IgG4 IC).[155]

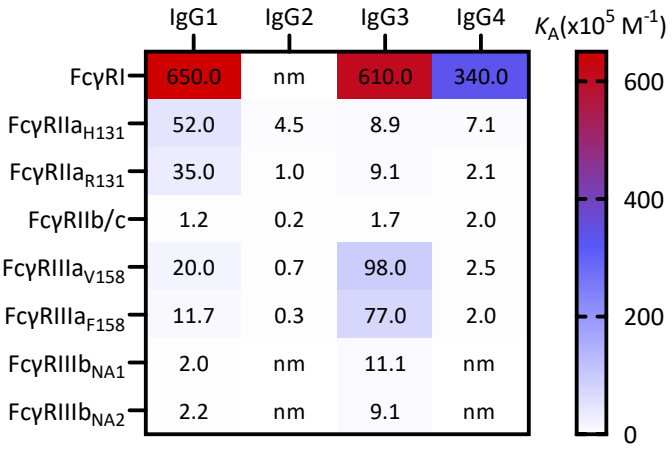

Figure 1.17| Binding affinities of human FcγRs to hIgG1-4. The Binding of hFcγRs to hIgG subclasses was determined by SPR. Red indicates high-affinity constants, whilst white indicates low-affinity constants. nm: not measurable (adapted from Bruhns *et al.*[155]).

The expression of FcγRs on adaptive and innate immune cells can be fairly broad or highly cell-specific, depending on the FcγR (Table 1.2). The majority of myeloid cells such as monocytes, macrophages, neutrophils and DCs express a combination of activating and inhibitory FcγRs. In contrast, NK cells only express the activating FcγRIIIa and B cells only express the inhibitory FcγRIIb on their cell surface.[149,156] FcγRIIIb can not only be found on neutrophils, but has also been detected on basophils.[157] The activating FcγRIIc can be expressed on NK cells and rarely on B cells, but only in individuals expressing the open reading frame (ORF) variant of FcγRIIc (7-15% of people).[158] The expression of FcγRs on T cells of the adaptive immune system remains controversial.[159]

Table 1.2| Distribution of human FcγRs on immune cell subsets. Myeloid cells express a combination of activating and inhibitory FcγRs, whereas B cells only express the inhibitory FcγRIIb and NK cells only express the activating FcγRIIIa. (+) indicates expression of FcγR in individuals with the according ORF. (Data adapted from Gillis *et al.*, 2014, Li *et al.*, 2013 and Nimmerjahn *et al.*, 2008[149,156,158])

	FcγRI (activating)	**FcγRIIa** (activating)	**FcγRIIb** (inhibitory)	**FcγRIIc** (activating)	**FcγRIIIa** (activating)	**FcγRIIIb** (activating)
B cells	-	-	+	(+)	-	-
T cells	-	-	-	-	-	-
NK cells	-	-	-	(+)	+	-
Monocytes	+	+	+	-	+	-
Macrophages	+	+	+	-	+	-
DCs	+	+	+	-	-	-
Neutrophils	+	+	-	-	-	+

To maintain immune homeostasis, a balance between the expression of activating and inhibitory receptors on immune cells is crucial. The negative regulatory FcγRIIb, increases the threshold for the activation of an immune response when co-expressed with activating FcγRs on myeloid cells.

The engagement of FcγRs is thereby dependent on the IgG subclass. The ability of a mAbs to bind to activating FcγRs relative to the inhibitory FcγRIIb also defines the activating to inhibitory (A:I) binding ratio, which is essential for the efficacy of therapeutic mAbs[160], as was shown for therapeutic mAbs that directly target tumour cells. It was demonstrated that human IgG1 (hIgG1; h1) or mouse IgG2a (mIgG2a; m2a) mAbs in particular have a high affinity to activating FcγRs relative to the inhibitory FcγR and therefore provide the required A:I ratio for appropriate therapeutic efficacy[160,161].

In contrast, the activity of immunostimulatory mAbs which bind to co-receptors on immune cells with the aim of stimulating them, is not mediated through the ligation of activating FcγRs. In this case, the mAbs require engagement of the inhibitory FcγRIIb. This facilitates crosslinking of the mAb's Fc and, in turn, clustering of target molecules such as members of the TNFRSF. As h1 mAbs have a high A:I ratio and therefore preferentially bind activating FcγRs, they only show weak therapeutic efficacy as immunostimulators.[162,163]

Consequently, Chu *et al.* generated mutations of h1 mAbs to specifically enhance their affinity to hFcγRIIb. Insertion of SE (S267E) and SE/LF (S267E/L328F) mutations into the Fc-domain of h1 mAbs led to a 30-fold and 430-fold enhanced binding affinity to hFcγRIIb, respectively.[164] Enhanced affinity of h1 SE and SE/LF mAbs has also been demonstrated for the CD40-targeting mAb CP-870,893 (SE: 30-fold and SE/LF: 70-fold, respectively).[165] *In vivo* administration of the hCD40 h1 SE and SE/LF mAbs to humanised CD40/FcγR mice resulted in increased cell activation (compared to WT h1 and hIgG2 (h2)) and reduced tumour growth. However, there is evidence that the h1 SE/LF mutant not only shows an enhanced affinity to the hFcγRIIb (Mimoto *et al.*:355-fold; Smith *et al.*: 166-fold), but also an increase in the affinity to the polymorphic $hFc\gamma RIIa_{R131}$ (Mimoto *et al.*: 864-fold; Smith *et al.*: 147-fold).[166,167] To circumvent this problem, Mimoto *et al.* engineered further h1 Fc-variants, to specifically enhance the binding affinity to hFcγRIIb only. The mAbs possessing the required features contained the following substitutions: G237D/P238D/P271G/A330R for the h1 V9-variant and G237D/P238D/H268D/P271G/A330R for the h1 V11-variant. Both of these Fc-engineered mAbs exhibited a 33-fold and 40-fold enhanced affinity to the hFcγRIIb but not to the hFcγRIIa.[166] Dahan *et al*. also developed, in addition to the SE and SE/LF variants of CP-870,893, h1 V9 and h1 V11 Fc-versions to specifically enhance the binding affinity to the hFcγRIIb only. SPR demonstrated a 32-fold (CP-870,893 h1 V9) and 97-fold (CP-870,893 h1 V11) increased binding affinity to hFcγRIIb. Furthermore, both mAb variants showed enhanced T-cell activating potential compared to the WT h1/h2 or SE/SE/LF anti-hCD40 mAbs *in vivo*. Regarding tumour clearance, administration of the anti-hCD40 h1 V11 mAb led to a reduction of metastasis in B16 melanoma bearing humanised CD40/FcγR mice (compared to the WT mAbs and the SE and SE/LF mutants).

Furthermore, in humanised CD40/FcγR mice injected with MC38, anti-hCD40 h1 V11 treatment resulted in complete tumour clearance.[165]

In contrast, h2 mAbs seem to mediate agonistic therapeutic efficacy independently of FcγR engagement, as was shown for anti-hCD40 mAbs.[163] This phenomenon may arise from the special conformational structure that h2 mAbs can form. It is reported that h2 mAbs are able to shuffle between two subclass configurations: "IgG2A" and "IgG2B".[168] IgG2A possesses four disulphide bonds linking the two heavy chains of the antibody and each light chain to its heavy chain. The IgG2B isoform in contrast is characterised by a different formation of disulphide bonds, linking the light chains of the Fab-arms directly to the hinge region. It is hypothesised that this conformational change gives the IgG2B mAb a more compact conformation and unique agonistic properties.[160,163,168,169] However, the studies described above were conducted in hCD40tg mice that still bear murine FcγRs.[163] Dahan *et al.* also investigated subclass-dependent therapeutic efficacies of anti-CD40 mAbs. In contrast to White *et al*., the mAb was administered in a mouse model transgenic for both hCD40 and hFcγRs. However, also in contrast to the above, they could not show the superior effect of the anti-hCD40 h2 and anti-hCD40 h2B mAbs over the h1 counterpart. Indeed, it was demonstrated that in this mouse model, engagement of hFcγRs is essential for the agonistic activity of the anti-hCD40 h2 mAbs.[165]

Dependent on the target expression, mAbs for cancer immunotherapy can be categorised into two subgroups: tumour targeting mAbs, which mediate direct cell destruction (section 1.5.1), and immunomodulatory mAbs, which include mAbs targeting co-inhibitory and co-stimulatory molecules (section 1.5.2)

1.5.1 Tumour targeting mAbs

Direct targeting antibodies bind directly to cancer cells and mediate their effector function either Fc-independently (complement-dependent cytotoxicity (CDC) or programmed cell death (PCD)) or via the recruitment of FcγR expressing immune cells, leading to the deletion of cancerous cells via ADCC or ADCP (Figure 1.18).[170] Moreover, mAb binding to tumour cells can also result in the inhibition of pathways leading to oncogenesis.[171]

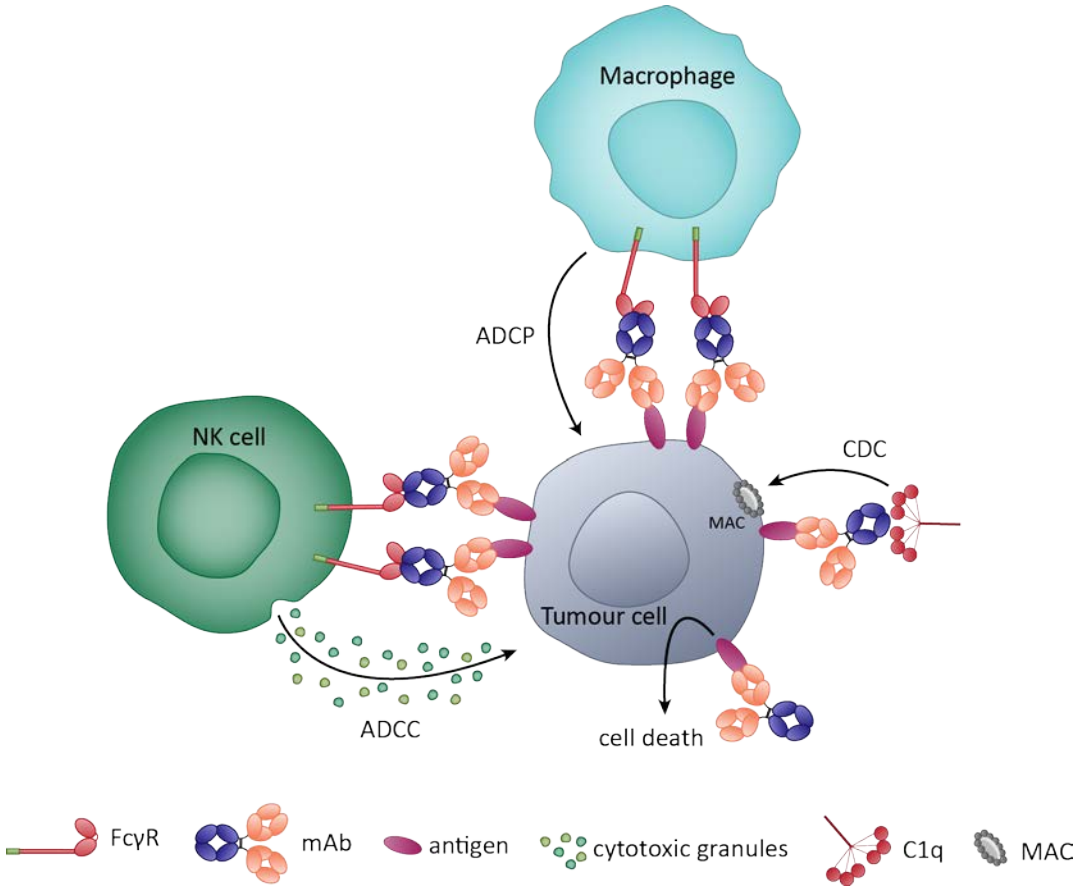

Figure 1.18| Effector functions of direct-targeting mAbs. Direct-targeting mAbs facilitate various effector functions. These included ADCC (mainly NK-cell mediated), ADCP (mediated by professional APCs), CDC (activation of the complement cascade by binding of C1q and formation of the membrane attack complex (MAC)) or tumour cell killing through the induction of PCD. All induced pathways eventually result in the killing of the target cell.

A prominent member of this tumour-targeting mAb family is rituximab, the first mAb approved by the FDA for cancer therapy in 1997. Today it is mainly used for the treatment of non-Hodgkin's lymphoma.[171] Rituximab targets CD20, which is expressed on normal B cells from the pre-B cell to the activated B-cell stage as well as on malignant B cells. Due to its broad expression on B-cell lymphomas, and absence from plasma cells and progenitor B cells , CD20 presents a viable target for anti-tumour mAbs, such as rituximab.[172] The mAb mediates its effector functions through Fc:FcγR interactions. It is also suggested that the antibody facilitates anti-tumour activity by CDC and induction of apoptosis (PCD). Whether or not CDC and PCD are mediated by anti-CD20 mAbs is still not fully clarified. However, it is clearly shown that binding of the rituximab to CD20 on malignant cells elicits direct tumour cell killing, which must occur through one or more of the described mechanisms.[173]

Another molecule targeted by tumour targeting mAb in cancer immunotherapy is CD38[174,175] The CD38 molecule functions as a receptor for CD31, and ligation results in the activation of signalling cascades beginning with phosphorylation and leading to an eventual increase of intracellular Ca^{2+} levels.[176] Besides its receptor function, CD38 also acts as a bi-functional ecto-enzyme with

adenosine diphosphate ribosyl (ADPR) cyclase and cyclic ADPR hydrolase activities. CD38 is broadly expressed on human immune cells; it can be found on thymocytes and T-cell subsets[177,178], and is also highly detectable on BM precursor cells and terminally differentiated plasma cells. Furthermore, its expression was detected on PBMC-derived monocytes[179], mature DCs[180], NK cells (residential and circulating)[181] and granulocytes[182]. CD38 can also be found on osteoclasts and osteoblasts[182] and non-immune tissues such as prostatic epithelial cells.[182]

Besides its expression on benign immune and non-immune cells, a high abundance of CD38 was also reported on malignant cells. High levels of CD38 were detected on patient-derived primary multiple myeloma (MM) cells and BM biopsies as well as on several human MM cell lines. [183] The high CD38 expression on MM cells prompted the development of direct targeting mAb against CD38 for the treatment of MM. Four anti-CD38 mAbs are currently under pre-clinical and clinical investigation and their characteristics, as well as therapeutic efficacies, are summarised in Table 1.3. Anti-CD38 mAbs show some anti-tumour properties as a monotherapy in clinical trials.[184]. However, their efficacy might be further improved by combining CD38-targeting with other reagents such as co-stimulatory mAbs (see Chapter 5).

Table 1.3| Anti-hCD38 direct targeting mAbs for the treatment of MM. The table lists the mAb format as well as their efficacy in pre-clinical and clinical trials. SCID: severe combined immune deficiency. ORR: overall response rate; CR: complete response; overall survival; PFS: progression-free survival; pt: patient.

CD38-targeting mAb	Isotype	Effector functions	Pre-clinical trial results	Clinical trial results
Daratumumab	human IgG1	CDC, ADCC, ADCP, PDC upon Fc-crosslinking[185-187]	inhibition of tumour development and full protection against tumour growth in Daudi-luc/UM9:SCID MM mouse models[185]	ORR: 32.1% (of 148 pts) CR: 4/148 pts PR: 13/148 pts median PFS: 4.0 month OS: 21.0 month[184,188,189]
Isatuximab (SAR650984)	humanised IgG1	CDC, ADCC, ACDP, PCD without Fc-crosslinking[190]	delayed tumour growth or tumour protection in lymphoma and MM xenograft mouse models[190]	CR: 11% (of 35 pts) PR: 22% (of 35 pts) OS: 33% (of 35 pts)[191]
MOR202	humanised IgG1	ADCC, ADCP[192,193]	improved median survival in Ramos xenograft mouse model reduction of bone lysis and serum monoclonal protein[192]	SD: 19% (of 31 pts; treated weakly SD: 75% (of 4 pts; treated every 2 weeks)[194]
Mezagitamab (TAK-079)	human IgG1	CDC, ADCC[195,196]	mAb tested in monkeys for pharmacokinetics and pharmaco-dynamics (data on anti-tumour performance not available)[197]	ORR: 33% (of 34 pts)[198]

1.5.2 Immunomodulatory mAbs

In contrast to direct targeting mAb, the employment of immunomodulatory mAbs aims to enhance immune effector functions in order to boost anti-tumour responses. This can either be achieved by evoking an anti-tumour response through the inhibition of negative signalling pathways or through the binding of co-stimulatory molecules.

1.5.2.1 Checkpoint inhibitory mAbs

One of the immunomodulatory mAbs that inhibits such a negative regulatory molecule is the checkpoint inhibitor ipilimumab, targeting CTLA-4. The negative regulatory function of CTLA-4 is based on its homology to the co-stimulatory molecule CD28 expressed on T cells. CD28 binds to CD80/86 on APCs and thereby provides the essential second signal for T-cell activation. CTLA-4 is upregulated upon T-cell activation and binds CD80/86 with a higher affinity than CD28. Mediating intrinsic and extrinsic effects, ligation of CTLA-4 with CD80/86 leads to cell cycle arrest and inhibition of T-cell proliferation and cytokine release by APCs.[30] Blocking this interaction with anti-CTLA-4 mAbs results in abrogation of the negative regulating signal and sustained T-cell activation[30,199] Furthermore, selective Treg depletion by CTLA-4 targeting mAbs was shown to substantially contribute to anti-tumour activity and this is now thought to be the prevailing mechanism of action of anti-CTLA-4 mAbs.[30,200] In clinical Phase III trials, ipilimumab, administered

either as a monotherapy or in combination with chemotherapy, demonstrated an improvement in overall survival in patients with unresectable, metastasised melanoma. [201,202]

Another checkpoint thatis targeted by immunotherapeutic mAbs is the PD-1/PD-L1 interaction.[31] Under inflammatory conditions, the interaction of PD-1 and PD-L1 normally attenuates the immune reaction of T cells to prevent autoimmunity and tissue destruction at the inflammatory site. However, Dong *et al.* demonstrated that PD-L1 is upregulated on various tumour types and that its interaction with PD-1 on tumour infiltrating T cells impairs their anti-cancer activity.[203] Hence, blockage of the PD-1/PD-L1 interaction is an attractive approach for cancer immunotherapy. Over the last decades, numerous PD-1 and PD-L1 mAbs have been invented, investigated in clinical trials, and subsequently approved by the FDA for the treatment of various cancers due to the promising clinical outcomes after treatment.[204] Furthermore, combination therapies of ipilimumab with PD-1 blocking mAbs such as nivolumab have been explored. This combination not only reduced the toxicity of the anti-CTLA-4 treatment but also induced a greater anti-tumour response in patients with metastatic melanoma [205].

1.5.2.2 Immunostimulatory mAbs

Alongside the aforementioned checkpoint-inhibitory mAbs, immunomodulatory mAbs are also employed in cancer immunotherapy. They are used to activate the patient's own immune system, and T cells in particular. The majority of these mAbs target molecules that are members of the IgSF or TNFRs, such as CD28, ICOS, OX40, GITR, 4-1BB or CD27 (Figure 1.7).

To date, a huge variety of mAbs targeting these molecules have been generated and are currently under pre-clinical and clinical investigation for the treatment of various solid and haematological cancers. Table 1.4 summarises the clinical trials of mAbs targeting T-cell co-stimulatory molecules, their T-cell modulating properties and clinical outcomes upon treatment.

Table 1.4| Summary of mAbs in clinical trials, targeting T-cell co-stimulatory molecules. "-": data not reported; "*":Fc-dysfunctional aglycosylated; "**": isotype unknown. mIgG1: mouse IgG1; GC: gastric cancer; TNBC: triple negative breast cancer; HNSCC: head and neck squamous cell carcinoma; RCC: renal cell carcinoma. pt: patient; CR: complete response; PR: partial response; SD: stable disease; PD: progressive disease; ORR: overall response rate; OS: overall survival; PFS: progression-free survival.

mAb/clinical trial identifier	Target	mAb format	Clinical trial phase	Indication	Evidence of T-cell agonism	Clinical efficacy	Ref
TAB08 (NCT03006029)	CD28	humanised IgG4	I (completed)	advanced solid malignancies	-	-	-
JTX-2011 (NCT02904226)	ICOS	humanised IgG1	I/II (completed)	advanced solid malignancies	- emergence of distinct blood peripheral $ICOS^{hi}$ $CD4^+$ T cells	- PR in heavily pre-treated GC (1/7 pts) - SD in heavily pre-treated TNBC (2/5 pts)	204,205
GSK3359609 (NCT02723955)	ICOS	humanised IgG4	I (active, not recruiting)	advanced solid malignancies	- increased numbers of intra-tumoural T cells, granzyme-B expressing $CD8^+$ T cells, PD-1 expressing T cells and proliferating T cells (patient with stage IIIc nodular melanoma)	-	206
KY1044 (NCT03829501)	ICOS	hIgG1	I/II (recruiting)	advanced malignancies	- reduction of intra-tumoural $ICOS^+$ Tregs - maintenance of intra-tumoural $CD8^+$ T cells - increased intra-tumoural Treg/$CD8^+$ ratio - T cell co-stimulation	- CR: 1/36 pts with TNBC - PR : 4/36 pts with TNBC, HNSCC, penile or pancreatic cancer	207,208
9B12 (NCT01644968)	OX40	mIgG1	I (completed)	advanced solid malignancies	- dose-dependent blood peripheral $Ki67^+CD4^+$ and $CD8^+$ memory T-cell proliferation - decreased intra-tumoural $OX40^+FoxP3^+$ T cells	- Tumour shrinkage in 12/30 pts, but no PR (>30% overall tumour shrinkage)	209
MEDI6469 (NCT02274155)	OX40	mIgG1	Ib (active)	neoadjuvant for locally advanced head and neck squamous cell carcinoma	- proliferation of blood peripheral and intra-tumoural $CD4^+$ and $CD8^+$ T cells - increase in anti-tumour reactive $CD8^+$ ($CD103^+$ $CD39^+$) T cells	- OS after 3 years: 82% (of 17 pts) - PFS after 3 years: 71% (of 17 pts)	210

PF-04518600 (NCT02315066)	OX40	hIgG2	I (completed)	advanced malignancies	- increase in blood peripheral $CD4^+$ T cell, $CD4^+$ T_{CM} and $CD8^+$ memory T cell proliferation
					- upregulation of activation markers
						- PR: 5.8 % (of 52 pts)
						- disease control: 56% (of 52 pts)
						  - SD: 26/52 pts
						  - PD: 19/52 pts
							211,212

Table 1.4| Summary of mAbs in clinical trials, targeting T-cell so-stimulatory molecules (continued). "-": data not reported; "*":Fc-dysfunctional aglycosylated; "**": isotype unknown. mIgG1: mouse IgG1; GC: gastric cancer; TNBC: triple negative breast cancer; HNSCC: head and neck squamous cell carcinoma; RCC: renal cell carcinoma. pt: patient; CR: complete response; PR: partial response; SD: stable disease; PD: progressive disease; ORR: overall response rate; OS: overall survival; PFS: progression-free survival.

mAb/clinical trial identifier	Target	mAb format	Clinical trial phase	Indication	Evidence of T-cell agonism	Clinical efficacy	Ref
MEDI0562 (NCT02318394)	OX40	humanised IgG1	I (completed)	advanced solid malignancies	- dose-dependent blood peripheral $Ki67^+CD4^+$ and $CD8^+$ memory T-cell proliferation - decreased intra-tumoural $OX40^+FoxP3^+$ T cells	- OS after 12 month: 47% - ORR: 4% (of 50 pts) with immune-related PR - SD: 44% (of 50 pts) - PD: 38% (of 50 pts)	215-217
MOXR0916 (NCT02219724)	OX40	humanised mIgG1	I (completed)	advanced solid malignancies	-	- SD: 16% (of 70 pts)	218
BMS-986178 (NCT02737475)	OX40	hIgG1	I/Ia (completed)	advanced solid malignancies	- Wang et al.: increase of proliferating T_{EM} - Gutierrez et al.: no effect on intra-tumoural $CD8^+$ T cells or Tregs	- no objective responses observed - SD: 35% (of 20 pts)	219,220
INCAGN01949 (NCT02923349)	OX40	hIgG1	I/II (completed)	advanced solid tumours	- increase of stromal T-cell infiltrates in on-treatment biopsies in one patient	- Pt 1: initial SD with subsequent PD - Pt 2: PD	221
GSK3174998 (NCT02528357)	OX40	humanised IgG1	I (completed)	advanced solid malignancies	- possible increase of intra-tumoural NK cells and reduction of intra-tumoural Tregs	- PR: 1/45 pts - SD: 1/45 pts	222
GWN323 (NCT02740270)	GITR	humanised IgG1	I/Ib (completed)	advanced solid malignancies	- transient increase in blood peripheral proliferating NK cells, $CD8^+$ T cells and $CD8^+$ T_{EM} during treatment - in some patients: decrease of peripheral effector Treg during treatment	- No CR or PR - SD: 17% (7/39 pts) - PD: 66.7% (26/39 pts)	223
TRX-518 (NCT02628574)	GITR	humanised IgG1*	I (completed)	advanced solid malignancies	- reduction of blood peripheral and intra-tumoural Treg	- SD: 9.3% (4/43 pts) - PD: 67.4% (29/43 pts)	224
MK-4166 (NCT02132754)	GITR	humanised IgG1	I (completed)	advanced solid malignancies	-	- SD: 22.9% (of 48 pts) - PD: 64.6% (of 48 pts)	225

Table 1.4| Summary of m mAbs in clinical trials, targeting T-cell so-stimulatory molecules (continued). "-": data not reported; "*":Fc-dysfunctional aglycosylated; "**": isotype unknown. mIgG1: mouse IgG1; GC: gastric cancer; TNBC: triple negative breast cancer; HNSCC: head and neck squamous cell carcinoma; RCC: renal cell carcinoma. pt: patient; CR: complete response; PR: partial response; SD: stable disease; PD: progressive disease; ORR: overall response rate; OS: overall survival; PFS: progression-free survival.

mAb/clinical trial identifier	Target	mAb format	Clinical trial phase	Indication	Evidence of T-cell agonism	Clinical efficacy	Ref
MK-1248 (NCT02553499)	GITR	humanised IgG4	I (completed)	advanced solid malignancies	- increase of intra-tumoural $CD3^+$, $CD8^+$ and $FoxP3^+$ T cells (in pts with SD compared to pts with PD)	- SD: 15% (3/20 pts) - reduction of target lesion size in 3 pts	226
AMG228 (NCT02437916)	GITR	hIgG1	I (completed)	advanced solid malignancies	- no evidence of T-cell activation	- SD: 23% (7/30 pts) - PD: 57% (17/30 pts)	227
BMS-986156 (NCT02598960)	GITR	hIgG1	I/IIa (completed)	advanced solid malignancies	- trend towards increase in NK-cell and $CD8^+$ T-cell proliferation	- No CR or PR observed.	228
ADG106 (NCT03707093)	4-1BB	hIgG4	I (active, not recruiting)	advanced malignancies and Non-Hodgkin lymphoma	- increase in secretion of IFN-γ and IL-6 - increase of blood peripheral NK-cell and T-cell subsets and proliferating $CD8^+$ T cells and T_{EM}	- SD: 60% (12/20 pts) with tumour shrinkage	229-231
ATOR-1017 (NCT04121676)	4-1BB	hIgG4	I (recruiting)	advanced cancer	- increase of blood peripheral activated $CD8^+$ T cells and $CD8^+$ T_{EM} and $ICOS^+CD8^+$ T cells	- SD: 23% (3/13 pts) - PD: 38.5% (5/13 pts)	232
PF-05082566 (NCT01307267)	4-1BB	humanised IgG2	I (completed)	advanced cancer	- increase in blood peripheral T-cell and NK-cell populations	- PFS: 1.7 month for pts with solid tumours - median OS: 11.2 month	233
BMS-663513 (NCT00309023)	4-1BB	hIgG4	I/II (terminated)	advanced cancer	- increase of blood peripheral activated ($HLA\text{-}DR^+$, $CD69^+$) $CD8^+$ and $CD4^+$ T cells - increased expression of CD8 and IFN-γ in post-treatment biopsies	- PR: 3.6% (3/83 pts) - SD: 4.8% (4/83 pts)	234
YH004 (NCT05040932)	4-1BB	humanised IgG1	I (recruiting)	advanced solid malignancies and relapsed/ refractory Non-Hodgkin lymphoma	-	-	-

Table 1.4| Summary of mAbs in clinical trials, targeting T-cell so-stimulatory molecules (continued). "-": data not reported; "*":Fc-dysfunctional aglycosylated; "**": isotype unknown. mIgG1: mouse IgG1; GC: gastric cancer; TNBC: triple negative breast cancer; HNSCC: head and neck squamous cell carcinoma; RCC: renal cell carcinoma. pt: patient; CR: complete response; PR: partial response; SD: stable disease; PD: progressive disease; ORR: overall response rate; OS: overall survival; PFS: progression-free survival.

mAb/clinical trial identifier	Target	mAb format	Clinical trial phase	Indication	Evidence of T-cell agonism	Clinical efficacy	Ref
(AGEN2373 (NCT04121676)	4-1BB	hIgG1	I (recruiting)	advanced solid malignancies	-	- best response: prolonged disease stabilisation in 26.3% (5/19 pts)	235
EU101 (NCT04903873)	4-1BB	human**	I/II (recruiting)	advanced solid malignancies	-	-	-
CDX-1127 (NCT01460134)	CD27	hgG1	I (completed)	haematologic or solid malignancies	Haematological malignancies: - increase of serum levels of soluble CD27 - increased secretion of pro-inflammatory cytokines and chemokines (CXCL9, IL-12, CCL4, CCL2) - no consistent changes in $CD4^+$ and $CD8^+$ T cell numbers, but decrease in $CD4^+$ Tregs in some patients Solid tumours: - increase of serum levels of soluble CD27 - increased secretion of pro-inflammatory cytokines and chemokines (predominantly CXCL10) - decrease of $CD4^+$ Treg, but no effect on $CD8^+$ T-cell or B-cell numbers in the periphery - increase of blood peripheral NK cells with cytotoxic phenotype (in some patients)	Haematological malignancies: - Hodgkin lymphoma: 1/10 pts with CR and 1/10 pts with SD, 8/10 pts with PD - Non-Hodgkin B-cell lymphoma: 3/18 pts with SD, 15/18 pts with PD - Non-Hodgkin T-cell lymphoma: 1/5 pts with SD, 4/5 pts with PD Solid tumours: - 1/56 pts: PR with durable and significant tumour regression (pt with RCC) - 1/56 pts: SD with initial tumour shrinkage (pt with RCC) - 8/56 pts (with RCC, melanoma, colorectal adenocarcinoma) with SD	236,237
MK-5890 (NCT03396445)	CD27	humanised IgG1	I (recruiting)	advanced solid malignancies	-	- PR: 4% (1/25 pts)	238

1.5.3 Anti-CD27 mAbs under pre-clinical and clinical investigation

Several studies have examined the therapeutic efficacy of anti-CD27 mAb monotherapy *in vivo*. CD27 as a possible target for immunotherapy was first described by French *et al*., where the application of agonistic anti-CD27 mAb in BCL_1-tumour bearing mice resulted in complete protection against the tumour.[32] Additionally, the anti-tumour efficacy was confirmed in further murine tumour models. Administration of an anti-CD27 mAb (AT124-1) to C57Bl/6 mice injected with B16 melanoma cells led to the reduction of lung metastasis and subcutaneous tumour volume[239]. Furthermore, AT124-1 demonstrated and anti-tumour efficacy in the EG.7 thymoma tumour model[240]. The main cell population mediating the anti-tumour effect was identified to be intra-tumoural $CD8^+$ T cells. In addition, suppression of intra-tumoural $CD4^+FoxP3^+$ T cells was detected and the anti-tumour effect also seemed to be dependent on NK cells.[239] Vitale *et al*. tested the anti-tumour efficacy of 1F5, a fully human anti-CD27 mAb (not cross-reactive with mCD27), in a xenograft mouse model. Administration of this mAb resulted in delayed tumour growth after Raji cell injection and improved survival in mice bearing Raji or Daudi cells. Since 1F5 is not cross-reactive with mCD27, the authors suggest that the tumour reduction could only be achieved through mAb effector mechanisms, such as ADCC. These data indicate that 1F5 may not only display immunostimulatory properties but also facilitate direct anti-tumour effects against $CD27^+$ malignancies.[96] The anti-tumour activity of 1F5 was further demonstrated hCD27tg BALB/c mice. BCL_1-bearing hCD27tg BALB/c mice showed prolonged survival, which was also seen in solid tumour models such as CT26 and EG7. In the solid tumour models, tumour regression was detectable and anti-tumour activity was crucially dependent on $CD4^+$ and $CD8^+$ T cells and the formation of a long-lived memory response. Moreover, it was demonstrated that the activity of 1F5 is only facilitated upon Fc:FcγR interaction.[241] Follow up studies compared 1F5 as different mAb formats, namely 1F5 mouse IgG1 (mIgG1, m1) and 1F5 m2a, and compared their therapeutic efficacy in the BCL_1 lymphoma and solid tumour models. m1 mAb bind FcγRIIb with high affinity, whereas m2a mAb preferentially engage with activating FcγRs.[33] Therefore, in BCL_1, which highly expresses mFcγRIIb, 1F5 m1 but not m2a induced substantially prolonged survival. However, the high co-stimulatory activity was accompanied by terminal differentiation, T-cell exhaustion and eventual apoptosis. On the contrary, in solid tumours, 1F5 m2a but not m1 induced prolonged survival alongside tumour regression. Anti-tumour activity was thereby not only mediated through co-stimulatory effects but also through depletion of suppressive Tregs. Together, these studies indicate that targeting CD27 can elicit potent anti-tumour activity and that this activity can be modulated for therapeutic benefit.[242]

Turaj *et al*. combined an immunostimulatory mAb targeting CD27 with the direct tumour-targeting CD20 mAb in order to provide an enhanced anti-tumour effect.[243] Using various B cell lymphoma mouse models, significant therapeutic effects of the combination therapy were demonstrated; notably tumour depletion and cure of all mice treated with the anti-CD20/CD27 mAb combination, whereas treatment with anti-CD20 mAb alone did not show such anti-tumour efficacy. These results clearly indicate the capability of the anti-CD27mAbs to enhance the anti-tumour properties of the anti-CD20-targeting mAb. Turaj *et al*. further investigated the expression of CD27 on the respective tumour cells and noted that CD27 was not detectable. This suggests that the anti-CD27 mAb in this setting is not effective as a direct targeting mAb. Indeed, the anti-tumour effect was mediated by anti-CD27 mAb activated T cells, NK cells, and the subsequent recruitment and activation of myeloid effector cells.[243] In addition to the *in vivo* investigation, anti-CD27 mAb was also examined *in vitro*. Stimulation of human PBMCs with the mAb led to an increase in the percentage of monocytes and their viability in culture, which was accompanied by a downregulation of CD14. As monocytes, in contrast to T cells, in PBMCs cultures do not express CD27, the presumption is that CD14 downregulation occurs as an indirect effect downstream of the T cell stimulation by the hCD27 mAb.[243] However, the underlying mechanism and consequence of the CD14 downregulation on monocytes upon anti-CD27 mAb stimulation of PBMCs has not yet been clarified.

Research has also been undertaken to combine the immunostimulatory function of anti-CD27 mAb with the blocking function of anti-PD-L1 mAb in one bispecific mAb (BsAb) to enhance T-cell activity. The BsAb CDX-527 comprises h1 PD-L1 mAb 9H9, which binds to human and macaque PD-L1 but not rodent PD-L1, and the scFv of the CD27 mAb 2B3 linked in V_L-V_H orientation to the C-terminus of 9H9. *In vitro* studies of CDX-527 in a T-cell activation assay demonstrated increased IL-2 and IFN-γ production and T-cell proliferation compared to 2B3 alone, indicating enhanced T-cell activation after treatment. However, the assay also revealed that TCR-engagement and receptor cross-linking are crucial for CDX-527 mediated T-cell stimulation. Since CDX-527 contains the anti-PD-L1 h1 mAb, it is able to engage activating FcγRs via its Fc region and experiments confirmed the mediation of ADCC against cell lines and tumour cell lines transfected with PD-L1 or CD27. Subsequent *in vivo* experiments in hCD27tg mice demonstrated enhanced IFN-γ production of OVA-specific T cells after stimulation with AVEx2B3 (PD-L1 mAb cross-reacting with mouse PD-L1) or a combination of avelumab (AVE, anti-PD-L1) and 2B3 compared to single mAb treatments, implying an enhanced antigen-specific T-cell response. Furthermore, the administration of the BsAb in BCL_1-bearing mice led to long-term survival. Assessment of ADCC against CD27 expressing Raji cells in severe combined immune deficiency (SCID) mice revealed no benefit in the addition of anti-PD-L1 to CD27 mAb. CDX-527 was also assessed in a preliminary non-human primate study to investigate safety

and pharmacokinetics. Body weight, temperature, and clinical as well as haematological parameters remained unchanged after BsAb administration.[244]

Based on the *in vitro* and *in vivo* studies detailed above, various clinical trials have been initiated to test CD27 mAbs as a monotherapy or in combination with other therapeutic mAbs. In a phase I clinical trial, monotherapy with the CD27 mAb varlilumab (varli) has demonstrated potential anti-tumour efficacy and safety in patients with solid tumours. Treatment with varli achieved stable disease for > 3 months in eight out of sixty-five patients (four with renal cell carcinoma (RCC), three with melanoma, one with colorectal adenocarcinoma) including one patient with metastatic RCC demonstrating a progression-free survival > 3.9 years. Another patient suffering from metastatic RCC not only showed progression-free survival > 2.3 years but also demonstrated a tumour shrinkage of 78%.[237] In addition to the anti-CD27 monotherapy, varli was also tested in combination with the PD-L1-inhibitor nivolumab. In a phase I/II clinical trial including patients with CRC, ovarian cancer [245] and recurrent glioblastoma[246] the safety profile and efficacy of the combination treatment were assessed (NCT02335918). The combination therapy was well tolerated and there was no evidence of additive toxicities. Anti-CD27/PD-L1 mAb combination treatment of patients with CRC or ovarian cancer led to a partial response (PR) in 5% or 10% of the patients, respectively. Of those, 39% of the ovarian cancer patients and 17% of the CRC patients showed stable disease. On-treatment tumour biopsies showed increased levels of PD-L1 expression on $CD8^+$ T cells of patients with ovarian cancer. Elevated PD-L1 levels were most common in patients with better disease outcomes. In contrast, $CD8^+$ T cells of patients with CRC did not consistently display this expression pattern.[245] For patients suffering from recurrent glioblastoma, combination treatment led to a 12-month overall survival of 38.5% and a median overall survival of 9.7 months. Of the treated patients, 9% demonstrated a PR, and 9 out of 22 patients enrolled showed stable disease.[246]

Varli therapy has not only been investigated in combination with PD-1 and PD-L1 targeting mAbs. Based on the results from Turaj *et al.*[243], a phase IIa clinical study has been initiated and is currently ongoing to evaluate the combination therapy of varli with the CD20-targeting mAb rituximab in patients with relapsed or refractory B cell malignancies (RiVa-study; NCT03307746[247]).

Recently, another CD27-targeting mAb (MK-5890) has entered clinical trials.[238] MK-5890 is a humanised agonistic mAb that enhances T-cell immune responses. It is currently being tested as a monotherapy and in combination with the PD-1 targeting mAb pembrolizumab for safety and efficacy in a phase I clinical trial for patients with solid tumours (NCT03396445). Out of 44 patients recruited, one patient receiving MK-5890 alone and one patient receiving the combination therapy showed a PR. Common related adverse events with MK-8590 were fatigue and infusion-related reaction and in the combination treatment arm fatigue and pruritus. To date, the therapy with

MK-5890 alone or in combination with pembrolizumab has shown an acceptable safety and efficacy profile.[238] A phase II clinical trial has been announced aiming to investigate the efficacy of the combination of MK-5890 with pembrolizumab in patients with advanced squamous or non-squamous non-small cell lung cancer.[248]

Furthermore, a phase I clinical trial including the aforementioned BsAb CDX-527 has been initiated and is currently recruiting patients suffering from advanced malignancies to assess the safety, tolerability and activity of the therapy (NCT04440943). To date, CDX-527 therapy has been well tolerated with the most common adverse events being influenza-like illness, fatigue and arthralgia.[249]

1.6 Hypothesis and aims

As detailed above, targeting CD27 demonstrates anti-tumour activity in pre-clinical models. However, the clinical efficacy of the FDA approved anti-CD27 mAb varli has been modest and its agonistic activity remains uncertain. Identifying the key features that govern anti-CD27 mAb agonism might lead to the development of more effective clinical reagents.

In order to do so, novel anti-hCD27 mAbs, in addition to varli, were generated and the following objectives were set:

1. Characterisation of anti-hCD27 mAb binding *in vitro*, to understand the influence of epitope specificity on the agonistic activity of immunostimulatory anti-hCD27 mAb
    - Determination of binding and affinity as well as identification of specific epitopes for each anti-hCD27 mAb.
    - Identification of specific epitopes for each anti-hCD27 mAb
2. Characterisation of the anti-hCD27 mAbs regarding their functional properties *in vitro* using immunological assays (such as NF-κB/green fluorescent protein (GFP) reporter assays, T-cell proliferation assays) to understand the significance of the mAb's isotype on its agonistic activity.
3. Identification of the best hCD27-targeting candidate for further assessment *in vivo*.

Turaj *et al.* have previously demonstrated that an agonistic anti-CD27 mAb is able to improve therapeutic efficacy of a tumour-targeting anti-CD20 mAb.[243] Therefore, it was hypothesised that anti-CD27 mAbs can also augment the therapeutic efficacy of other direct tumour targeting mAbs such daratumumab (anti-hCD38 mAb).

In order to test this hypothesis, the following objectives were set:

1. Establishment of appropriate mouse models bearing hCD38 transfected A20 tumours or NSG mice injected with human PBMCs and human Daudi lymphoma cells.
2. Investigation of hCD27 monotherapy followed by assessment of hCD27/hCD38 combination therapy to assess modes of action and effects on effector cell populations.

Lastly, the mechanism underlying the bystander effects of the anti-hCD27 mAb treatment in PBMCs cultures, reported by Turaj *et al*. should be deciphered.[243]

Chapter 2 Methods

2.1 Animals

Balb/c mice, hCD27tg BALB/c mice, hCD27tg C57/BL6 mice[241] and NOD.*Cg-Prkdc*^{scid}*Il2rg*^{tm1Wjl}*/SzJ mice* (NSG mice) were bred in local facilities (all mice were originally sourced from Charles River). Mice had water freely and were fed regular chow. For experiments mice were age- and sex-matched, randomly assigned into treatment groups and housed under the same experimental conditions. All experiments were performed in accordance with UK Home Office Regulations. Procedures carried out were approved by the local ethics committee (ERGO: 64937 or 65400), and performed in accordance with the Animals (Scientific Procedures) Act 1986, as set out in the Procedure Project Licences: P81E129B7 and P4D9C89EA. Any work using tissue from animals was ethically approved by the local ethics committee (ERGO: 67204).

2.2 Cell lines

2.2.1 Generation of stably transfected cell lines

Throughout this project, a variety of cell lines were employed. These included hCD27 WT, hCD27 R214STOP, hCD27/GFP (for construct sequences see Appendix B.1) and hCD27 transfected NF-κB/Jurkat/GFP Jurkat cells (hCD27 NF-κB/GFP Jurkat). hCD27 NF-κB/GFP Jurkat cells express hCD27 and bear a GFP-gene under the control of a minimal cytomegalovirus (mCMV)-NF-κB (Figure 2.1[250]) (generated by System Biosciences (2007) and Antibody and Vaccine Group (AVG) Southampton). Activation of the NF-κB pathway leads to GFP reporter gene expression, which can be detected using flow cytometry. In addition, hCD38 transfected A20 cells (hCD38 A20) were generated (sequence displayed in Appendix C.1). All cell lines listed above were generated using transfection methods, such as lipofection or nucleofection, as described in sections 2.2.1.1 and 2.2.1.2.

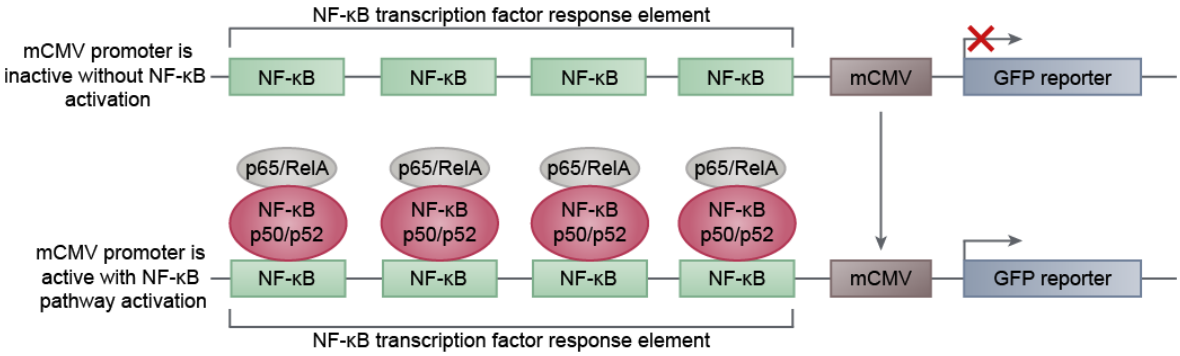

Figure 2.1| NF-κB/GFP reporter assay. Human T lymphocyte-derived Jurkat cells were transduced with an expression vector containing a GFP reporter gene and a mCMV promoter with an upstream NF-κB transcription factor response element. Binding of the NF-κB complex, consisting of p65 (RelA) and p50 (NF-κB1) or p52 (NF-κB2), resulting from the interaction of hCD27 on hCD27/NF-κB Jurkat cells with anti-hCD27 mAbs[250] leads to activation of the NF-κB transcription factor response element. Following this, the mCMV promoter becomes activated and the GFP-reporter gene is transcribed and translated, inducing GFP expression, which can be detected by flow cytometry (adapted from[250]).

2.2.1.1 Lipofection

One day prior to the lipofection, cells were plated in a 24-well plate at a concentration of $2x10^5$ cells/ml in 500 µl of antibiotic-free growth Roswell Park Memorial Institute (RPMI) 1640 medium supplemented with 10% foetal calf serum (FCS; Sigma Aldrich), 2 mM L-glutamine (Life Technologies), 1 mM pyruvate (Life Technologies) at 37°C and 5% CO_2 atmosphere in a humidified incubator. On the day of transfection, cells were diluted to $4x10^5$ cells/ml with antibiotic-free supplemented RPMI. 1 µg plasmid DNA and 2 µl lipofectamine 2000 (Invitrogen) were diluted in 50 µl Opti-MEM (Invitrogen), respectively. After 5 minutes incubation at room temperature (RT), the diluted plasmid DNA was added to diluted Lipofectamine 2000 reagent, gently inverted and incubated for 20 minutes at RT. Following this, the lipofectamine-DNA mixture was added to the cells and incubated for 72 hours at 37°C and 5% CO_2 atmosphere in a humidified incubator. Six wells (of a six-well plate) of cells transfected with each DNA construct were pooled, counted and seeded into a flat-bottom 96-well plate at either 5000 or 10,000 cells per well in RPMI medium supplemented with 10% FCS, 2 mM L-glutamine, 1 mM pyruvate and 100 U/ml penicillin/100 µg/ml-streptomycin (Life Technologies (complete RPMI (cRPMI) medium)) and the according selection reagent was added (see 2.2.2). Cells were incubated for approximately 3 weeks until cell colonies became visible. For cells undergoing geneticin (Invitrogen) selection, the medium containing selection reagent was replaced twice a week.

2.2.1.2 Nucleofection

Nucleofection was performed using the Amaxa Cell line Nucleofector Kit V (Lonza) and conducted according to the manufacturer's protocol. In brief, cells were seeded to the required concentration prior to the transfection (Jurkat cells: $0.2x10^6$ cells/ml 3 days before nucleofection, A20 cells: $1.5x10^6$ cells/ml one before nucleofection). On the day of nucleofection cells (Jurkat cells: $1x10^6$

cells, A20 cells: $2x10^6$ cells) were centrifuged at RT for 10 minutes at 90 g. After complete removal of the supernatant, cells were resuspended in 100 µl prepared nucleofection solution (82 µl nucleofector solution + 18 µl supplement provided with the kit) and 2 µg of plasmid DNA was added. The DNA/cell/nucleofection mix was then transferred into a cuvette and nucleofection was performed on an Amaxa nucleofector device II, using the program recommended for the respective cell line (Jurkat cells: X-001, A20 cells: L-013). Following this, cells were either rested in the cuvette for 10 minutes (Jurkat cells) or directly transferred (A20 cells) into a 12-well plate to 500 µl pre-warmed cRPMI medium and incubated for 48 hours at 37°C and 5% CO_2 atmosphere in a humidified incubator. Cells were then seeded into a flat-bottom 96-well plate in a final volume of 200 µl cRPMI medium containing the according selection reagent (see 2.2.2). Cells were incubated for approximately 3 weeks until cell colonies became visible. Cultures containing geneticin as a selection reagent were fed twice a week to exchange the selection medium.

2.2.2 Maintenance of cell lines

Cell lines were maintained as outlined in Table 2.1. All cell lines, except 293F cells, were cultured in cRPMI medium. Where required, selective antibiotics such as puromycin (InvivoGen) or geneticin (Life Technologies) were added. Cell passaging was performed every second day. For adherent cell lines, trypsin/ethylenediaminetetraacetic acid (EDTA) (Sigma) was added prior to the cell passage to detach the cells from the culture flask and cell density was kept below 95% confluency.

Table 2.1 | Culture conditions for cell lines. Cells lines were suspension cells and kept and 5% CO_2 atmosphere unless stated otherwise under "Additional information". CHO: Chinese hamster ovarian.

Cell line	Media	Supplements	Cell density [cells/ml]/ split ratio	Additional information
A20[251] (ATCC TIB-208)	RPMI	10% FCS L-glutamine pyruvate penicillin/streptomycin	1-2x10^6	-
hCD38 A20 (parental A20 cells from ATCC, transfected in-house)	RPMI	10% FCS L-glutamine pyruvate penicillin/streptomycin	1-2x10^6	2.5 µg/ml puromycin
CHO-K1 (ATCC CCL-61)	RPMI	5% FCS L-glutamine pyruvate penicillin/streptomycin	1:8	adherent

CHO-K1 FcγRIIb[252]	RPMI	10% FCS L-glutamine pyruvate penicillin/streptomycin	1:8	adherent, + 1 mg/ml geneticin
parental Jurkat (ATCC TIB-152)	RPMI	10% FCS L-glutamine pyruvate penicillin/streptomycin	0.7-2x10^6	-
hCD27 Jurkat (parental Jurkat cells from ATCC, transfected in-house)	RPMI	10% FCS L-glutamine pyruvate penicillin/streptomycin	0.7-2x10^6	+ 0.5 µg/ml puromycin
hCD27 R214 STOP (parental Jurkat cells from ATCC, transfected in-house)	RPMI	10% FCS L-glutamine pyruvate penicillin/streptomycin	0.7-2x10^6	+ 0.5 µg/ml puromycin
hCD27/GFP Jurkat (parental Jurkat cells from ATCC, transfected in-house)	RPMI	10% FCS L-glutamine pyruvate penicillin/streptomycin	0.7-2x10^6	+ 0.5 µg/ml puromycin
hCD27 NFKB/GFP Jurkat [250], transfected in-house)	RPMI	10% FCS L-glutamine pyruvate penicillin/streptomycin	0.7-2x10^6	+ 5 µg/ml puromycin
Daudi[253] (ATCC CCL-213)	RPMI	10% FCS L-glutamine pyruvate penicillin/streptomycin	0.5-1.5x10^6	-
293F (ThermoFisher Scientific)	Freestyle 293F	-	0.3-2x10^6	shaking incubator (125 rpm), 8% CO_2

2.3 Cell quantification

A range of cell quantification methods was utilised:

1. Beckman Coulter: Cells were diluted 1:500 in 10 ml isotone (Beckman Coulter Life Sciences) and measured with a Coulter Particle counter Z1 (Beckman Coulter Life Sciences). For samples containing erythrocytes, such as PBMCs, cells were diluted 1:500 in 10 ml isotone and three drops of Zap-Oglobin (Beckman Coulter Life Sciences) were added to lyse red blood cells before counting.
2. CellDrop (DeNovix, Cambridge Bioscience): Cells were diluted 1:1 with CellDrop Acridine Orange/Propidium Iodide (PI) viability dye (DeNovix, Cambridge Bioscience). Acridine Orange as a membrane-permeable nucleic acid-binding fluorophore indicates live cells. PI also binds nucleic acids but is not membrane permeable and hence indicates dead cells.[254] Cell numbers were quantified according to the manufacturer's instructions.
3. Haemocytometer: Cells were diluted 1:1 with trypan blue solution (0.4%, Gibco) to determine cell numbers and viability. Trypan blue stains permeable cells such as non-viable cells blue and is not taken up by viable cells.

2.4 Cryopreservation and recovery of cells

For cryopreservation, cells were resuspended in FCS containing 10% dimethylsulfoxide (DMSO) at desired cell concentrations and promptly transferred to -80°C. After a maximum of 7 days at -80°C, cells were transferred to liquid nitrogen (vapour phase) for long term storage. Frozen cells were thawed from liquid nitrogen by rapidly resuspending them in pre-warmed culture medium. After two wash steps (5 minutes, 400 g) cells were cultured as described in section 2.2.

2.5 Antibodies and reagents

The anti-hCD27 mAbs varli and hCD27.15 were produced in-house using patented sequences published by Keler *et al*. (varli)[255] and Van Eenennaam *et al*. (hCD27.15)[256]. Constructs as well oligonucleotides of varli and hCD27.15 were purchased from GeneArt (Thermo Fisher Scientific). Anti-hCD27 mAbs AT133-2, AT133-5, AT133-11, and AT133-14 were generated in-house by A.L. Tutt by immunisation of mice with recombinant human CD27/TNFRSF7 Fc chimera protein (R&D Systems). Using standard hybridoma technology[257], spleens from immunised mice were fused with NS-1 myeloma cells. Selection of anti-hCD27 mAbs was determined by ELISA and flow cytometry.

Isotype-switching of mAbs to h1 and h2 as well as mutation of h1 mAbs to SE/LF[164,167], V9 and V11[166] variants was performed by C.H.T. Chan (Table 2.2).

Transient mAb production was performed using ExpiFectamine Chinese hamster ovarian (CHO) Transfection kit (Gibco). De-aggregation of mAbs was performed by size exclusion high-performance liquid chromatography (Agilent) and purified by affinity chromatography. All mAbs underwent testing for endotoxin levels (≤ 5 EU/mg) (endotoxin assay, Charles River) and were regularly checked (every 2 months) for aggregation by high-performance liquid chromatography. Only samples with less than 1% aggregation and ≤ 5 EU/mg (endotoxin) were used in experiments.

The soluble ligand CD70 used throughout this project was a kind gift from A. Al-Shamkhani and O. Dadas. Its structure is based on the soluble CD70 fusion protein comprised of the murine CD70 extracellular domain and a h1 Fc region[98]. Since in this project the target molecule CD27 is of human origin, soluble human CD70 (hCD70), comprised of the human extracellular domain of CD70 fused to either a h1 Fc region or a m1 Fc region (hCD70 Fc) was employed. The hCD70 Fc fusion protein was used to mimic the natural hCD27/CD70 ligation and served as a comparison for the anti-hCD27 h1/h2 mAbs.

Table 2.2| Un-conjugated antibodies and isotype controls for *in vitro* and *in vivo* experiments.

Antigen	Clone	Isotype	Source
hCD27	varlilumab	hIgG1, hIgG1 V11, hIgG2	in-house, based on patented sequence information from Keler *et al*. [255]
hCD27	hCD27.15	hIgG1, hIgG1 V11, hIgG1 SELF, hIgG2, hIgG2σ	in-house, based on patented sequence information from Van Eenennaam *et al*. [256]
hCD27	AT133-2	hIgG1, hIgG1 V11, hIgG2	in-house
hCD27	AT133-5, AT133-11, AT133-14	hIgG1, , hIgG1 V11, hIgG1 SELF, hIgG2	in-house
hCD27	daratumumab	hIgG1	Southampton General Hospital Pharmacy
hCD3	OKT3	mIgG2a	in-house
mCD40	3/23	mIgG1	in-house
p-IκBα (Ser32/36)	5ª5	mIgG1	Cell Signalling
IκBα,	44D4	rbIgG	Cell Signalling
tubulin	11H10	rbIgG	Cell Signalling
secondary anti rabbit			
IL16	14.1	mIgG2a	BioLegend
MIF	M1	mIgG1	Sigma Aldrich
EGFR (isotype control hIgG1)	cetuximab	hIgG1	Southampton General Hospital Pharmacy
isotype control hIgG2	-	hIgG2	BioXcell

Antigen	Clone	Isotype	Source
hCD16 isotype control mIgG1	3G8	mIgG1	in-house
mCD32b isotype control mIgG2a	AT130-2	mIgG2a	in-house
Secondary antibodies			
Anti-mouse IgG HRP-linked F(ab')$_2$ fragment			Sigma Aldrich
Anti-rabbit IgG HRP-linked F(ab')$_2$ fragment			Sigma Aldrich

Table 2.3 and Table 2.4 list anti-human and anti-mouse fluorochrome-conjugated mAbs as well as fluorochrome-conjugated secondary mAbs, which were used for flow cytometric analysis throughout this project.

Table 2.3| Fluorochrome-conjugated anti-human mAbs targeting used for flow cytometric analysis.

Antigen	Clone	Isotype	Fluorochrome	Source
Human antigen targeting mAbs				
CD3	SK7	mIgG1 κ	FITC/PerCP Cy 5.5	eBiosceince
CD4	OKT4	mIgG2b κ	FITC/PE Cy-7	eBioscience
CD4	RPA-T4	mIgG1 κ	PE	eBioscience
CD5	OKT1	mIgG1	FITC	in-house
CD8	SK1	mIgG1 κ	APC	eBioscience
CD8	MIH1	mIgG1 κ	APC eF780	eBioscience
CD14	M5E2	mIgG2a κ	Pacific Blue	BioLegend
CD16	3G8 Fab$_2$	Fab$_2$	FITC	in-house
CD16	3G8	mIgG1	PerCP eF710	eBioscience
CD16	eBioCB16	mIgG1 κ	PE-Cy7	eBioscience
CD19	J3-129	mIgG1 κ	PerCP eF710	eBioscience
CD19	HIB19	mIgG1 κ	PE-Cy 7	eBioscience
CD20	AT80	hIgG1	FITC	in-house
CD20	rituximab	hIgG1	FITC	in-house
CD25	BC96	mIgG1 κ	PE/eF450	eBioscience
CD27	O323	mIgG1 κ	PE/PerCP eF710	eBioscience
CD27	1F5, AT133-2, hCD27.15	hIgG1/hIgG2	Alexa Fluor 488	in-house
CD33	WM53	mIgG1 κ	PerCP Cy5.5	eBioscience
CD38	HIT2	mIgG1 κ	APC	eBioscience/ in-house
CD45	2D1	mIgG1 κ	PE	eBioscience
CD56	MY31	mIgG1 κ	PE	BD

Antigen	Clone	Isotype	Fluorochrome	Source
CD86	BU63	mIgG1 κ	PE	Invitrogen
FoxP3	236AE7	mIgG1 κ	APC	eBioscience
Ki67	20Raj1	mIgG1 κ 1	PE-Cy7	eBioscience
Secondary mAb				
phycoerythrin-labelled F(ab)$_2$ fragment goat anti-human IgG Fc (anti-hFc)				Jackson ImmunoResearch
Other reagents for flow cytometric analysis				
Alexa Fluor 488	-	rabbit IgG1	-	Thermo Fisher Scientific
LAMP-1	H4A3	mIgG1 κ	-	Biolegend
fixable viability dye	-	-	eF506	eBioscience

Table 2.4| Fluorochrome-conjugated anti-mouse mAbs used for flow cytometric analysis.

Antigen	Clone	Isotype	Fluorochrome	Source
Murine antigen targeting mAbs				
A20 idiotype	1G6	mIgG1	FITC	kind gift from R. Levy
B220	RA3-6B2	rat IgG2b	PerCP	Biolegend
CD3	17A2	rat IgG2b	FITC/PerCP eF710	eBioscience
CD4	GK1.5	rat IgG2b	eF450	eBioscience
CD8	53-6.7	rat IgG2a	APC eF780	eBioscience
CD11b	M1/70	rat IgG2b	eF450	eBioscience
CD19	1D3	rat IgG2a	APC	eBioscience
CD25	PC61.5	rat IgG1	APC	eBioscience
CD38	90	rat IgG2a	FITC	in-house
F4/80	CI:A3-1	rat IgG2b	Alexa Fluor 647	Serotec BioRad
Fox P3	NRRF-30	rat IgG2	PE	eBioscience
Ly6C	HK1.4	rat IgG2c	APC eF780	eBioscience
Ly6G	RB6-8C5	rat IgG2b	PE	eBioscience
NKp46	29A1.4	rat IgG2a	PE/PE-Cy7	eBioscience
Secondary mAb				
fluorescein (FITC)-labelled goat anti-mouse IgG Fc (anti-mFc)				Jackson ImmunoResearch
Alexa Fluor 647-labelled goat anti-mouse IgG Fc				Thermo Fisher Scientific
Other reagents for flow cytometric analysis				
H-2K^b/SIINFEKL tetramer	MHC-I tetramer	-	PE	in-house

2.6 Flow cytometry

All samples were acquired on a BD FACS Calibur or BD FACS Canto II flow cytometer. Data were analysed using BD FACS Diva and Cytobank software[258] and plotted graphically with GraphPad Prism 9.

If it was not possible to acquire samples on the same day, cells were fixed in 2% paraformaldehyde (PFA), stored at 4°C and analysed within 48 hours.

2.6.1 Staining with primary fluorochrome-conjugated mAb

Fluorescently labelled antibodies targeting antigens of interest (Table 2.3 and Table 2.4) were added to 100 µl single-cell suspension (1-2x10^6 cells). Cells were incubated for 15 minutes at RT in the dark and washed twice with staining buffer (phosphate-buffered saline (PBS) with 1% w/v bovine serum albumin (BSA), 0.1% w/v sodium azide) for 5 minutes at 400 g and resuspended in fluorescence-activated cell sorting (FACS) Flow (BD Biosciences) for flow cytometric analysis.

For intracellular FoxP3 staining, single-cell suspensions were fixed and permeabilised by adding 1 ml of FoxP3 transcription factor fixation/permeabilisation concentrate (eBioscience) for 30 minutes at RT. After two washes (5 minutes, 400 g) intracellular staining was performed for 20 minutes at RT, and cells were washed twice again, before flow cytometry.

2.6.2 Staining with secondary fluorochrome-conjugated antibodies

For staining with fluorochrome-conjugated secondary antibodies, cells were first incubated with the primary mAb for 30 minutes at 4°C in dark (see section 2.6.1). After two wash steps with staining buffer to remove non-specific binding, cells were stained with a secondary anti-hFc or anti-mFc (Table 2.3 and Table 2.4) for 30 minutes at 4°C in dark. Cells were washed twice with staining buffer (5 minutes, 400 g) and resuspended in FACSFlow for flow cytometry.

2.6.3 Processing and staining of mouse blood and tissue

Blood obtained by venesection was promptly diluted into heparin after withdrawal and further diluted with PBS to a final volume of 100 µl. To process tumours, tissue was chopped into small pieces, digested with Liberase TL (Sigma Aldrich) for 15 minutes at 37°C and mashed into single-cell suspensions using a 100 µm cell strainer. Following, cells were incubated for 10 minutes with 20 µg/ml mFcγR-block (2.4G2) to block mFcγRII and mFcγRIII[252]. Where FcγRs were of interest, no Fc-block was used. Cells were then stained with surface markers of interest as outlined in section 2.6.1.

Without washing, red blood cell lysis reagent (Invitrogen) was added for 2-3 minutes and cells were then washed twice (5 minutes, 400 g). For intracellular staining, cells were washed once after staining of surface antigens and fixed using 1 ml of fixative (1:4 dilution, eBioscience) for 30 minutes at RT in the dark. After two washes with 1 ml of PermWash (eBioscience) for 5min at 800 g mAbs specific for intracellular antigens were added for 30 minutes at RT in the dark. After two final wash steps with 1 ml PermWash, cells were analysed by flow cytometry.

2.7 Isolation of human PBMCs from leukocyte cones

PBMCs were isolated from fresh leukocyte cones received from anonymised, healthy donors through the National Health Service Blood and Transplant (NHSBT) service. The use of human leukocyte blood cones was approved by the East of Scotland Research Ethics Service (IRAS Project ID: 186605; ERGO: 19660.A7), in accordance with the Declaration of Helsinki. For PBMC isolation, blood was diluted 1:5 in 50 ml PBS/EDTA (2 mM). Diluted blood (25 ml) was layered onto 15 ml Lymphoprep (Stemcell technologies) and centrifuged for 20 minutes at 800 g (acceleration (acc): 9, deceleration (dcc): 5). Subsequently, the PBMC-containing layer was removed and topped up with PBS/EDTA (2 mM) to 50 ml and centrifuged for 5 minutes at 400 g (acc: 9, dcc: 9). After an additional washing step with PBS/EDTA (5 minutes, 300 g (acc: 9, dcc: 9)) the cell pellet was gently resuspended in cRPMI medium.

2.8 Surface plasmon resonance analysis

For SPR analysis, anti-His-antibodies (GE Healthcare Life Sciences) were immobilised onto a CM5-SPR-chip at different response units (RU). Subsequently, His-tagged hCD27 (produced by C.I. Mockridge using His Capture Kit, GE Healthcare Life Sciences) was added (Figure 2.2). For determination of IgG binding affinities, anti-hCD27 mAbs were diluted to 0.4, 2, 10, 50 and 250 nM in HBS-EP running buffer (0.01 M HEPES pH 7.4, 0.15 M NaCl, 3 mM EDTA, 0.005% v/v Surfactant P20, GE Healthcare) and the mAb:receptor interaction was measured using a Biacore T100 system. After association and dissociation of the anti-hCD27 mAbs, the CM5 chip was regenerated using 10 mM glycine (pH1.5) (conditions see Table 2.5). Binding was detected by the change of mass on the chip upon the interaction of the analyte (anti-hCD27 mAbs) with the ligand (His-tagged hCD27) and displayed as a sensorgram for further analysis (Figure 2.2). For the determination of association (k_a) and dissociation (k_d) constants as well as the calculation of the affinity (K_D), a 1:1 binding fitting curve was applied using Biacore T100 Evaluation software and Graph Pad Prism 9.

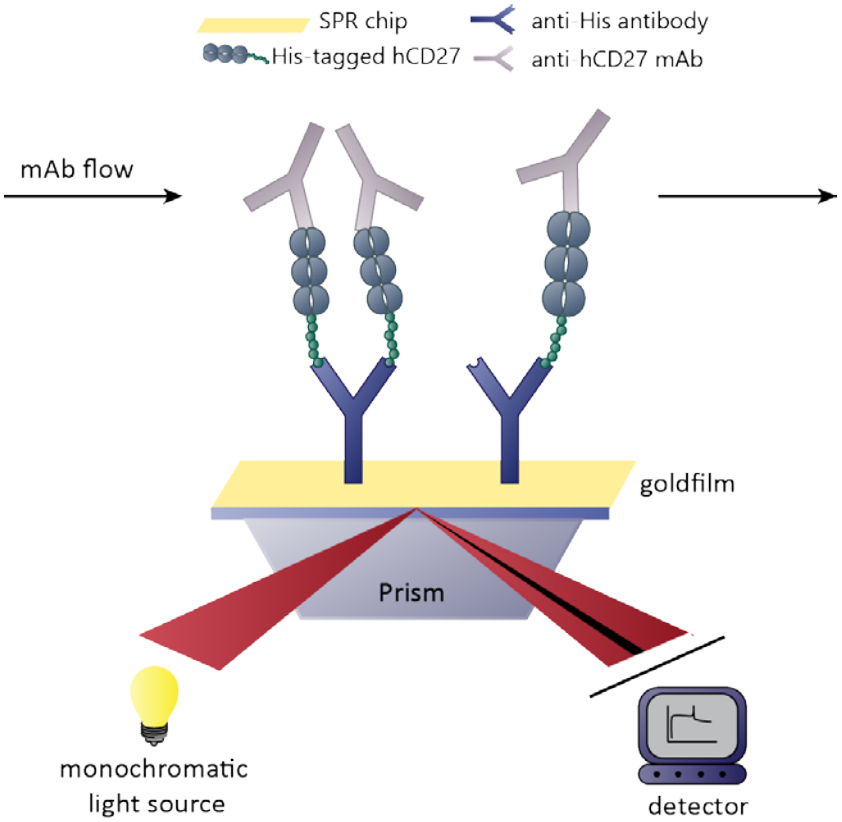

Figure 2.2| Schematic display of SPR analysis. Anti-His mAbs were immobilised onto a biosensor chip (glass surface covered with a thin gold layer coated with a dextran layer). Following, His-tagged hCD27 was captured and anti-hCD27 mAbs were added at different concentrations. Measuring principle: SPR occurs at an interface between media of different refractive indices. When SPR takes place, a decrease in the reflected light intensity at a specific angle takes place. Once a molecule binds to its ligand immobilised on the SPR chip, the angle of the reflected light intensity shifts. This change of angel is proportional to a change in mass and measured in RU (Schematic picture adapted from Zimmermann et al. (2002)[259]).

Table 2.5| Assay conditions of SPR analysis. The table summarises the experimental parameters of the SPR analysis of anti-hCD27 mAbs at three different hCD27 receptor densities (His-tagged hCD27; 20, 100, 180 response units (RU)).

		Cycle steps		
hCD27 receptor density on SPR chip	**Times and flow rate**	**hCD27-His capture**	**Analyte injection**	**Chip regeneration**
20 RU	contact time	90 s	300 s	60 s
	dissociation time	-	300 s	-
	flow rate	30 µl/min	30 µl/min	30 µl/min
80 RU	contact time	90 s	300 s	60 s
	dissociation time	-	300 s	-
	flow rate	30 µl/min	30 µl/min	30 µl/min
180 RU	contact time	120 s	300 s	60 s
	dissociation time	-	300 s	-
	flow rate	10 µl/min	30 µl/min	30 µl/min

2.9 Determining the binding site of the anti-hCD27 mAbs

2.9.1 Domain mapping

Domain mapping was performed using hCD27 truncation mutants, generated (by C.H.T. Chan) through site-directed mutagenesis and polymerase chain reaction (PCR) cloning. Constructs either containing solely CRD1, CRD3 or combinations of CRD1 and 2, CRD1 and 3 or CRD2 and 3 (schematic display of hCD27 constructs is shown in section 3.3.1, Figure 3.4; for truncated receptor sequences see Appendix A.2) were transiently transfected into 293F cells, which were cultured at $0.7x10^6$ cells/ml one day before the transfection. On the day of transfection, DNA-lipid complexes were prepared by diluting 10 µl of FreeStyle MAX Reagent (Invitrogen) or 10 µg of plasmid DNA to 300 µl Opti-MEM medium, respectively. After 5 minutes incubation at RT, the diluted plasmid DNA was added to the FreeStyle MAX reagent, gently inverted and incubated for 20 minutes at RT to allow the formation of DNA-lipid complexes. Subsequently, the DNA-lipid complex solution was added to 10 ml of 293F cells (at $1x10^6$ cells/ml) and cultured in a humidified shaking incubator for 24 hours and 8% CO_2 atmosphere. For binding analysis, cells were subsequently incubated with anti-hCD27 mAbs or hCD70 h1 Fc fusion protein and after two washes with a secondary anti-hFc for 30 minutes at 4°C (as outlined in section 2.6.2). Cells were washed twice more and analysed by flow cytometry.

2.9.2 Anti-hCD27 mAb competition assay

For the competition analysis of anti-hCD27 mAb/hCD70 Fc, PBMCs were isolated as outlined in section 2.7. $1x10^6$ cells were incubated with 10 µg/ml of anti-hCD27 m1 mAb or hCD70 m1 Fc fusion protein or the respective isotype control for 30 minutes at 4°C. Without washing, 10 µg/ml anti-hCD27 h1 mAb or hCD70 h1 Fc fusion protein was added to the cells for 30 minutes at 4°C. PBMCs were washed twice and incubated with secondary anti-hFc PE (1:500) and CD3 and CD4-specific mAbs for another 30 minutes at 4°C. After the final two washes, cross-blocking of the mAbs was assessed on $CD3^+CD4^+$ T cells by flow cytometry. For analysis, the ratio of PBMCs incubated with anti-hCD27 mAb/hCD70 Fc and PBMCs incubated with the irrelevant isotype controls was calculated.

2.9.3 Fine epitope mapping using alanine scanning mutagenesis

Surface alanine scanning mutagenesis is commonly used to finely map the epitope bound by mAbs or protein ligands on their cognate receptor. To remove reactive site chains within a protein, non-alanine residues are sequentially substituted with alanine, which carries a chemically inert methyl group, prohibiting side-chain interactions.

To map the binding sites of the anti-hCD27 mAbs on hCD27, alanine-mutated DNA constructs were purchased from GenScript. The constructs were generated by substituting either two consecutive amino acids or selected single amino acids with an alanine. Pre-existing cysteines, which contribute to protein stability through disulphide bonds were left unmutated to maintain protein integrity. The hCD27 constructs contained a hCD27 leader sequence, the extracellular region containing CRD1-3, the TMD and ICD). Furthermore, a rituximab epitope tag (RTX-10: ACPYSNPSLC^{260})was inserted between the leader sequence and extracellular region (see section 3.3.3,Figure 3.6 A for the schematic display of the hCD27 receptor construct). Protein expression on the cell surface was confirmed by detecting the epitope tag with fluorescently labelled rituximab.

The purchased DNA constructs were transiently transfected into 293F cells as described in section 2.9.1. After 24 hours of incubation, 200 µl of cell suspension was taken from each transfectant, washed once (5 minutes at 400 g) and resuspended in 100 µl PBS. Following, cells were incubated with anti-hCD27 mAbs, hCD70 Fc or the respective isotype control at 10 µg/ml for 30 minutes at 4°C and washed twice with staining buffer at 400 g for 5 minutes. Cells were subsequently stained with a secondary anti-hFc (1:500) as outlined in section 2.6.2. To confirm protein expression on the cell surface, cells were also stained with FITC-labelled rituximab at 10 µg/ml for 30 minutes at 4°C in a separate tube and washed twice with staining buffer (400 g for 5 minutes) before analysis. The binding of anti-hCD27 mAbs or hCD70 Fc to the mutated constructs was determined by flow cytometry and further analysed using GraphPad Prism 9 and Pymol software.

2.10 NF-κB-GFP reporter assay

2.10.1 Determination of hCD27 surface expression

To determine the expression level of hCD27 on the surface of hCD27 NF-κB/GFP, hCD27 WT, hCD27 R214 STOP and hCD27/GFP Jurkat cells, staining with a fluorochrome-conjugated anti-hCD27 mAb was performed (see section 2.6) and the median fluorescence intensity (MFI) was measured by flow cytometry.

2.10.2 Investigation of anti-hCD27 mAb transcriptional activating properties

To examine the ability of the anti-hCD27 mAbs to induce NF-κB transcriptional activity, hCD27 NF-κB/GFP Jurkat cells were transferred to puromycin-free cRPMI medium 24 hours prior to the assay. Jurkat cells were then cultured in a flat-bottom 96-well plate at a concentration of $1.5x10^6$ cells/ml in a final volume of 200 µl and stimulated with 10 µg/ml anti-hCD27 mAb. Cells

were subsequently incubated for 6 hours at 37°C and 5% CO_2 unless stated otherwise. As a positive control, a combination of 50 ng/ml phorbol 12-myristate 13-acetate (PMA) and 1 µg/ml ionomycin (both Sigma Life Science) was used. PMA activates the cellular PKC, whereas ionomycin increases intracellular Ca^{2+} levels. Together, these mitogens activate the cells by eliciting intracellular signalling pathways, bypassing engagement of surface receptors.[261] At the indicated time points, the Jurkat cells were examined under a microscope (Motic AE 2000). hCD27 NF-κB/GFP Jurkat cells are auto-fluorescent upon stimulation. Therefore, cells were resuspended in a 96-well plate, harvested and transferred to a tube and transcriptional activity was determined by analysing the strength of the GFP signal by flow cytometry.

To investigate whether the anti-hCD27 mAb-mediated transcriptional activation of NF-κB was dependent on hFcγR cross-linking, hCD27 NF-κB/GFP Jurkat cells were co-cultured with hFcγRIIb-transfected CHO cells. The latter highly express the hFcγRIIb, hence providing a cross-linking scaffold for anti-hCD27 mAbs. To ascertain hFcγRIIb expression the cells were stained with an anti-hFcγRIIb mAb and the expression level was assessed by flow cytometry. For the co-culture with hCD27 NF-κB/GFP Jurkat cells, hFcγRIIb-transfected CHO cells or parental CHO cells (control) were transferred to geneticin-free media 24 hours prior to the assay. On the day of the assay, the media was removed from the hFcγRIIb CHO cells and hCD27 NF-κB/GFP Jurkat cells were added at a concentration of $1x10^5$ cells/ml in a final volume of 200 µl. Subsequently, cells were stimulated with 10 µg/ml of anti-hCD27 mAb and incubated for 6h at 37°C and 5% CO_2 in a humidified incubator (unless stated otherwise), before GFP expression was assessed by flow cytometry.

As hFcγRIIb-transfected CHO cells express super-physiological levels of hFcγRIIb, hCD27 NF-κB/GFP Jurkat cells were also co-cultured with PBMCs from different healthy donors reflecting a more physiological hFcγRIIb-expression. Therefore, PBMCs were thawed as described in section 2.4 and seeded in a flat-bottom 96-well plate at a concentration of $1x10^5$ cells/ml in a final volume of 100 µl. hCD27 NF-κB/GFP Jurkat cells were subsequently added at a concentration of $2x10^4$ cells/ml. For T-cell activation, anti-hCD27 mAbs were added at a final concentration of 10 µg/ml and the GFP fluorescence was determined by flow cytometry.

2.11 Immunofluorescence microscopy

For clustering analysis, hCD27/GFP Jurkat cells were cultured at $1.5x10^6$ cells/ml in 200 µl cRPMI in a flat-bottom 96-well plate. Cells were stimulated with 10 µg/ml anti-hCD27 mAb for 30 minutes, 2, 6 and 24 hours at 37°C and 5% CO_2 atmosphere in a humidified incubator. After the incubation, cells were washed once with PBS and subsequently fixed with 4% PFA for 10 minutes at RT. After fixation, cells were washed once with PBS and transferred to a Poly-L-Lysine (Sigma Life Science)

covered µ-Slide 8-wWell microscopy chamber slide (Ibidi) and centrifuged at 250 g for 10 minutes to gently attach the cells to the chamber slide and stored in PBS at 4°C. To assess hCD27 receptor clustering, cells were acquired in confocal mode (100x objective lens) using an ONI Nanoimager (ONI Oxford) device and analysed using NimOS 1.18 and ImageJ software. Clusters ≥0.126 μm^2 were quantified.

For analysis of hCD27 internalisation, $2x10^6$ hCD27 WT Jurkat cells were incubated with 10 µg/ml Alexa Fluor 488 (Alexa488)-conjugated anti-hCD27 h1/h2 mAbs for 2 or 6 hours at 37°C and 5% CO_2 in a humidified incubator. Cells were then washed twice with ice cold PBS (400 g, 5 minutes, 4 °C) and fixed in 4% PFA for 20 minutes at RT in darkness. Subsequently, cells were washed twice more with PBS and permeabilised for 4 minutes in 0.5% Triton/PBS at RT in darkness. After additional two washes, cells were incubated in 2.5% normal goat serum (Vector Laboratories) in PBS for 30 minutes at RT to block unspecific binding of subsequent mAbs. Cells were washed once more and incubated with 8 µg/ml anti-LAMP-1 mAb (BioLegend) at 4°C overnight. For the detection of anti-LAMP-1 mAb binding, cells were washed twice more and incubated with a secondary goat anti-mouse Alexa Fluor 647 antibody (Thermo Fisher Scientific) (1:1000) for 1 hour at RT in darkness. After two final washes, cells were transferred to a Poly-L-Lysine (Sigma Aldrich) covered µ-Slide 18 Well microscopy chamber slide (Ibidi) and centrifuged at 250 g for 10 minutes to gently attach the cells to the chamber slide and stored in PBS at 4°C until imaging. For the analysis of hCD27 receptor internalisation, imaging was performed with a Leica SP5 confocal microscope (Leica microsystems) (100x objective lens (HCX PL APO, Leica microsystems)) and analysis was conducted using Adobe Photoshop CS6 software.

2.12 Quenching assay for the assessment of receptor internalisation assay

Human PBMCs were thawed as described in section 2.4 and $1x10^6$ PBMCs were incubated with 10 µg/ml Alexa488 labelled anti-hCD27 mAb. After 0, 2 or 6 hours, cells were moved on ice and washed twice with staining buffer (5 minutes, 400 g, 4°C). After resuspension, cells were divided into two separate tubes ($0.5x10^6$ cells per tube, respectively) and incubated with or without anti-Alexa488 for 30 minutes at 4°C at a concentration of 25 µg/ml to quench remaining anti-hCD27 Alexa488 surface fluorescence. PBMCs were then washed once more (5 minutes, 400 g, 4°C) and anti-hCD27 Alexa488 fluorescence was assessed on $CD4^+$ T cells by flow cytometry. Surface accessible anti-hCD27 mAb was calculated according to the following equation:

$$\frac{(\text{MFI unquenched - MFI quenched})}{\text{MFI unquenched}} \text{ x100}$$

2.13 Western blot

As previously reported, CD27 ligation results in the induction of the canonical NF-κB pathway (see section 1.3.4, Figure 1.10).[90] Therefore, the signalling downstream of hCD27 was investigated upon binding of anti-hCD27 mAbs by investigating the protein expression of molecules such as IκBα and p-IκBα.

2.13.1 Preparation of cell lysates

hCD27 WT Jurkat cells ($5x10^6$) were cultured at $1.5x10^6$ cells/ml in cRPMI media. Cells were subsequently stimulated with 10 µg/ml anti-hCD27 mAbs and the respective isotype controls for 5, 10, 15, 20 and 30 minutes. The reaction was stopped promptly by transferring the cells to ice followed by centrifugation at 400 g for 5 minutes at 4°C. After removing the supernatant and transferring the cells to 1.5 ml tubes, cells were centrifuged for 5 minutes at 400 g at 4°C. The supernatant was fully removed, the pellets resuspended in 30 µl radioimmunoprecipitation buffer (1 M sodium fluoride (NaF), protease inhibitor, 700 mM sodium orthovanadate (Na_3VO_4)) and incubated on ice for 30 minutes. Generated cell lysates were stored at -20°C.

2.13.2 Bradford assay for determination of protein concentration

To determine the protein concentration of the cell lysates, a Bradford assay was performed. A BSA protein standard curve was obtained by 1:2 dilutions of BSA, starting from 2 mg/ml. Cell lysates were thawed and spun for 5 minutes at 16.000 g and 4°C and the supernatant was diluted 1:10 with ultrapure H_2O (produced with a milliQ H_2O purification system) in a volume of 10 µl. Samples were measured in duplicates (Epoch BioTek Microplate Spectrophotometer) and protein concentrations were calculated using a BSA standard curve.

2.13.3 SDS PAGE

For Sodium dodecyl sulfate polyacrylamide gel electrophoresis (SDS PAGE), final volume reactions of 30 µl were prepared by adding 7.5 µl of 4x NuPAGE LDS sample buffer (Invitrogen; containing lithium dodecyl sulfate, SERVA blue G250 and phenol red), 3 µl of NuPAGE sample reducing agent (Invitrogen; 500 mM dithiothreitol), 15 µg of protein and ultrapure H_2O. Lysates were then heat-denatured at 95°C for 5 minutes and centrifuged for 5 minutes at 16.000 g. Samples were loaded onto a NuPAGE 10% Bis-Tris Protein Gel (Invitrogen) and ran for 30 minutes at 100 V, followed by 120 V until the leading band reached the bottom of the gel.

2.13.4 Protein transfer

Western blot was performed using an iBlot 2 Gel transfer device (Invitrogen) and the according iBlot 2 transfer stacks (either nitrocellulose or polyvinylidene difluoride; Invitrogen). Blotting was performed following the manufacturer's instructions using blotting template P0.

2.13.5 Blocking and staining

After the protein transfer, the membrane was rinsed with H_2O and stained with ponceau red to confirm a successful protein transfer by visualising protein bands. After destaining the membrane with H_2O, it was blocked with 5% non-fat dried milk (Marvel) diluted in Tris-buffered saline with Tween 20 (TBS-T) for 2 hours at room temperature. Subsequently, the membrane was stained with primary antibody (1:500 in staining buffer (TBS-T, 5% BSA, 0.05% sodium azide), see Table 2.2) overnight at 4°C. Following this, the membrane was rinsed 3 times with TBS-T and washed 3 times for 5 minutes in TBS-T. Staining with secondary antibodies (1:5000 in 5% non-fat dried milk diluted in TBS-T, see Table 2.2) was performed for 1-2 hours at RT. The membrane was washed with TBS-T 3 times for 5 minutes to remove any unbound secondary antibody. Enhanced chemiluminescence substrate (Abcam) was prepared by mixing the lumino/enhancer solution (Abcam) with the peroxide chemiluminescent detection reagent (Abcam) in a 1:1 ratio. The enhanced chemiluminescence substrate (2 ml) was applied onto the membrane and incubated for 5 minutes at room temperature. Excess substrate was removed and the membrane was imaged using a Biospectrum AC Imaging system device and analysed using ImageJ and Microsoft Office PowerPoint.

2.14 T-cell proliferation assay

To investigate the ability of anti-hCD27 mAbs to induce T-cell proliferation, PBMCs isolated from various donors were thawed as described in section 2.4. Following, $10x10^7$ PBMCs were labelled with CFSE at 2.5 µM in a final volume of 10 ml un-supplemented RPMI for 10 minutes at RT in darkness. To quench the reaction, 40 ml of FCS-containing cRPMI medium was added and cells were centrifuged for 5 minutes at 400 g. After an additional washing step with cRPMI medium, PBMCs were resuspended in cRPMI medium and cultured at high density ($1x10^7$ cells/ml) in a final volume of 1.5 ml in a 24-well plate for 24 hours at 37°C and 5% CO_2 atmosphere in a humidified incubator to upregulate hFcγRIIB on monocytes.[262] CFSE-labelled PBMCs were harvested using a Pasteur pipette, washed once with cRPMI medium for 5 minutes at 400 g and plated in a U-bottom 96-well plate at a concentration of $1x10^6$ cells/ml in a final volume of 100 µl. Cells were subsequently

stimulated with 0.5-0.05 ng/ml soluble anti-CD3 (see Table 2.2; anti-CD3 dose titrated for each donor) and anti-hCD27 mAbs of different isotypes and the respective isotype controls. After a 96 hour incubation at 37°C and 5% CO_2 atmosphere in a humidified incubator, T-cell proliferation was investigated by assessing CFSE-dilution in $CD8^+$ T cells by flow cytometry.

2.15 High density PBMC stimulation assay

Isolated PBMCs were plated at high density ($1x10^7$ cells/ml) in 1.5 ml in a 24-well plate. PBMCs were stimulated with soluble anti-hCD27 mAbs of different isotypes as well as with the respective controls at a concentration of 10 µg/ml for 48 hours at 37°C and 5% CO_2 atmosphere in a humidified incubator. Cells were then resuspended with a Pasteur pipette and 100 µl of the suspension was stained for flow cytometry (see section 2.6).

For the high density PBMC assay with IL-16 and MIF neutralisation, cells were isolated as described in section 2.7, seeded at high density as described above, and anti-IL16 mAb or anti-MIF (see Table 2.2) were added 10 min before 10 µg/ml anti-hCD27 mAbs were added. After 48 hours incubation at 37°C and 5% CO_2 atmosphere in a humidified incubator, 100 µl of cell suspension was harvested, stained for surface markers and assessed by flow cytometry (see section 2.6)

2.16 Cell death assay

Cell death was assessed using Annexin V and PI staining. Both dyes are membrane impermeable. However, during early apoptosis, intracellularly located membrane phosphatidylserine (PS) residues are translocated to the extracellular side. Annexin V, a natural ligand of PS residues, binds these externalised residues and is an indicator for early apoptosis. If cells are necrotic, the membrane ruptures but PS residues are not translocated. Due to the deteriorated membrane integrity PI can enter the cell and bind to DNA and is hence an indicator of cell necrosis. However, Annexin V^+ is also able to enter necrotic cells and to bind to intracellular PS residues contained in the cell membrane. Cells in early apoptosis are therefore Annexin V^+ and PI^-, whilst apoptotic/necrotic cells appear Annexin V^+ and PI^+. Daudi cells were cultured at $1x10^6$ cells/ml in 200 µl cRPMI medium in a U-bottom 96-well plate and incubated with 10 µg/ml anti-hCD27 mAbs or daratumumab or the respective isotype controls for 24 or 48 hours at 37°C and 5% CO_2 atmosphere in a humidified incubator. After the incubation, cells were stained with FITC-labelled Annexin V and PI, diluted in 1x binding buffer (100 mM HEPES (pH7.4), 1.4 M sodium chloride (NaCl), 25 mM calcium chloride ($CaCl_2$) in H_2O) containing Ca^{2+}, which is essential for the function of Annexin V. Cell death was subsequently assessed by flow cytometry.

2.17 *In vivo* mouse models

2.17.1 Endogenous response to anti-hCD27 mAb stimulation

For the assessment of the endogenous response to anti-hCD27 mAb treatment *in vivo* hCD27tg C57BL/6 mice were immunised with 5 mg OVA (Sigma Aldrich) in combination with 200 µg anti-hCD27 mAb or the irrelevant isotype control. To assess $SIINFEKL^{+}CD8^{+}$ T-cell expansion, blood was taken via venesection on days 3, 5, 7 and 14 after OVA/mAb injection. Blood was processed as described in section 2.6 and analysed by flow cytometry.

2.17.2 Assessment of hCD38 A20 cells *in vivo*

Kinetics of the hCD38 expression on hCD38 A20 cells was initially assessed in BALB/c mice. Therefore, mice were either inoculated with $5x10^6$ A20 or hCD38 A20 cells in 100 µl PBS via subcutaneous injection. To monitor hCD38 expression on hCD38 A20 cells, tumours were harvested: first, when the tumour was first palpable; second, two days after the tumour was first palpable; third, 4 days after the tumour was first palpable; fourth, 7 days after the tumour was first palpable. Tissue was processed as outlined in section 2.6.3 and hCD38 expression on A20 cells was analysed by flow cytometry.

2.17.3 Anti-hCD27/anti-hCD38 mAb combination therapy *in vivo*

hCD27tg BALB/c mice were subcutaneously injected with $5x10^6$ hCD38 A20 cells. Once the tumour was palpable (day X, 2-8 days post tumour inoculation), mice were treated with either 200 µg anti-hCD38 h1 (daratumumab) or irrelevant isotype control on day X or 100 µg anti-hCD27 m1 (hCD27.15) or respective isotype control on days X+1 and X+2 or the combination. Survival and tumour growth was monitored and mice were sacrificed once the tumour exceed 15 mm in diameter (measured using a calliper) or at an earlier time point if signs of tumour-associated symptoms such as laboured respiration, abdominal distension or impairment of the overall condition and behaviour (according to Foltz and Ullman-Cullere[263]) was detectable.

2.17.4 Hu-PBL-SCID:Daudi xenograft mouse model for anti-hCD27 monotherapy

$5x10^6$ PBMCs (obtained from Stemcell technologies) were administered via intravenous injection to NSG mice. Six days after cell transplantation, mice were checked for PBMC engraftment. Therefore, 20 µl of blood was withdrawn by venesection, processed and stained as described in sections 2.6.3 and 2.6.1 and analysed for the percentage of $hCD45^{+}$ cells. On day 7, mice were subcutaneously

inoculated with $5x10^6$ Daudi cells and subsequently treated with anti-hCD27 h2 c4d (hCD27.15) on days 10 and 11 after PBMC transplantation. Tumours were harvested on day 17 post PBMC injection and processed as outlined in 2.6.3. The bodyweight of the mice was regularly assessed throughout the time course of the experiment by using an Ohaus CS200 scale.

2.18 Statistics

Statistical analysis was performed using Graph Pad Prism 9. Two-tailed paired t-tests or one way-ANOVA were performed. p values ≤ 0.05 were considered as significant ($p \geq 0.05$: ns; $p \leq 0.05$: *; $p < 0.01$: **; $p < 0.001$: ***; $p < 0.0001$: ****). All graphs show medians and error bars represent ranges unless stated otherwise.

Chapter 3 Characterisation of anti-hCD27 mAb binding

3.1 Chapter introduction

Pre-clinical investigations of anti-CD27 mAbs as either monotherapy or in combination with anti-CD20 mAbs have shown promising anti-tumour responses in lymphoma mouse models.[243,264] Based on these anti-tumour activities, anti-CD27 mAbs were taken into the clinic and investigated as monotherapy[236,237]; and then in combination with other components such as the direct targeting mAb rituximab (NCT03307746[247]); checkpoint inhibitors (atezolizumab (NCT04941287), nivolumab (NCT030386702/ NCT02335918[245]); or in the context of the bispecific antibody CDX-527 (NCT04440943[249]. However, the success of anti-CD27 mAbs in anti-tumour responses seen in the pre-clinical models was not observed in clinic, and this may have been due to the mAb format utilised. Previous research has shown that the efficacy of mAbs targeting members of the TNFRSF can be dependent on a variety of factors including epitope specificity and isotype. As such, anti-CD40 mAb CP870,893 mediated optimal agonism when binding to membrane-distal domains[169], whereas membrane-proximal binding was best for OX40-mediated agonism[265].

In this study, the impact of epitope specificity and the use of different IgG isotypes on the agonistic activity of anti-hCD27 mAbs was investigated. For this, a new panel of anti-hCD27 mAbs (AT133-2, AT133-5, AT133-11, AT133-14) was generated by immunisation and standard hybridoma technology (by A.L. Tutt) or raised based on patented sequences in the case of hCD27.15[256] and clinically relevant varli[255]. These anti-hCD27 mAbs bind specifically to hCD27 and are not cross-reactive with mCD27 (Appendix A.1). In this chapter, the avidity, affinity and mAb binding site were determined.

3.2 Target binding of anti-hCD27 mAbs

3.2.1 Binding of anti-hCD27 mAbs by flow cytometry

The hCD27 receptor is expressed on naïve T cell subsets (constitutively) and can also be found on subsets of B and NK cells. Thus, binding of the anti-hCD27 mAbs to the hCD27 receptor was assessed on CD4⁺ T cells (Figure 3.1 A, B). Human PBMCs were isolated and incubated with the anti-hCD27 mAbs as either h1 or h2 isotype (Figure 3.1 C and D, respectively) and binding was subsequently determined using a secondary fluorochrome-conjugated anti-hFc (Figure 3.1 A, B).

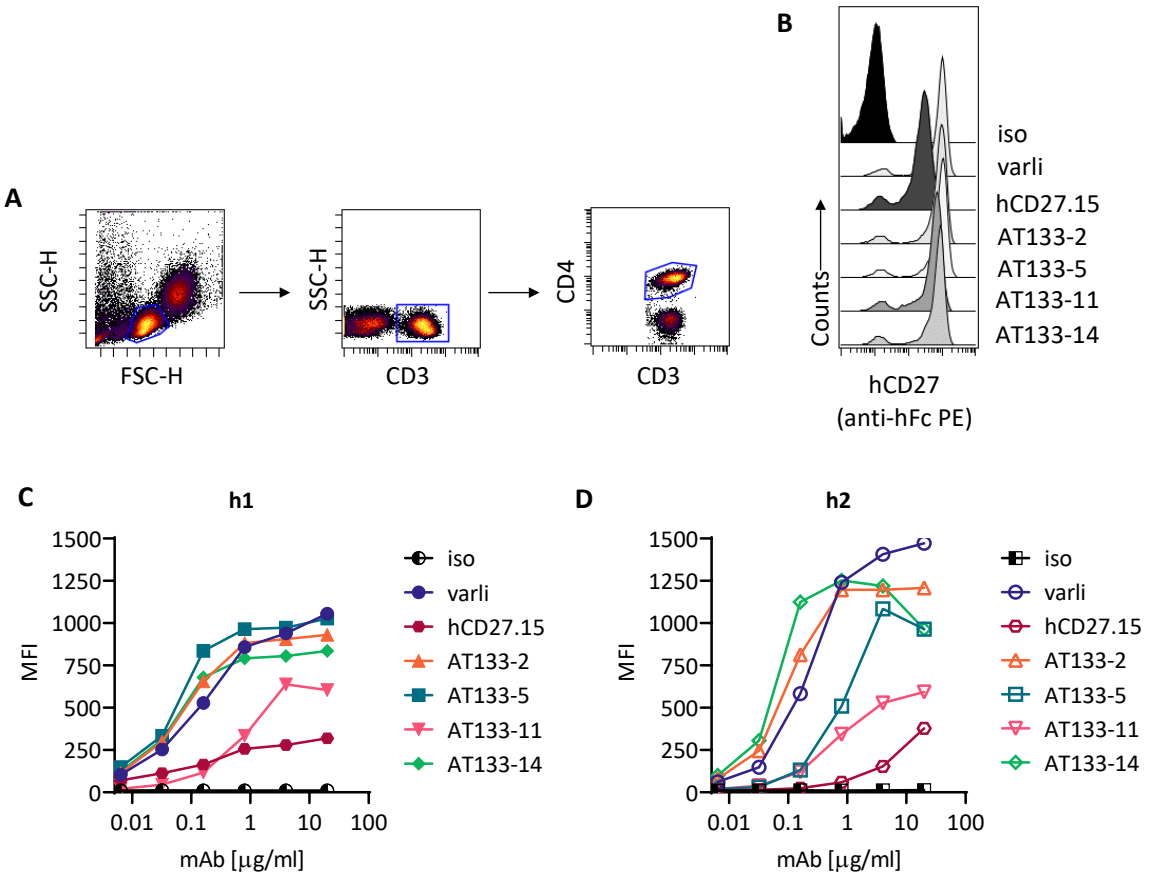

Figure 3.1| **Binding of anti-hCD27 mAbs to hCD27 on T cells.** PBMCs were incubated with anti-hCD27 h1/h2 mAbs or the respective h1/h2 isotype controls at 0.0064, 0.032, 0.8, 0.4, 4 and 20 µg/ml and binding to human CD4⁺ T cells was detected by flow cytometry. **A**: Gating strategy for CD3⁺CD4⁺ T cells. **B**: Representative histogram plots of anti-hCD27 mAb-binding to human CD4⁺ T cells at 4 µg/ml (populations identified as shown in (A)), detected with a fluorochrome-conjugated secondary anti-hFc. **C**, **D**: Binding curves of anti-hCD27 h1 (C) or anti-hCD27 h2 (D) mAbs to CD4⁺ T cells (as identified in (A) and (B)). The graphs show the median fluorescence intensity (MFI) of hCD27 on CD4⁺ T cells. Data is representative of n=3 independent experiments.

At low mAb concentrations (0.0064 µg/ml), h1 mAbs varli, AT133-2, AT133-5 and AT133-14 showed binding to CD4⁺ T cells, which increased further with rising mAb concentrations. This was not seen with AT133-11 or hCD27.15. Varli, AT133-2, AT133-5 and AT133-14 displayed similar binding profiles and maximum specific binding (Bmax, highest MFI per anti-hCD27 mAb), and saturated at

1 µg/ml. In contrast, hCD27.15 (saturating at 1 µg/ml), and AT133-11 (saturating at 4 µg/ml) showed reduced Bmax (hCD27.15: 3.4-fold, AT133-11: 1.5-fold). Similar to their h1 counterparts, varli h2, AT133-2 h2 and AT133-14 h2 bound to hCD27 at low concentrations (0.0064 µg/ml). AT133-2 h2 and AT133-14 h2 saturated at 1 µg/ml, whereas varli h2 did not reach saturation up to 20 µg/ml. AT133-5 h2, saturating at 4 µg/ml, showed reduced binding at concentrations of 0.0064-0.16 µg/ml, but a comparable binding profile to AT133-2 h2 and AT133-14 h2 at higher mAb concentrations. Similar to their h1 isotype, AT133-11 h2 an hCD27.15 h2 also demonstrated reduced Bmax to hCD27 on $CD4^+$ T cells and did not reach saturation.

3.2.2 Determination of binding affinities by SPR

Next, the bivalent binding affinities of anti-hCD27 mAbs to hCD27 were assessed by SPR analysis. SPR analysis allows a sensitive and quantitative assessment of the affinity, specificity and binding kinetics of the interaction between the mAb's paratope and its epitope in real-time. To do so, hCD27 was immobilised onto a CM5-SPR chip at different RU. Densities of 20, 100 and 180 RU were selected to optimise curve fitting and to assess the impact of ligand density on mAb binding. Subsequently, anti-hCD27 mAbs were injected as h1 or h2 isotypes (at 180 RU only as h1). Representative sensorgrams at 20 RU are displayed in Figure 3.2 (sensorgrams for 100 and 180 RU are displayed in Appendix A.4 Figure A.2 and Figure A.3, respectively).

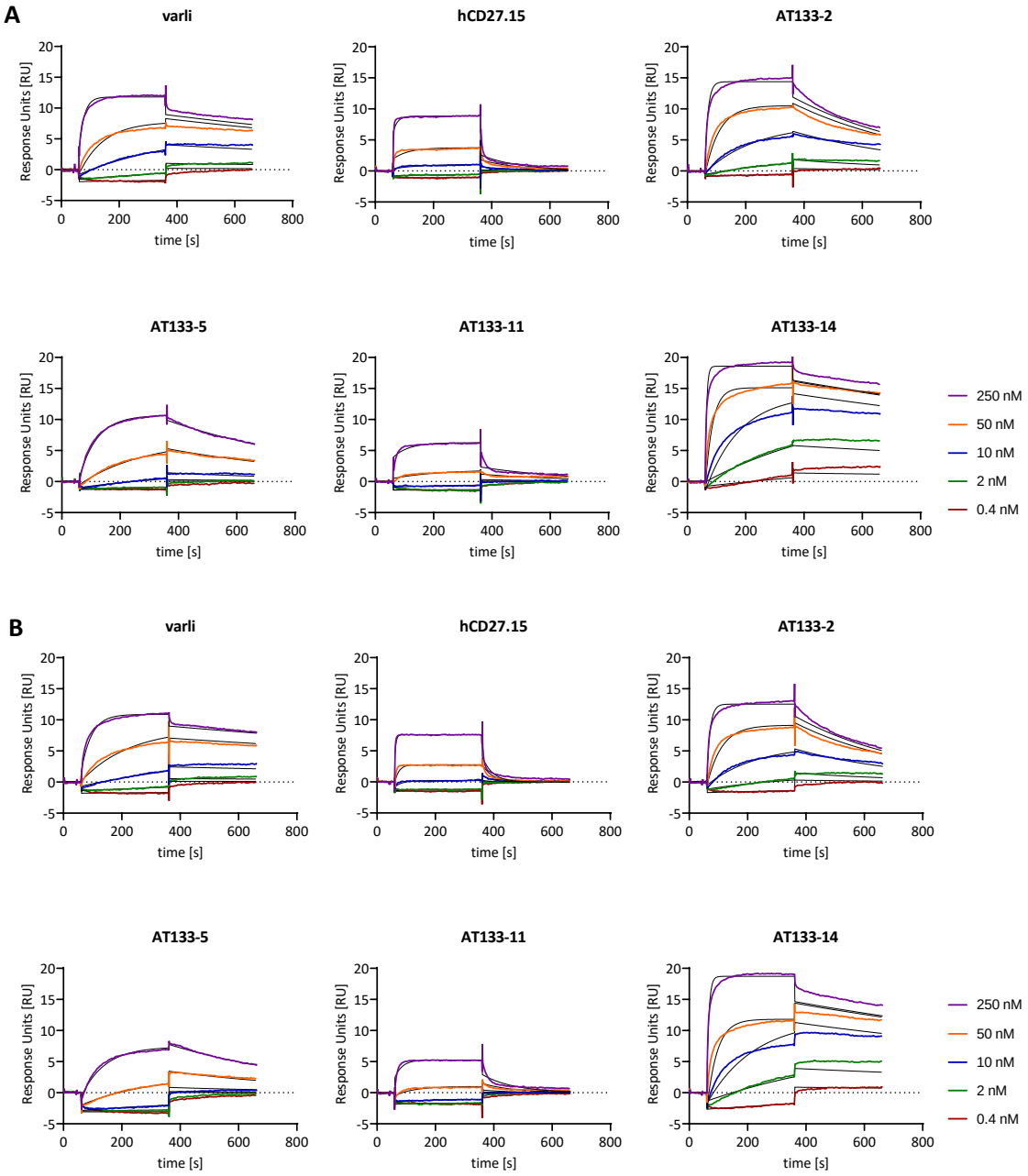

Figure 3.2| Sensorgrams of the binding of anti-hCD27 mAb to hCD27. A, B: Anti-hCD27 h1 (A) and anti-hCD27 h2 (B) mAbs were diluted to 0.4, 2, 10, 50 and 250 nM and binding curves were achieved by plotting the RU over time. His-tagged hCD27 was immobilised at 20 RU. A 1:1 binding fitting was applied (black line) (n=1).

SPR analysis showed different k_a and k_d for each of the anti-hCD27 mAbs. With regards to K_D, AT133-14 showed the highest bivalent affinity at 20 RU, followed by varli, AT133-2, AT133-5, hCD27.15 and AT133-11 (Figure 3.2 and Table 3.1). The h2 mAbs, when compared to their h1 counterparts, mostly showed a marginally lower K_D. Apart from AT133-5, all mAbs demonstrated a relatively high k_a. However, the k_d varied between mAbs, with hCD27.15 dissociating 2.3-14.9-times faster than the other anti-hCD27 mAbs.

Table 3.1| SPR analysis of anti-hCD27 mAbs. His-tagged hCD27 ligand was immobilised onto the SPR chip at 20, 100 and 180 RU. Displayed are k_a, k_d and K_D of the anti-hCD27 mAbs.

		varli		hCD27.15		AT133-2		AT133-5		AT133-11		AT133-14	
		h1	**h2**	**h1**	**h2**	**h1**	**h2**	**h1**	**h2**	**h1**	**h2**	**h1**	**h2**
20 RU	k_a (x10^5 $M^{-1}s^{-1}$)	2.2	1.1	2.4	8.0	3.7	3.5	0.6	0.4	0.6	1.2	8.0	5.6
	k_d (x10^{-4} s^{-1})	6.7	4.5	74.1	288.2	21.0	24.8	16.5	18.7	32.3	92.3	5.0	5.7
	K_D (xE^{-9})	3.0	4.1	30.8	35.8	5.7	7.1	28.2	44.1	50.4	75.9	0.6	1.0
100 RU	k_a (x10^5 $M^{-1}s^{-1}$)	3.3	2.7	16.5	15.9	4.1	0.9	5.6	0.8	2.9	2.3	10.9	8.5
	k_d (x10^{-4} s^{-1})	6.7	6.8	95.4	79.1	8.4	7.0	9.9	8.3	34.0	33.0	4.9	4.8
	K_D (xE^{-9})	2.0	2.5	5.8	5.0	2.1	7.7	1.8	10.2	11.9	14.2	0.5	0.6
180 RU	k_a (x10^5 $M^{-1}s^{-1}$)	7.5	-	36.5	-	5.3	-	1.1	-	1.2	-	12.2	-
	k_d (x10^{-4} s^{-1})	5.7	-	95.0	-	2.9	-	2.3	-	22.3	-	3.0	-
	K_D (xE^{-9})	0.8	-	2.6	-	0.6	-	2.1	-	18.0	-	0.2	-

Next, the impact of different hCD27 receptor densities on the bivalent affinity of the anti-hCD27 mAbs was compared. Each anti-hCD27 mAb was tested at three different hCD27 receptor densities (20, 100 and 180 RU) to observe changes in binding kinetics. Figure 3.3 A and B shows representative sensorgrams for the lowest-affinity mAb AT133-11 and the highest-affinity mAb AT133-14 at hCD27 receptor densities of 20, 100 or 180 RU. With increasing hCD27 receptor densities both, the k_a and k_d of AT133-11 decreased. In contrast, the receptor density did not have a notable impact on k_a and k_d of the highest-affinity mAb AT133-14 (Figure 3.3 A and Table 3.1). Plotting of the bivalent affinities against the hCD27 receptor densities shows the impact on antibody affinity for all anti-hCD27 mAbs (Figure 3.3 C); for the higher affinity mAbs varli, AT133-2 and AT133-14, the hCD27 density only had a marginal impact (20 RU vs 100 RU for h1 mAbs: 1.5 to 2.7-fold decrease in affinity). However, a more prominent effect was observed with decreasing receptor densities for medium to low-affinity mAbs such as AT133-5, AT133-11 and hCD27.15 (20 RU vs 100 RU for h1 mAb: 4.2 to 15-6-fold decrease in affinity), indicating a potential impact of hCD27 receptor density on low-affinity mAbs. The same trends were detectable for the h2 mAbs (data shown in Appendix A.4 Figure A.4). However, despite these differences the order of mAbs according to their affinity remained unchanged: AT133-14 > varli > AT133-2 > hCD27.15 > AT133-5 > AT133-11.

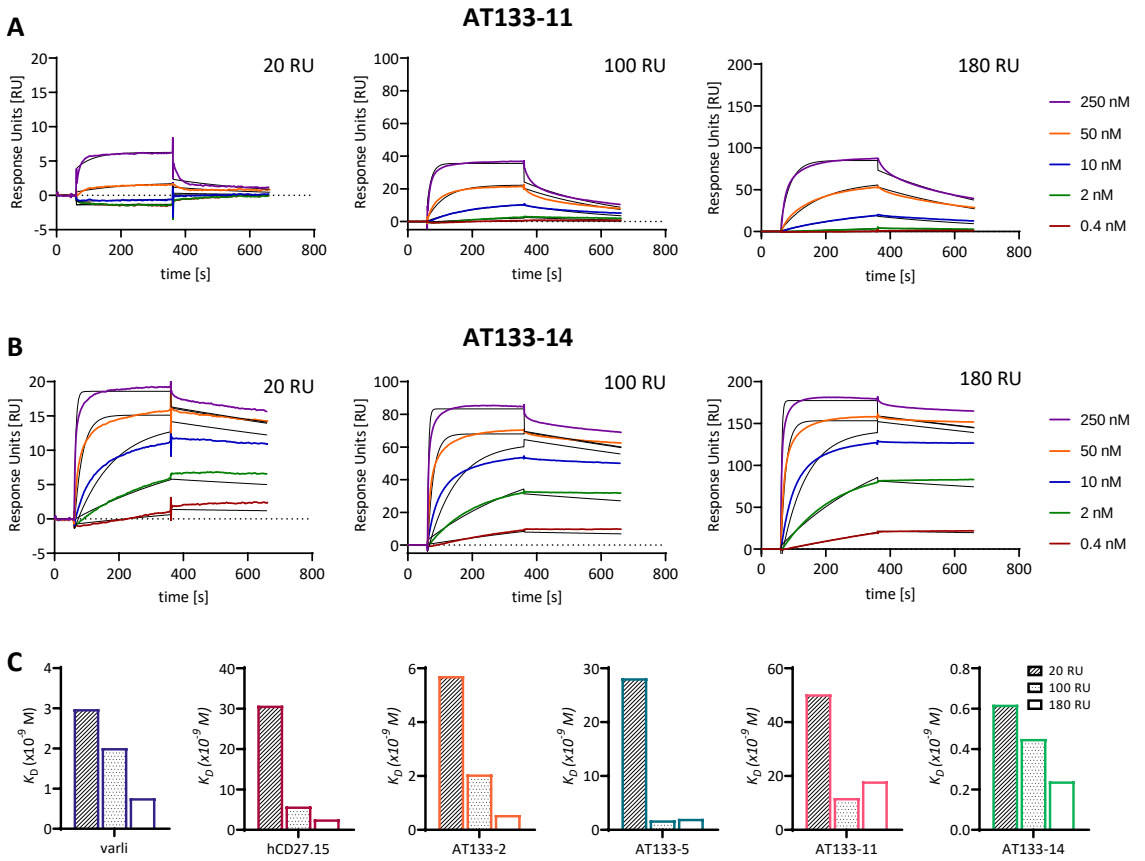

Figure 3.3| Impact of hCD27 receptor density on mAb affinity. A, **B**: Representative sensorgrams for a low (AT133-11(A)) and high-affinity (AT133-14 (B)) mAb at hCD27 receptor densities of 20, 100 and 180 RU. A 1:1 binding fitting was applied (black line). **C**: Comparison of K_D of anti-hCD27 h1 mAbs at hCD27 ligand densities of 20, 100 or 180 RU (n=1 for 20, 100 and 180 RU, respectively).

3.3 Epitope

Studies on other immunostimulatory molecules such as CD40, OX40 or 4-1BB suggest that mAb epitope location affects mAb agonistic performance.[169,170,265] It has been shown that anti-CD40 mAbs displayed enhanced activity upon binding to membrane distal epitopes of CD40[169], whereas OX40 performed best upon binding to membrane-proximal domains.[265] Furthermore, the importance of epitope location has also been demonstrated for CD20, where enhanced effector functions were associated with mAb epitopes located within membrane-proximal domains of the receptor.[170] However, whether the agonistic activity of anti-hCD27 mAbs is similarly dependent on epitope specificity has not been investigated yet. Therefore, domain mapping and cross-blocking assays were performed followed by surface alanine scanning mutagenesis to identify the epitopes crucial for the binding of anti-hCD27 mAbs.

3.3.1 Domain mapping of anti-hCD27 mAbs

To identify the CRDs the anti-hCD27 mAb bind to and confirm the hCD70 binding site within CRD2[37,38], truncation mutants of the hCD27 receptor were generated. Constructs consisting of CRD1 or CRD3 or a combination of CRD1 and 2, or CRD1 and 3, or CRD2 and 3 (Figure 3.4) were transiently transfected into 293F cells. The transfectants were incubated with the anti-hCD27 mAbs or soluble hCD70 h1 Fc fusion protein (hCD70 Fc) and binding to the truncation mutants was determined with a secondary anti-hFc using flow cytometry (Figure 3.4).

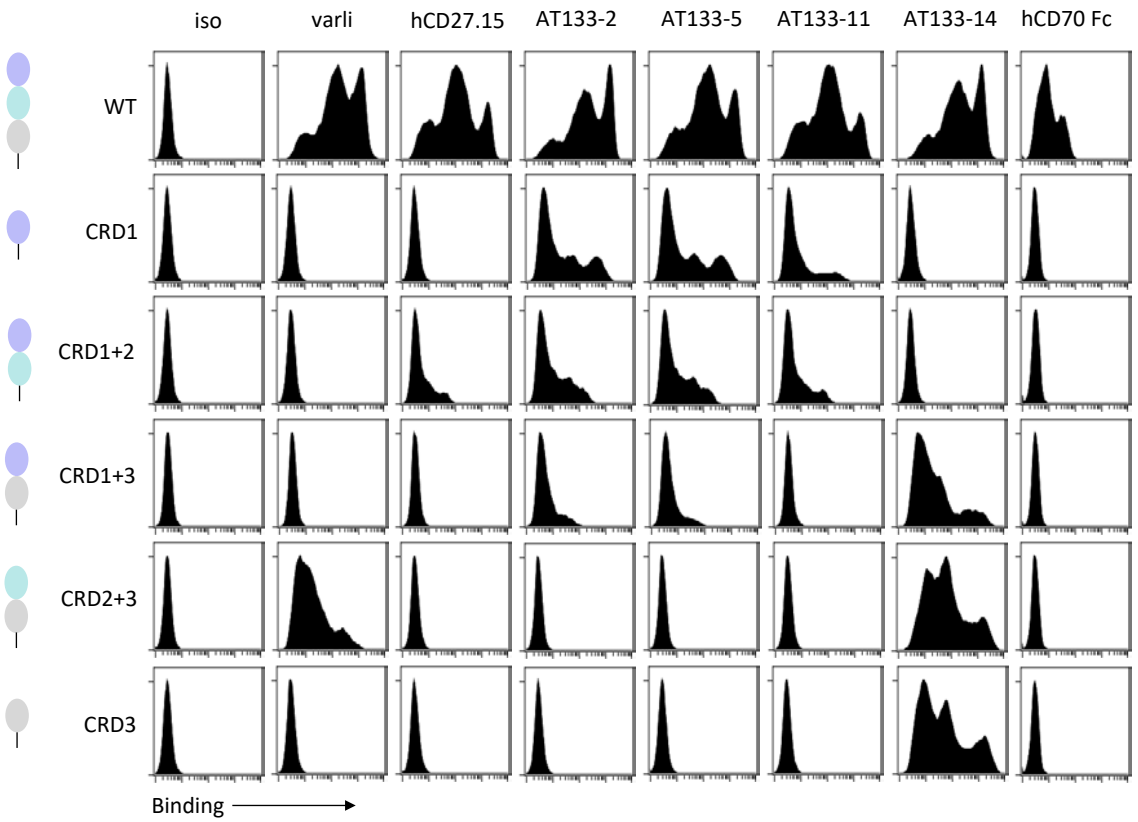

Figure 3.4| Domain mapping of anti-hCD27 mAbs. WT hCD27 and truncation mutants (CRD1, CRD1+2, CRD1+3, CRD2+3) were transiently transfected into 293F cells. After 48 hours cells were incubated with 10 µg/ml anti-hCD27 h1 mAb or hCD70 h1 Fc fusion (hCD70 Fc) protein or the irrelevant isotype control. Binding to hCD27 receptor truncation mutants was detected by flow cytometry using a fluorochrome-conjugated secondary anti-hFc. Plots show representative histograms for the binding of anti-hCD27 mAbs or hCD70 Fc to WT and truncated hCD27. Data is representative of n=3 independent experiments.

All anti-hCD27 mAbs as well as hCD70 Fc bound to WT hCD27 (Figure 3.4). Varli only bound receptor mutants concurrently containing CRD2 and CRD3. AT133-5 and AT133-2 showed similar binding profiles, as epitopes of both mAbs were restricted to CRD1-bearing receptor mutants (CRD1, CRD1+2, CRD1+3), suggesting their binding site is located within CRD1. AT133-11 also bound to CRD1 and CRD1+2 truncation mutants but not to the CRD1+3 construct. AT133-14 only displayed binding to CRD3-containing receptor mutants, strongly suggesting its binding site is exclusively within CRD3. Similar to varli, the binding profiles for hCD27.15 and hCD70 Fc were ambiguous:

hCD27.15 only bound to CRD1+2 but no other truncation mutant and hCD70 Fc did not bind to any of the mutants, indicating the requirement of a broader contact surface on the hCD27 receptor.

3.3.2 Competition assay for the determination of anti-hCD27 mAb binding sites

The domain mapping suggested that mAbs such as AT133-2, AT133-5 and AT133-11 bind epitopes located within CRD1, whereas the epitope of AT133-14 might be located in CRD3 (Figure 3.4). However, for the other mAbs, no clear domain preference could be defined. To confirm the results of the domain mapping and to gain further information about potentially overlapping epitopes, a competition assay was performed (Figure 3.5).

For the competition assay, anti-hCD27 mAbs and hCD70 Fc were employed as two different isotypes (h1 and m1), o be able to detect binding of the competing reagent. Human PBMCs were firstly incubated with anti-hCD27 m1 mAb or hCD70 m1 Fc fusion protein (initial reagent). Without washing, anti-hCD27 h1 mAb or hCD70 h1 Fc fusion protein were added (detected competing reagent), excess mAb washed off and binding of the competing mAb detected with a secondary fluorochrome-conjugated anti-hFc by flow cytometry (Figure 3.5 A). Figure 3.5 B displays representative dot plots for the binding of the competing anti-hCD27 mAb to WT hCD27 and Figure 3.5 C summarises the competition analysis in a heatmap.

All proposed CRD1-binding mAbs (AT133-2, AT133-5, AT133-11) cross-blocked each other and pre-incubation with any other anti-hCD27 mAb did not affect binding. However, when hCD70 Fc was added first, binding of AT133-5 and AT133-11 was reduced (Figure 3.5 C). Binding of hCD27.15 was only blocked by AT133-2 and enhanced binding to the hCD27 receptor was detected after primary incubation with AT133-11 and hCD70 Fc. Varli showed normal binding to hCD27, except when cells were incubated with hCD70 Fc or AT133-14 first, then reduced binding was detected. Binding of neither AT133-2 nor hCD27.15 affected binding of hCD70 Fc. However, hCD70 Fc binding was blocked after pre-incubation with varli and AT133-14. Moreover, initial binding of AT133-5 and AT133-11 resulted in reduced binding of hCD70 Fc, supporting the assumption that hCD70 Fc's epitope might span a broader contact surface on the hCD27 receptor. AT133-14 binding was not affected by any other anti-hCD27 mAb, strongly indicating its epitope is located within CRD3. Based on the results obtained in section 3.3.1 and 3.3.2, the hCD27 mAbs and hCD70 Fc could be classified as follows: CRD1-binding: AT133-2, AT133-5, AT133-11, hCD27.15; CRD2-binding: varli, hCD70 Fc; CRD3-binding: AT133-14.

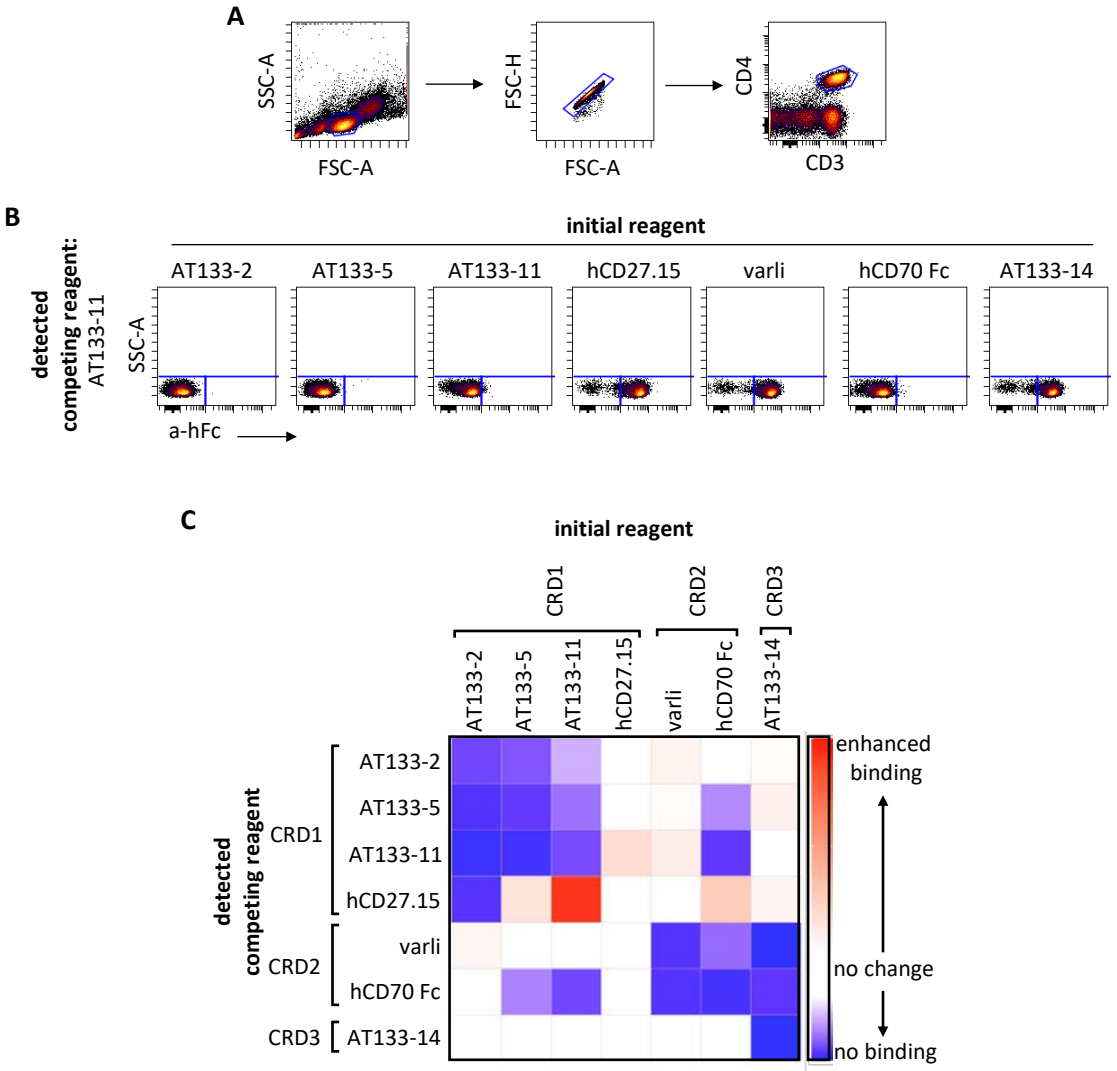

Figure 3.5| Competition assay for determination of anti-hCD27 mAb cross-blocking. Human PBMCs were incubated with 10 µg/ml anti-hCD27 m1 mAb or hCD70 m1 Fc fusion protein (initial reagent). Secondly, 10 µg/ml anti-hCD27 h1 mAb or hCD70 h1 Fc fusion protein was added (detected competing reagent). Binding of the anti-hCD27 mAbs to hCD27 was determined on $CD4^+$ T cells by flow cytometry after staining the cells with fluorochrome-conjugated anti-hFc. **A:** Shown is the gating strategy for $CD4^+$ T cells. **B**: Representative dot plots showing the binding of AT133-11 h1 to hCD27 in competition with the indicated anti-hCD27 m1 mAbs or hCD70 m1 Fc fusion protein. **C**: Heatmap showing the ratio of the MFI of PBMCs incubated with the competing reagent and PBMCs treated with the respective isotype control. Red represents enhanced and blue reduced binding or blocking of the competing reagent. Data representative of n=3 independent experiments.

3.3.3 Fine epitope mapping of anti-hCD27 mAb binding sites by surface alanine scanning mutagenesis

To validate and refine the above findings, epitope mapping by site-directed surface alanine scanning mutagenesis was performed. This method allows the identification of single amino acid residues that are crucial for protein-protein interactions[266] by substituting non-alanine residues with alanine. The hCD27 receptor construct used for the site-directed mutagenesis contained a rituximab-epitope tag[260] inserted between the leader sequence and the three CRDs of hCD27[260] (Figure 3.6 A). The epitope tag allowed the assessment of surface protein expression with

fluorochrome-conjugated rituximab. Additionally, the construct contained the hCD27 receptor transmembrane and intracellular domain (Figure 3.6 A). Mutated hCD27 constructs were generated by site-directed mutation of consecutive amino acids to alanine. Subsequently, based on the experiment with pairwise mutated amino acids, single point mutations (of selected amino acids to alanine) experiments were performed. To retain tertiary protein structure stability, cysteine residues remained un-mutated (Figure 3.6 B) (mutated constructs were purchased from GenScript).

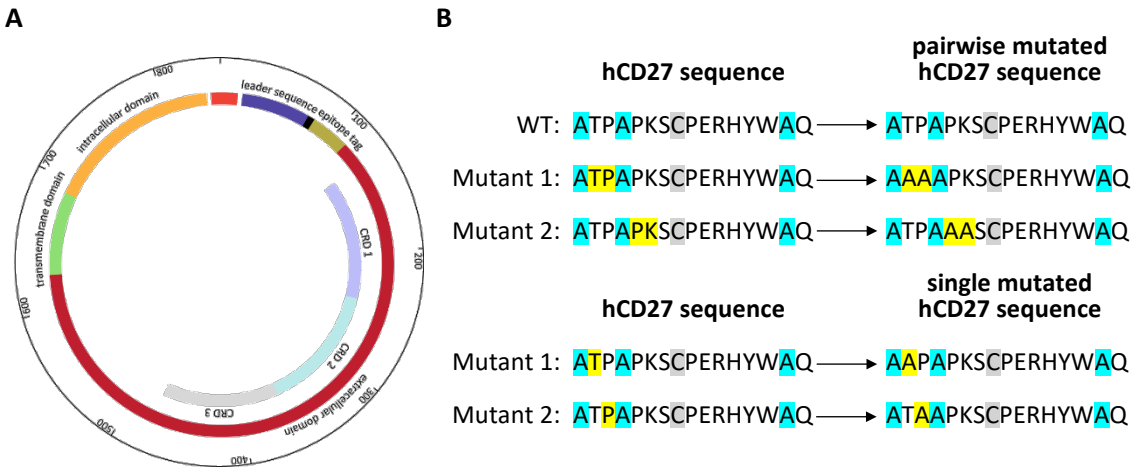

Figure 3.6| hCD27 construct for epitope mapping by surface alanine scanning mutagenesis. A: WT hCD27 and the mutated constructs were composed of a hCD27 leader sequence followed by a rituximab-epitope tag (RTX-10: ACPYSNPSLC[260]), CRD1, CRD2, CRD3 and the transmembrane and intracellular domain of hCD27. **B**: Shown is the mutation of consecutive and single amino acids of the hCD27 receptor to alanines. Pre-existing alanines and cysteines remained unchanged.

The hCD27 receptor mutants were transiently expressed on the surface of 293F cells and the binding of anti-hCD27 mAbs and hCD70 Fc was determined by flow cytometry (Figure 3.7). A gate was initially drawn on live cells (Figure 3.7 A) and hCD27 receptor expression confirmed by addition of fluorochrome-conjugated rituximab (Figure 3.7 B). Binding of the anti-hCD27 mAbs or hCD70 Fc was detected using a secondary anti-hFc as depicted in Figure 3.7 C. The representative dot plots show binding of the anti-hCD27 mAbs and hCD70 Fc to a hCD27 receptor construct. When residues G48 and K49 were pairwise mutated, the binding of AT133-5 and AT133-11 was abrogated, suggesting these residues are crucial for binding of these mAb.

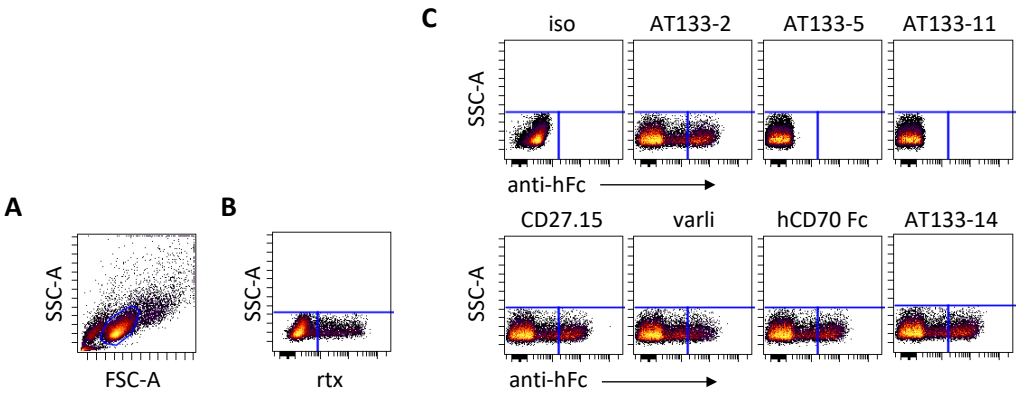

Figure 3.7| Gating strategy and representative dot plots of anti-hCD27 mAb binding to hCD27 mutants. 293F cells were transiently transfected with hCD27 mutants, incubated with 10 µg/ml of the respective indicated anti-hCD27 mAbs or hCD70 Fc and binding was analysed using a secondary anti-hFc by flow cytometry. **A**: Gating strategy for 293F cells. **B**: The dot plot shows cells stained with fluorochrome-conjugated rituximab to confirm the expression of the hCD27 constructs. **C**: Shown are representative dot plots for anti-hCD27 mAb binding to the hCD27 construct containing a pairwise mutation at the positions G48 and K49.

From the dot plots, the ratio of the percentage of anti-CD27 mAb-binding and the percentage of the highest hCD27-binding per mutant was calculated and displayed in a heatmap (Figure 3.8 A, Appendix A.5). Mutation of amino acid pairs such as H43/Y44, M54/E56, T59/F60, L61/V62, G80/V81, S82/F83, N107/T109 and N113/E115 led to a reduction of binding for all anti-hCD27 mAbs, with the exception of AT133-14 (Figure 3.8 A, amino acid pairs marked with an *). Their requirement for binding, although being broadly spread across the extracellular domain of the hCD27 receptor, might indicate their critical contribution to receptor stability and integrity. Further amino acids were identified as essential for binding of each anti-hCD27 mAb. AT133-2, AT133-5, AT133-11 required residue pairs located within CRD1 (AT133-2: H68/R69; AT133-5: W45/Q47, G48/K49; AT133-11: W45/Q47, G48/K49, H68/R69) and hCD27.15's were located in CRD1 and CRD2 (K63/D64, D75/P76, I110/T111). CD70's epitope was found within CRD2 (R90/P91 and H92/E94) in accordance with previous literature[37,38], whereas varli's epitope was stretched across CRD2 and CRD3 (S95/R97, R119/N120, G121/W122). The binding site of AT133-14 was exclusively located within CRD3 (D126/K127).

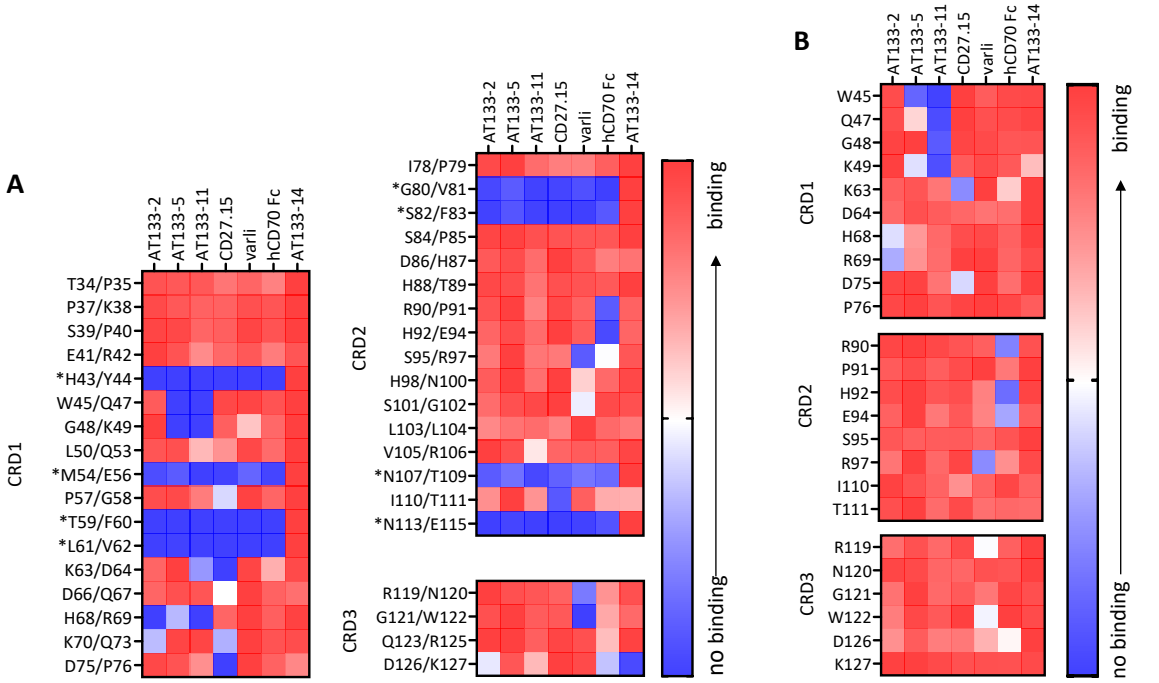

Figure 3.8| Alanine scanning mutagenesis with pairwise and single mutated amino acids. A, **B**: Heatmaps of anti-hCD27 mAbs and hCD70 Fc, binding to hCD27, containing mutations of consecutive residues (A) or single amino acids (B). Red indicates no change in binding and dark blue no binding. Amino acid pairs marked with an asterisk (*) were not considered as crucial for mAb binding (n=1 for alanine scan with pairwise and single mutations, respectively).

Next, the identified amino acid pairs crucial for binding of each anti-hCD27 mAb were individually mutated (Figure 3.6 B). This allowed further refinement and detailed identification of the epitopes for each mAb. A key residue for CRD1-binding AT133-5 was W45, whereas W45, Q47, G47 and K49 were crucial for binding of AT133-11. As already identified by using pairwise mutations, AT133-2 required H68 and R69 for binding. Amino acids crucial for binding of hCD27.15 were also located solely within CRD1 (K63, D75). Binding of varli and hCD70 Fc was identified within CRD2, relying on R97 (varli) and R90, H92 and E94 (hCD70 Fc). Single mutation of D126 and K127, located in CRD3, the residues, which were crucial for binding of AT133-14 after pairwise mutation, did not abrogate the binding, suggesting that concurrent presence of these residues is essential for AT133-14-binding.

Based on the results presented in this chapter, the binding sites of the different anti-hCD27 mAbs were highlighted using PyMol software, as demonstrated in Figure 3.9. The presented hCD27 molecular model (5TL5) is based on the crystal structure of the extracellular domain of hCD27 in complex with the Fab fragment of mAb 2177, published by Teplayakov *et al.*[38] For the display of epitopes, only the residues exclusively necessary for binding of each mAb are depicted (Figure 3.9).

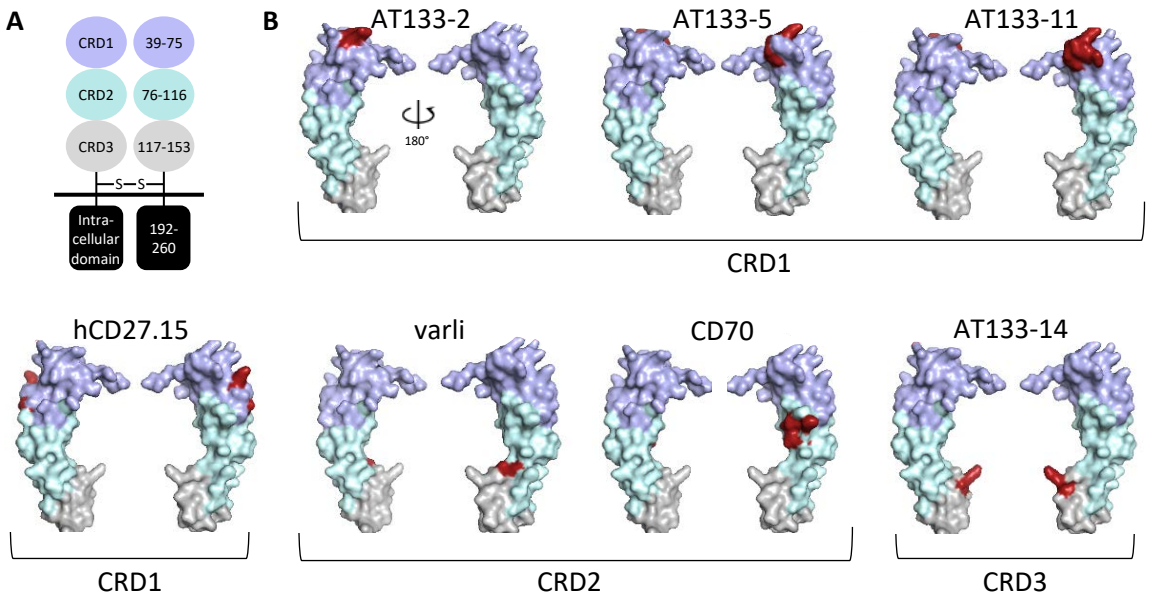

Figure 3.9| Structural display of anti-hCD27 mAb binding sites. A: Cartoon depicting the structure of a hCD27 homodimer. **B**: Displayed is a two-dimensional view from two directions of the extracellular domain (CRD1, CRD2, CRD3) of hCD27 without transmembrane or intracellular domain. Light blue: CRD1, light green: CRD2, light grey: CRD3, red: residues crucial for mAb binding. The crystal structure used for the structural display of hCD27 was extracted from Teplyakov *et al*. (5TL5).[38] Structures were generated using PyMol software.

The structure revealed that CRD1 binding AT133-2, AT133-5 and AT133-11 engaged the most distal epitopes at the N-terminus of hCD27. The epitope of hCD27.15, still located distally to the membrane within CRD1, was positioned more membrane-proximal on the interface to CRD2. Of note, these residues were located on the opposite side of the binding sites of AT133-5, AT133-11, varli and AT133-14 on the hCD27 homodimer. The ligand hCD70 Fc bound residues in the middle of the receptor within CRD2. In contrast, varli required residues located in membrane-proximal CRD2 and AT133-14 in CRD3. Taken together, these data gave a detailed positional map of the binding sites on the extracellular domain of hCD27 for each of the anti-hCD27 mAbs (Table 3.2).

Table 3.2| Summary of the characterisation of anti-hCD27 mAb binding. The table displays the epitope location of the anti-hCD27 mAbs on the hCD27 receptor as well as their Bmax and bivalent affinities (K_D). na: not assessed.

	AT133-2	**AT133-5**	**AT133-11**	**hCD27.15**	**varli**	**CD70**	**AT133-14**
Epitope location	CRD1 (H68/R69)	CRD1 (W45, K49)	CRD1 (W45, Q47, G48, K49)	CRD1 (K63, D75)	CRD2 (R97)	CRD2 (R90, H92, E94)	CRD3 (D126, K127)
Bmax	1014	923.9	661.9	283.6	1000	na	825.2
K_D (x10^{-9})	2.06	1.78	11.85	5.77	2.01	na	0.45

3.4 Chapter discussion

In this chapter, the binding of novel and clinically relevant anti-hCD27 mAbs to the hCD27 receptor was characterised. Avidities and bivalent affinities were determined by flow cytometry and SPR. Specific epitopes for each of the anti-hCD27 mAbs were identified through hCD27 truncation mutants, cross-blocking and fine epitope mapping by alanine scanning mutagenesis.

Initial investigation of the mAb binding showed that the majority of mAbs have high binding levels to hCD27 except for AT133-11 and hCD27.15 (Figure 3.1). SPR revealed different bivalent affinities for the anti-hCD27 mAbs, which could be ranked as follows: AT133-14 > varli > AT133-2 > hCD27.15 > AT133-5 > AT133-11 (Table 3.1). The data obtained from the binding and affinity analyses were in congruence for most of the mAbs (Figure 3.1 and Figure 3.2). However, hCD27.15, which bound to hCD27 with medium affinity showed low target binding (Figure 3.1 and Table 3.1). A possible explanation could be its epitope orientation on the hCD27 receptor (Figure 3.9) which will be further elucidated in Chapter 7.

In addition to the determination of bivalent affinities, the impact of hCD27 receptor density on mAb affinity was investigated. SPR at three different ligand densities revealed that high-affinity mAbs were less susceptible to changes in receptor densities than lower affinity mAbs (Figure 3.3). These observations may be partially explained by mass transfer effects, which can be associated with high ligand densities, wherein the analyte binds faster to the immobilised ligand than it can be supplied to the SPR chip surface. The consequence is a k_a that is slower than the true k_a and a delay of analyte dissociation (k_d) due to delayed analyte diffusion and re-binding to the immobilised receptor. To minimise mass transport limitations, determination of the optimal ligand density on the chip is crucial. To avoid this phenomenon, the density of the immobilised ligand can be lowered and the flow rate can be increased.[267] To exclude mass transfer effects, the interpretation of the bivalent affinities of the anti-hCD27 mAbs was therefore evaluated with the results obtained at a hCD27 receptor density of 20 RU.

Other groups have also noted a relation between receptor density and mAb affinity. Similar relations between immobilised ligand density and mAb affinity (as observed in this project) were indicated for HIV-1 neutralising mAbs targeting epitopes on the HIV envelop glycoprotein gp120. Variations of the antigen-density had less impact on the binding of high-affinity mAbs, whereas low-affinity were more susceptible to antigen-density variations.[268] Furthermore, Velders and colleagues evaluated the impact of mAb affinity and ligand density on ADCC. They found that high-affinity mAbs targeting epithelial cell adhesion molecule (Ep-CAM) were more effective in mediating tumour cell killing *in vitro* and *in vivo* than low-affinity mAbs and simultaneously less

impacted by the ligand density on the cell surface.[269] Taken together, these studies might indicate the importance of ligand density on mAb effector functions.

Binding sites of the anti-hCD27 mAbs were determined by employing various epitope-mapping methods. The anti-hCD27 mAbs bound epitopes across all three CRDs of the hCD27 receptor. The data obtained with truncated hCD27 receptors (Figure 3.4) and the observation that AT133-2, AT133-5 and AT133-11 were cross-blocking each other (Figure 3.5) strongly indicated their binding site is located within CRD1 and this was confirmed by alanine scanning mutagenesis (Figure 3.8 and Figure 3.9). Screening of AT133-14 unambiguously identified its epitope within CRD3 and binding essentially relied on the presence of both D126 and K127, since mutations of either amino acid abrogated binding. The hCD27 binding sites were less distinct for varli and hCD70 Fc. Varli only bound when CRD2 and CRD3 were concurrently present and hCD70 Fc seemed to have a broader contact surface, spanning across CRD1-3 (Figure 3.4). Reduced binding was detected when varli was competing with hCD70 Fc and AT133-14, confirming the predicted epitope location within CRD2 and CRD3 (Figure 3.5). On the other hand, binding of hCD70 Fc was reduced when competing with varli or AT133-14, implying that both hCD70 Fc and AT133-14 have overlapping epitopes located within membrane-proximal CRDs, possibly due to steric hindrance. Indeed, alanine scanning mutagenesis revealed that binding of varli and hCD70 Fc is reliant on residues in close proximity within CRD2 (varli: R97; CD70: R90, H92, E94) (Figure 3.9). Currently, there are no crystal structures available depicting the anti-hCD27 mAbs in complex with hCD27. However, in parallel undertaken *in silico* docking analyses by H. Fisher determined the likelihood of the identified epitopes to be the binding sites of the anti-hCD27 mAbs. Docking was performed in a restraint manner based on the previously identified epitopes for each anti-hCD27 mAb and the best binding model for each mAb selected based on its HADDOCK score. The *in silico* models agree with the putative binding sites of the anti-hCD27 mAbs identified by alanine scanning mutagenesis.

Furthermore, the binding site of hCD70 Fc was identified within CRD2, which is in concordance with previously published data by Teplayakov *et al*. and Liu *et al*.[37,38]. Liu *et al.* resolved the crystal structure of hCD27 in complex with trimeric hCD70. hCD70 thereby bound residues on the hCD27 receptor located on the internal surface of a homodimer. Based on these data, epitopes pointing in the same direction as the hCD70 Fc binding sites could be identified as internally facing, whereas epitopes on the opposite could be defined as externally facing (Figure 3.9). Accordingly, AT133-5, AT133-11, varli and AT133-14 suggest internal binding, whereas the epitopes of AT133-2 and hCD27.15 are located on the outer surface. This classification could also account for the reduced binding when hCD70 Fc competed with AT133-5 or AT133-11. Although these mAbs bind to different CRD (AT133-5 and AT133-11: CRD1, CD70: CRD2), steric hindrance caused by the epitopes

being orientated internally facing could still explain the reduced binding. Interestingly, hCD27.15 did not block any of the other anti-hCD27 mAbs or hCD70 Fc binding. One possible explanation could be its high k_d, which allows the mAb to rapidly dissociate from the receptor, giving other mAbs the ability to bind and outcompete hCD27.15 (Figure 3.2 and Table 3.1). However, this data is different to the results published by Van Eeneennam et al., where hCD27.15 was identified as ligand-blocking.[256] These differences might be due to different experimental conditions. Although the anti- hCD27 mAb and hCD70 Fc used in Van Eenennaam *et al.* were the same as in this study, the authors conducted experiments using hCD27 transfected CHO-K1 cells, which possibly express higher hCD27 levels than PBMCs.

Apart from reduced binding, enhanced binding was also detected with two of the combinations: AT133-11 (initial binder) with hCD27.15 (competing mAb) and hCD70 Fc (initial binder) with hCD27.15 (competing mAb) (Figure 3.5). Despite their epitopes not overlapping, binding of the initial reagent might drive mAb- or ligand-induced conformational changes within the hCD27 receptor, therefore enhancing the binding of hCD27.15. Conformational changes of receptors upon mAb binding have also been observed for CD20. Binding of type 1 anti-CD20 mAbs (e.g. rituximab) prompted an open CD20 configuration, whereas binding of type 2 mAbs (e.g. GA101) left the receptor in a closed configuration limiting the amount of mAb bound to one cluster.[270]

In this chapter, the binding properties and epitope specificities of the anti-hCD27 mAb panel were characterised (Table 3.2). It has been shown by many research groups that epitope specificity can influence the biological effect of multiple immunostimulatory mAbs.[169,170,265] For example, Zhang *et al*. demonstrated that anti-OX40 mAbs that bind to membrane-proximal epitopes in CRD2-4 mediate superior agonistic activity over CRD1-binding mAbs, resulting in enhanced T-cell stimulation and anti-tumour efficacy in a CT26 colon carcinoma mouse model.[265] In contrast, only binding to distal epitopes in CRD1 of the CD40 receptor by the immunostimulatory anti-CD40 mAb CHiLob7/4 led to strong agonistic activities.[169] It is hypothesised that mAbs, which bind to CRD1 can engage cognate receptors due to good accessibility of their Fc-region. In contrast, mAbs which bind closer to the membrane may not be able to sufficiently engage with relevant receptors due to steric and conformational hindrance and hence display weaker agonism. Indeed, anti-CD40 mAbs that bound epitopes in CRD2-4 function as potent antagonists due to CD40L-blocking.[169] Moreover, safety studies of urelumab[271] and utomilumab[233] revealed different toxicity profiles which might be due to differences in their agonistic activities or epitope binding sites. Chin *et al*. found that urelumab bound distally to CRD1 of 4-1BB whereas utomilumab engaged the more proximal junction between CRD3 and CRD4. Comparison of functional properties of both mAbs revealed enhanced agonistic activity in NF-κB reporter assays and stronger activation of isolated human $CD8^+$

T cells when anti-4-1BB mAb urelumab bound membrane-distal epitopes in CRD1.[272] However, the studies mentioned above also demonstrated that therapeutic efficacy of the mAbs is not entirely dictated by the epitope specificity but also dependent on the mAb isotype and its ability to engage with FcγRs. Considering these findings, the impact of the isotype on anti-hCD27 mAb mediated agonism will be elaborated in the following section.

Chapter 4 Functional investigation of anti-hCD27 mAbs

4.1 Chapter introduction

Clinical application of the anti-hCD27 mAb varli has displayed modest anti-tumour activity.[236,237] Research on other TNFRSF-targeting mAbs suggests that this may be due to the utilisation of the wrong mAb format and that poor agonism might be overcome by the use of different mAb formats. Current evidence implies that agonism of immunomodulatory TNFRSF-targeting mAbs is influenced by mAb isotype.[162,165,169,273-277] Depending on which isotype is employed, activity could either be mediated through Fc-independent TNFR clustering (by h2 mAbs) or cross-linking through Fc:FcγRIIb interactions.[160] However, to what extent these observations are also applicable to anti-hCD27 mAbs is unknown. Therefore, in this chapter the agonistic activity of a novel anti-hCD27 mAb panel (detailed in Chapter 3) was characterised. Using h1, h2 or Fc-engineered (enhanced affinity to FcγRIIa/b) isotypes, their ability to induce NF-κB transcriptional activity, immediate hCD27 receptor downstream signalling, receptor clustering, and $CD8^+$ T-cell proliferation, was explored.

4.2 NF-κB transcriptional activity

It has been demonstrated that ligation of hCD27 with CD70 results in TRAF2-and TRAF5-mediated activation of the NF-κB signalling pathway.[93] Thus, to examine the agonistic properties of the anti-hCD27 mAb panel, a NF-κB/GFP reporter assay using hCD27 NF-κB/GFP Jurkat cells was employed.

4.2.1 Kinetics of NF-κB transcriptional activity

To identify the time point of maximal NF-κB transcriptional activity, the kinetics of the hCD27 stimulation with anti-hCD27 mAbs were investigated (Figure 4.1). hCD27 NF-κB/GFP Jurkat cells were treated with anti-hCD27 mAbs as h1 or h2 isotypes for 2, 6, or 24 hours, and GFP expression was assessed by flow cytometry (Figure 4.1 A). Incubation of Jurkat cells with all mAbs induced GFP within two hours (Figure 4.1 B and C, respectively). However, the comparison between the 2 and 6 hour time points showed that Jurkat cells displayed an increase in GFP levels with all mAbs (except varli h2 (Figure 4.1 C)), independent of isotype. Similar results were obtained for the comparison between the 6 and 24 hour time points. A 1.8-3.3-fold higher GFP expression was shown with all h1

mAbs after 6 hours incubation (compared to 24 hours), although this was not significant. Anti-hCD27 h2 mAbs showed a significantly stronger GFP induction after 6 hours with AT133-14 h2 (2.3-fold), but all other mAbs investigated also exhibited stronger expression after 6 hours (AT-133-2 h2: 1.3-fold, AT133-5 h2: 2.1-fold, AT133-11 h2: 2.3-fold, varli h2: 2.1-fold). Hence, these results indicate that maximal GFP expression was reached within 6 hours. Accordingly, all subsequent experiments investigating NF-κB transcriptional activity were analysed 6 hours after initial mAb stimulation.

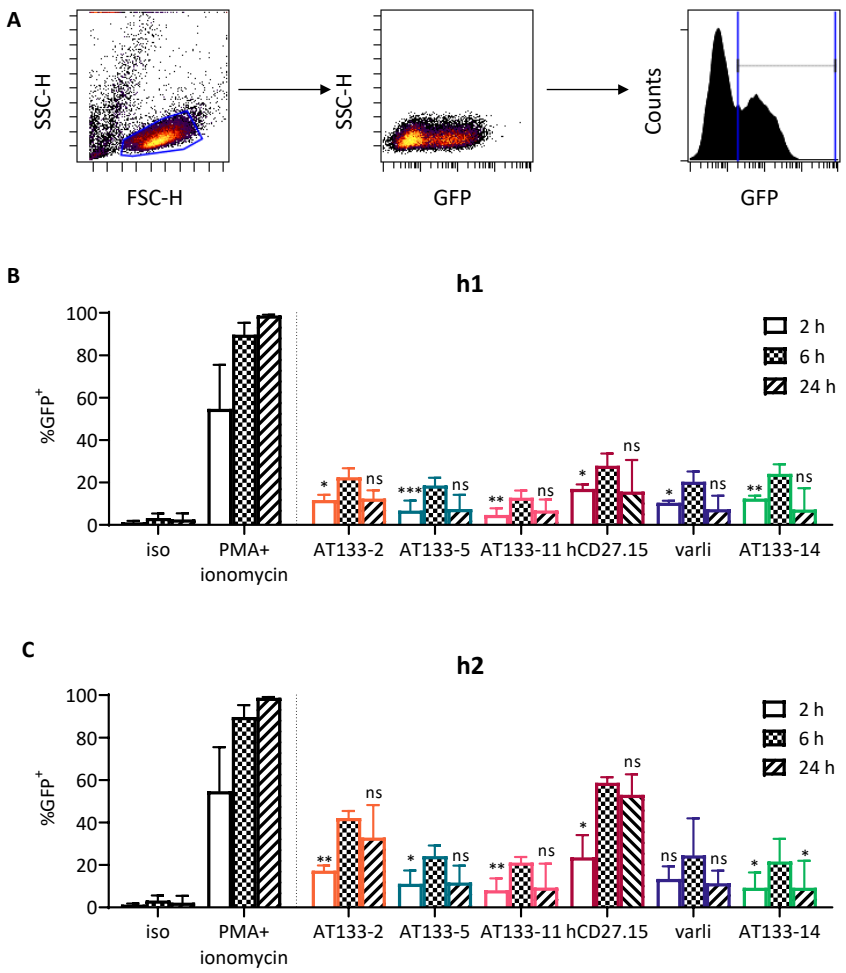

Figure 4.1| Kinetics of anti-hCD27 mAb-induced activation of NF-κB signalling. A: Gating strategy for GFP⁺ hCD27 NF-κB/GFP Jurkat cells upon anti-hCD27 mAb stimulation. **B, C**: hCD27 NF-κB/GFP Jurkat cells were treated with either anti-hCD27 h1 mAbs (B) or anti-hCD27 h2 mAbs (C) at 10 µg/ml, the respective control or PMA and ionomycin as a positive control for 2, 6 and 24 hours. Transcriptional activity, represented by GFP expression, was analysed by flow cytometry (n=4-5). Graphs show the percentage of GFP⁺ hCD27 NF-κB/GFP Jurkat cells. Bars display median with range. Data were assessed using one-way ANOVA with Tukey's test. Displayed is the comparison of the 6 hour with either the 2 hour (asterisk above 2 hour bars) or the 24 hour (asterisk above 24 hour bars) time point; ns: $p > 0.05$, *$p \leq 0.05$, **$p \leq 0.01$.

4.2.2 Agonistic activity of anti-hCD27 mAbs

As discussed in Chapter 1, mAbs of different isotypes can have varying agonistic properties and this seems partially to be dependent on the FcγRs these isotypes engage.[160,169] Thus, anti-hCD27 mAbs

were employed as h1 or h2 to explore the impact of isotype on their ability to activate NF-κB signalling in Jurkat cells (Figure 4.2).

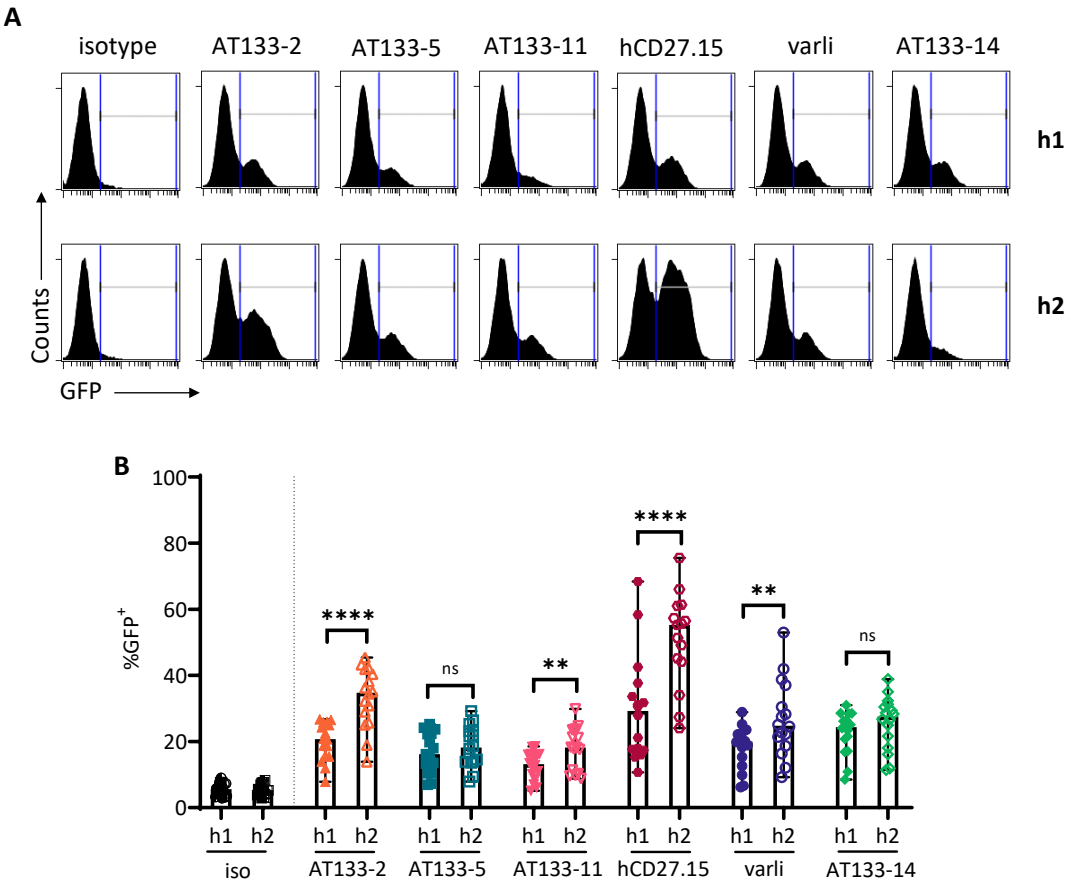

Figure 4.2| Comparison of the agonistic activity of anti-hCD27 h1 and h2 mAbs using an NF-κB/GFP reporter assay. hCD27 NF-κB/GFP Jurkat cells were stimulated with anti-hCD27 h1 or h2 mAbs at 10 µg/ml for 6 hours. GFP expression, representing transcriptional activity, was determined by flow cytometry. **A**: Displayed are representative histogram plots of the GFP expression on hCD27 NF-κB/GFP Jurkat cells after anti-hCD27 h1 or h2 mAb treatment. **B**: The graph shows the percentage of GFP⁺ hCD27 NF-κB/GFP Jurkat cells after stimulation with either anti-hCD27 h1 or h2 (n=15-16). Graph shows median with range and data analysis was performed using one-way ANOVA with Sidak's test; ns: p> 0.05, * p ≤ 0.05, **p ≤ 0.01, ***p ≤ 0.001, ****p ≤ 0.0001.

Treatment of hCD27 NF-κB/GFP Jurkat cells with all anti-hCD27 h1 and anti-hCD27 h2 mAbs resulted in NF-κB signalling as determined by GFP expression (Figure 4.2). Across all mAbs tested, hCD27.15 induced the highest GFP levels (h1: 29.3%, h2: 55.3%) followed by AT133-2 (h1: 20.6%; h2: 34.8%), varli (h1: 20.0%; h2: 24.8%), AT133-14 (h1: 24.4%, h2: 27.6%), AT133-5 (h1: 16.2%, h2: 18.2%) and AT133-11 (h1: 13.2%; h2: 18.2%). All h2 mAbs, with the exception of AT133-5 and AT133-14, induced significantly higher GFP expression when compared to their h1 counterparts; this was also seen with AT133-5 and AT133-14, but to a lesser extent.

As previously discussed, different isotypes can promote varied effector functions, based on their interaction with FcγRs. It was demonstrated that h1 mAbs bind the activating hFcγRI and III with high affinity[155], which can result in cell depletion and weak agonistic activity.[160] However, the

inhibitory hFcγRIIb can function as a cross-linking scaffold for TNFR-targeting h1 mAbs, leading to receptor clustering and enhanced downstream signalling.[162,165,169,265,272,275,276,278] Thus, it was of interest, whether h1-mediated agonism could be improved by Fc-engineering to augment Fc:FcγRIIb interactions, as it was shown for anti-CD40 mAbs. Enhanced agonistic activity with anti-CD40 mAbs was achieved when mAbs were employed as isotypes with enhanced affinity to FcγRIIa and FcγRIIb (h1 SE/LF) or FcγRIIb alone (h1 V9 or h1 V11).[165,279] To investigate, whether this approach was also applicable to anti-hCD27 mAbs, Fc-mutated h1 mAb variants were generated in addition to the WT anti-hCD27 h1 mAbs.

Before the impact of Fc:FcγR interactions on agonistic mAbs was explored, the dose-response of the anti-hCD27 mAbs was investigated in an NF-κB/GFP reporter assay. hCD27 NF-κB/GFP Jurkat cells were incubated with anti-hCD27 h1, h1 V11 (representative for Fc-engineered h1 mAbs) and h2 mAbs at different concentrations, and agonistic activity was assessed by flow cytometry (Figure 4.3).

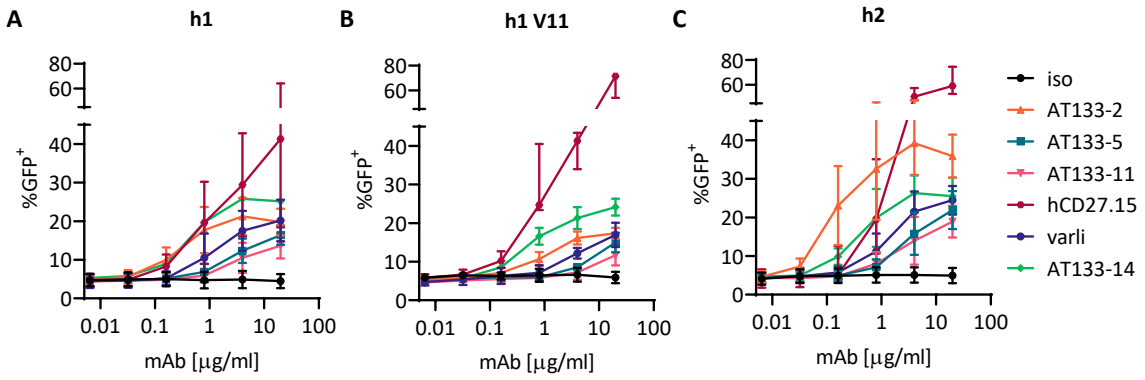

Figure 4.3| Dose titration of anti-hCD27 h1, h1 V11 and h2 mAbs. A-C: hCD27 NF-κB/GFP Jurkat cells were incubated with anti-hCD27 h1 (A), h1 V11 (B) and h2 (C) mAbs at a concentration range of 0.0064-20 µg/ml. After 6 hours, GFP expression was assessed by flow cytometry (n=3-7). Graphs display the percentage of GFP+ NF-κB/hCD27 Jurkat cells and data points show median with range.

Induction of GFP expression with AT133-2 h1, hCD27.15 h1 and AT133-14 h1 was detected at a concentration of 0.16 µg/ml, whereas AT133-5 h1, AT133-11 h1 and varli h1 induced expression at 0.8 µg/ml (Figure 4.3 A). It was observed that AT133-2 h1 V11, hCD27.15 h1 V11 and AT133-14 h1 V11 evoked GFP expression at a concentration of 0.16 µg/ml. In contrast, the h1 V11 variants of AT133-5 and varli displayed a higher activation threshold (4 µg/ml) and AT133-11 only induced GFP expression when added at 20 µg/ml (Figure 4.3 B). The dose titration of anti-hCD27 h2 mAbs differed from h1 and h1 V11 mAbs. Again, AT133-2 and AT133-14 displayed GFP expression when added at 0.16 µg/ml and AT133-5, AT133-11, hCD27.15 and varli at a concentration of 0.8 µg/ml (Figure 4.3 C). Although AT133-2 and AT133-14 induced the highest GFP expression at a

concentration of 4 µg/ml, the majority of the anti-hCD27 mAbs did not induce maximal activation, even at 20 µg/ml (Figure 4.3 C).

However, despite most of the mAbs not reaching maximal activation, the binding analysis (section 3.2.1, Figure 3.1) demonstrated that receptor saturation for the majority of anti-hCD27 mAbs was achieved at a concentration of 4 µg/ml (Figure 4.3). Therefore, all subsequent experiments were performed at an anti-hCD27 mAb concentration of 10 µg/ml to ensure consistent receptor saturation.

4.2.3 Impact of hFcγRIIb engagement and Fc-engineering on mAb mediated agonism

To investigate, whether the agonistic activity of h1 mAbs can be enhanced through Fc-engineering and augmented through hFcγRIIb-mediated cross-linking hCD27 NF-κB/GFP Jurkat cells were co-cultured with WT CHO cells or hFcγRIIb transfected CHO cells and treated with anti-hCD27 mAbs of various isotypes (Figure 4.4): All mAbs were generated as h1, h1 V11, and h2 isotypes, and AT133-5, AT133-11, AT133-14 and hCD27.15 were additionally available as the h1 SE/LF isotype.

Stimulation of hCD27 NF-κB/GFP Jurkat cells with all h1 and h2 mAbs induced GFP expression in the presence of WT CHO cells (Figure 4.4, filled bars), and a trend towards higher GFP levels was detected with h2 mAbs, compared to their h1 counterparts. However, co-culture of hCD27 NF-κB/GFP Jurkat cells with hFcγRIIB expressing CHO cells led to a significantly higher GFP expression with both, anti-hCD27 h1 and h2 mAbs (Figure 4.4, open vs filled bars). Furthermore, the addition of anti-hCD27 h1 variants (h1 V11 and h1 SE/LF) led to significantly higher levels of GFP when cells were co-cultured with hFcγRIIB expressing CHO cells (Figure 4.4, open bars). The comparison of the WT h1 mAbs with their Fc-engineered variants (h1 vs h1 V11 or h1 SE/LF) in presence of hFcγRIIB, revealed significantly higher GFP expression for AT133-11, hCD27.15 (h1 V11 only) and AT133-14.

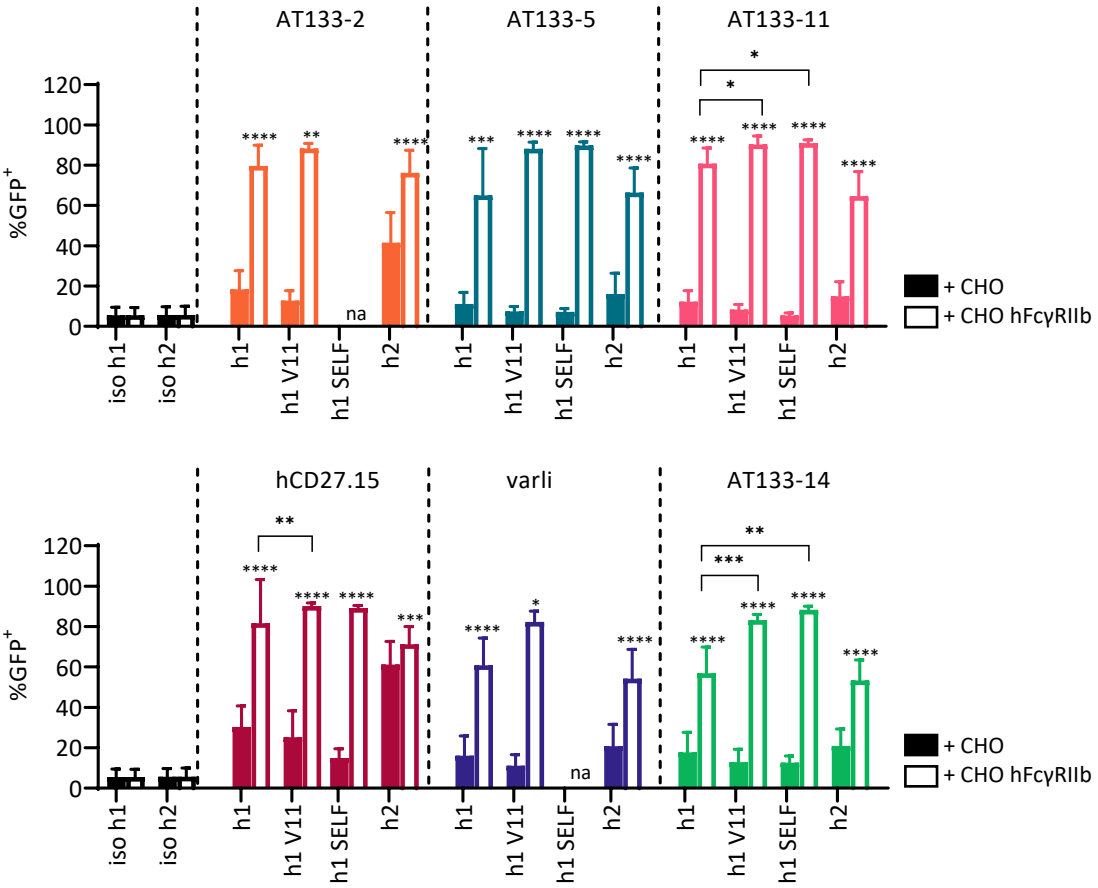

Figure 4.4| Stimulation of hCD27 with anti-hCD27 mAbs in the presence of hFcγRIIb-expressing cells. hCD27 NF-κB/GFP Jurkat cells were either co-cultured with WT CHO cells or hFcγRIIb transfected CHO cells and treated with 10 µg/ml anti-hCD27 h1 or h2 mAbs, the indicated h1 Fc mutants or the respective isotype controls for h1 and h2 mAbs (na: not available). After 6 hours incubation, cells were harvested and GFP expression was analysed by flow cytometry (n=4-15). Graph shows the median percentage of GFP$^+$ cells and error bars show range. Filled bars represent hCD27 NF-κB/GFP Jurkat cells in co-culture with WT CHO cells and open bars in co-culture with hFcγRIIb expressing CHO cells. For statistical analysis, one-way ANOVA with Tukey's test was performed. Non-underlined statistics show the comparison of %GFP after co-culture with WT or hFcγRIIb CHO cells; *p ≤ 0.05, **p ≤ 0.01, ***p ≤ 0.001, ****p ≤ 0.0001.

The hFcγRIIB-transfected CHO cells used in Figure 4.4 express super-physiological levels of hFcγRIIB (Appendix B.2). To investigate the influence of hFcγR engagement in a more physiological environment, human PBMCs, expressing physiological levels of activating hFcγRs and the inhibitory hFcγRIIb, were co-cultured with hCD27 NF-κB/GFP Jurkat cells and stimulated with h1, h1 V11 and h2 isotypes of the anti-hCD27 mAbs (Figure 4.5).

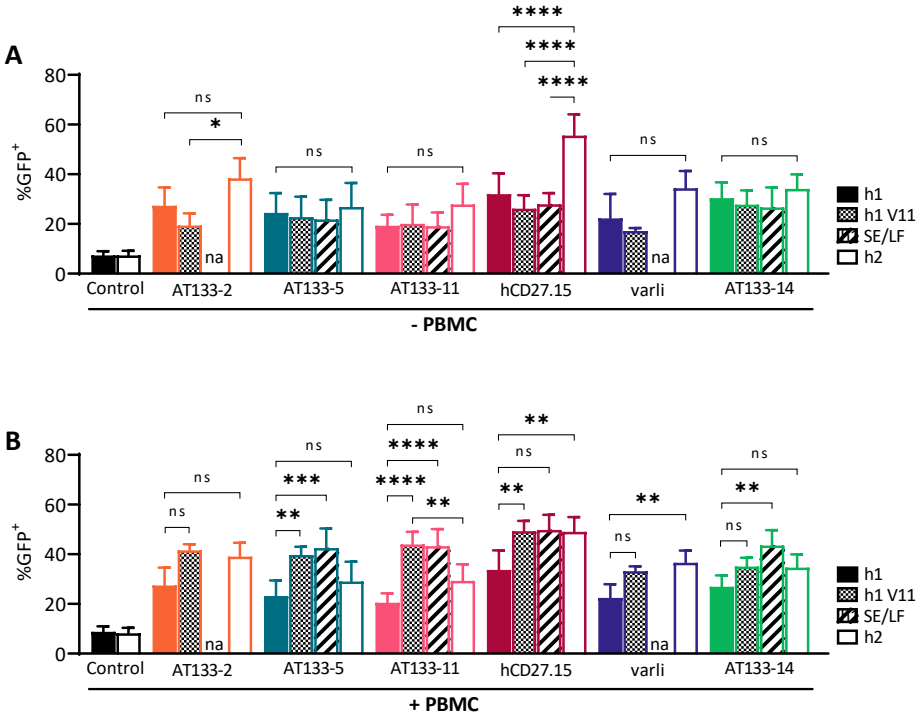

Figure 4.5| Activation of hCD27 NF-κB/GFP Jurkat cells by anti-hCD27 h1, h2 and h1 Fc-variants in the absence or presence of hFcγR-expressing PBMCs. A, **B**: hCD27 NF-κB/GFP Jurkat cells were cultured alone (-PBMC; (A)) or co-cultured with human PBMCs (+PBMC; (B)) and stimulated with 10 µg/ml anti-hCD27 mAb or the respective isotype control for 6 hours at 37°C. Graphs show the percentages of GFP⁺ hCD27 NF-κB/GFP Jurkat cells upon mAb stimulation. Bars represent mean +SD (n=3-9). For statistical analysis one-way ANOVA with Tukey's test was performed; ns: $p > 0.05$, *$p \leq 0.05$, **$p \leq 0.01$, ***$p \leq 0.001$, ****$p \leq 0.0001$.

Stimulation of Jurkat cells (-PBMC; Figure 4.5 A) with all mAbs induced GFP expression, regardless of the isotype. The majority of h2 mAbs evoked stronger agonistic activity than their WT or Fc-mutated h1 counterparts, but this was only significant for AT133-2 (h1 V11 vs h2: 2-fold) and hCD27.15 (h1 vs h2: 1.7-fold, h1 V11 vs h2: 2.1-fold, h1 SE/LF vs h2: 2-fold). However, when Jurkat cells were co-cultured with PBMCs (+PBMC; Figure 4.5 B), the h1 V11 Fc-variant (with enhanced affinity to hFcγRIIb) of AT133-5, AT133-11 and hCD27.15 significantly increased GFP expression in comparison to h1. This trend was also evident for AT133-2, varli and AT133-14. Stimulation with AT133-5, AT133-11 and AT133-14 h1 SE/LF mAbs also resulted in increased GFP levels when compared to h1 and this trend was also apparent for hCD27.15. When h2 mAbs were added to the co-culture of Jurkat cells with PBMCs (Figure 4.5 B), GFP expression was stronger than with WT h1 counterparts. However, with the exception of hCD27.15, Fc-mutated mAbs induced stronger agonism than their h2 counterparts.

Next, the affinities of the anti-hCD27 mAbs measured by SPR and flow cytometry were correlated with their ability to induce NF-κB activation. Bmax, the K_D, k_a and k_d (see section 3.2.2) were compared against the percentage of GFP⁺ hCD27 NF-κB/GFP Jurkat cells after anti-hCD27 mAb stimulation and the correlation coefficient R^2 as well as the p-values calculated (Figure 4.6). None

of the comparisons showed a significant association (Figure 4.6 A). However, removal of hCD27.15, a visual outlier, resulted in significant correlations between the k_a or K_D and NF-κB transcriptional activity, respectively (Figure 4.6 B). Thus, an increase in k_a resulted in elevated GFP expression. The relationship between K_D and activity (%GFP) showed an inverse correlation, where increasing mAb affinities were associated with higher GFP expression. The correlation of the k_d and agonistic activity was not statistically significant. However, a slower k_d and high Bmax were associated with a higher agonistic activity.

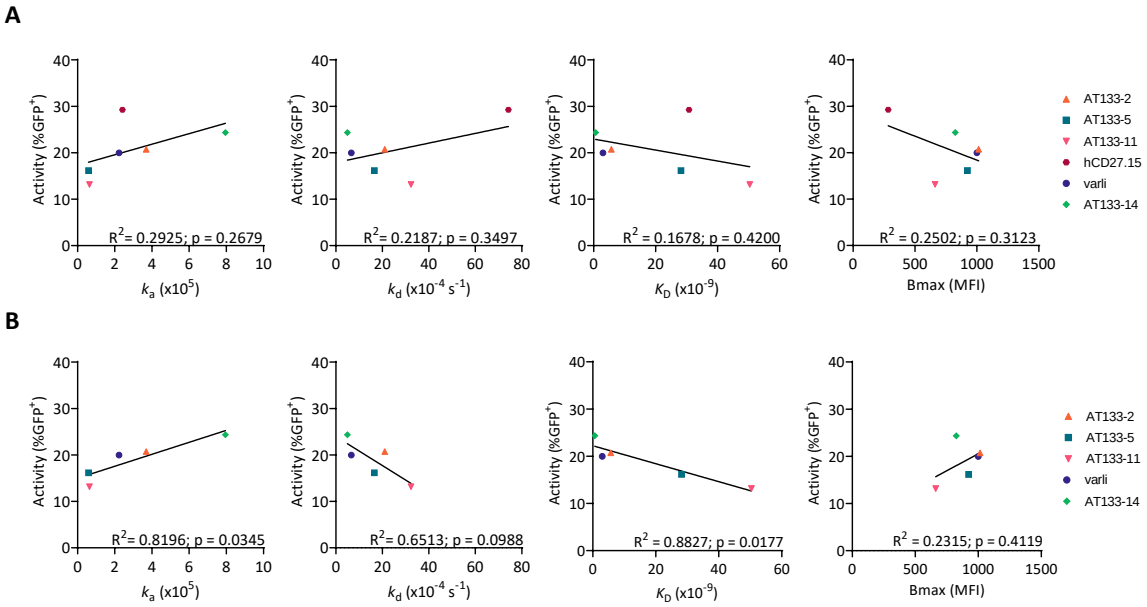

Figure 4.6| Correlation of NF-KB transcriptional activity with k_a, k_d, K_D and Bmax of anti-hCD27 mAbs. Graphs show the correlation of the k_a, k_d, K_D and Bmax of the anti-hCD27 mAbs with their agonistic activity after 6 hours of mAb stimulation (%GFP+). (**A**) Correlation of AT133-2, AT133-5, AT133-11, hCD27.15, varli and AT133-14. (**B**) Correlation of all mAbs, except hCD27.15; ns: $p > 0.05$, *$p \leq 0.05$.

4.3 Downstream signalling of hCD27 through the canonical NF-κB pathway

Ramakrishnan *et al*. previously demonstrated that ligation of hCD27 with CD70 leads to the induction of the canonical NF-κB pathway.[90] Based on these findings, the kinetics of the immediate downstream signalling of the ligation of hCD27 with the anti-hCD27 mAbs were investigated. WT hCD27 transfected Jurkat cells (here referred to as hCD27 Jurkat cells) were stimulated with varli (as currently being tested in the clinic) or hCD27.15 (as the strongest agonist) both as h1 and h2 isotype, or hCD70 Fc (positive control for ligand-mediated signalling) for 5, 10, 15, 20 and 30 minutes. After stimulation, the presence of downstream proteins of the canonical NF-κB signalling pathway such as IκBα and p-IκBα was assessed by western blotting (Figure 4.7).

Stimulation of hCD27 Jurkat cells with varli h1/h2, hCD27.15 h1/h2 and hCD70 Fc led to increased p-IκBα expression, which was most apparent 5 to 10 minutes after mAb stimulation (Figure 4.7 A). Concurrently, a reduction of IκBα was observed for both the anti-hCD27 mAbs and hCD70 Fc, suggesting activation of the canonical NF-κB pathway. Although only weakly, p-IκBα was detectable up to 10 minutes after stimulation with varli and hCD27.15, regardless of the isotype, whereas it was still faintly present upon 15 minutes of incubation with hCD70 Fc. At later time points, p-IκBα was not detectable with any of the indicated reagents. Treatment with hCD27.15 resulted in comparable p-IκBα levels as hCD70 Fc, and higher levels than after stimulation with varli (Figure 4.7 A and B). Across isotypes, h2 mAbs appeared to induce stronger IκBα reduction than the respective h1 counterparts. However, no differences were detected between isotypes for p-IκBα levels.

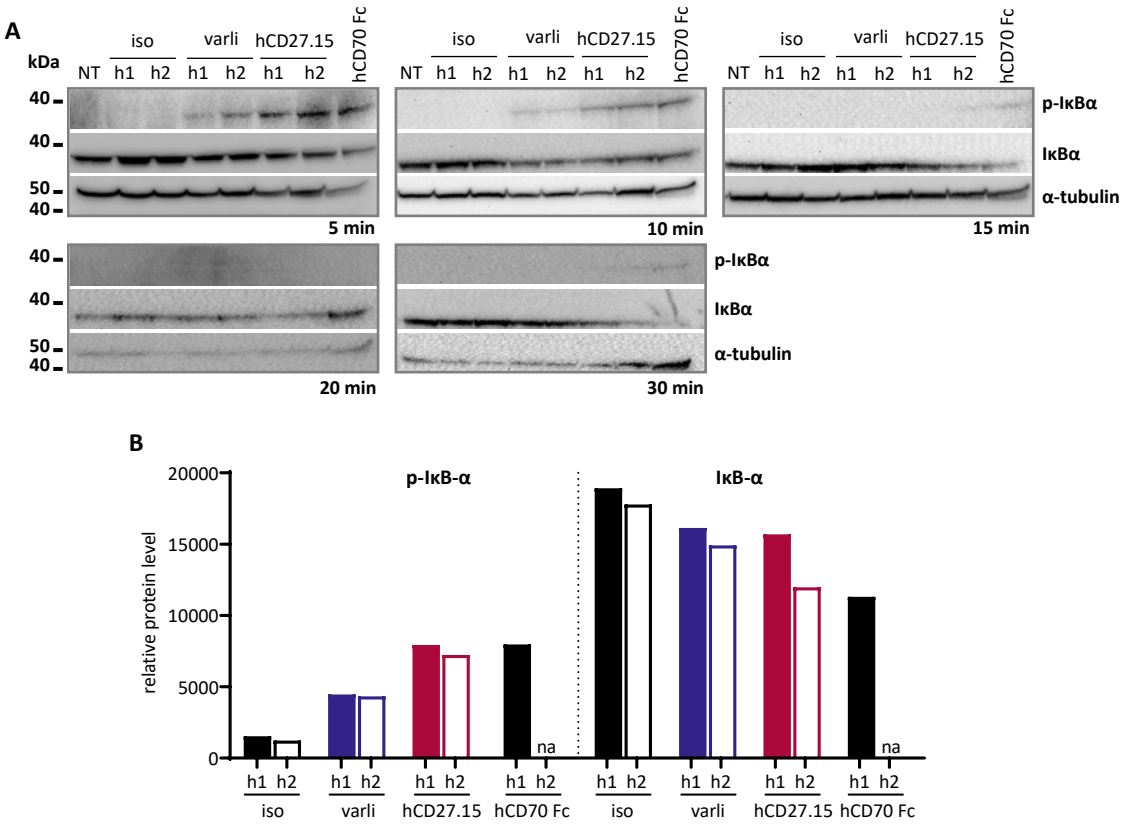

Figure 4.7| Protein levels of IκBα and p-IκBα upon stimulation of hCD27 with anti-hCD27 mAbs or hCD70 Fc. A: hCD27 Jurkat cells were incubated with varli h1, varli h2, hCD271.5 h1, hCD27.15 h2 or hCD70 h1 Fc fusion protein (hCD70 Fc) or the respective isotype controls for 5, 10, 15, 20 and 30 minutes. The abundance of p-IκBα (40 kDa) and IκBα (39 kDa) was determined by western blot. α-tubulin (50 kDa) was used as a positive control. **B**: Graph shows the relative protein levels of p-IκBα and IκBα 5 minutes after stimulation with the anti-hCD27 mAbs or hCD70 Fc. Relative protein levels were determined by densitometry. Data is representative of one experiment.

4.4 Clustering of hCD27 upon mAb stimulation

Activation of TNFRSF members can be dependent on clustering and be mediated either through binding of the cognate receptor ligand or mAbs.[160] It has been demonstrated that the mAb isotype

defines whether the clustering relies on Fc:FcγR engagement, or is facilitated Fc-independently. White *et al.* demonstrated that CD40, a member of the TNFRSF, can be efficiently clustered in a FcγR-independent manner by anti-CD40 h2 mAbs but not their h1 counterparts.[163] Based on these findings, the ability of the anti-hCD27 h1 and h2 mAbs to cluster hCD27 was investigated. Jurkat cells that were stably transfected with a hCD27-GFP fusion protein (hCD27/GFP Jurkat) were treated with anti-hCD27 mAbs for 30 minutes, 2, 6 and 24 hours. These time points were selected based on the NF-κB reporter assay, where the strongest GFP expression was detected 6 hours post-stimulation; and then upon the investigation regarding the hCD27-downstream signalling, where activation of the NF-κB pathway occurred already upon 30 minutes post-stimulation. The assay was performed with anti-hCD27 mAbs selected for distinct features: varli as the clinically relevant mAb with high affinity but moderate agonistic properties. hCD27.15 as the strongest agonist and AT133-2 representative for a moderately agonistic and medium affinity mAb. Lastly, AT133-14 was selected as a weak agonist with high affinity. Figure 4.8 shows hCD27 receptor clustering after 6 hours of anti-hCD27 mAb stimulation (immunofluorescence images for the 30 minutes, 2 and 24 hour time points are displayed in Appendix B.30).

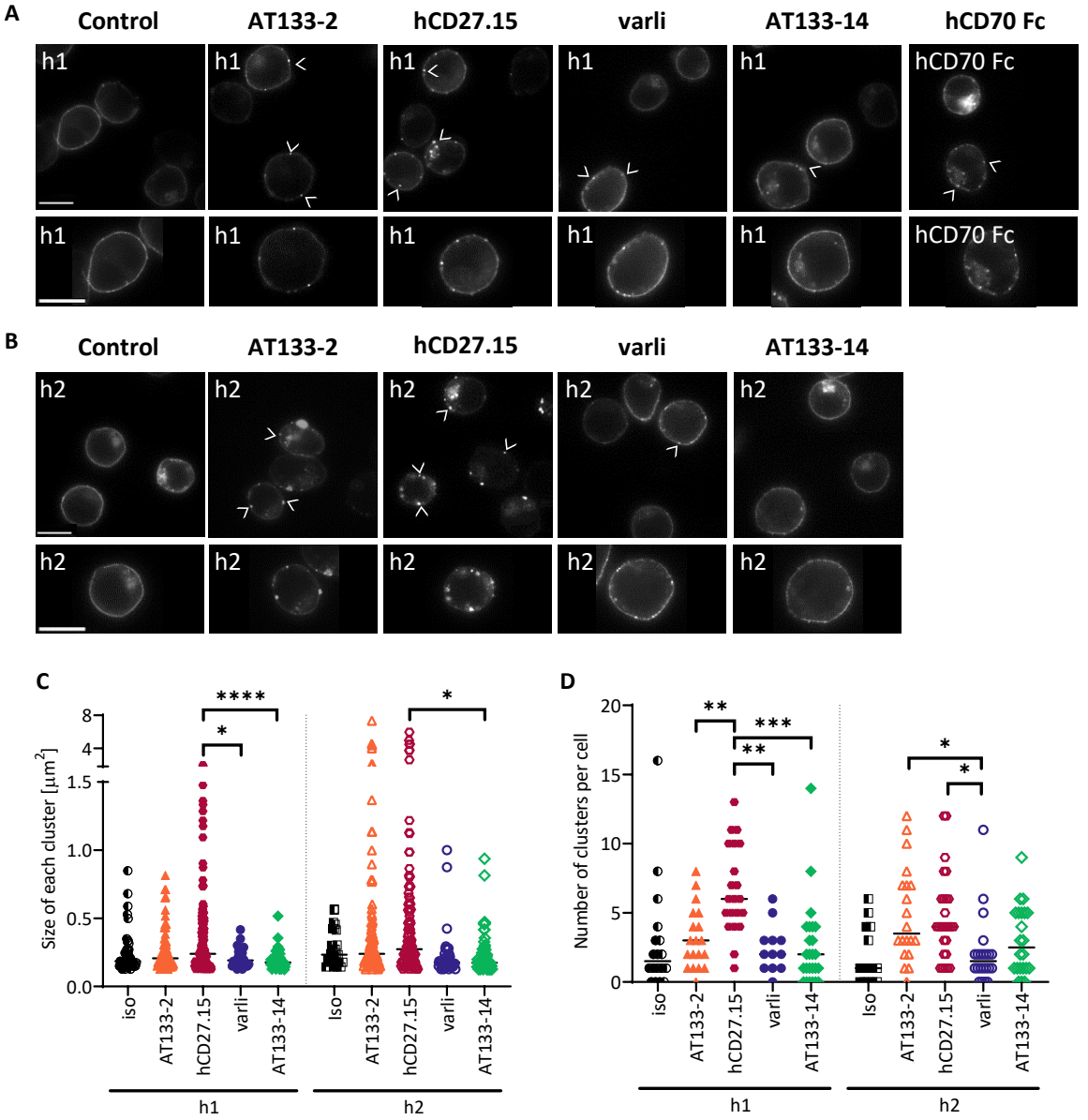

Figure 4.8| Clustering of hCD27 upon anti-hCD27 mAb binding. hCD27/GFP Jurkat cells were incubated for 6 hours with 10 µg/ml of the h1 and h2 isotype of AT133-2, hCD27.15, varli or AT133-14 or hCD70 h1 Fc fusion protein (hCD70 Fc) as well as with the respective controls. Cells were acquired on an ONI Nanoimager in confocal mode (100x lens). **A, B**: Displayed are representative images of receptor clustering after 6 hours of stimulation with either anti-hCD27 h1 (A) or anti-hCD27 h2 (B) mAbs. The bottom panel of A and B shows amplification of selected single cells for each mAb, respectively. The scale bar represents 10 µm. White arrows indicate hCD27 receptor clusters on the cell surface. **C, D:** The size of each cluster per cell (C) and the number of clusters on the cell surface (D) after 6 hours of incubation was determined manually using Image J. Clusters ≥ 0.126 µm^2 were counted. Per condition following numbers of cells were counted: iso h1: 19, varli h1: 12, CD27.15 h1: 21, AT133-2 h1:19, AT133-14 h1: 25, Iso h2: 14. varli h2: 22, CD27.15 h2: 27, AT133-2 h2: 20, AT133-14 h2: 22. Graphs show medians and p-values were determined using one-way ANOVA with Tukey's test; ns: $p > 0.05$, *$p \leq 0.05$, **$p \leq 0.01$, ***$p \leq 0.001$, ****$p \leq 0.0001$.

Puncti were visualised, which were differentially distributed on the cell surface, dependent on the mAb treatment. For mAbs such as AT133-2 and hCD27.15, the puncti were bigger and more concentrated, which is likely to represent receptor clustering. In contrast, puncti observed after varli and AT133-14 treatment appeared smaller (compared to AT133-2 and hCD27.15) and were more evenly distributed, which implies a lower level of receptor clustering. Comparison of the

isotypes revealed marginal differences between varli h1 and varli h2. AT133-14 h1 only led to low levels of clustering, and stimulation with AT133-14 h2 did not show surface clustering. In contrast, treatment with AT133-2 h2 showed more clustering than with the h1 isotype. Across all mAbs, the strongest clustering was observed upon stimulation with hCD27.15, specifically with the h2 isotype compared to the h1 isotype, suggesting more clustering. The clustering ability of AT133-2 and hCD27.15 was thereby similar to those observed with hCD70 Fc.

Following imaging, surface clusters were quantified (intracellular clusters not included), and an average of clusters per cell was calculated (Figure 4.8). The quantification confirmed the visual observations. Treatment of cells with AT133-2 and hCD27.15 led to the formation of bigger clusters as compared to the other anti-hCD27 mAbs (Figure 4.8 C). Furthermore, more clusters were generated upon hCD27.15 binding followed by AT133-2 (Figure 4.8 D). Varli and AT133-14 generally showed smaller clusters and fewer receptor complexes on the cell surface.

Besides the surface clusters, the confocal microscopy also displayed some internal fluorescence in cytoplasmic compartments, possibly indicating hCD27 receptor internalisation upon anti-hCD27 mAb binding (Figure 4.8 A and B).

4.5 Internalisation of hCD27:anti-hCD27 mAb complexes

Receptor internalisation can be evaluated using a surface fluorescence quenching assay (see section 2.12). To investigate hCD27 receptor internalisation, hCD27 Jurkat cells were incubated with Alexa 488-conjugated anti-hCD27 mAbs (AT133-2 and hCD27.15 as strongest agonists, varli as clinically relevant) for 2 and 6 hours (for comparisons, the hCD27 baseline expression at 0 hours was also determined). Subsequently, cells were either left untreated or incubated with anti-Alexa 488 to quench the fluorescence of surface-bound mAbs (Figure 4.9 A and B). Therefore, only the fluorescence of mAbs on the cell surface was subjected to fluorescence quenching, whereas cells, where mAbs were internalised remained fluorescent. This was expressed as % of surface accessible anti-hCD27 mAb (Figure 4.9 C).

No significant reduction of AT133-2 h1 was detectable on hCD27 Jurkat cells, but a trend towards decreased levels of surface accessible AT133-2 h2 was observed (Figure 4.9 C). A reduction of hCD27.15 on the cell surface was detected; nevertheless, this was only significant with hCD27.15 h2. Surface levels of varli were decreased to some extent, but this was not significant.

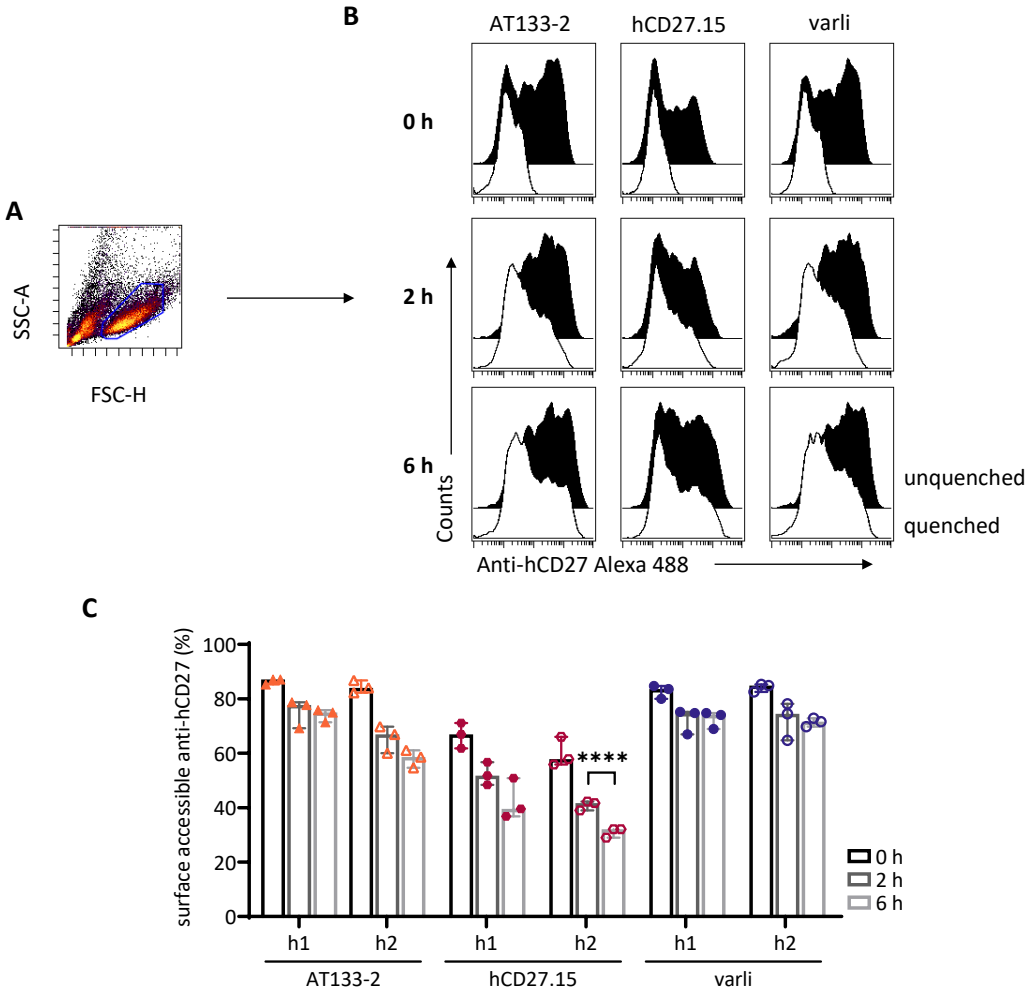

Figure 4.9| Internalisation of hCD27 upon anti-hCD27 mAb binding on hCD27 Jurkat cells. hCD27 Jurkat cells were incubated for 0, 2 or 6 hours with 10 µg/ml Alexa488-labelled AT133-2 h1/h2, CD27.15 h1/h2 and varli h1/h2. After the incubation, cells were split into two tubes. One tube was left untreated, whilst the Alexa-488 fluorescence in the other tube was quenched by adding 25 µg of anti-Alexa488. Fluorescence intensity was subsequently determined by flow cytometry. **A**: Gating strategy for live hCD27 Jurkat cells. **B**: Representative histograms of anti-hCD27 Alexa488 fluorescence (MFI) of paired unquenched and quenched samples after 0, 2 and 6 hours incubation. **C**: The percentage of surface accessible anti-hCD27 was calculated by subtracting the MFI of quenched samples from the MFI of unquenched samples divided by the MFI of unquenched samples. Graph shows median with range from n=3 independent experiments and p-values were determined using one-way ANOVA with Tukey's test; ****p ≤ 0.001.

In addition, internalisation was also investigated on primary human $CD4^+$ T cells (Figure 4.10 A). Receptor internalisation was evident upon incubation with all anti-hCD27 mAbs after 2 hours of incubation (Figure 4.10 B). However, the biggest reduction of surface accessible anti-hCD27 was most prominent after the 6 hour incubation time point for all mAbs investigated (0 vs 6 hours: AT133-2 h1: 1.6-fold, AT133-2 h2: 2.1-fold, hCD27.15 h1: 3-fold, hCD27.15 h2: 2.1-fold, varli h1/h2: 1-4-fold). At the time point of greatest reduction (6 hour time point), the comparison across the h1 mAbs showed that hCD27.15 induced stronger internalisation (Figure 4.10 C). Comparison between the h2 mAbs also showed that hCD27.15 induced the strongest internalisation compared to AT133-2 or varli. However, AT133-2 also resulted in significantly stronger internalisation than varli. Binding of anti-hCD27 mAb to both hCD27 Jurkat cells (Figure 4.9) and PBMCs (Figure 4.10) induced

receptor internalisation and this process was more prominent in PBMCs than in hCD27 Jurkat cells. However, the greatest reduction of surface accessible anti-hCD27 was detected with hCD27.15 in both settings, followed by AT133-2 and varli.

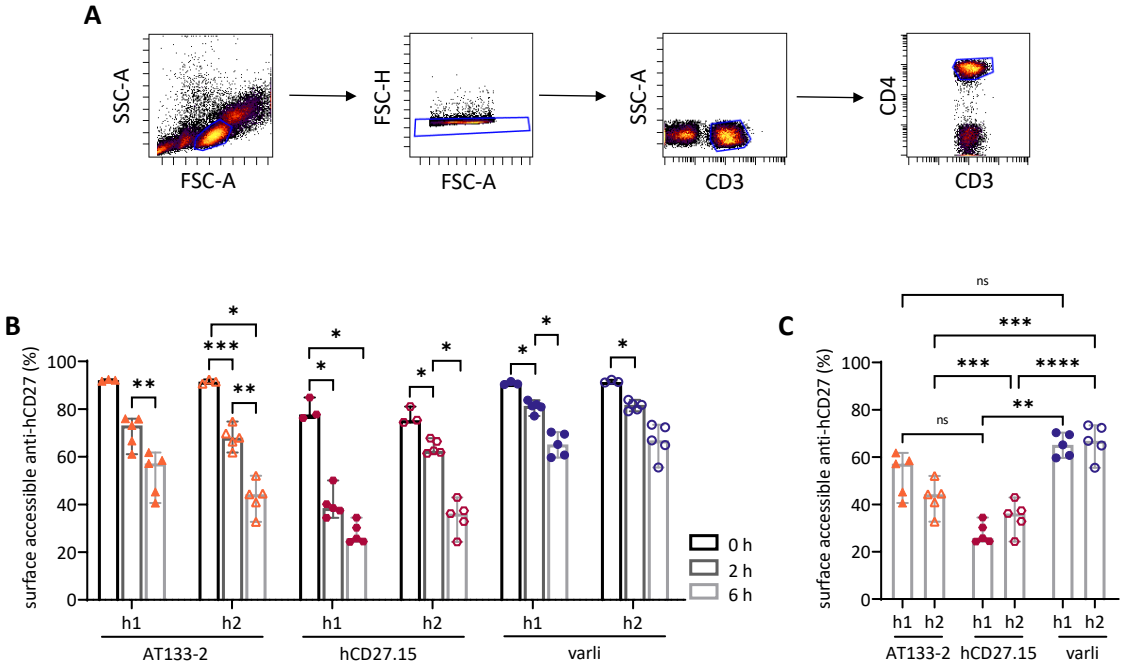

Figure 4.10| Internalisation of hCD27 upon anti-hCD27 mAb binding on human PBMCs. Human PBMCs were incubated for 0, 2 or 6 hours with 10 µg/ml Alexa488-labelled varli h1/h2, CD27.15 h1/h2 and AT133-2 h1/h2. After the incubation, Alexa-488 fluorescence was quenched by adding 25 µg of anti-Alexa488. Fluorescence intensity was subsequently determined by flow cytometry. **A**: Gating strategy used for the identification of $CD4^+$ T cells. **B**: Graph shows the percentage of surface accessible hCD27 after 0, 2 and 6 hours of incubation. Surface accessible hCD27 was calculated by subtracting the MFI of quenched samples from the MFI of unquenched samples divided by the MFI of unquenched samples. **C**: Graph shows the same data as in (B) but only the 6 hour time point for the comparison of internalisation between the anti-hCD27 mAbs. Graphs (B, C) show median with ranges representative of n=3-5 experiments and p-values were determined using one-way ANOVA with Tukey's test; ns: $p > 0.05$, *$p \leq 0.05$, **$p \leq 0.01$, ***$p \leq 0.001$, ****$p \leq 0.0001$.

Receptor internalisation can be facilitated through endocytosis. Upon internalisation, the receptors are packed into vesicles (early endosomes), in which they are selected for two distinct pathways. The receptors can either become recycled and subsequently re-expressed on the cell surface or degraded via the endo-lysosomal degradation pathway.[280] Confocal microscopy was used to investigate the internalisation of the hCD27:anti-hCD27 mAb complexes by detecting their co-localisation with lysosomes, identified by staining for the lysosomal-associated membrane protein (LAMP) 1.[281] Jurkat cells transfected with hCD27 were incubated with fluorochrome-conjugated (Alexa 488) AT133-2, hCD27.15 and varli as h1 or h2 isotypes. After 2 hours (see Appendix B.4) or 6 hours (Figure 4.11), the co-localisation of hCD27:anti-hCD27 mAb complexes with lysosomes was visualised. While some co-localisation was observed with all mAbs of both isotypes, no clear differences were apparent.

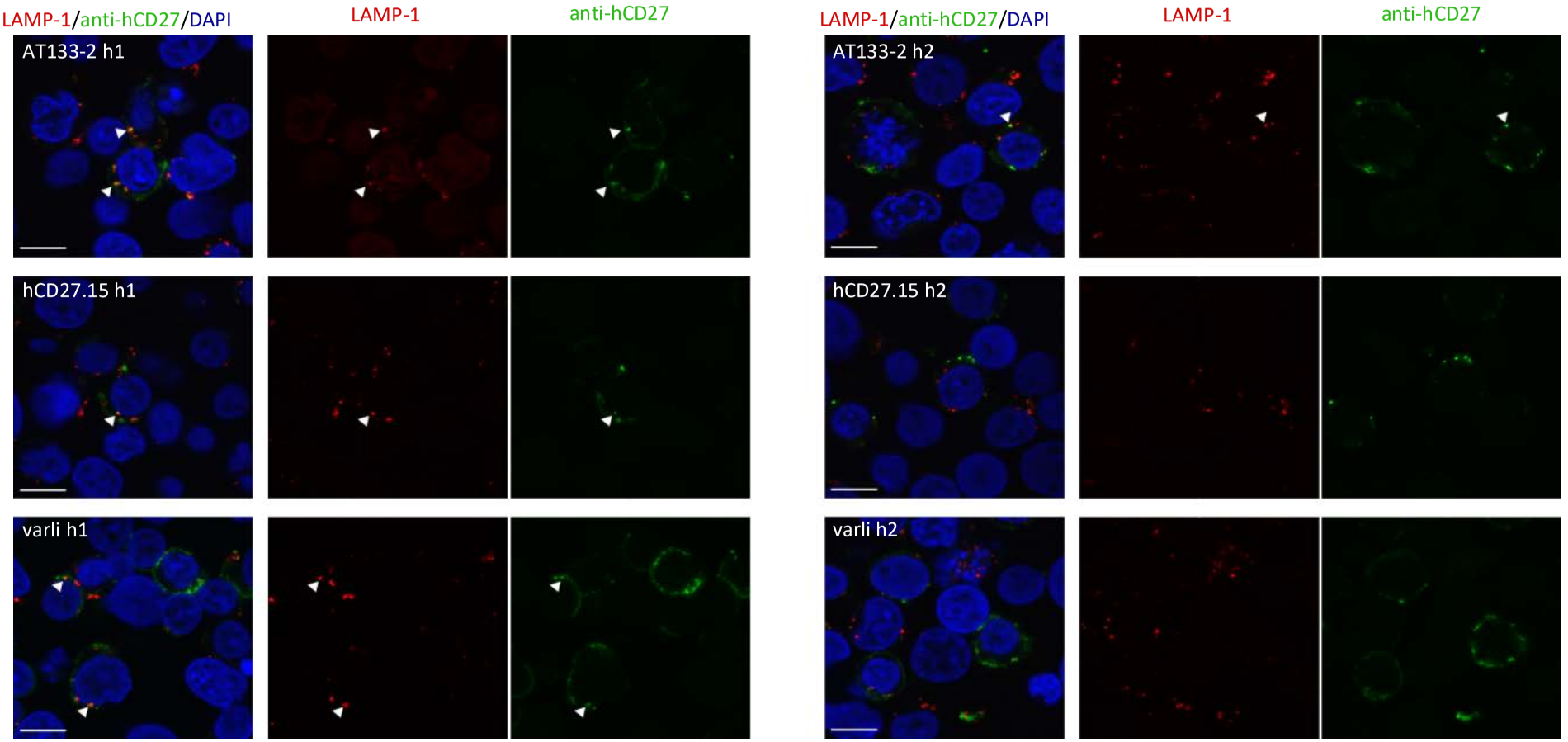

Figure 4.11| Assessment of co-localisation of hCD27:anti-hCD27 mAb complexes with lysosomes by confocal microscopy. Jurkat cells expressing hCD27 Jurkat cells were incubated with the indicated Alexa488-labelled anti-hCD27 h1/h2 mAbs. After 6 hours, cells were stained with a primary antibody to detect LAMP-1 and following with a secondary fluorochrome conjugated antibody (Alexa 647) to detect anti-LAMP-1 binding. Shown are representative images for the 6 hour incubation time point. DAPI was used to visualise cell nuclei (blue) and anti-LAMP1 for lysosomes (red). Binding of anti-hCD27 mAbs to hCD27 is indicated in green. White arrows indicate co-localisation of LAMP-1 and anti-hCD27 mAb staining. The scale bar represents 10 µm. Images were analysed using Adobe Photoshop CS6 software and adjusted for brightness.

4.6 T-cell proliferation in response to anti-hCD27 mAb stimulation

In vitro studies and *in vivo* mouse models of immunisation and infection have demonstrated that stimulation of the CD27 receptor with either CD70 or anti-CD27 mAbs induces $CD8^+$ T-cell proliferation.[85,97-99,106] The NF-κB reporter assay, as described above (see section 4.3), only addresses the immediate downstream signalling upon hCD27-stimulation. Thus, it was of interest, whether hCD27 stimulation with the anti-hCD27 mAbs and subsequent signalling results in $CD8^+$ T-cell proliferation. Isolated human PBMCs were labelled with CFSE and stimulated with a sub-optimal dose of a CD3-specific mAb and the anti-hCD27 mAbs. Four days post-stimulation T-cell proliferation was assessed by determining the CFSE-dilution of $CD8^+$ T cells by flow cytometry.

Microscopic evaluation of PBMCs after anti-hCD27 mAb stimulation showed differences between the various isotypes (Figure 4.12 A). Small cell clusters, indicating proliferating cells, were visible in PBMC cultures treated with the isotype control, whereas no clusters were detected upon h1 mAb treatment. Stimulation with h1 V11 and h2 mAbs, in contrast, resulted in the increased formation of bigger cell clusters. However, the clusters were more abundant with anti-hCD27 h1 V11 than with the anti-hCD27 h2 mAbs. These differences were also apparent in the representative histogram plots displayed in Figure 4.12 B, where CFSE dilution was representative of $CD8^+$ T-cell divisions. Figure 4.12 C, D and E summarise the $CD8^+$ T-cell proliferation after stimulation with anti-hCD27 h1, h1 V11 and h2 mAbs. Treatment of $CD8^+$ T cells with anti-hCD27 h1 mAbs did not evoke T-cell proliferation (Figure 4.12 C). On the contrary, T-cell proliferation was reduced or even suppressed upon the addition of h1 mAbs. Stimulation of PBMCs with anti-hCD27 h2 mAbs induced proliferation to some extent. However, this was not significantly different from isotype-treated cells (Figure 4.12 E). In contrast, h1 V11 mAbs induced substantial T-cell proliferation and this was significant for all mAbs, except varli. Comparisons within the h1 V11 mAbs showed that AT133-5 and AT133-11 were the strongest agonists, followed by hCD27.15 and AT133-2 (Figure 4.12 D). Across isotypes, AT133-2, AT133-5, AT133-11, hCD27.15 and AT133-14 h1 V11 induced more T-cell proliferation then their h2 counterparts (AT133-2: 1.1-fold, AT133-5: 1.3-fold, AT133-11: 2.2-fold, hCD27.15: 1.9-fold, AT133-14: 1.6-fold). In contrast, varli induced 1.6-fold higher $\%CD8^+$ T-cell proliferation when added as h2 compared to h1 V11.

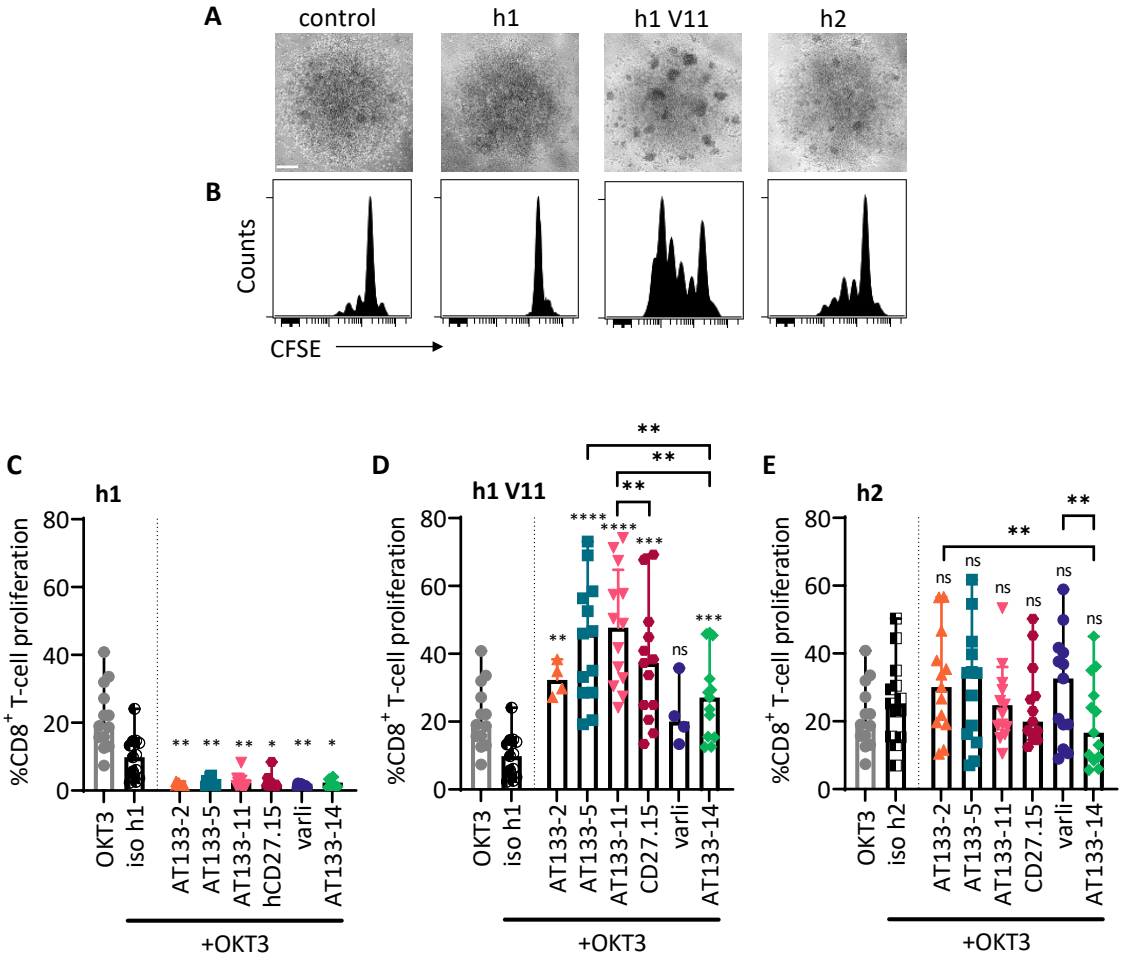

Figure 4.12| Proliferation of CD8⁺ T cells upon anti-hCD27 mAb co-stimulation. Frozen PBMCs were thawed and stimulated with anti-CD3 mAb (clone OKT3, mIgG2a, 0.5-0.005µg/ml) and 10 µg/ml anti-hCD27 h1, h1 V11 or h2 mAbs. Four days after stimulation, cells were harvested and proliferation of CD8⁺ T cells was assessed. **A:** Representative microscopy images of PBMCs after stimulation with anti-hCD27 h1, h1 V11 or h2 mAbs. Images were acquired with an Olympus CKX41 microscope (40x lens) and scale bar represents 200 µm. **B**: Representative histograms of the proliferation of CD8⁺ T cells upon stimulation with anti-hCD27 h1, h1 V11 and h2 mAbs. **C-E:** Graphs show the median percentage of CD8⁺ T-cell proliferation represented by cells that have undergone more than one division upon anti-hCD27 h1 (C), h1 V11 (D) and h2 (E) stimulation (n=4-13). Each data point indicates one donor and shows the mean of technical triplicates. Error bars show range and statistical analysis was performed using one-way ANOVA with Tukey's test; ns: $p > 0.05$, *$p \leq 0.05$, **$p \leq 0.01$, ***$p \leq 0.001$, ****$p \leq 0.0001$. Non-underlined statistics show comparisons between the isotype control and the mAbs and underlined statistics display comparisons between anti-hCD27 mAbs.

Next, the dose-response of the CD8⁺ T-cell proliferation upon anti-hCD27 mAb stimulation was investigated for h1 V11 and h2 mAbs (Figure 4.13). Titration of anti-hCD27 h1 mAbs was not performed, since these mAbs did not induce CD8⁺ T-cell proliferation at a concentration of 10 µg/ml as shown in Figure 4.12.

Stimulation of PBMCs with anti-hCD27 h1 V11 mAbs implied dose-dependency; maximal dose-response was reached with all mAbs (AT133-2, varli, AT133-14: 0.1 µg/ml, hCD27.15: 1 µg/ml), except with AT133-5 and AT133-11. With decreasing mAb concentrations, %CD8⁺ T-cell proliferation decreased concurrently and this was true for all mAbs (Figure 4.13 A). Most of the anti-hCD27 h2 mAbs did not follow a typical dose-response (Figure 4.13 B). Although not reaching

maximal proliferation, AT133-2 induced the highest T-cell proliferation at a concentration of 5 µg/ml. Stimulation of PBMCs with different concentrations of AT133-5 h2 did not show notable differences in T-cell proliferation. AT133-11 and hCD27.15 displayed similar dose-response patterns; both mAbs reached the highest $CD8^+$ T-cell proliferation at concentrations of 0.05 and 5 µg/ml and were less effective at lower concentrations. Varli h2 in contrast differed from the other mAbs and evoked the highest $CD8^+$ T-cell proliferation at 0.05 µg/ml. Concentrations below or above led to marginally lower levels of proliferated $CD8^+$ T cells.

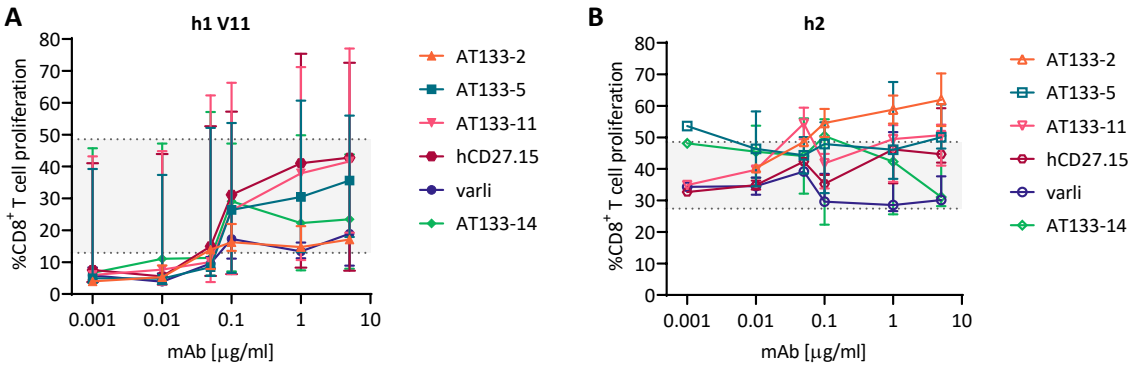

Figure 4.13| Dose-response of $CD8^+$ T-cell proliferation upon anti-hCD27 mAb stimulation. A, B: Frozen PBMCs were thawed and stimulated with anti-CD3 mAb (clone OKT3, mIgG2a, 0.5-0.005 µg/ml) and 0.001, 0.01, 0.05, 0.1, 1 and 5 µg/ml anti-hCD27 h1 V11 (A) or h2 (B) mAbs. After 4 days of incubation, cells were harvested and $CD8^+$ T-cell proliferation was assessed by flow cytometry. Data points represent the median percentage of $CD8^+$ T-cell proliferation (from the mean of technical triplicates of n=3-6 donors) represented by cells that have undergone more than one division. Error bars show range. The grey-shaded area shows the range of suboptimal CD3 stimulation.

Next, it was investigated, whether the results obtained in the *in vitro* T-cell proliferation assay translated to an *in vivo* endogenous response in hCD27tg C57/BL6 mice. These mice are transgenic for hCD27, but express mFcγRs. Thus, the anti-hCD27 m1 mAb format was selected for its specificity to hCD27 and its ability to bind the inhibitory mFcγRIIb with high affinity, which can contribute to receptor clustering and enhanced activity. The hCD27tg C57/BL6 mice were immunised with OVA and treated with the anti-hCD27 m1 mAbs and the percentage of $SIINFEKL^+CD8^+$ T cells was assessed in the blood over a time course of 14 days (Figure 4.13 A). Treatment with all anti-hCD27 mAbs and anti-CD40 mAb increased $SIINFEKL^+CD8^+$ T cells (Figure 4.13 B and C). The percentage of $SIINFEKL^+CD8^+$ T cells increased over time and the peak response was reached 7 days post mAb treatment (Figure 4.13 D).

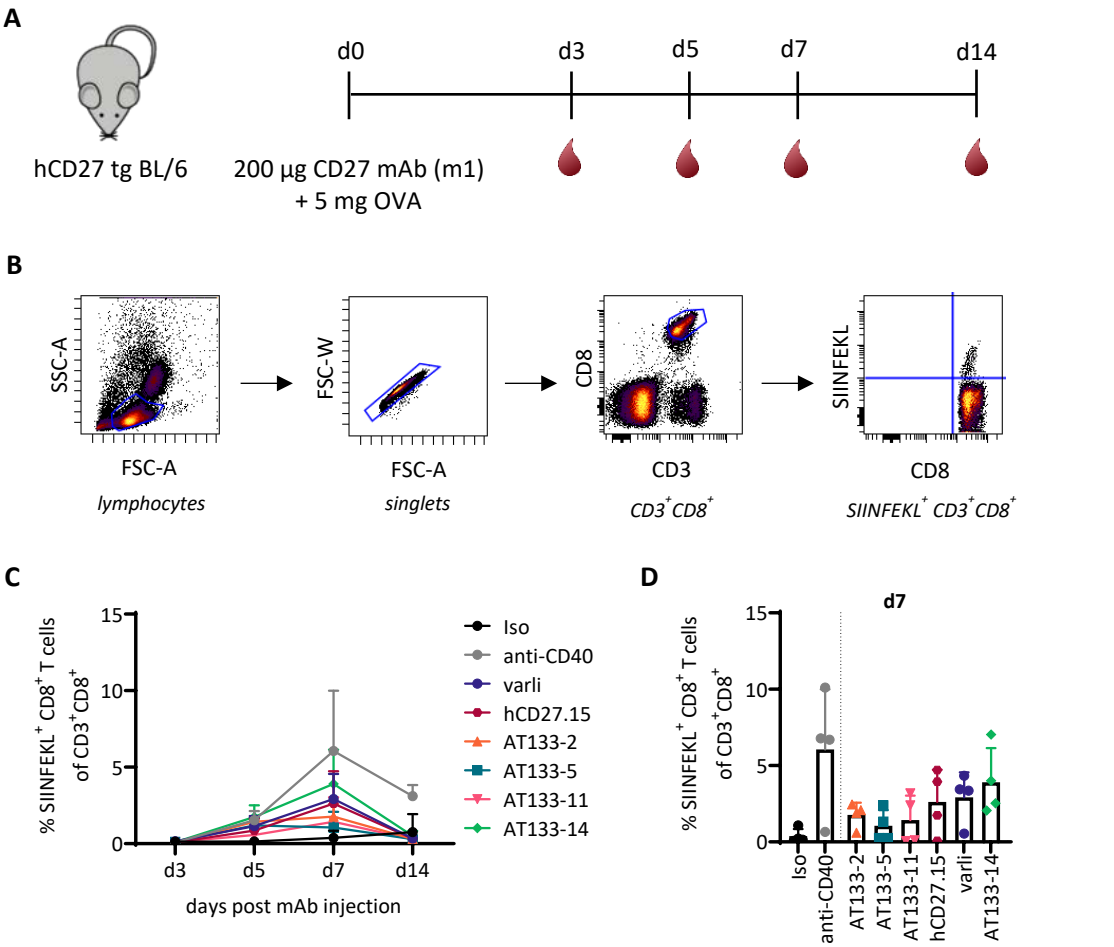

Figure 4.14| Endogenous CD8⁺ T-cell response to anti-hCD27 mAb treatment *in vivo*. A: hCD27tg C57/BL6 mice were intraperitoneally (i.p.) immunised with 5 mg OVA and treated with anti-hCD27 m1 mAbs, anti-mCD40 m1 mAb (3/23) or the irrelevant isotype control (3G8 m1) (200 µg, i.p.) on day 0. Subsequently, the percentage of SIINFEKL⁺ CD8⁺ T cells was determined in the blood on days 3, 5, 7 and 14 by flow cytometry. **B**: Gating strategy for SIINFEKL⁺CD8⁺ T cells. **C**: Graph shows the percentage of SIINFKEL⁺CD8⁺ T cells of CD3⁺CD8⁺ T cells (n=4 mice per group from one experiment). **D**: Graph shows same data as in (C) for comparison of %SIINFEKL⁺CD8⁺ T cells in response to the anti-hCD27 mAbs on day 7 post-immunisation. Graphs (C and D) show mean + SD.

4.7 Chapter discussion

In this chapter, the agonistic activity of the anti-hCD27 mAbs was investigated *in vitro* and *in vivo*. Using NF-κB-GFP reporter assays, western blotting and T-cell proliferation assays, the impact of mAb isotype on hCD27 agonism was assessed. Furthermore, the ability of the anti-hCD27 mAbs to mediate receptor clustering as well as the impact of the mAb isotype was explored.

It was shown previously that mAb effector functions rely on Fc:FcγR interactions and are dictated by the mAb isotype.[155,282] Thus, the choice of the isotype might have a substantial impact on the efficacy of therapeutic mAbs. Literature suggests that the therapeutic potential of direct targeting mAbs of the h1 isotype such as rituximab is crucially dependent on the engagement with activating hFcγRs.[283] In contrast, immunostimulatory h1 mAbs have been shown to require cross-linking to be therapeutically active, which can be provided by the sole inhibitory hFcγRIIb.[162,276] In contrast, h2 mAbs were able to mediate receptor-crosslinking hFcγR-independently and were more agonistic than h1 mAbs.[163] Similarly, when the isotypes of the anti-hCD27 mAbs were compared, it was generally observed that h1 mAbs induced less NF-κB transcription than h2 mAbs (Figure 4.2 and Figure 4.4). However, the agonistic activity of h1 mAbs was dramatically improved in the presence of hFcγRIIb (Figure 4.4 and Figure 4.5), further confirming the contention that agonistic activity of immunomodulatory TNFRSF-targeting h1 mAbs is crucially reliant on Fc:FcγRIIb interactions. Employment of Fc-engineered anti-hCD27 h1 mAbs (h1 V11, h1 SE/LF[164,166]) with increased affinity to hFcγRIIb was shown to further enhance the agonistic activity in presence of hFcγRIIb expressing cells (Figure 4.4 and Figure 4.5) and this is congruent with published research. For example, Zhang and colleagues reported a 2-fold increase in transcriptional activity after hOX40 expressing HEK-Blue reporter cells were co-cultured with hFcγRIIb expressing Raji cells and treated with Fc-engineered OX40SF2 h1 SE/LF or h1 V12 mAbs. However, and in contrast to the results obtained in this project, the presence of hFcγRIIb could not improve the agonistic activity of the WT anti-hOX40 h1 mAb.[278] Of note, stimulation of hCD27 NF-κB/GFP Jurkat cells with anti-hCD27 h2 mAbs resulted in increased transcriptional activation when co-cultured with hFcγRIIb expressing CHO cells. Despite the aforementioned studies, which proposed h2 mAbs to mediate agonism independent of Fc[163,169], the work by Zhang *et al*. and Dahan *et al*. suggests otherwise.[165,278] They proposed that the agonistic efficacy of immunostimulatory anti-CD40 h2 mAbs is dependent on Fc:FcγR interactions.[165,278] However, hFcγRIIb transfected CHO cells express super-physiological levels of hFcγRIIb that might account for this observation. Therefore, to investigate the anti-hCD27 h1 and h2 mAbs in a more physiological manner, hCD27/NF-κB Jurkat cells were cultured in presence of human PBMCs and stimulated with anti-hCD27 mAbs (Figure 4.5). PBMCs contain multiple immune cell subsets, which not only provide cells expressing the inhibitory hFcγRIIb but also activating hFcγRs. As elucidated

above, anti-hCD27 h1 mAb mediated agonism was improved in the presence of hFcγRIIb expressing cells. However, this could not be reproduced when h1 mAbs were co-cultured with PBMCs. It is known that h1 mAbs bind to activating hFcγRs with higher affinity than to the inhibitory hFcγRIIb. [284], and hence have a higher A:I receptor engagement ratio. This is theoretically accompanied with lower agonistic activity and could be a possible explanation for the lack of agonism when used in an environment with both, inhibitory and activating hFcγRs (Figure 4.5). However, decreasing the A:I ratio by employing Fc-engineered anti-hCD27, h1 V11 and h1 SE/LF mAbs, resulted in enhanced agonistic efficacy of the WT h1 mAbs. This confirmed the hypothesis that the agonistic activity of h1 mAbs crucially relies on hFcγRIIb-crosslinking and that it can be enhanced through Fc-engineering as shown for other TNFR targeting mAbs[165,278]. Further, anti-hCD27 h2 mAb activity was not affected by the changed A:I ratio upon co-culture with PBMCs (Figure 4.5), indicating that h2 mAb mediated agonism is not reliant on Fc engagement. This differs from the results obtained in the aforementioned NF-κB/GFP reporter assay (Figure 4.4). However, PBMCs more accurately resemble a physiological hFcγR environment than the hFcγRIIb expressing CHO cells, which generates more valid and representative results. Furthermore, these results are supported by literature on other TNFRs, which suggests that h2 mAb activity does not rely on hFcγRIIb-interactions due to its very low affinity to hFcγRs.[160,163,169,277]

NF-κB transcriptional activation and T-cell proliferation are closely interlinked. Proliferation of $CD8^+$ T cells upon hCD27 stimulation was observed *in vivo* and *in vitro* (Figure 4.12 and Figure 4.14). Differences between h1 and h2 mAbs observed in the NF-κB reporter assays (Figure 4.2) were also, to some extent, reflected in the T-cell proliferation assay. T-cell proliferation was only moderately induced with h2 mAbs, whereas h1 mAbs were inactive and induced a reduction of T-cell proliferation. This might due to h1 mAbs interacting with activating hFcγRs on effector cells[284], leading to cell death via ADCC, resulting in reduced T-cell proliferation. However, isotype switching of WT h1 into Fc-mutated h1 V11 mAb variants dramatically enhanced T-cell proliferation, highlighting the importance of the requirement of hFcγRIIb engagement for h1 mAb agonism. Interestingly, Fc mutation did not enhance T-cell proliferation with all anti-hCD27 mAbs equally, possibly indicating that agonism may also be affected by other determinants such as epitope specificity (detailed in Chapter 7).

Similar results were obtained for other immunostimulatory mAbs such as anti-CD40 mAbs. Studies investigating B-cell proliferation (either splenic B cells from hCD40tg mice[169] or human PBMCs[163]) in response to anti-CD40 mAbs (ChiLob 7/4, SGN40, CP870,893) of different isotypes demonstrated that only the addition of anti-hCD40 h2 mAbs resulted in B-cell proliferation, whereas the h1 counterparts were inactive. However, and in accordance with the results presented here, when B

cells were cultured in presence of cells super-physiologically expressing hFcγRIIb, similar levels of activation upon anti-hCD40 mAb stimulation were observed, and this was independent of the isotype.[169] Dahan *et al*. further generated the SE/LF and V11 variants of the anti-hCD40 h1 mAb CP870,893. Treatment with anti-CD40 h1 V11, but not h1 SE/LF or h2, resulted in an anti-tumour specific T-cell expansion in OVA-DEC immunised mice and a superior anti-tumour response in MC38 or B16 melanoma bearing hCD40/FcγRtg mice.[165] *In vivo* studies comparing m1 and m2a isotypes of TNFR-targeting mAbs further underline the impact of the isotype on agonistic activity.[242,273,274,276] mIgG2a mAbs preferentially engage activating FcγR similar to h1 mAbs.[282] In contrast, m1 mAbs display strong affinity to the inhibitory mFcγRII[284] and mediate agonism through receptor-crosslinking. Therefore, treatment with anti-mCD40 m1 mAb resulted in substantial $CD8^+$ T-cell expansion, whereas the m2a isotype failed to induce agonism.[276] Similar results were obtained for mAbs targeting OX40, 4-1BB or CD27. However, in contrast to anti-CD40 mAb, the m2a isotype was not inactive but resulted in $CD8^+$ T-cell expansion in response to mAb-mediated Treg depletion.[242,273,274] Of note, the study conducted by Wasiuk *et al*. demonstrated that mAb performance might be dependent on the tumour type.[242]

Members of the TNFRSF are crucial for immune homeostasis since they are associated with immune cell activation but also facilitate negative signals to dampen immune responses. It is well known, that agonistic TNFR mediated signalling requires receptor oligomerisation. This was demonstrated in a recently published study investigating TNFR clustering (CD40, OX40, 4-1BB) in response to TNFR targeting mAbs of different isotypes. Generally, h2 mAbs showed greater receptor clustering than h1 mAbs and this correlated with stronger agonistic activity.[277,285] Anti-hCD27 mAbs resembled these observations. Thus, stronger agonistic mAbs such as hCD27.15 or AT133-2 induced more receptor clustering on the surface, whereas the weaker agonists varli and AT133-14 displayed weak receptor clustering. However, the impact of the mAb isotype was not as prominent. Interestingly, and against expectations, Yu *et al.* found that bigger receptor clusters were not associated with stronger agonism. On the contrary, stochastic optical reconstruction microscopy (STORM) analysis showed the formation of smaller clusters with high receptor density for highly agonistic mAbs, whereas weak agonists failed to induce notable receptor clusters. This data supports the notion that receptor clustering is essential for effective TNFR mediated agonism and highlights that secondary receptor clustering might be necessary for h1 mAb efficacy. However, to date, the underlying mechanism governing higher receptor oligomerisation has not been fully elucidated. A two-step model for ligand-mediated oligomerisation has been proposed; step 1 entails the assembly of a trimeric TNFR ligand with its TNFR followed by step 2, where trimeric receptor-ligand complexes are drawn into higher-order oligomerisation through the pre-ligand assembly domain

(PLAD).[286] However, receptor clustering facilitated by TNFRSF-targeting mAbs might be more complex and needs further investigation.

In conjunction with receptor clustering, internalisation of hCD27:anti-hCD27 complexes was investigated by flow cytometry and confocal microscopy. Some co-localisation of hCD27:anti-hCD27 mAb complexes with lysosomes was observed (Figure 4.11) and greater internalisation was detected with the more agonistic mAbs by flow cytometry (Figure 4.9 and Figure 4.10). Martinez-Forero and colleagues also investigated internalisation of the TNFR 4-1BB upon anti-4-1BB mAb ligation. 4-1BB agonists induced receptor internalisation on 4-1BB expressing HEK293T cells and primary $CD4^+$ and $CD8^+$ T cells *in vitro* and on TCR-tg OT-1 $CD8^+$ T cells *in vivo*. Furthermore, the group found that greater internalisation occurred, when mAbs were cross-linked with a secondary mAb, indicating that greater oligomerisation might lead to greater receptor internalisation.[287] To date, the impact of TNFR internalisation upon mAb binding is not fully clarified. However, the authors suggest the formation of a "4-1BB signalosome" upon internalisation, which is able to maintain intracellular signalling. Furthermore, it was proposed that mAb-mediated removal of the receptor from the cell surface might prevent mAb:complement interactions or the formation of autoantibodies against circulating TNFRSF targeting mAbs.[287]

Taken together, the results obtained from the functional characterisation of the anti-hCD27 mAb panel revealed the isotype to be a pivotal determinant of the anti-hCD27 mAb-mediated agonism. h2 mAbs generally were stronger agonists, but weak agonism of h1 mAbs was overcome by hFcγRIIb cross-linking and augmented by Fc-engineering. However, research shows that the efficacy of therapeutic mAbs can be affected by other aspects, such as the abundancy of cross-linking hFcγRIIb in the tumour microenvironment, the expression of mAb targets on various cell types, the presence of Tregs and their TNFR expression in the tumour microenvironment, epitope specificity and the isoform of the mAb isotype (in the case of h2 mAbs). White *et al.* and Yu *et al.* demonstrated that conformational changes of the immunostimulatory anti-hCD40 h2 mAbs into the h2B isoform, which is hypothesised to be more rigid and constrained, leads to increased agonistic activity.[163,169] Moreover, the importance of epitope binding has previously been demonstrated for the direct targeting anti-CD20 mAb, rituximab[170] and mAbs targeting TNFRs CD40[169], OX40[274] and 4-1BB[272]. The aforementioned aspects, particularly the complex interplay of both epitope and isotype should be carefully evaluated when generating clinically relevant therapeutic mAbs (discussed in Chapter 7).

Chapter 5 Anti-CD27/anti-CD38 mAb combination therapy *in vivo*

5.1 Introduction

Anti-cancer immunity is mediated through immune surveillance. This process, also referred to as the cancer immunity cycle, entails seven major steps: It is initiated through the release of cancer antigens (step 1) and their cross-presentation to MHC on APCs (step 2). APCs that have encountered cancer antigens subsequently migrate to SLOs where they mediate T-cell priming and activation (step 3). Activated tumour-antigen specific T cells subsequently migrate to (step 4) and infiltrate (step 5) tumour sites and mediate tumour cell destruction through antigen recognition on the tumour cells via their TCR (step 6 and 7). Each step of this cycle is tightly regulated by a number of inhibitory and activating components such as immune checkpoint (e.g. CTLA-4) and co-stimulatory molecules (e.g. CD28, 4-1BB, OX40, CD27) in the stage of T-cell priming and activation (step 3).[288] Anti-cancer reagents target specific steps of this cycle with the aim to induce or enhance anti-tumour responses. As such, for example mAbs targeting check point molecules are commonly utilised to counteract negative immunosuppressive signals. However, it has been shown that the administration of agents directed at a single target often has limited anti-tumour efficacy (see section 1.5.2.2, Table 1.4) and this might be due to their ability to only target one or two steps of the cancer immunity cycle. To overcome these limitations, immunotherapy increasingly focusses on the combination of anti-cancer reagents[247,289]. To date, numerous combination therapies are FDA approved or being investigated in pre-clinical and clinical trials. Beside the combination of mAbs targeting check point molecules, other approaches such as the combination of immunomodulatory mAbs with checkpoint blockade (e.g. anti-CTLA-4 mAb [290]) or direct targeting mAbs[243,247] have achieved promising results. Addition of the anti-hCD27 mAb to the anti-CD20 mAb enhanced anti-CD20's tumour cell depleting potency and resulted in potent anti-tumour efficacy. These findings led to the hypothesis that anti-CD27 mAbs could also enhance the efficacy of other direct targeting mAbs such as anti-CD38, which is approved by the FDA for the treatment of MM.[189]

MM is a haematological malignancy of terminally differentiated antibody-secreting plasma cells and an incurable disease. The prevalence of MM appears to correlate with age, with 44% of newly

diagnosed patients being 75 years of age or above. MM is associated with a poor prognosis, with 52% of patients surviving 5 years or more and only 29.1% 10 years or more.[291] This highlights the need to find new approaches that efficiently treat patients suffering from MM. Thus, a variety of mono- and combination therapies (e.g. with chemotherapy, immunomodulatory imide drugs, autologous stem cell transplantation, proteasome inhibitors[292]) are currently investigated in pre-clinical and clinical trials. Based on the promising pre-clinical results obtained with the combination of anti-CD27 and anti-CD20 mAb by Turaj *et al*.[243], the combination of anti-CD27 mAbs with anti-CD38 mAbs was investigated as a novel therapeutic approach for MM.

5.2 Anti-mCD27/anti-mCD38 mAb combination therapy *in vivo*

Preliminary experiments (conducted by A.H. Turaj) assessed the survival of BCL_1-bearing mice in response to the combination of anti-mCD27 mAbs and anti-mCD38 mAbs (Figure 5.1) (for mCD38 expression on murine immune cell subsets see Appendix C.2). Firstly, BCL_1-bearing BALB/c mice were treated with either anti-mCD27 m1 or anti-mCD38 rat IgG2a (rIgG2a, r2a) monotherapy or the combination (Figure 5.1A). Median survival of the combination arm (53 days) was significantly greater than the control (26 days) and both monotherapy arms (anti-mCD27: 43 days, anti-mCD38: 25 days) (Figure 5.1 B). However, r2a is not the ideal isotype for a direct targeting, tumour-depleting mAb due to its low affinity to activating mFcγRs.[33] Thus, mice were treated with anti-mCD38 m2a (instead of r2a) (Figure 5.1 C), which binds with high affinity to the activating mFcγRs I and IV[33]. The control group showed a median survival of 21 days and anti-mCD38 m2a treated mice a median survival of 22 days (Figure 5.1 D). Anti-mCD27 monotherapy and in combination with anti-mCD38 m2a resulted in median survivals of 62 days, respectively, and this was significantly different to the anti-mCD38 monotherapy arm. The combination treatment did not produce greater survival than the anti-mCD27 therapy alone. Nevertheless, based on the survival benefit seen in these experiments, the combination of anti-hCD27 mAbs with the fully human anti-CD38 h1 mAb daratumumab (no cross-reactivity with mCD38, see Appendix C.3) was investigated *in vivo*.

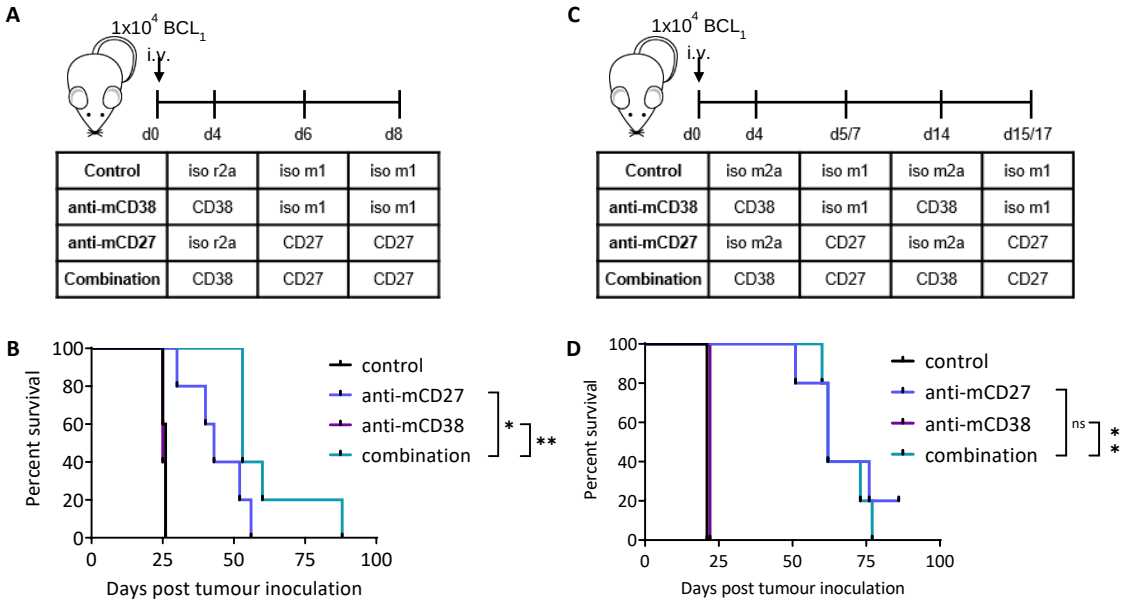

Figure 5.1| Survival of BCL_1-bearing BALB/c mice upon anti-mCD27/anti-mCD38 combination therapy. A: BALB/c mice were intravenously (i.v.) inoculated with $1x10^4$ BCL_1 cells and treated with either anti-mCD38 r2a (Clone 90,500 µg) on day 4 or anti-mCD27 m1 (AT124-1, 100 µg) on days 6 and 8 or the combination. **B:** Survival of mice treated as described in (A) with n=5 mice per group from one experiment. **C**: BCL_1-bearing BALB/c mice were treated with either anti-mCD38 m2a (Clone 90, 200 µg) on days 4 and 14 or anti-mCD27 m1 (AT124-1, 100 µg) on days 5, 7, 15 and 17 or the combination. **D:** Survival of mice treated as described in (C) with n=5 mice per group from one experiment. Data (B, D) were assessed using Log-rank test; ns: $p > 0.05$, *$p \leq 0.05$, **$p \leq 0.01$.

5.3 Establishment of tumour mouse models for the investigation of anti-hCD27/anti-hCD38 mAb combination therapy

Firstly, to explore the anti-hCD27/anti-hCD38 mAb combination therapy *in vivo*, suitable tumour mouse models had to be established. As such, pilot experiments were performed in naïve and hCD27tg BALB/c mice bearing A20 cells transfected with hCD38 (herein referred to as hCD38 A20 cells) and humanised mouse models for the investigation of the combination of fully anti-hCD27 and anti-hCD38 mAbs.

5.3.1 Investigation of the anti-hCD27/anti-hCD38 combination therapy in hCD38 A20 lymphoma:hCD27tg mouse model

Due to the lack of a mouse model for MM in our laboratory, the A20 lymphoma mouse model was considered as a suitable representative. A20 cells is a B cell lymphoma cell line, which derived from a spontaneous reticulum cell neoplasm in an old BALB/c AnN mouse.[251] In order to investigate the anti-hCD27/anti-hCD38 combination therapy, parental A20 cells expressing hCD38 were generated (Figure 5.2)

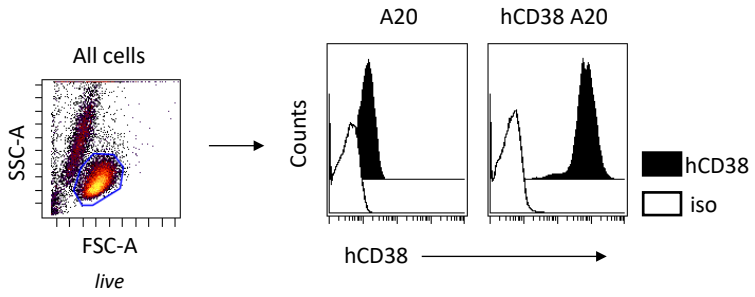

Figure 5.2| Expression of hCD38 on parental A20 and hCD38 A20 cells. hCD38 A20 cells were generated by nucleofection and hCD38 expression determined by flow cytometry using a fluorochrome conjugated anti-hCD38 mAb. Shown is the gating strategy for live A20 cells and the histograms depict the hCD38 expression on parental and hCD38 A20 cells after staining with anti-hCD38 mAb or the respective isotype control.

Parental A20 or hCD38 A20 cells were injected into WT BALB/c mice to evaluate the sustainability of the hCD38 expression (Figure 5.3). Subsequently, subcutaneous tumours were harvested at four different time points: first, when the tumour was first palpable (day X, which occurred 2-8 days post tumour inoculation), second, 2 days post day X (day X+2), third, 4 days post day X (day X+4) and fourth, 7 days post day X (day X +7)) (Figure 5.3 A). Tumour cells were identified by flow cytometry using an A20 idiotype targeting mAb (Figure 5.3 B). Expression of hCD38 was not detectable on parental A20 cells (negative control) after injection at any of the time points investigated. On the contrary, hCD38 was detectable on hCD38 A20 cells at all harvest time points (Figure 5.3 C and D). However, comparison between day 0 and each of the four harvest time points showed a significant reduction of %hCD38^{+}A20 cells, implying that hCD38 A20 cells loose hCD38 surface expression over time *in vivo*.

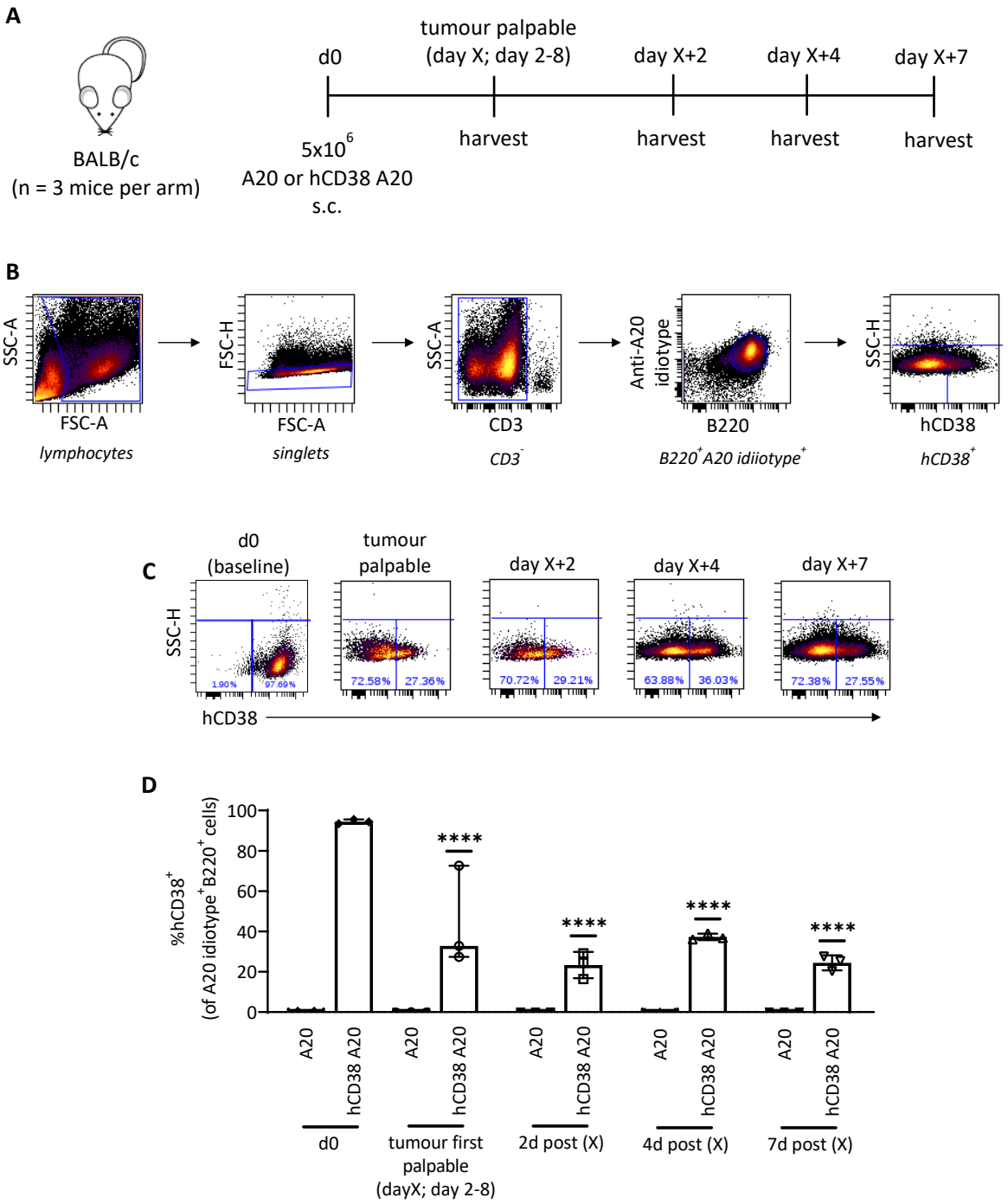

Figure 5.3| Kinetics of the hCD38 expression on hCD38 A20 cells *in vivo*. A: WT BALB/c mice subcutaneously (s.c.) received either $5x10^6$ parental A20 or hCD38 A20 cells on day 0. Tumour growth was monitored and tumours were harvested when first palpable (day X, between days 2 and 8 post tumour inoculation) and 2, 4 and 7 days post day X. **B**: Gating strategy for hCD38 expression on tumour cells. **C**: Representative dot plots for the hCD38 expression on hCD38 A20 cells for each harvest time point. **D**: Shown is the % of hCD38$^+$ B220$^+$A20 idiotype$^+$ cells. Graph is representative of one experiment with n=3 mice per arm. Shown is median with range and one-way ANOVA and Sidak's multiple comparison test were used to assess p values; $^{****}p \leq 0.0001$. Statistics represent the comparison of %hCD38$^+$ cells on each harvest time point with the %hCD38$^+$ cells on day 0.

Despite the reduction of the percentage of hCD38$^+$ A20 cells, the combination therapy was tested in a pilot experiment using the hCD38 A20 lymphoma:hCD27tg mouse model. It was hypothesised that, although the percentage of hCD38$^+$ A20 cells was reduced when the tumour was first palpable, early administration of daratumumab followed by anti-hCD27 might still result in some notable

anti-tumour effects. Thus, hCD27tg BALB/c mice were inoculated with hCD38 A20 cells and once the tumour was palpable, treated with the combination of daratumumab and anti-hCD27 (hCD27.15) (Figure 5.4 A). Treatment with hCD27.15 monotherapy and in combination with daratumumab marginally delayed tumour growth compared to the control arm (Figure 5.4 B). In contrast, no differences in tumour size were detectable when mice were treated with daratumumab alone. Median survivals of mice in the daratumumab monotherapy group (22 days) and control group (22 days) did not differ (Figure 5.4 C). The combination of daratumumab and hCD27.15 prolonged median survival (24 days), but this was not significantly different to the median survival obtained after hCD27.15 monotherapy (27 days).

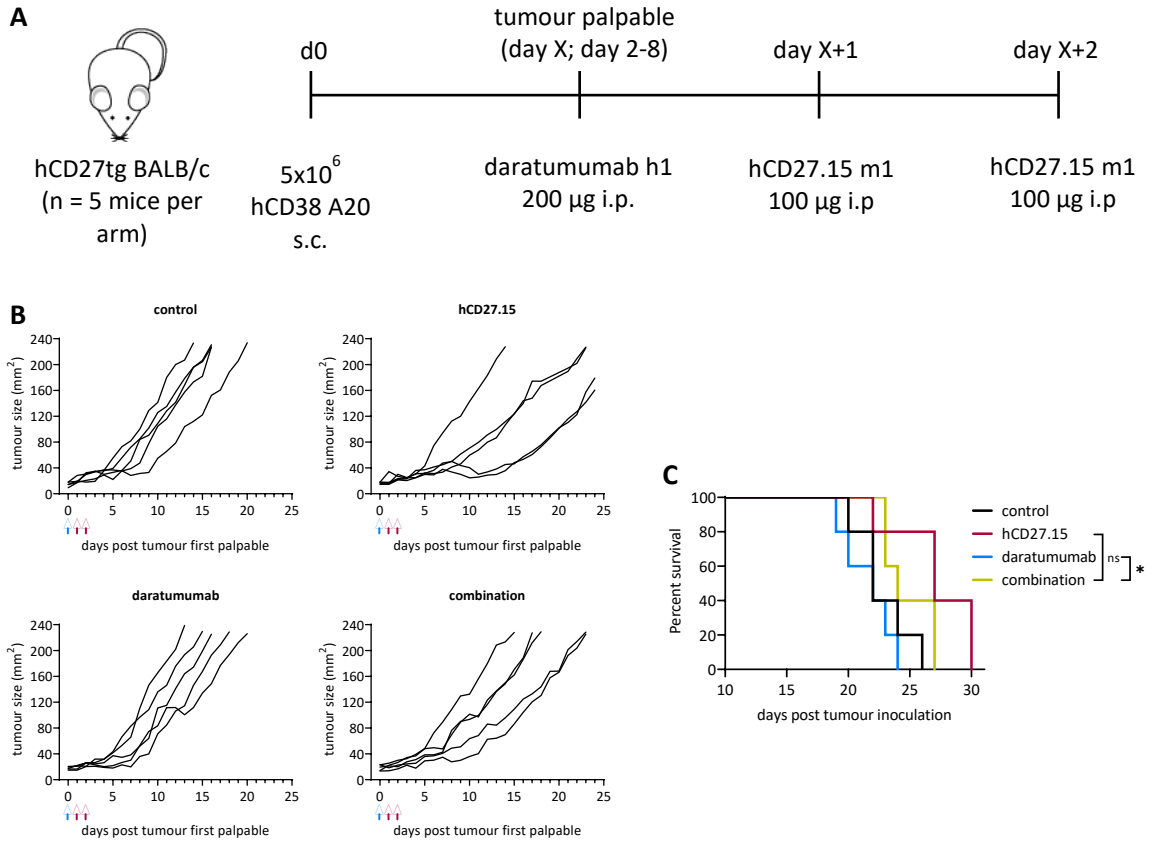

Figure 5.4| Tumour growth and survival of hCD38 A20-bearing hCD27tg BALB/c mice upon anti-hCD27/anti-hCD38 combination therapy. A: hCD27tg BALB/c mice were subcutaneously (s.c.) inoculated with $5x10^6$ hCD38 A20 cells on day 0. When the tumour was palpable (day X, between days 2 and 8 post tumour cell injection) mice were treated with either daratumumab (anti-hCD38 h1, 200 µg) on day X or hCD27.15 (anti-hCD27 m1, 100 µg) on day X+1 and day X+2 or the irrelevant isotype control or the combination of hCD27.15 and daratumumab. Mice were sacrificed when the tumour size reached 15 mm^2 **B**: Tumour growth in individual mice treated as described in (A). Arrwos indicate the timepoint of mAb treatments (blue: daratumumab, red: hCD27.15). **C**: Survival of mice treated as described in (A) (n=5 mice per group from one experiment). Log rank test was used to assess p values; ns: $p > 0.05$, $^*p \leq 0.05$.

5.3.2 Investigation of the anti-hCD27/anti-hCD38 combination therapy in Hu-PBL-SCID:Daudi *in vivo* mouse model

Investigations of fully human mAbs *in vivo* require a mouse model which recapitulates a human immune system (i.e. expressing hFcγR). As such, NSG (NOD.Cg-*Prkdc*^{scid}*Il2rg*^{tm1Wjl}/SzJ) mice have been used for studies involving engraftment of human cells or tissue. These mice have a severe SCID phenotype, which results from a mutation of the protein kinase DNA-activated catalytic polypeptide (*Prkdc*) gene, leading to defects in the autologous T-and B-lymphocyte development[293]. In addition, NSG mice are back-crossed with mice on the non-obese diabetic (NOD) background and show a knockout of the common γ-chain of the IL2 receptor[294], leading to the lack of NK cells and impaired macrophage activity. Together, these genetic alterations and the associated lack of functional murine immune cell subsets allow the engraftment of human cells and tissues.[293-295] Humanising NSG mice can be achieved through different approaches, such as through human PBMC injection (Hu-PBL-SCID model). Transplantation of healthy donor PBMCs results in the engraftment of mainly activated and memory T cells (equal parts of $CD4^+$ and $CD8^+$ T cells) and in low levels of myeloid cells and B cells. However, one drawback of this model is the early onset of lethal graft versus host disease (GvHD), manifested by severe weight loss.[294,295]

Before the investigation of the anti-hCD27/anti-hCD38 mAb combination therapy in the Hu-PBL-SCID mouse model, the anti-tumour efficacy of anti-hCD27 as monotherapy was explored. As a representative for a haematological malignancy such as MM, Daudi B-cell lymphoma cells, expressing both hCD27 and hCD38 (see Appendix C.4), were utilised. Research suggested that CD38 possesses enzymatic and receptor properties, and that it is involved in regulatory immune functions and proliferation.[175,176] Hence, the ability of daratumumab to induced proliferation, and the immunostimulatory potential of varli (representative for anti-hCD27 mAbs) were investigated in Daudi cells *in vitro*. Cell proliferation was assessed via flow cytometry by detection of intracellular Ki67, a protein absent in resting cells and present during active phases of the cell cycle (Figure 5.5 A).

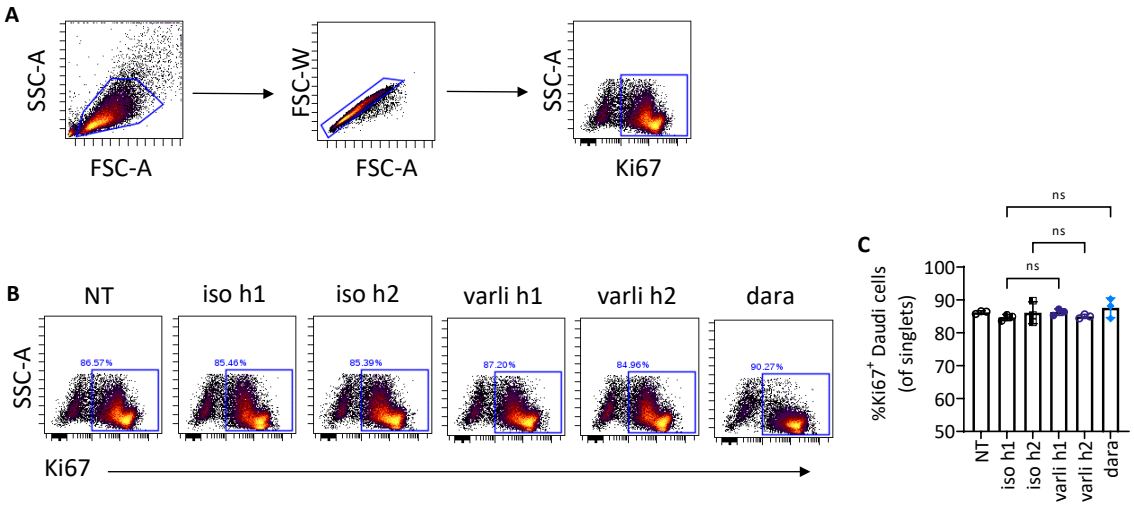

Figure 5.5| Assessment of Ki67 expression in Daudi cells upon treatment with varli or daratumumab *in vitro*. Daudi cells ($1x10^5$) were incubated with 10 µg/ml varli h1, varli h2 or daratumumab (dara) or the respective isotype controls or left untreated (NT). Three days after stimulation, the presence of intracellular Ki67 was assessed by flow cytometry. **A**: Gating strategy for $Ki67^+$ Daudi cells. **B**:. Shown are representative dot plots for intracellular Ki67 in response to the indicated treatments. **C**: Graph shows the percentage of $Ki67^+$ Daudi cells (n=3). Data were assessed using one-way ANOVA with Tukey's test; ns: $p > 0.05$.

Untreated Daudi cells displayed high levels of Ki67 (baseline level), implying that the cells were actively proliferating. When daratumumab or varli h1/h2 were added, no increase in Ki67 levels was observed beyond the baseline (Figure 5.5 B and C). As untreated Daudi cells were already highly proliferative, additional mitogenic effects might not have been possible to detect. Assessment of Daudi cell proliferation by CFSE dilution showed similar results (see Appendix C.5)

A previous study from Overdijk et al. reported that daratumumab is able to induce PCD in MM cell lines upon mAb-mediated cross-linking *in vitro*.[186] Thus the ability of daratumumab or anti-hCD27 mAbs to induce Daudi cell death was investigated next by using an Annexin V and PI cell death assay (see section 2.16). Daudi cells were incubated with the indicated mAbs for 48 hours (Figure 5.6). The tumour cells were subsequently stained with Annexin V and PI to examine early apoptosis (Annexin V^+PI^- cells) and late apoptosis/necrosis (Annexin V^+PI^+ cells) by flow cytometry (Figure 5.6). Neither varli h1, varli h2 or daratumumab induced notable cell death *in vitro*.

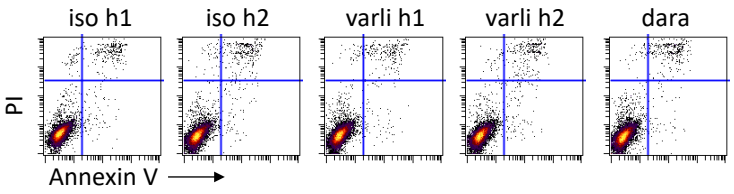

Figure 5.6| Assessment of early and late apoptosis on Daudi cells upon varli h1/h2 or daratumumab stimulation. Daudi cells were incubated with either varli h1, varli h2 or daratumumab (dara) as well as with the respective isotype controls for 48 hours. Cells were harvested and stained with Annexin V and PI to examine induction of early and late apoptosis. Shown are representative dot plots (n=1).

Next, the hCD38 expression was investigated on various PBMC-derived immune cell subsets (Figure 5.7). High expression of hCD38 was detected on $CD4^+$ T cells, $CD56^+$ NK cells and $CD19^+$ B cells. Weaker hCD38 expression was observed on $CD8^+$ T cells and $FoxP3^+$ T cells compared to other lymphocyte populations (Figure 5.7 A). On myeloid cells, hCD38 was highly abundant on $CD14^+CD16^-$ (classical) and $CD14^+CD16^+$ (intermediate) monocytes. A weaker expression of hCD38 was detected on $CD14^{++}CD16^+$ (non-classical) monocytes and $CD11b^+CD16^+$ macrophages (Figure 5.7 B).

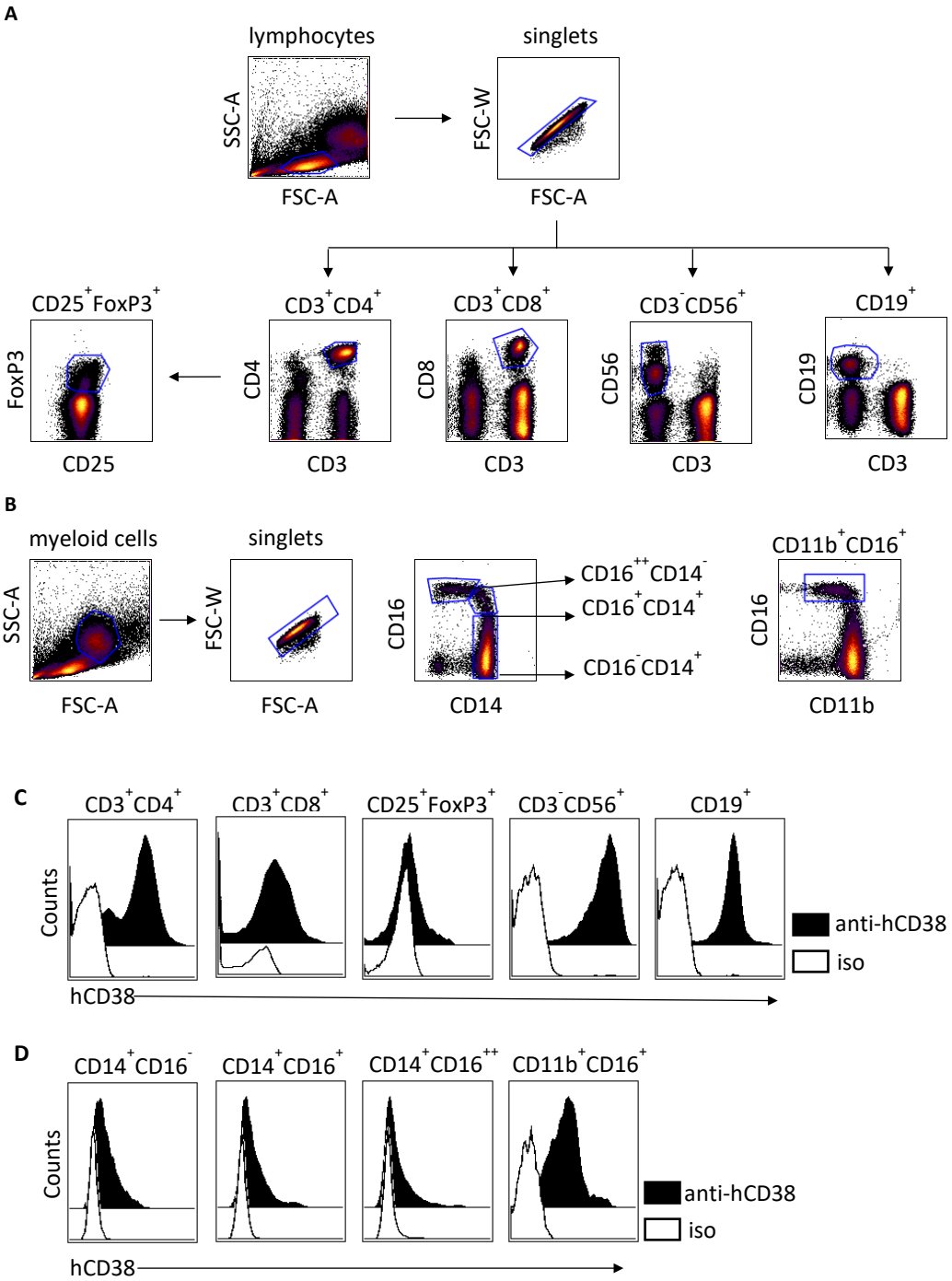

Figure 5.7| Expression of hCD38 on human PBMC-derived immune cell subsets. Isolated human PBMCs were stained with fluorochrome-conjugated mAbs to determine the hCD38 expression on lymphoid and myeloid immune cell subsets by flow cytometry. **A**: Gating strategy for $CD3^+CD4^+$ and $CD3^+CD8^+$ T cells, $CD56^+$ NK cells and $CD19^+$ B cells. Additionally $FoxP3^+$ T cells were determined form $CD3^+CD4^+$ T cells. **B**: Gating strategy for classical ($CD14^+CD16^-$), intermediate ($CD14^+CD16^+$) and non-classical ($CD14^+CD16^{++}$) monocytes and $CD11b^+CD16^+$ macrophages. **C, D**: Histograms show the MFI of hCD38 on the indicated lymphoid and myeloid immune cells subsets. Filled histograms show PBMCs stained with an anti-hCD38 mAb and clear histograms show PBMCs stained with the respective isotype control (n=1).

The anti-tumour efficacy of anti-hCD27 mAb monotherapy was tested in a pilot experiment using the previously described Hu-PBL SCID:Daudi model. To do so, NSG mice were intravenously injected with human PBMCs, subcutaneously inoculated with Daudi cells and subsequently treated with anti-hCD27 mAb (Figure 5.8 A). As the immunostimulatory mAb, hCD27.15 was selected since the data described in Chapter 4 indicated this mAb to be the strongest agonist. To ensure Fc-independency, hCD27.15 was employed as a Fc-engineered h2σ isotype. The hσ2 isotype contains V234A/G237A/P238S/H268A/V309L/A330S/P331S substitutions, which abrogate binding to activating hFcγRs and the inhibiting hFcγRIIb and engagement with C1q of the complement pathway. As a result h2σ variants lose the ability to mediate Fc-dependent effector functions such as ADCC, ADCP and CDC.[296]

Engraftment of PBMCs was assessed 6 d post PBMC injection, and the reconstitution of %hCD45$^+$ cells in the blood ranged from 0.38% to 1.8% (Figure 5.8 B and C). Since the Hu-PBL-SCID model is associated with severe GvHD manifested by weight loss, body weight was regularly monitored over the experimental time course (17 days) as displayed in Figure 5.8 D. No reduction in weight could be detected in either treatment group, indicating no onset of GvHD.

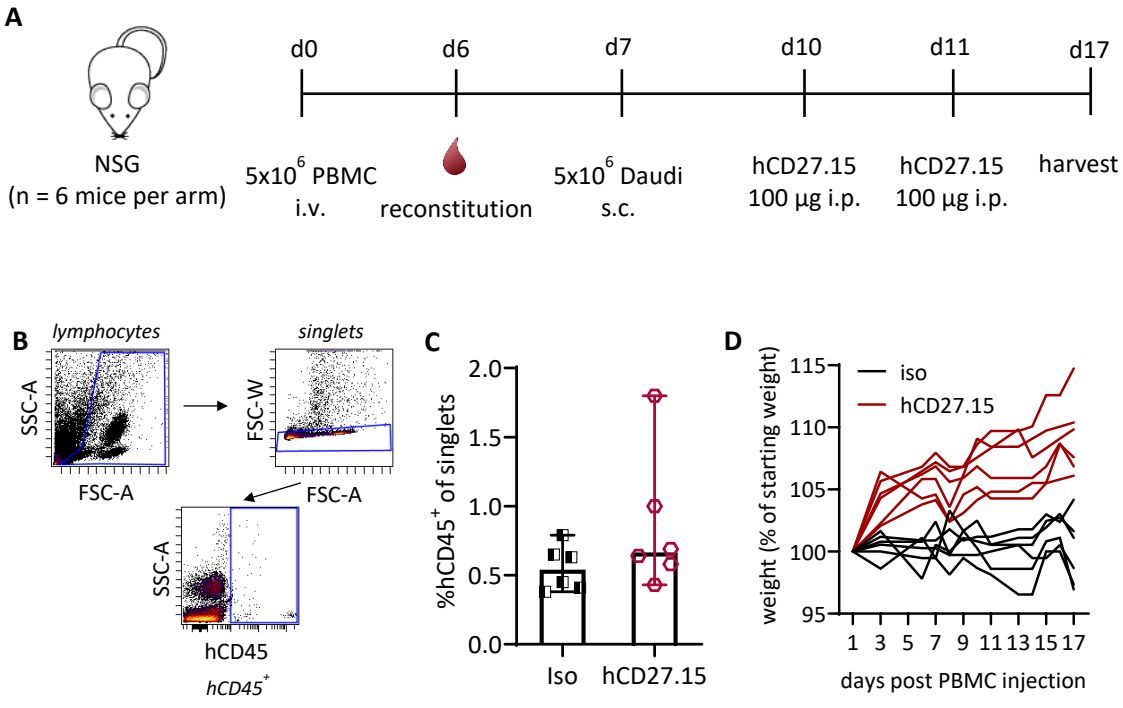

Figure 5.8| Assessment of PBMC engraftment and body weight in Hu-PBL-SCID mice after PBMC injection. A: NSG mice were intravenously (i.v.) injected with 5x10^6 human PBMCs on day 0 and engraftment of human PBMCs was determined in the blood on day 6. Following, 5x10^6 Daudi cells were administered via subcutaneous injection. On days 10 and 11 post PBMC injection, mice were treated with anti-hCD27 h2σ (hCD27.15, 100 µg) or the irrelevant control (h2) and tumours were harvested on day 17 (n=6 per group). **B**: Gating strategy for hCD45$^+$ cells on day 6 post PBMC injection. **D**: Graph shows the median percentage of hCD45$^+$ cells in blood on day 6 post PBMC injection. **C**: Weight of PBMC-injected mice over the experimental time course of 17 days. Graph shows the percentage of the starting weight for individual mice.

Treatment with hCD27.15 marginally delayed tumour growth in comparison to isotype treated mice, but full tumour clearance was not achieved (Figure 5.9 A). However, assessment of the weight of the resected tumours on day 17 showed a decrease in tumour weight in the hCD27.15 treatment group, indicating some slowing of tumour growth.

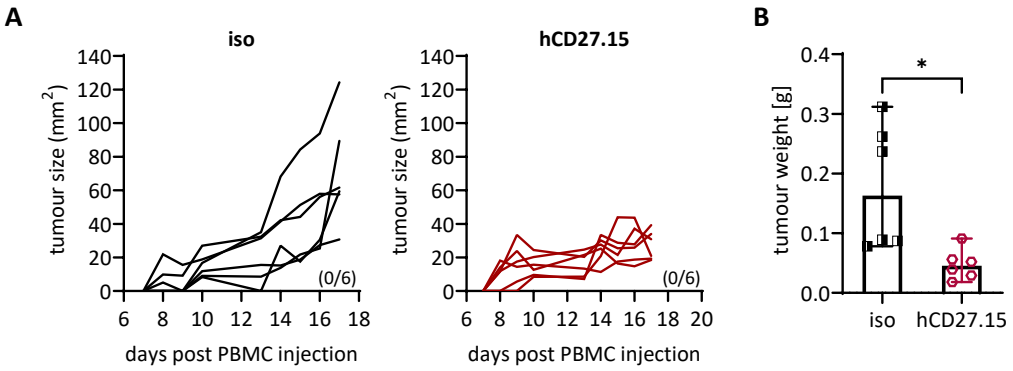

Figure 5.9| Anti-tumour efficacy of anti-hCD27 mAb monotherapy Hu-PBL-SCID:Daudi mice. A: Tumour growth in individual mice treated with either isotype control or hCD27.15 h2σ (as described in Figure 5.9 A) **B**: Tumour weight on day 17 post tumour inoculation. Graphs show n=6 mice per group from one experiment and (B) shows median with range. Data in (B) were assessed using Mann-Whitney test; *p ≤ 0.05.

Next, intra-tumoural human lymphoid immune cell subsets were investigated by flow cytometry (Figure 5.10 A). Treatment with hCD27.15 led to a 1.9-fold reduction of $CD3^+$ T cells (Figure 5.10 B). However, within the $CD3^+$ T-cell population an elevation of $CD4^+$ T cells (Figure 5.10 C) and a reduction of $CD8^+$ T cells (Figure 5.10 D) was detectable in response to hCD27.15 treatment. A difference in the $\%CD19^+$ B cells was not apparent between treatment groups (Figure 5.10 E).

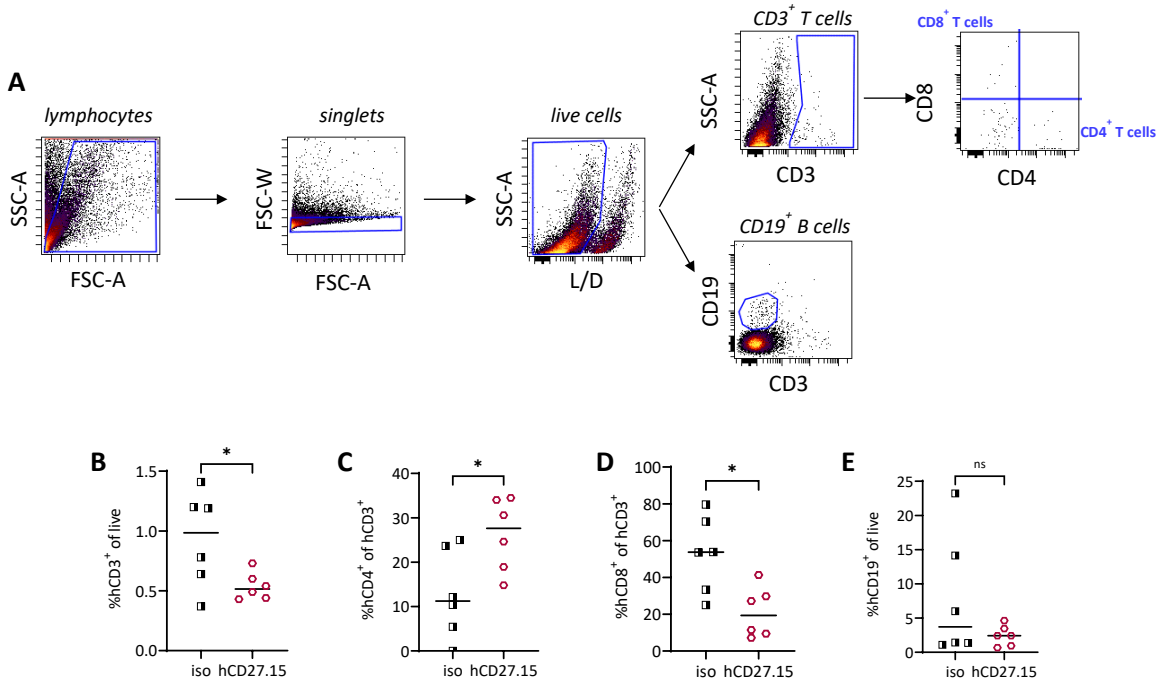

Figure 5.10| Intra-tumoural human lymphocyte subsets after hCD27.15 treatment. Mice were treated as described in Figure 5.8 A. Subcutaneous Daudi cell tumours were harvested 17 days after PBMC injection and investigated for human lymphoid immune cell subsets. **A**: Gating strategy for human lymphoid immune cell subsets. **B-D**: Graphs show percentages of human CD3$^+$ (A), CD4$^+$ (B) and CD8$^+$ (C) T cells and CD19$^+$ B cells (D). Shown is median and statistical analysis was performed using paired Student's t-test; ns: $p > 0.05$, *$p \leq 0.05$.

Analysis of intra-tumoural myeloid immune cell subsets (Figure 5.11 A) showed increased CD33$^+$ myeloid cell infiltration in the hCD27.15 treatment group (Figure 5.11 B). Within the CD33$^+$ cells, a trend towards reduced percentages of CD14$^+$CD16$^-$ (Figure 5.11 C) and elevated percentages of CD14$^+$CD16$^+$ (Figure 5.11 D) monocytes were observed.

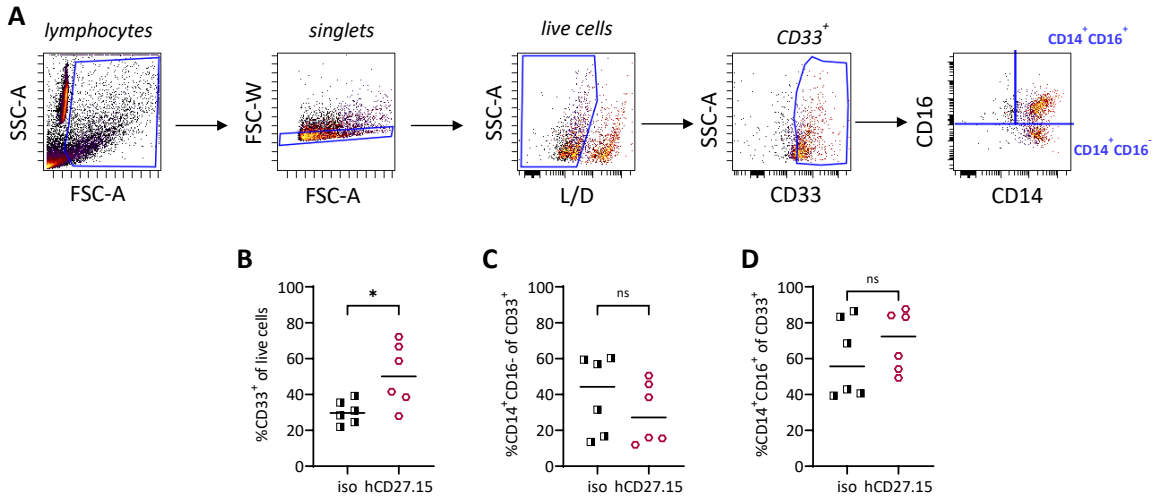

Figure 5.11| Intra-tumoural human myeloid cell subsets after hCD27.15 treatment. Mice were treated as described in Figure 5.8 A. Subcutaneous Daudi cell tumours were harvested 17 days after PBMC injection and investigated for myeloid immune subsets. **A**: Gating strategy for myeloid cells. **B-D**: Graphs show percentages of human CD33$^+$ (A), CD14$^+$CD16$^-$ (B) and CD14$^+$CD16$^+$ (C) cells. Shown is median and statistical analysis was performed using paired Student's t-test; ns: $p > 0.05$, *$p \leq 0.05$.

These data is to some extent in agreement with data published by Turaj *et al*.[243] and Heckel *et al.*[290], where anti-CD27 mAb monotherapy also increased myeloid cell infiltration in several tumour models. However, the results obtained for the intra-tumoural lymphoid subsets in those publications differed and showed decreased $CD4^+$ T-cell levels (especially Tregs) with an increase in $CD8^+$ T-cells infiltrates.[243,290] The screening for $hCD45^+$ cells on day 6 after PBMC injection showed very low percentages, possibly indicating poor tissue engraftment. Moreover, the gating for intra-tumoural immune cell subsets was performed without a $hCD45^+$ gate due to technical difficulties. Thus, the results presented here should be evaluated with caution. Optimisation of this mouse model will be necessary to overcome poor tissue engraftment, which could possibly be achieved through sub-lethal irradiation of NSG mice prior to PBMC injection.[297]

5.4 Chapter discussion

In this chapter the combination therapy of anti-hCD38 mAb with anti-hCD27 mAb was explored *in vivo*. The initial investigations in BCL_1-bearing BALB/c mice demonstrated some therapeutic benefit (Figure 5.1) leading to further investigations in other mouse models. As such, a hCD38 A20 lymphoma mouse model was to be established. hCD38 A20 cells generated by nucleofection formed tumours upon subcutaneous inoculation, but the percentage of $hCD38^+$ A20 cells was reduced over the experimental time course (Figure 5.3 C and D). Administration of the anti-hCD27/anti-hCD38 mAb combination therapy in this model resulted in prolonged survival but was less effective than the anti-hCD27 mAb monotherapy (Figure 5.4). Lastly, a Hu-PBL-SCID:Daudi mouse model was to be established for the investigation of the combination of anti-hCD27 mAb with anti-hCD38 mAb in a fully human context. Anti-hCD27 mAb monotherapy was first tested in this model and, although no complete tumour regression was achieved, delayed tumour growth was observed (Figure 5.9).

Mice bearing hCD38 A20 tumours did not show differences in median survival following either the anti-hCD27/anti-hCD38 mAb combination therapy or anti-hCD27 mAb monotherapy (Figure 5.4 C). This may indicate that the prolonged survival seen in the combination therapy resulted from anti-hCD27 alone rather than from the combination with anti-hCD38 mAb. One possible explanation for the lack of efficacy might be the early reduction of hCD38 expressing A20 cells (Figure 5.3), which may not allow daratumumab to effectively target the tumour.

The hCD38 A20 lymphoma mouse model was not an optimal model for the investigation of mAbs targeting hCD38. Therefore, as an alternative the Hu-PBL-SCID:Daudi mouse model was attempted, allowing the investigation of the combination therapy of human mAbs in the context of a human immune system (including hFcγR). It has previously been reported that one of daratumumab's effector function is the induction of PCD in $hCD38^+$ MM cell lines.[186] Thus, an *in vitro* cell death assay was performed to assess the PCD-inducing abilities of daratumumab on Daudi cells (Figure 5.6). The mAb did not induce cell death, which is different to the observations obtained by Overdijk *et al*.[186] However, the mAb-mediated PCD reported by Overdijk *et al*. was dependent on Fc-crosslinking.[186] Thus, the lack of a crosslinking might explain the absence of PCD in Daudi cells and co-culture with hFcγR-expressing cells might lead to cell death.

Based on the study by Turaj *et al.* a proposed mode of action of the combination therapy of anti-hCD27 mAbs with a direct targeting mAb is the cytokine-mediated recruitment of intra-tumoural myeloid cells, which in turn act as the key mediators of tumour clearance *in vivo*.[243] Phenotyping of human PBMCs (Figure 5.7) and murine splenocytes (Appendix C.2C.1) revealed that CD38 is

expressed on a wide range of immune cell subsets, which is in accordance with current literature (see section 1.5.1). However, this broad expression pattern might result in the depletion of crucial effector cells (macrophages, NK cells, T cells) through anti-CD38 mAb mediated effector functions (ADCC, ADCP), and may also account for the moderate therapeutic efficacy seen in the initial investigation of the combination therapy in BCL_1-bearing mice (Figure 5.1). Future experiments determining whether daratumumab is able to induce cell death in the proposed effector cells (macrophages, T cells, NK cells) *in vivo*, might aid to clarify this assumption.

Furthermore, to fully investigate and evaluate the anti-hCD27/anti-hCD38 mAb combination therapy suitable mouse models are essential. Due to the unstable hCD38 expression, the hCD38 A20 mouse model turned out not to be suitable and therefore alternatives were considered. As one possibility, the Hu-PBL-SCID:Daudi model was investigated. However, the low percentages of $hCD45^+$ cells observed at day 6 after PBMC injection and the absence of GvHD strongly suggest insufficient engraftment efficacy (Figure 5.8). A study by Ye *et al*. compared intravenous PBMC engraftment in NSG mice which were irradiated or not irradiated prior to PBMC transplantation. Pre-conditioning of mice (compared to non-irradiated mice) led to an improved engraftment efficacy with a significant increase of $hCD45^+$ cells 5 days post PBMC injection. Of note, the group injected a substantially higher amount of PBMCs ($30x10^6$ cells).[297] Therefore, improvement of the engraftment success may be achieved through pre-conditioning as well as injection of higher PBMC numbers. This might allow more accurate gating and subsequently a more compelling interpretation of the treatment effects on intra-tumoural immune cell subsets.

Taken together, the experiments investigating the combination therapy of anti-hCD27 and anti-hCD38 mAb so far show moderate anti-tumour activity. However, the mouse models used to explore the therapeutic efficacy need more optimisation to allow a firm conclusion about the effectiveness of the combination therapy and whether further investigations should be pursued in clinical trials. These pre-clinical experiments would include the optimisation and administration of the anti-hCD27/anti-hCD38 combination therapy in the Hu-PBL-SCID model and the identification of mouse models specific for human MM.

Chapter 6 *In vitro* myeloid stimulation by anti-hCD27 mAbs

6.1 Chapter introduction

Turaj *et al.* demonstrated in *in vitro* studies that the treatment of human PBMCs with the anti-hCD27 mAb varli results in off-target effects on monocytes with a 2-fold downregulation of the expression of the monocyte antigen CD14.[243]

Monocytes develop in the bone marrow from haematopoietic precursor cells and comprise approximately 10% of PBMCs. As part of the innate immunity, they are involved in the clearance of bacterial and viral infections. Under inflammatory conditions, monocytes migrate to tissue or the site of infection, where they can differentiate into more specialised myeloid cells, such as macrophages or monocyte-derived dendritic cells.[298] Monocytes are highly heterogeneous and to date, three different subsets have been described. These are distinguished primarily by two surface antigens: CD14 and CD16.[299] The CD14 molecule is a GPI-anchored protein expressed on mature monocytes and macrophages.[300] Together with TLR4 and the accessory molecule MD-2, CD14 forms a complex that is able to respond to LPS, the main component of Gram-negative bacterial membranes. As a result, signalling cascades are induced leading to translocation of NF-κB and secretion of type-I IFNs. Furthermore, CD14 can mediate signalling independent of TLR4 and MD-2 leading to the nuclear translocation of NFAT.[301] The second monocyte differentiation marker is the low-affinity hFcγRIII (CD16) (see Chapter 1). According to these markers, monocytes can be divided into classical ($CD14^{++}CD16^{-}$), intermediate ($CD14^{+}CD16^{+}$) and non-classical ($CD14^{+}CD16^{++}$) monocytes.[302] These subpopulations can be further characterised by cell surface markers such as CD86 (for additional differentiation markers see Table 6.1). The costimulatory molecule CD86 is expressed on professional APCs and interacts with CD28 or CTLA-4 during T-cell activation.[24] Fleischer *et. al.* demonstrated that CD86 is weakly expressed on freshly isolated monocytes, but upregulated upon stimulation with IFN-γ. [303] The expression of CD86 is dynamic and differs between the monocyte subsets.[304] Hence it gradually increases with the transition of the classical to the intermediate to the non-classical monocyte phenotype.[304,305]

Gene expression analysis of the three monocyte subsets by Wong *et al*. and Zwada *et al*. showed that the transcriptomes were most similar between the intermediate and non-classical monocytes[306,307], whereas another independent study conducted by Cros and colleagues suggests more similarity between transcriptomes of classical and intermediate monocytes.[308] Nevertheless, Patel *et al*. implied that classical monocytes sequentially differentiate into intermediate and non-classical monocytes.[304]

Table 6.1| Characteristics of human monocyte subsets. Summarised are the surface markers and gene expression as well as functions of classical, intermediate and non-classical monocytes. The cytokines listed were detected in response to LPS stimulation. G-CSF: granulocyte colony-stimulating factor, ROS: reactive oxygen species.[306-309]

	Classical monocytes	**Intermediate monocytes**	**Non-classical monocytes**
Abundance in peripheral blood	~90% of monocytes	~5% of monocytes	~10% of monocytes
Surface expression markers	$CD14^+CD16^-CD36^+CCR2^+HLA\text{-}DR^{mid}CD11c^{mid}CD64^+CD62L^+$	$CD14^+CD16^+HLA\text{-}DR^+CD86^+$ $CD11c^+CCR5^+CD74^+$	$CD14^+CD16^{++}CX3CR1^+CXCR4^+$ $SLAN^{+/-}HLA\text{-}DR^+$
Gene expression	– pro-inflammatory genes of the S100-family (*S100A12/9/8*) – genes linked to phagocytotic processes (e.g. *CD64, CD16*)	– genes associated with antigen processing (e.g. *CD74)* and presentation (e.g. *HLA-DRB3*, *HLA-DRA*) – *CD40*	– cytoskeleton rearrangement (e.g. *VAV2*) – FcγR-mediated phagocytosis (e.g. *FCGR3B, LYN*) – complement components (e.g. *C1QA/B, C2, C3*)
Secreted cytokines and chemokines	IL-10, CCL2, CCL3, IL-6, IL-8, G-CSF	TNFα, IL-1β, IL-10, IL-6, IL-8, CCL3	TNF-α (not as high as intermediate), IL-1 receptor agonist, proinflammatory cytokines
Function	– angiogenesis – wound healing – coagulation – phagocytosis – ROS production – anti-microbial responses	– MHC class II antigen processing and presentation – $CD4^+$ T-cell stimulation – ROS production – cytokine secretion – apoptosis regulation	– cell motility/ tissue patrolling – FcγR-mediated phagocytosis – anti-viral responses

The monocyte subsets not only differ in their phenotypes and transcriptomic profile but also in their functionality. A summary of the main characteristics of the three monocyte subsets is shown in Table 6.1. Classical monocytes are phagocytic and involved in anti-microbial immune responses. They express high levels of CCR2, which enables tissue invasion during inflammation. Furthermore, classical monocytes possess the ability to differentiate into monocytes-derived macrophages or DCs.[309] Intermediate monocytes have less peroxidase activity than classical monocytes and produce IL-1β and TNF-α in response to LPS. Due to their high expression of MHC class II genes, they are considered to be involved in inflammatory responses as well as in antigen presentation and T-cell activation.[306,310,311] Non-classical monocytes patrol the vascular epithelium. Interaction of CX3CR1 and CCL3 in a lymphocyte functional antigen (LFA-1)/intercellular adhesion molecule-1 (ICAM-1) dependent manner enables tissue invasion. $CD14^-CD16^{++}$ monocytes do not produce reactive oxygen species (ROS) and poorly respond to LPS. However, it was reported that stimulation with

viruses and nucleic acids induces the production of pro-inflammatory cytokines such as TNF-α, IL-1β or CCL3.[308]

6.2 Effects on monocytes upon anti-hCD27 mAb stimulation

The expression of CD14, CD16 and CD86 was evaluated on PBMC-derived monocytes in response to anti-hCD27 mAb treatment. Human PBMCs were isolated, cultured at high density and stimulated with anti-hCD27 h1 and h2 mAb, the respective isotype controls or hCD70 Fc (Figure 6.1.). After 48 hours, the CD14 expression on monocytes was assessed by flow cytometry (Figure 6.1 A and B). Significant downregulation of CD14 was detected with varli h1 (2-fold compared to iso h1), as shown before by Turaj *et al*.[243] (Figure 6.1 C). Treatment with all other anti-hCD27 mAbs did not induce CD14 downregulation on the surface of monocytes.

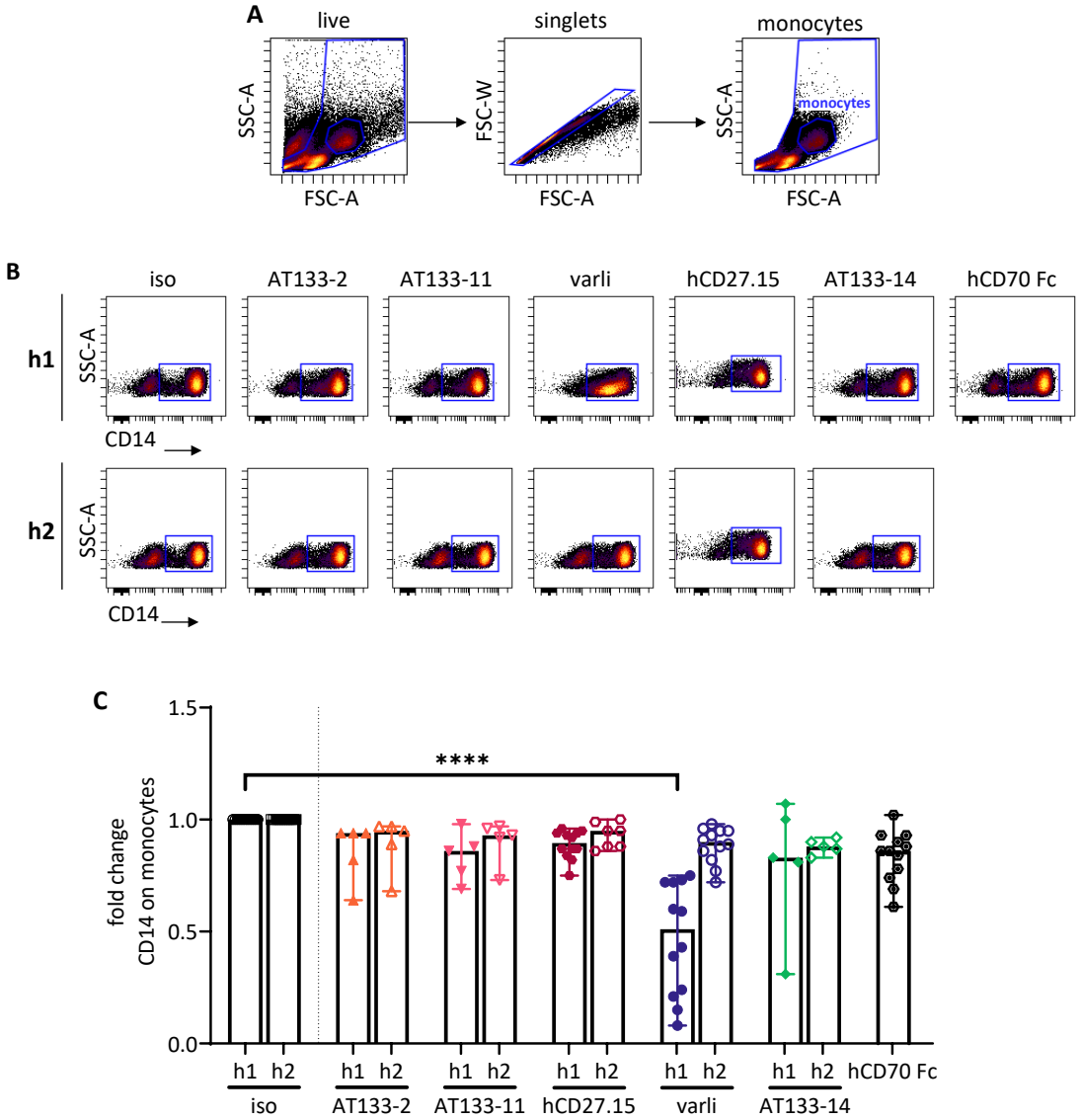

Figure 6.1| Expression of CD14 on monocytes after anti-hCD27 mAb treatment of human PBMCs. Human PBMCs were isolated, cultured at high density and stimulated for 48 hours with 10 µg/ml of anti-hCD27 mAbs, hCD70 Fc (h1 Fc fusion protein) or the respective isotype controls. **A**: Gating strategy used to identify PBMC-derived monocytes. **B**: Representative dot plots for the CD14 expression on monocytes. **C**: Fold change of CD14 expression on monocytes after anti-hCD27 mAb treatment. Graph shows median with range of n=5-12 independent experiments. Data were assessed using one-way ANOVA with Tukey's test. Only significant results are indicated; ns: $p > 0.05$, ****$p \leq 0.0001$.

To analyse the CD16 expression on monocytes (Figure 6.2), PBMCs were gated according to Figure 6.1 A. The representative dot plots in Figure 6.2 A display $CD14^+CD16^+$ monocytes. A significant increase in $\%CD14^+CD16^+$ monocytes was detected with AT133-2 h1 (6.3%), AT133-14 h1 (7.8%) and hCD70 Fc (10.35%) and similar trends were observed for the remaining h1 mAbs (AT133-11 h1: 6.1%, hCD27.15 h1: 4.9%, varli h1: 5.4%) (Figure 6.2 B). Anti-hCD27 h2 mAbs also elevated the percentage of $CD14^+CD16^+$ monocytes. However, this was not significant. Treatment with h1 mAbs generally induced higher percentages of $CD14^+CD16^+$ monocytes, with the exception of hCD27.15.

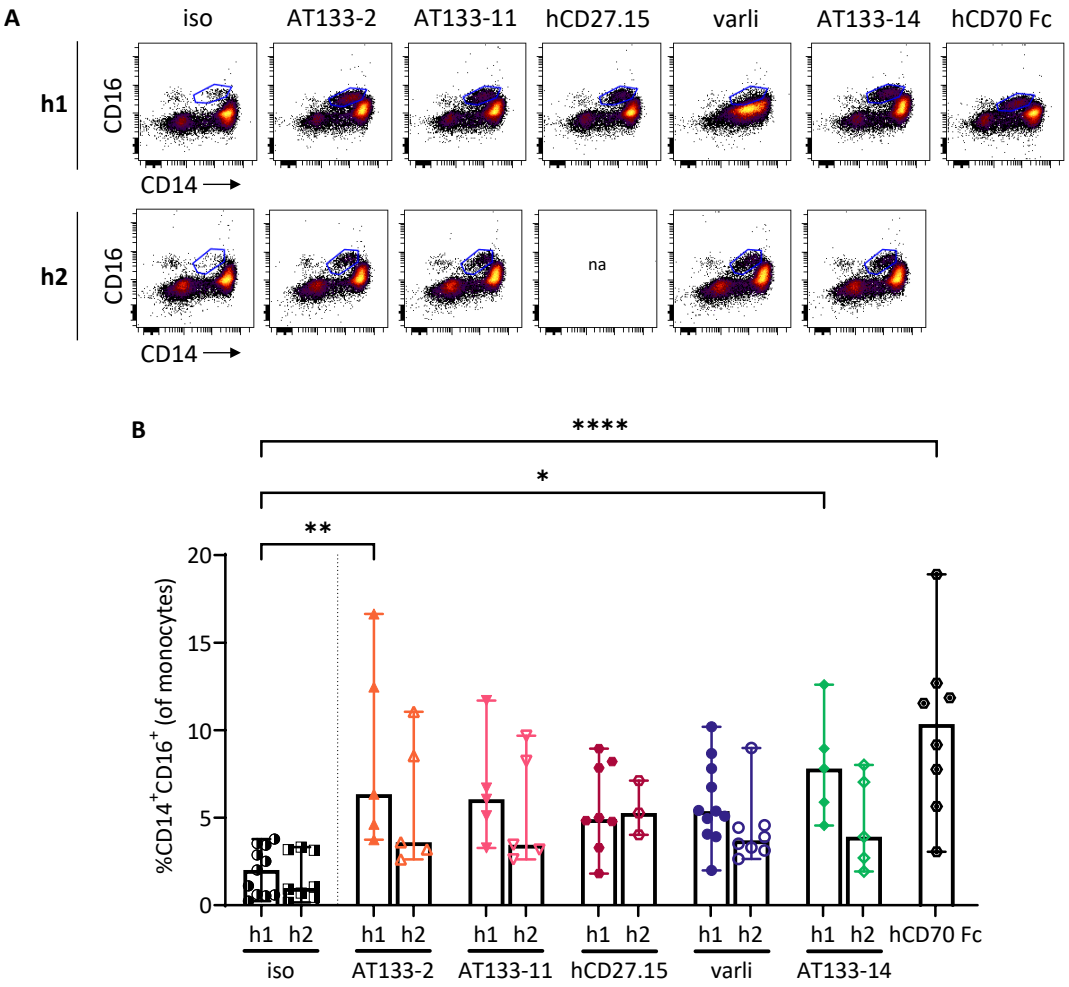

Figure 6.2| Expression of CD16 on monocytes upon anti-hCD27 mAb treatment. Human PBMCs were treated as described in Figure 6.1. Monocytes were identified as depicted in Figure 6.1 A. **A**: Representative dot plots of the CD14 and CD16 expression on monocytes. **B**: Graph shows the median percentage of $CD14^+CD16^+$ monocytes (of initial monocyte gate, FSC-A vs SSC-A). Data is representative of n=3-11. Statistical analysis was performed using one-way ANOVA with Tukey's test. Only significant results are indicated; ns: $p > 0.05$, *$p \leq 0.05$, **$p \leq 0.01$, ****$p \leq 0.0001$.

In addition, treatment of PBMCs with varli h1 led to a significant increase of $\%CD14^+CD86^+$ monocytes (varli h1: 19.1%). AT133-2 h1 (10.5%), AT133-11 h1 (6.2%), hCD27.15 h1 (4.8%), AT133-14 h1 (6.3%) and hCD70 Fc (8.2%) also elevated CD86 surface expression, although not statistically significant (Figure 6.3 A, B). Furthermore, a trend towards increased $\%CD14^+CD86^+$ monocytes was observed with h2 mAbs, if compared to the respective isotype control. However, when compared to their h1 counterparts, the percentage was lower.

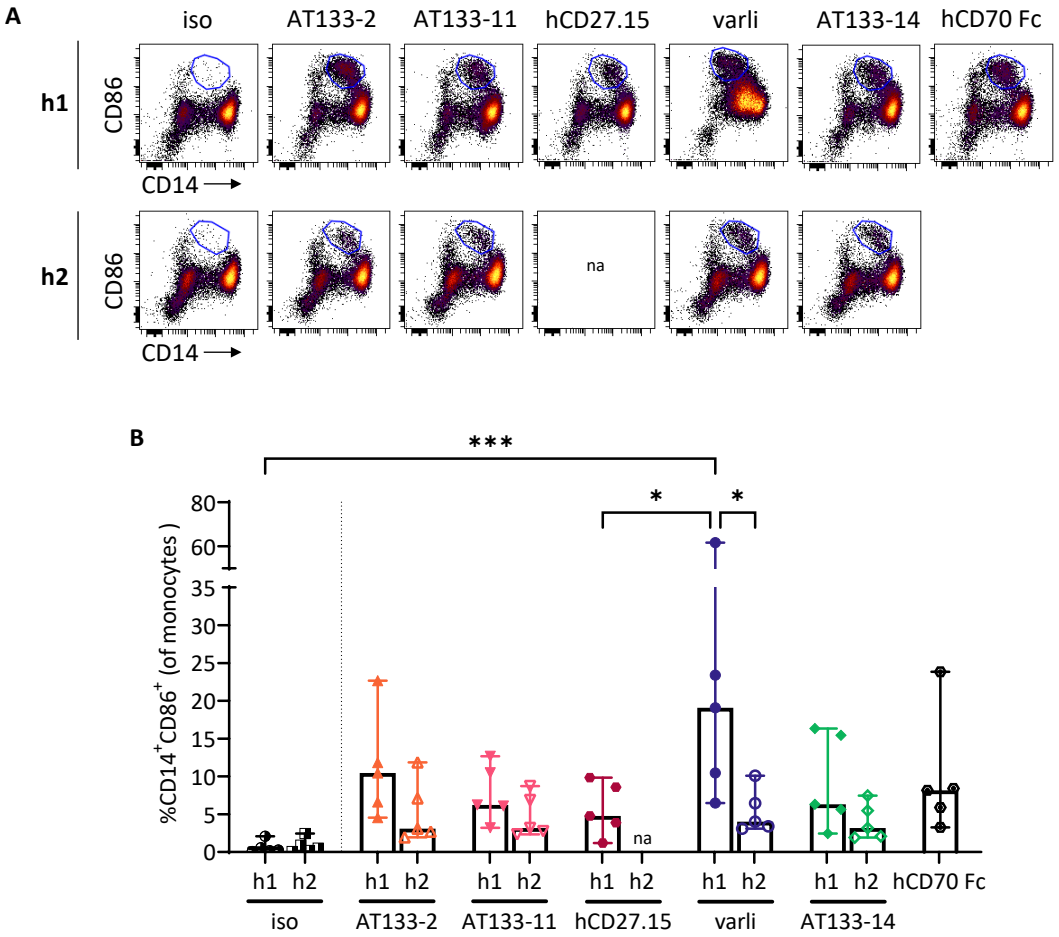

Figure 6.3| Expression of CD86 on monocytes upon anti-hCD27 mAb treatment. Human PBMCs were treated as described in Figure 6.1. Cells were gated as depicted in Figure 6.1 A. **A**: Representative dot plots of the CD14 and CD86 expression on monocytes. **B**: Graph shows the median percentage of $CD14^{+}CD86^{+}$ monocytes (of initial monocyte gate, FSC-A vs SSC-A). Data is representative of n=5. Statistical analysis was performed using one-way ANOVA with Tukey's test. Only significant results are indicated; ns: $p>0.05$, *$p \leq 0.05$, ***$p \leq 0.001$.

Table 6.2 summarises the phenotypic changes in monocytes observed after PBMCs were stimulated with the different anti-hCD27 mAbs. Thus, AT133-2, AT133-11, hCD27.15 and AT133-14 induced the formation of $CD16^{+}CD86^{+}$ monocytes but were not able to trigger the CD14 downregulation, as was observed after varli h1 treatment.

Table 6.2| Phenotypic changes in monocytes upon anti-hCD27 mAb stimulation of PBMC cultures. The table summarises the effects on monocyte differentiation markers observed after the stimulation of PBMC cultures with anti-hCD27 mAbs *in vitro*. For the CD14 expression: - indicates no change, whilst ↓ indicates CD14 downregulation. For %CD14$^+$CD16$^+$: ↑ represents an increase >2% ≤ 5% and ↑↑ indicates an increase >5%. For %CD14$^+$CD86$^+$: ↑ represents an increase >0.5% ≤ 10% and ↑↑ indicates an increase >10%. Data were compiled from Figure 6.1, Figure 6.2 and Figure 6.3.

	AT133-2		**AT133-11**		**hCD27.15**		**varli**		**AT133-14**	
	h1	h2	h1	h2	h1	h2	h1	h2	h1	h2
CD14 expression	-	-	-	-	-	-	↓	-	-	-
%CD14$^+$CD16$^+$	↑↑	↑	↑↑	↑	↑↑	↑↑	↑↑	↑	↑↑	↑
%CD14$^+$CD86$^+$	↑↑	↑	↑	↑	↑	↑	↑↑	↑	↑	↑

6.3 Mechanisms of the CD14 downregulation upon varli h1 stimulation

6.3.1 Dependence of the CD14 regulation on TCR signalling

The above data suggest that varli h1 induces phenotypic changes in monocytes, while other anti-hCD27 mAb have no effect. To decipher the mechanism of the CD14 downregulation on monocytes in response to varli h1 treatment, the contribution of TCR signalling was investigated.

TCR activation was selectively blocked using cyclosporine A (CSA). CSA in complex with cyclophilin binds to calcineurin, a phosphatase involved in the NFAT signalling pathway. This blocks the calcineurin function, which eventually results in the inhibition of T-cell activation, T-cell dependent IL-2 production and T-cell proliferation. T-cell activation was evaluated by the inducible T-cell marker CD137. The latter is a member of the TNFRSF and is induced on CD4$^+$ and CD8$^+$ T cells upon T-cell stimulation. To assess successful TCR signalling blockade, PBMCs were stimulated with anti-CD3 mAb alone or in combination with CSA (Figure 6.4). Stimulation with anti-CD3 mAb alone increased %CD137$^+$CD4$^+$ T cells and to a greater extent %CD137$^+$CD8$^+$ T cells. The addition of CSA resulted in a significant decrease of %CD137$^+$CD8$^+$ T cells and this trend was also detectable for CD4$^+$ T cells. The results suggest that anti-CD3 mAb-induced TCR signalling was inhibited by the addition of CSA in CD8$^+$ T cells and to some extent in CD4$^+$ T cells.

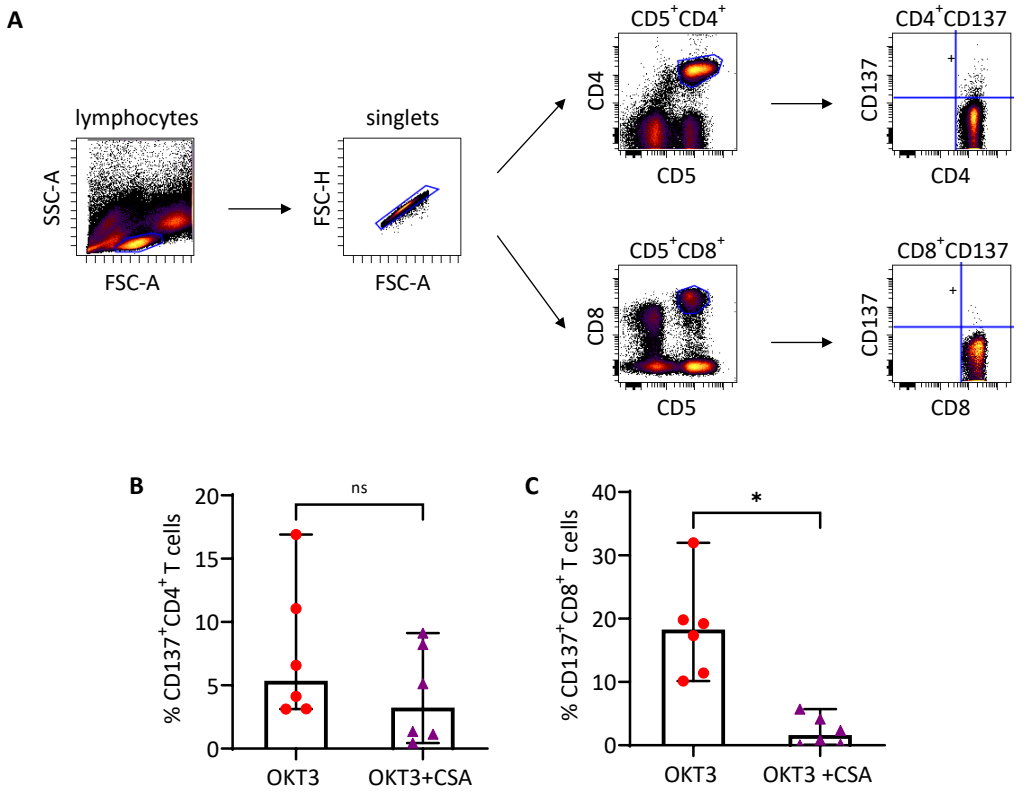

Figure 6.4| Activation of T cells upon blockage of TCR signalling with CSA. Human PBMCs were isolated, cultured at high density and stimulated with either 0.1 µg/ml anti-CD3 mAb (clone OKT3, mIgG2a) alone or in combination with 1 µg/ml CSA. After 48 hours the percentage of CD137$^+$ T cells was determined by flow cytometry. **A**: Displayed is the gating strategy for CD4$^+$CD137$^+$ or CD8$^+$CD137$^+$ T cells. **B**, **C**: Percentage of CD137$^+$CD4$^+$ T cells (B) and CD137$^+$CD8$^+$ T cells (C). Graphs show median with range of n=6. Data were assessed using paired student's t-test; ns: $p > 0.05$, *$p \leq 0.05$.

After establishing that CSA successfully blocked TCR signalling in activated T cells, the impact of TCR blockade on the CD14 expression on monocytes upon varli h1 treatment was investigated (Figure 6.5). To do so, PBMCs were treated with varli h1 or hCD70 Fc (as a positive control) alone or in combination with CSA to inhibit TCR signalling. Varli h1 or hCD70 Fc treatment induced only a small increase of %CD4$^+$CD137$^+$ (Figure 6.5 A) or %CD8$^+$CD137$^+$ (Figure 6.5 B) T cells and the addition of CSA did not produce any differences. The CD14 expression on monocytes decreased with varli h1 but not hCD70 Fc (Figure 6.5 C). A difference in the CD14 expression on monocytes upon addition of CSA did not result in significant changes, possibly suggesting that the phenotypic changes observed in monocytes upon varli h1 treatment are not solely dependent on TCR signalling.

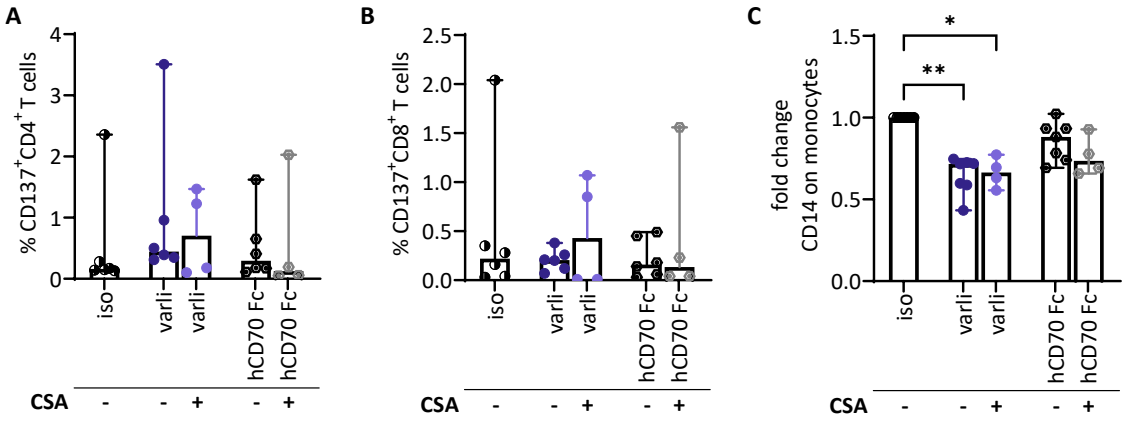

Figure 6.5| T-cell activation and CD14 expression on monocytes upon varli h1 stimulation and blockage of TCR signalling. Human PBMCs were isolated, cultured at high density and stimulated with either 10 µg/ml varli h1 or hCD70 Fc alone or in combination with 1 µg/ml CSA or with the respective isotype control. After 48 hours, the percentage of $CD137^+CD4^+$ T cells (A) and $CD137^+CD8^+$ T cells (B), as well as the CD14 expression on monocytes (fold change) (C) was determined by flow cytometry. Graphs (A-C) show median with range of n=4-6. Data were analysed using one-way ANOVA with Tukey's test. Only significant results are indicated; ns: $p > 0.05$, *$p \leq 0.05$, **$p \leq 0.01$.

6.3.2 Dependence of the CD14 downregulation on hCD27 signalling

To further explore the underlying mechanisms of the CD14 downregulation, it was of interest whether it was dependent on signalling through hCD27 or potentially induced through Fc:FcγR interactions on the monocytes. Monocytes were isolated from PBMCs and either cultured alone or with hCD27 Jurkat cells or hCD27 R214STOP Jurkat cells, lacking the intracellular hCD27 signalling domain. Subsequently, cultures were stimulated with varli h1 and the CD14 expression on monocytes was investigated (Figure 6.6). As shown before, addition of varli h1 induced downregulation of CD14 on monocytes (2-fold). Co-culture of monocytes with hCD27 Jurkat cells did not show differences after varli h1 treatment, whereas a marginal CD14 downregulation was detected upon co-culture with hCD27 R214STOP Jurkat cells. Moreover, there was no difference in CD14 expression when monocytes were cultured alone. Of note, varli h1 did not reduce CD14 expression in co-cultures to the same extent as seen in whole PBMC cultures. However, comparison of the CD14 levels upon co-culture with hCD27 Jurkat and hCD27 R214STOP Jurkat cells only showed marginal differences, suggesting that hCD27 signalling alone does not result in monocyte differentiation.

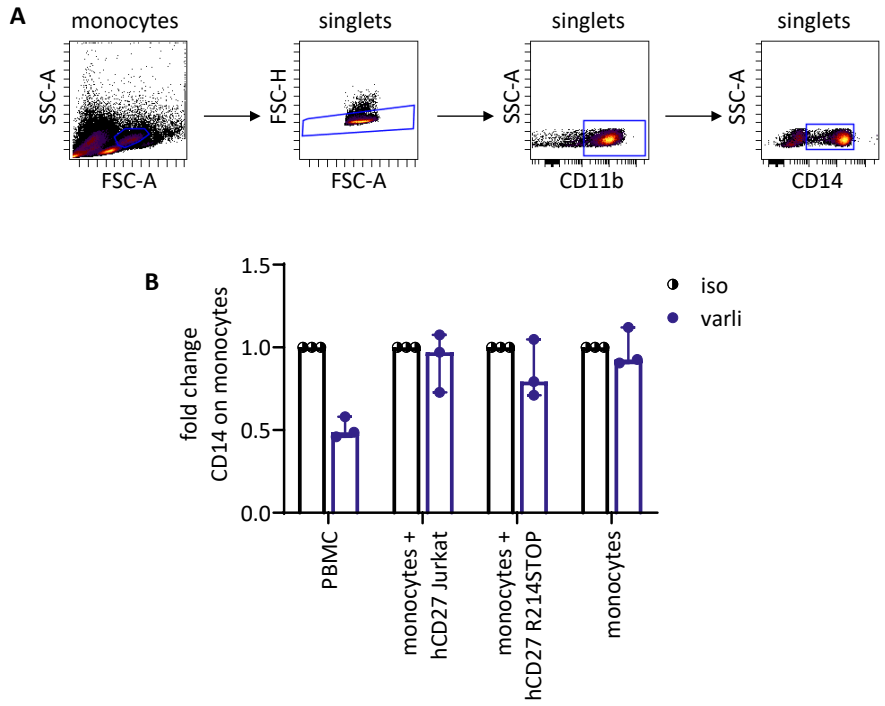

Figure 6.6| Co-culture of monocytes with hCD27 Jurkat cells lacking the hCD27 intracellular signalling domain. Monocytes were isolated from human PBMCs (using MACS pan monocyte isolation kit, Miltenyi) and were either cultured alone or in combination with hCD27 or hCD27 R214STOP Jurkat cells (in a 1:4 ratio) at high density. As a control for the CD14 downregulation, PBMCs were also cultured at high density. Subsequently, cells were stimulated with 10 µg/ml varli h1 or the respective isotype control for 48 hours and the CD14 expression was assessed by flow cytometry. **A**: Gating strategy for the CD14 expression on monocytes. **B**: CD14 expression on monocytes in PBMC cultures, monocytes in co-culture with hCD27 Jurkat cells or hCD27 R214STOP Jurkat cells, or monocytes alone. Graph shows median with range representative of n=3.

6.3.3 The role of IL-16 and MIF in the CD14 downregulation on monocytes

Concurrent with the above *in vitro* investigations, Michael Marshall and Heng Sheng Sow performed cellular indexing of transcriptomes and epitopes by sequencing (CITE-seq) on PBMCs treated with either varli h1 or the respective isotype control (data unpublished). CITE-seq is a single-cell RNA sequencing technique, which allows the simultaneous analysis of transcriptomics and proteomics data.[312] Six monocyte subsets were identified in response to varli h1 treatment: classical monocytes, classical IFN monocytes, classical secreted phosphoprotein (SPP) 1 monocytes, intermediate monocytes, DC-like monocytes and non-classical monocytes. All monocyte subsets showed increased proportions upon varli h1 treatment, with the exception of the classical monocyte population. To further investigate the CD14 downregulation upon varli h1 treatment, ligand:receptor analysis was performed between naïve or activated $CD4^+$ or $CD8^+$ T cells and the classical monocyte subset using CellChat[313]. CellChat analysis revealed five different signalling pathways. Among those, IL-16 and macrophage migration inhibitory factor (MIF) were identified to be the most activated pathways with activated T cells serving as the ligand source and monocytes as ligand recipients. IL-16, firstly identified as a T-cell chemoattractant cytokine, is secreted by a

variety of immune ($CD4^+$ and $CD8^+$ T cells, dendritic cells, eosinophils, mast cells, and monocytes) and non-immune cells (e.g. epithelial cells, fibroblasts)[314,315]. Depending on the cell type, IL-16 presents as either mRNA or bioactive IL-16 as a result of caspase-3 mediated cleavage of pro-IL16 (e.g. in $CD8^+$ T cells) or as mRNA only (e.g. in $CD4^+$ T cells, DC), which upon activation is converted into bioactive IL-16. Secreted IL-16 can bind to cells expressing the CD4 co-receptor (e.g. T cells, monocytes)[316]. Subsequential downstream signalling results in cell cycle progression of $CD4^+$ T-cell subsets, increase of intracellular Ca^{2+} levels and IP_3, and induction of chemoattractant properties.[317,318] The other activated pathway identified by CITE-seq was MIF signalling. MIF is a pro-inflammatory cytokine expressed in monocytes, macrophages and T cells, among others.[319] The receptor of MIF was identified to be CD74[320], but induction of downstream signalling requires the formation of a receptor complex with CD44[321] or members of the CXC chemokine receptor (CXCR) family (CXCR2, CXCR4[322], CXCR7[323]). MIF was described to have chemotactic activities. As such, it plays an important role in the CCL2 mediated cell adhesion and migration of myeloid cells[324], as well as leukocyte recruitment in general[325]. MIF:receptor interactions result in the phosphorylation of SRC leading to activating pathways such as MAPK (through phosphorylation of ERK)[326] or the PI3K pathway (through phosphorylation of AKT)[327]. Furthermore, it was reported that MIF:receptor interaction reverses the cell cycle arresting function of p53 in tumour cells, contributing to cell survival, proliferation and chemotaxis[328]. Also, MIF signalling through CXCR2 and 4 was associated with the recruitment of monocytes, neutrophils and T cells.[322]

Based on the CellChat analysis, the impact of IL-16 and MIF on the CD14 downregulation was investigated *in vitro*. To explore this, PBMCs were cultured in presence of varli h1 and cytokine neutralising mAb and the effect on the CD14 downregulation was monitored after 48 hours. Firstly, PBMCs were cultured with varli h1 with or without different concentrations of MIF or IL-16 neutralising mAb (Figure 6.7 A, B). As seen before, CD14 on monocytes was downregulated upon varli h1 treatment. Addition of anti-IL-16 (Figure 6.7 A) or anti-MIF (Figure 6.7 B) at the indicated concentrations did not abrogate the CD14 downregulation. Moreover, simultaneous addition of both neutralising mAb did also not abolish CD14 downregulation after varli h1 treatment (Figure 6.7 C). Taken together, these results indicate that oppressed IL-16 and MIF signalling does not affect the CD14 expression on monocytes.

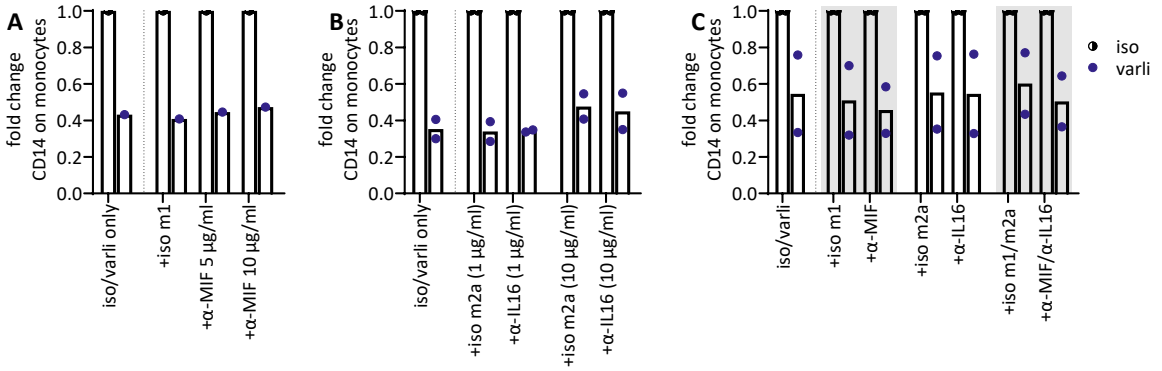

Figure 6.7| CD14 expression on monocytes upon IL-16 or/and MIF neutralisation. A, B: PBMC were cultured at high density and MIF (A) or IL-16 (B) neutralising antibody was added at the indicated concentrations (or the respective isotype controls: iso m1: 3/23, iso m2a: AT130-2) 10 minutes prior to varli h1 or isotype (10 µg/ml) treatment. **C** For the combination of MIF and IL-16 neutralisation, anti-MIF (1 µg/ml) and anti-IL-16 (1 µg/ml) or the combination were added 10 minutes prior varli h1 (10 µg/ml) or isotype treatment. Additionally, PBMC were stimulated with 10 µg/ml varli h1 or the respective isotype control only. CD14 expression on monocytes was assessed 48 hours post-stimulation by flow cytometry (A-C). Data are representative of n=1 (A) or n=2 (B, C).

6.4 Chapter discussion

Turaj *et al.* reported in their study that varli h1 treatment of human PBMCs leads to an alteration of the monocyte phenotype represented by a 2-fold downregulation of the cell surface antigen CD14. As human monocytes do not express hCD27, the varli h1 might have mediated bystander effects on monocytes through hCD27 expressing T cells. This hypothesis has further been supported by the observation that the removal of T cells from the culture abrogated the CD14 downregulation on monocytes, which was reversed by the re-addition of T cells.[243] Therefore, in this chapter the bystander myeloid effects of anti-hCD27 mAbs were explored. Only varli h1 induced notable phenotype changes in the monocyte subset. To decipher the underlying mechanism, a variety of immunological assays was performed. The data suggest that the observed CD14 downregulation might partially be dependent on TCR activation and hCD27 signalling but not the cytokines MIF and IL-16.

Treatment of PBMCs with varli h1 produced a $CD14^{-}CD16^{+}CD86^{+}$ monocyte phenotype (Figure 6.1-Figure 6.3). The CD14 downregulation in concordance with the CD86 upregulation may suggest a skewing of classical monocytes towards a non-classical monocyte phenotype. Of note, PBMCs were only stimulated for 48 hours which is not sufficient time for a complete monocyte differentiation. Vitale *et al.* demonstrated that the stimulation of purified T cells with the hCD27 targeting mAb 1F5 results in the secretion of IFN-γ and TNF-α.[96] According to the literature, these cytokines can prompt the differentiation of monocytes into pro-inflammatory M1-macrophages, which have an $IL\text{-}12^{high}$, $IL\text{-}23^{high}$, $IL\text{-}10^{low}$ phenotype and simultaneously express CD16, CD86 and CD64 (hFcγRI). They secrete pro-inflammatory cytokines such as IL-1β, TNF-α and IL-6 and thus participate in

inflammatory immune responses.[329] Moreover, M1-macrophages are able to initiate T_h1-cell responses and provide anti-tumour activities.[330] As mentioned previously, Ziegler-Heitbrock *et al*. demonstrated that classical $CD14^{++}$ monocytes can differentiate into a monocyte subpopulation ($CD14^{-}CD16^{++}$ non-classical monocytes), which is associated with a more mature stage[331] and can be prompted via cytokine stimulation to develop into macrophages. Further, CITE-seq data from PBMCs stimulated with varli h1 *in vitro* (generated in the AVG Southampton) suggests that classical monocytes might differentiate beyond the non-classical monocyte stage into monocyte-derived DCs upon varli h1 treatment (data unpublished). Trajectory inference (allowing the investigation of cell differentiation) of the six identified monocyte subsets proposed that varli h1 treatment triggers differentiation of classical monocytes into DC-like monocytes via the type-1 classical, non-classical, intermediate and SPP-1 classical monocyte stage. Concomitantly, a downregulation of CD14 and myeloid related proteins 8 and 14 (MRP8/14, S100A8/A9) was observed, which had been reported to be associated with the progression of monocyte differentiation into monocyte-derived DCs[332]

Different approaches have been undertaken to decipher the varli h1 induced CD14 downregulation. First, TCR signalling was blocked by the addition of CSA. Only marginal trends towards dependence of the CD14 downregulation on simultaneous TCR and hCD27 signalling were detected (Figure 6.5). Of note, the activation of $CD4^{+}$ and $CD8^{+}$ T cells (indicated by CD137 expression) was weak, even without blockade of TCR signalling, indicating that the T cells might not have been sufficiently activated. Indeed, Ramakrishna *et al*. demonstrated, that stimulation of T cells with 1F5 is crucially dependent on TCR signalling mediated by suboptimal concentrations of plate-bound anti-CD3 mAb.[34] Next, human monocytes were either cultured with Jurkat cells expressing hCD27 or Jurkat cells expressing hCD27 lacking the intracellular signalling domain. Congruent with Turaj *et al.*[243], monoculture of monocytes and stimulation with varli h1 did not evoke CD14 downregulation (Figure 6.6). In contrast, co-culture with T cells induced some CD14 downregulation, possibly suggesting that T cells, as providers of hCD27, are involved in the regulation of CD14 on monocytes (Figure 6.6). However, the results also indicate that this is not solely reliant on hCD27 signalling.

As elucidated above, CITE-seq analysis suggested that the CD14 expression on monocytes might be regulated by the cytokines IL-16 and MIF. Neutralisation of the respective cytokines either alone or in combination however could not abrogate the phenotypic change observed upon varli h1 treatment (Figure 6.7). Concentrations of the neutralising anti-MIF and anti-IL-16 mAbs have been titrated, but successful cytokine neutralisation was not confirmed in the experiments presented. A study by Mathy *et al.* identified the pro-inflammatory cytokines IL-1β, IL-6, IL-15 and TNF-α to be highly upregulated in PBMC cultures after the addition of recombinant human IL-16. However, when IL-16 neutralising mAb was added to the culture, the secretion of these cytokines was

abrogated.[333] Therefore, ELISA assessing the cytokine profile after the addition of neutralising mAb might aid to identify the correct neutralising concentration. Of note, hCD27 stimulation of PBMC cultures also induced elevated levels of IL-6 and TNF-α (measured by meso scale discovery, data unpublished). Another approach to abrogate MIF signalling may be the interruption of MIF:CD74 interaction through blockade of CD74 with blocking mAb. However, there have been reports that do not support the assumption that the MIF pathway is part of the monocyte differentiation into pro-inflammatory cell subsets. MIF overexpression has been observed in cancers, such as melanoma, glioblastoma or prostate cancer, and was associated with disease progression (reviewed in [334]). Also, a pre-clinical study by Yaddanapudi and colleagues demonstrated that MIF-deficiency or antagonising MIF (by small molecule inhibitors) results in a reduction of tumour growth with the ability to convert an immunosuppressive TME into a more pro-inflammatory TME.[335] The observation that neither MIF nor IL-16 mediated the CD14 downregulation in response to varli h1, might lead to the assumption that other pathways are involved in this process. Indeed, CITE-seq analysis identified three other pathways that were significantly upregulated upon varli h1 treatment (SPP-1, CCL and GALECTIN, data unpublished). However, to what extent these pathways contribute to the observed monocyte differentiation is subject to further investigations.

The downregulation of CD14, concomitant with the upregulation CD16 and CD86 was solely evident upon stimulation with varli h1 and not the h2 counterpart, suggesting that the effect might be isotype-dependent (Table 6.2 and Figure 6.1-Figure 6.3). However, this is in contradiction with the observation that other anti-hCD27 h1 mAbs did not induce the CD14 downregulation. Of note, anti-hCD27 mAbs were regularly tested for endotoxin levels to rule out monocyte activation through LPS contamination, which could have accounted for the phenotypic changes observed.

Chapter 7 General discussion

Over the last three decades, mAbs have been at the forefront of cancer immunotherapy. The first mAb approved by the FDA in 1986 was OKT3, a T-cell depleting mAb to prevent transplant rejection. In 2021, 35 years later, the FDA set a milestone by approving its 100th mAb product (anti-PD-1 blocking mAb (dostralimab)). Forty-one percent of these approved mAbs are used in cancer therapy, which highlights their rising success in this field.[336] However, the latest review of "Antibodies to watch in 2022" reported that the majority of mAbs in late-stage clinical trials for cancer indications are checkpoint inhibitory or direct targeting mAbs, but not immunostimulatory mAbs.[337] Immunostimulatory mAbs targeting co-stimulatory receptors such as 4-1BB, OX40, CD40 or CD27 have been, and still are extensively studied in pre-clinical trials and demonstrated promising anti-tumour activity in several solid tumour and lymphoma mouse models.[32,165,169,241-243,264,265,273,274] However, in clinic their efficacy has been modest (see section 1.5.2.2, Table 1.4) and in some instances accompanied with severe side effects, leading to the termination of the clinical investigation.[271,338]

There is now an extensive body of data indicating that the efficacy of immunostimulatory mAbs can be improved by modulating the mAb format. Research in the field suggests that agonism of immunostimulatory mAbs might be driven by two key determinants: mAb epitope specificity and isotype, and that this might be dependent on the mAb target. Studies have characterised aspects of this relation for OX40, CD40 and 4-1BB-mediated agonism[160,169,170,265], but there is no data on CD27 available yet. Thus, with a panel of six anti-hCD27 mAbs (including varli, currently in clinical trials) the impact of epitope specificity and isotype on the agonistic activity of anti-hCD27 mAb was investigated, to provide a guide towards the generation of therapeutically more effective anti-hCD27 mAbs.

Binding assays, SPR and *in vitro* functional characterisation revealed different target binding characteristics and agonistic activities of the anti-hCD27 mAbs. Correlation of the agonistic activity with affinity demonstrated an inverse relationship for all mAbs but hCD27.15, wherein high affinity was associated with a stronger activity. The strongest agonist hCD27.15, bound hCD27 with reduced Bmax and medium bivalent affinity (by K_D across the anti-hCD27 mAb), and its epitope was located within CRD1, possibly facilitating a unique mechanism of receptor clustering. Thus, hCD27.15 might

be able to bind across multiple hCD27 homodimer pairs (Figure 7.1). This ability may be driven by its rapid k_d and externally facing epitope. The mAb might evoke a "trigger and release" mechanism, whereby hCD27.15 binds to two hCD27 homodimers and facilitates clustering (trigger), and then rapidly dissociates from the receptor (release) to draw further hCD27 dimers into the cluster. A similar mechanism supporting this hypothesis has previously been described for mAbs targeting TNFR Fas, where it was proposed that the k_d is a crucial determinant for receptor clustering. Therefore, partial dissociation from the receptor is essential for anti-Fas mAb activity. The free F(ab) arm is then able to recruit further monomeric Fas molecules, which subsequently results in augmented receptor multimerisation and enhanced downstream signalling. On the contrary, it was suggested that mAbs with a low k_d lock the receptor in an inactivated, non-signalling stage, which is associated with less activity.[339] The "trigger and release" hypothesis would also account for hCD27.15's low avidity, yet strong agonistic activity across multiple isotypes. Less mAb molecules are required for receptor crosslinking and to evoke downstream signalling. Binding to internal aspects of a hCD27 dimer (e.g. varli) might prevent mAbs to reach across multiple dimers and instead only enable binding to one hCD27 dimer with both Fab arms. Thus, the number of surface-bound mAb is greater, accounting for the high avidity observed by flow cytometry.

The assumption that the mAb performance is influenced by epitope location is further exampled by the fact that AT133-5 and AT133-11 also bind epitopes located in CRD1, but do not evoke strong agonism as hCD27.15 or AT133-2. The discrepancy might be, as detailed above, due to the epitope orientation on the hCD27 homodimer (external versus internal binding). Furthermore, weak agonistic activity was also evident, when mAbs bound to membrane-proximal epitopes (varli: CRD2, AT133-14: CRD3).

Therefore, it can be summarised that the epitope has an influence on the agonistic activity of hCD27-mediated agonism, with mAbs binding to membrane-proximal, externally located epitopes being the strongest agonists and mAb binding either to internally facing or membrane-proximal residues being less agonistically potent. The data reiterate that fine-tuning of epitope location affects mAb activity as this is further supported by results reported for anti-CD40 mAbs. For example, the anti-CD40 mAbs Lob7/4 and CP870,893 bind within CRD1 of the CD40 receptor but show varying agonistic activities, with Lob7/4 being less agonistic than CP870,893.

Interestingly, enhanced binding of hCD27.15 (competing reagent) was detected when added to AT133-11 or hCD70 Fc (initial reagent). Considering the location of the epitopes of AT133-11 and hCD70 Fc (AT133-11: CRD1 and CD70: CRD2, internal surface, respectively) and hCD27.15 (CRD1, external surface), it is likely that binding of the initial reagent might alter the conformation and arrangement of hCD27 on the cell surface, enabling enhanced binding of hCD27.15. Microscopic

investigation of the co-localisation of fluorochrome-conjugated hCD27.15 and AT133-11 or hCD70 Fc by confocal microscopy might aid to elucidate this hypothesis. Further, it might be interesting to explore whether the enhanced binding of hCD27.15 after pre-incubation with AT133-11 or hCD70 Fc subsequently translates into enhanced downstream signalling in NF-κB/GFP reporter assays.

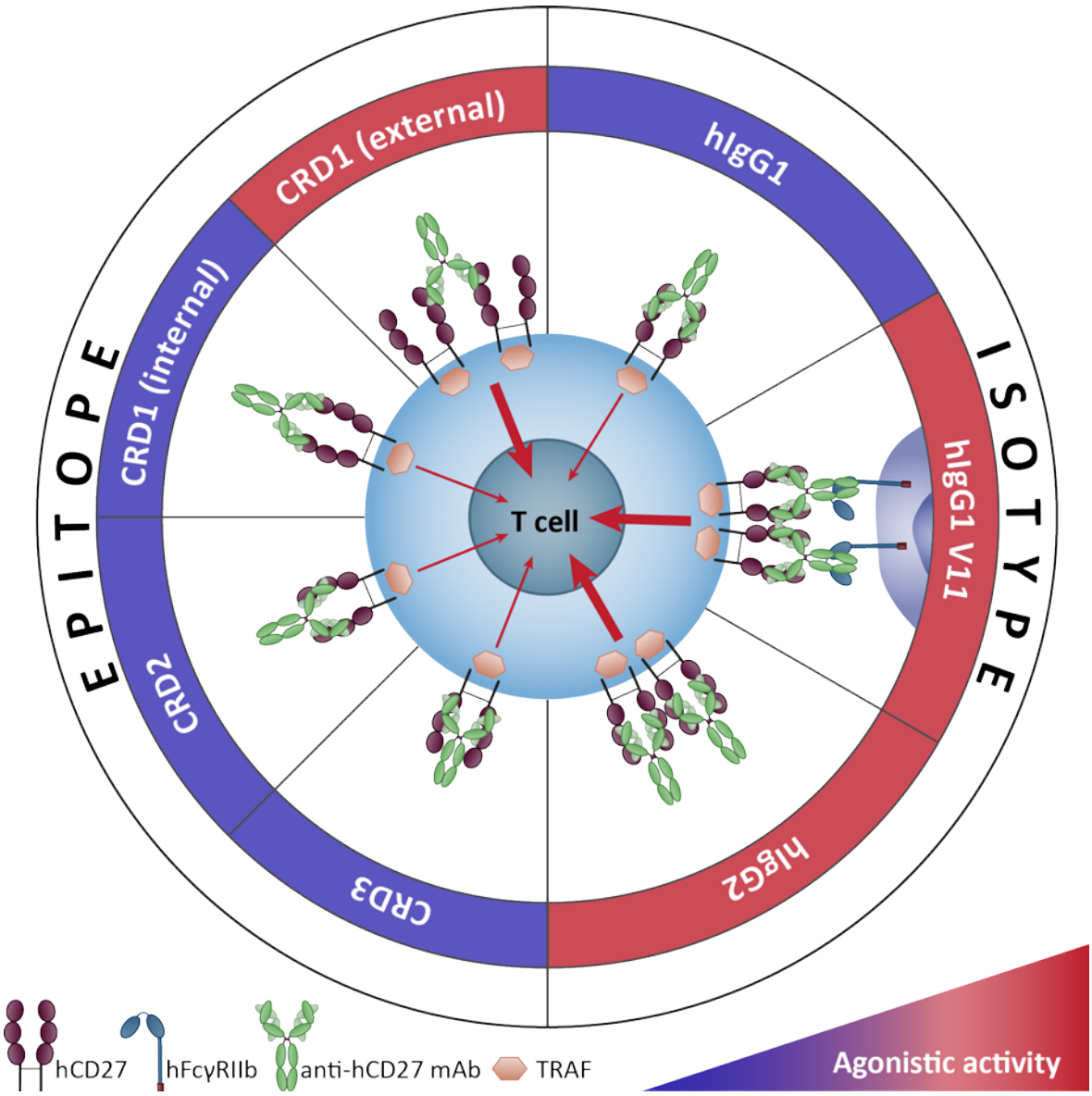

Figure 7.1 Schematic display of hypothesised hCD27-mediated agonism by anti-hCD27 mAbs. The illustration shows the proposed impact of epitope specificity (left half of the circle) and isotype (right half of the circle) on hCD27-mediate agonism. Anti-hCD27 mAbs, binding to the internal surface of CRD1 or membrane-proximal epitopes within CRD2 or CRD3 display moderate/weak agonistic activity. In contrast, anti-hCD27 mAbs with epitopes facing the outer surface of a hCD27 homodimer evoke more receptor clustering. Anti-hCD27 h1 mAbs mediate only weak agonism, but activity can be enhanced upon Fc-engineering (V11) and FcγRIIb-mediated clustering. Anti-hCD27 h2 mAbs mediate strong agonism Fc-independently.

As elucidated before, mAbs binding to the internal surface or membrane-proximal epitopes of the hCD27 homodimer showed moderate to weak agonistic activity as h1 isotypes, and marginally improved activity when used as a h2 format. However, engagement of FcγRIIb by h1 mAbs or Fc-

engineering of h1 mAb to gain improved affinity to FcγRIIa/b or FcγRIIb alone strongly augmented the activity of the weaker agonists and moderately enhanced the efficacy of the strong agonists in NF-κB reporter and T-cell proliferation assays. This indicates that weak agonism due to epitope location can partially be overcome by Fc:FcγRIIb interactions and that FcγRIIb-mediated crosslinking is indispensable for weaker agonists (Figure 7.1). Agonism of TNFRs OX40, CD40 and 4-1BB is also dependent on FcγRIIb engagement.[165,278,340,341] Similar to anti-hCD27 mAbs, the activity of strong agonistic anti-CD40 and anti-4-1BB mAbs is less dependent on FcγRIIb-engagement than of the activity of weaker agonists.[169,341] However, Fc:FcγR engagement might be limited by the epitope location as it was proposed for anti-CD40 mAbs[169]. Thus, closer binding of the mAbs to the N-terminus might compromise the accessibility of the mAb's Fc-domain for scaffolding FcγRs.

Nevertheless, Fc-engineering becomes more and more attractive for mAbs targeting members of the TNFRSF. Employment of the clinical anti-hOX40 mAb PF-04518600 as a h1 V11 and not the h2 isotype (as used in the clinic) led to expansion of TILs in tumour tissue of patients with liver metastasis, colorectal cancer and hepatocellular carcinoma.[340] The importance of FcγRIIb-mediated cross-linking was also shown for CD40 agonists [165] and 4-1BB targeting mAbs[341]. Superior anti-tumour activity was achieved with anti-CD40 h1 V11 mAb when compared to h2 or h1 SE/LF counterparts.[165] Qi *et al*. developed an anti-h4-1BB mAb with selective affinity for hFcγRIIb, which showed potent anti-tumour activity in h4-1BB knock-in mice. However, the group did not elucidate the specific Fc mutations leading to the selective affinity to FcγRIIb.[341]

The data obtained in this project suggest that both epitope specificity and isotype dictate hCD27-mediated agonism, but the isotype seems to be the dominating factor (Figure 7.1). Research on other TNFR members has also identified this link between epitope specificity and strength of agonism. For example, anti-CD40 mAbs[169] and anti-4-1BB mAbs[272] also require binding to distally located CRDs for optimal agonism, whereas OX40-mediated agonism requires residues in membrane-proximal CRD4[265].

When it comes to clinical application of immunostimulatory mAbs, it is important to carefully select the mAb format. Given the nature of h1 mAbs to engage activating FcγRs (high A:I ratio) and their ability to induce effector functions such as ADCC, h1 might not be the ideal isotype for immunostimulatory mAbs. Enhancing the affinity of h1 mAbs to FcγRIIb (lower A:I ratio) to augment agonistic signalling might also come with limitations. Since these mAb formats crucially rely on the presence of the inhibitory FcγRIIb, their efficacy might be compromised in tumours, where FcγRIIb abundancy is low. In this instance, mAb formats that facilitate receptor clustering FcγR-independently might be the better choice. Zhang *et al*. have characterised novel mutations that drive anti-OX40 mAb-mediated receptor clustering FcγR-independently. These mutations include

T437R and K248E, which facilitate anti-OX40 mAb hexamerisation and subsequent receptor clustering solely through Fc:Fc interactions once bound to the receptor.[342] An alternative approach is the usage of h2 mAb formats, which, based on the results observed in this project and by others[163,169], are supposed to mediate anti-tumour efficacy Fc-independently, and might be driven by the special conformation of its hinge. The underlying mechanism is yet unknown and requires further investigation. White *et* al. propose, that receptor-independent clustering of h2 mAbs may be caused by the more rigid h2B isoform. The special conformation such h2B mAbs adapt may allow tighter packing of receptors which contributes to enhanced downstream signalling.[163] This observation is supported by another study investigating the influence of hIgG hinges on mAb agonism, which additionally suggest that more rigid hinges might be able to more efficiently stabilise receptor multimerisation.[343] Hinge modulation might therefore be an alternative approach to improve mAb performance. Indeed, Buchan *et al*. combined two mAb effector functions (agonism and depletion) by combining a h2B CH1 hinge region and mIgG2a constant region of an immunostimulatory anti-4-1BB mAb. Administration *in vivo* not only led to Treg depletion (m2a mediated) but also increased intra-tumoural $CD8^+$ T-cell infiltration (possibly mediated through h2B CH1 hinge). These results highlight the great utility of Fc-engineering to adapt to specific requirements and increase therapeutic efficacy.[273]

In addition to the limitations for immunostimulatory mAbs discussed above, multiple other factors have to be considered, with the most important being safety and toxicity. The most dramatic toxicities have been observed upon over-stimulation of the immune system by highly agonistic mAbs, as was seen with the anti-CD28 mAb TGN1412 (hIgG4) in a first-in-human study in 2006. A single infusion of the mAb induced a systemic inflammatory response with a rapid “cytokine release syndrome” (CRS), characterised by exceptionally high secretion of inflammatory cytokines (TNF-α, IFN-γ, IL-10). All trial participants were taken into intensive care for appropriate medical treatment. To determine the dose of TGN1412 for the first-in human trial, the mAb was tested in non-human primates (cynomolgus and rhesus macaques). However, the CRS observed in the clinic was not apparent in these animal models. It was later revealed that CD28 is downregulated on $CD4^+$ T_{EM} cells in cynomolgus macaques but not humans, and that human CD28 differs from CD28 of non-human primates.[344] Further, Hussain *et al*. suggested that the superagonistic activity observed with TGN1412 and the concomitant systemic immune toxicity are triggered by FcγRIIb-mediated clustering of CD28.[262] On-target, but off-site effects also occurred with the strong agonistic anti-4-1BB mAb urelumab. Some patients developed severe dose-dependent hepatotoxicity upon administration of urelumab (at doses >1 mg/kg), leading to the termination of the phase I clinical trial.[271] In contrast, the less agonistic anti-4-1BB mAb utomilumab, showed a milder toxicity profile, implying that the strength of mAb agonism might be associated with toxic side effects.[345] Indeed, it

was hypothesised that FcγRIIb-mediated cross-linking of urelumab on activated $CD8^+$ T cells in the liver contributed to the observed side effects and that fine-tuning of the balance between Fc functions and mAb strength can help to overcome these limitations. Nevertheless, both immunostimulatory mAbs, urelumab and TGN1412, are back in clinical trials; this time at lower doses than before.[345,346] The observation that toxicities might be associated with FcγRIIb-mediated super-agonistic activity of immunostimulatory mAbs indicates another risk that has to be considered and investigated, particularly in the case of Fc-mutated mAbs with enhanced affinity to FcγRIIb.

To evaluate the aforementioned risks and limitations, testing of the anti-hCD27 mAbs in suitable *in vivo* mouse models is essential. In this project, only hCD27.15 h2σ was investigated in a pilot experiment *in vivo* and achieved some slowing of tumour growth. Thus, the next step is to select additional anti-hCD27 mAbs with different epitope specificities, and to evaluate their activity as different isotype formats in suitable tumour mouse models. This will aid to elucidate, whether the differences between the mAbs observed *in vitro* also translate to anti-tumour activity *in vivo*. To do so, appropriate mouse models have to be established and optimised, such as the Hu:PBL:SCID mouse model, inoculated with different tumour cell lines such as Daudi B-cell lymphoma or RPMI8226 MM. Further, a comparison of the mAbs in these models might help to unravel the difference observed in the myeloid differentiation upon treatment varli h1 and all other anti-hCD27 mAbs *in vitro*. Analysis of immune cell subsets, especially of the myeloid compartment might reveal differences in cell differentiation that aid to clarify the mechanism behind the CD14 downregulation. To date, no severe systemic toxicities have been reported upon anti-hCD27 mAb administration in pre-clinical (data unpublished) and clinical trials. However, especially with Fc-engineered mAbs with enhanced affinity to FcγRIIb, there is an increased risk of toxicity that has to be carefully evaluated when it comes to clinical application.

Turaj *et al*. demonstrated in previous studies that anti-CD27 mAb can enhance the efficacy of direct tumour-targeting mAbs such as anti-CD20 in B cell lymphoma mouse models.[243] The combination of anti-CD20 and anti-CD27 improved myeloid cell-mediated tumour phagocytosis by anti-CD20, in a T-cell dependent manner. Based on these promising findings, a clinical trial has been initiated, investigating the CD20/CD27 combination therapy. In the light of this study, this project also aimed to combine novel anti-hCD27 mAbs with the direct targeting anti-hCD38 mAb daratumumab for the therapy of MM. This combination therapy was tested in pilot experiments. However, in this project, an appropriate mouse model was not successfully established. Further efforts have to be made to improve the Hu:PBL:SCID model to be able to investigate the combination therapy in the context of a “fully” human immune system. Once this has been achieved, it might be interesting to see

whether the combination of daratumumab with different anti-hCD27 mAb clones shows different outcomes regarding survival, efficacy and intra-tumoural immune cell landscape.

To conclude, data obtained in this project and previously reported in the literature underline the importance of epitope specificity and more so, isotype for agonistic activity mediated by immunostimulatory mAbs, and the fact that this is target-dependent. In the case of hCD27-mediated agonism, it is proposed that potent agonistic activity is dependent on epitope location, with membrane-distal, externally binding mAbs being more active than membrane-proximal, internally binding mAbs. Furthermore, weak agonism can be overcome by Fc-engineering to enhance FcγRIIb mediated crosslinking and associated downstream signalling. The results highlight the importance of fine-tuning the balance between epitope-specificity and Fc-function and provide a guide towards engineering optimised anti-hCD27 mAb for optimal clinical efficacy.

Appendix A

A.1 hCD27 mAb sequences

Table A.1| hCD27 mAb sequences. The table shows the sequences of the hCD27 mAb panel. vh: variable region heavy chain; vκ: variable region κ-chain; mκ: mouse κ-chain; hκ: human κ-chain; SE/LF mutation in the h1 constant region is indicated in red (S267E/L328F) and V9 (G237D/P238D/P271G/A330R) and V11 (G237D/P238D/P271G/A330R/H268D) mutation in green.

Variable mAb regions		
varli	vh	MEFGLSWVFLVALLRGVQCQVQLVESGGGVVQPGRSLRLSCAASGFTFSSYDMHWVRQAPGK GLEWVAVIWYDGSNKYYADSVKGRFTISRDNSKNTLYLQMNSLRAEDTAVYYCARGSGNWGFF DYWGQGTLVTVSS
	vκ	MRVLAQLLGLLLLCFPGARCDIQMTQSPSSLSASVGDRVTITCRASQGISRWLAWYQQKPEKAPK SLIYAASSLQSGVPSRFSGSGSGTDFTLTISSLQPEDFATYYCQQYNTYPRTFGQGTKVEIK
hCD27.15	vh	MGWSWIFLFLLSGTAGVLSEVRLQQSGADLVKPGASVKLSCTASGFIIKATYMHWVRQRPEQGL EWIGRIDPANGETKYDPKFQVKATITADTSSSTAYLQLNSLTSDDTAVYYCARYAWYFDVWGAGT LVTVSS
	vκ	MGWSWIFLFLLSGTAGVLSDIQMTQSPASLSASVGDTVTITCRASENIYSFLAWYHQKQGRSPQL LVYHAKTLAEGVPSRFSGSGSGTQFSLKINSLQAEDFGSYYCQHYYGSPLTFGAGTKLEVK
	vκ	MRFPAQLLGLLLFWLHGAQCDIQMTQSPSSLSASLGGKVTITCKASQDINKYIAWYQHKPGKGP RLLIHYTSTLQPGIPSRFSGSGSGRDYSFSISNLEPEDIATYYCLQYDNPLNTFGGGTKLEIK
AT133-2	vh	MGWSWIFLFLVATATGVHSQVQLQQPGAELVRPGASVKLSCKASGYSFTSYWMNWVKQRPG QGLEWIGMIHPSDSETRLNQKFKDKATLTVDKSSSTAYMQFSSPTSEDSAVYYCARGPDVYYEAL DYWGQGTTLTVSS
AT133-5	vh	MAWVWTLLFLMAAAQSAQAQIQLVQSGPELKKPGETVKISCKASGYTFTNYGMNWVKQAPGK GLKWMGWINTYTGEATYVDDFKGRFAFSLETSASTAYLQTNNLKNEDTATYFCARNWEGAMDY WGQGALVTVSS
	vκ	MGIKMESQFLVFISILLWLYGADGNIVMTQSPKSMSMSVGERVTLSCKASENVGTFVSWYQQKS EQSPELLIYGASNRYTGVPDRFTGSGSATDFTLTISSVQAEDLADYHCGQSYSYPLTFGAGTKLELK
AT133-11	vh	MDWVWNLLFLMAAAQSIQAQIQLVQSGPELKKPGETVKISCKASGYTFTNYGMNWVKQAPGK GLKWMGWINTNTGEPTYAEEFKGRFAFSLETSASTAYLQINNFKNEDTATYFCARWDQGAMDY WGQGTLVTVSS
	vκ	METDTLLLWVLLLWVPGSTGNIVLTQSPASLAVSLGQRATISCRASESVDSYGNSFMHWYQQKP GQPPKLLIYLASNLESGVPARFSGSGSRTDFTLTIDPVEADDAATYYCQQNNEDPPTFGGGTKLEIK
AT133-14	vh	MGWSWNFHFLLSITAGVHCQVQLQQSGPELVKPGASVKFSCKASGYAFSRSWMNWVKQRPG QGLEWIGRIYPGDGDTNYNGKFKGKATLTADESSNTAYMQLSSLTSVDSAVYFCAIMITTVHAM DYWGQGTLVTVSS
	vκ	MESDTLLLWVLLLWVPGSTGDIVLTQSPASLTVSLGQRATISCRASQSFTASSSTYVHWYQQKPG QPPKLLIKYASNLGSGVPARFSGSGSGTDFTLTIHPVEEEDTATYYCQHSWEIPYTFGGGTKLEIK

Constant mAb regions		
h1		ASTKGPSVFPLAPSSKSTSGGTAALGCLVKDYFPEPVTVSWNSGALTSGVHTFPAVLQSSGLYSLSS VVTVPSSSLGTQTYICNVNHKPSNTKVDKKVEPKSCDKTHTCPPCPAPELLGGPSVFLFPPKPKDTL MISRTPEVTCVVVDVSHEDPEVKFNWYVDGVEVHNAKTKPREEQYNSTYRVVSVLTVLHQDWL NGKEYKCKVSNKALPAPIEKTISKAKGQPREPQVYTLPPSRDELTKNQVSLTCLVKGFYPSDIAVEW ESNGQPENNYKTTPPVLDSDGSFFLYSKLTVDKSRWQQGNVFSCSVMHEALHNHYTQKSLSLSP GK
h2		ASTKGPSVFPLAPCSRSTSESTAALGCLVKDYFPEPVTVSWNSGALTSGVHTFPAVLQSSGLYSLSS VVTVPSSNFGTQTYTCNVDHKPSNTKVDKTVERKCCVECPPCPAPPVAGPSVFLFPPKPKDTLMIS RTPEVTCVVVDVSHEDPEVQFNWYVDGVEVHNAKTKPREEQFNSTFRVVSVLTVVHQDWLNG KEYKCKVSNKGLPAPIEKTISKTKGQPREPQVYTLPPSREEMTKNQVSLTCLVKGFYPSDIAVEWES NGQPENNYKTTPPMLDSDGSFFLYSKLTVDKSRWQQGNVFSCSVMHEALHNHYTQKSLSLSPG K
hκ		RTVAAPSVFIFPPSDEQLKSGTASVVCLLNNFYPREAKVQWKVDNALQSGNSQESVTEQDSKDST YSLSSTLTLSKADYEKHKVYACEVTHQGLSSPVTKSFNRGEC
mIgG1		AKTTPPSVYPLAPGSAAQTNSMVTLGCLVKGYFPEPVTVTWNSGSLSSGVHTFPAVLQSDLYTLSS SVTVPSSTWPSETVTCNVAHPASSTKVDKKIVPRDCGCKPCICTVPEVSSVFIFPPKPKDVLTITLTP KVTCVVVDISKDDPEVQFSWFVDDVEVHTAQTQPREEQFNSTFRSVSELPIMHQDWLNGKEFK CRVNSAAFPAPIEKTISKTKGRPKAPQVYTIPPPKEQMAKDKVSLTCMITDFFPEDITVEWQWNG QPAENYKNTQPIMDTDGSYFVYSKLNVQKSNWEAGNTFTCSVLHEGLHNHHTEKSLSHSPGK
mκ		RTVAAPSVFIFPPSDEQLKSGTASVVCLLNNFYPREAKVQWKVDNALQSGNSQESVTEQDSKDST YSLSSTLTLSKADYEKHKVYACEVTHQGLSSPVTKSFNRGEC

A.2 Domain mapping – truncated hCD27 receptor sequences

Table A.2| hCD27 receptor truncation mutant sequences. The table lists the sequences for hCD27 WT and truncated mutants. Underlined are the signal peptide and the transmembrane region. Coloured in blue is CRD1, in red CRD2 and in green CRD3.

CD27 WT	MARPHPWWLCVLGTLVGLSATPAPKSCPERHYWAQGKLCCQMCEPGTFLVKDCDQHRKAAQCDPCIP GVSFSPDHHTRPHCESCRHCNSGLLVRNCTITANAECACRNGWQCRDKECTECDPLPNPSLTARSSQAL SPHPQPTHLPYVSEMLEARTAGHMQTLADFRQLPARTLSTHWPPQRSLCSSDFIRILVIFSGMFLVFTLAG ALFLHQRRKYRSNKGESPVEPAEPCRYSCPREEEGSTIPIQEDYRKPEPACSP
CRD1	MARPHPWWLCVLGTLVGLSATPAPKSCPERHYWAQGKLCCQMCEPGTFLVKDCDQHRKAAQCDPQP THLPYVSEMLEARTAGHMQTLADFRQLPARTLSTHWPPQRSLCSSDFIRILVIFSGMFLVFTLAGALFLHQ RRKYRSNKGESPVEPAEPCRYSCPREEEGSTIPIQEDYRKPEPACSP
CRD1+2	MARPHPWWLCVLGTLVGLSATPAPKSCPERHYWAQGKLCCQMCEPGTFLVKDCDQHRKAAQCDPCIP GVSFSPDHHTRPHCESCRHCNSGLLVRNCTITANAECPQPTHLPYVSEMLEARTAGHMQTLADFRQLPA RTLSTHWPPQRSLCSSDFIRILVIFSGMFLVFTLAGALFLHQRRKYRSNKGESPVEPAEPCRYSCPREEEGST IPIQEDYRKPEPACSP
CRD1+3	MARPHPWWLCVLGTLVGLSATPAPKSCPERHYWAQGKLCCQMCEPGTFLVKDCDQHRKAAQCDACR NGWQCRDKECTECDPLPNPSLTARSSQALSPHPQPTHLPYVSEMLEARTAGHMQTLADFRQLPARTLST HWPPQRSLCSSDFIRILVIFSGMFLVFTLAGALFLHQRRKYRSNKGESPVEPAEPCRYSCPREEEGSTIPIQE DYRKPEPACSP
CRD2+3	MARPHPWWLCVLGTLVGLSATPAPKPCIPGVSFSPDHHTRPHCESCRHCNSGLLVRNCTITANAECACR NGWQCRDKECTECDPLPNPSLTARSSQALSPHPQPTHLPYVSEMLEARTAGHMQTLADFRQLPARTLST HWPPQRSLCSSDFIRILVIFSGMFLVFTLAGALFLHQRRKYRSNKGESPVEPAEPCRYSCPREEEGSTIPIQE DYRKPEPACSP
CRD3	MARPHPWWLCVLGTLVGLSATPAPKACRNGWQCRDKECTECDPLPNPSLTARSSQALSPHPQPTHLPY VSEMLEARTAGHMQTLADFRQLPARTLSTHWPPQRSLCSSDFIRILVIFSGMFLVFTLAGALFLHQRRKYR SNKGESPVEPAEPCRYSCPREEEGSTIPIQEDYRKPEPACSP

A.3 Cross-reactivity of anti-hCD27 mAbs with mCD27

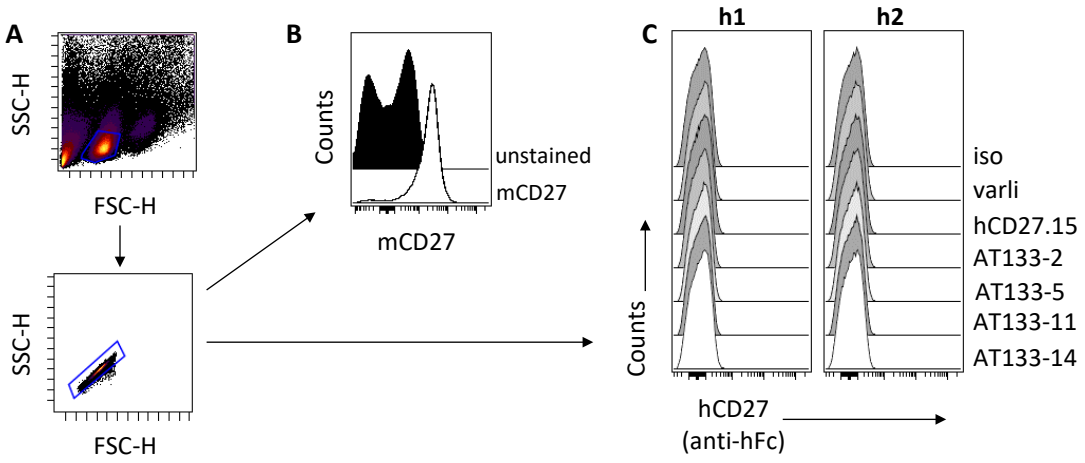

Figure A.1| Binding of anti-hCD27 mAbs to mCD27. Splenocytes of a naïve C57/BL6 mouse were incubated with 10 µg/ml anti-hCD27 h1/h2 mAb or anti-mCD27 mAb or the respective isotype control for 30 minutes at 4°C and binding to mCD27 was detected using a fluorochrome-conjugated anti-hFc. To confirm mCD27 expression on murine lymphocytes, splenocytes were also stained with a fluorochrome-conjugated anti-mCD27 mAb. **A**: Gating strategy for lymphocytes. **B**: Expression of mCD27 on murine lymphocytes. **C**: Histogram plots showing the binding of the anti-hCD27 mAbs to murine lymphocytes (n=1).

A.4 SPR analysis

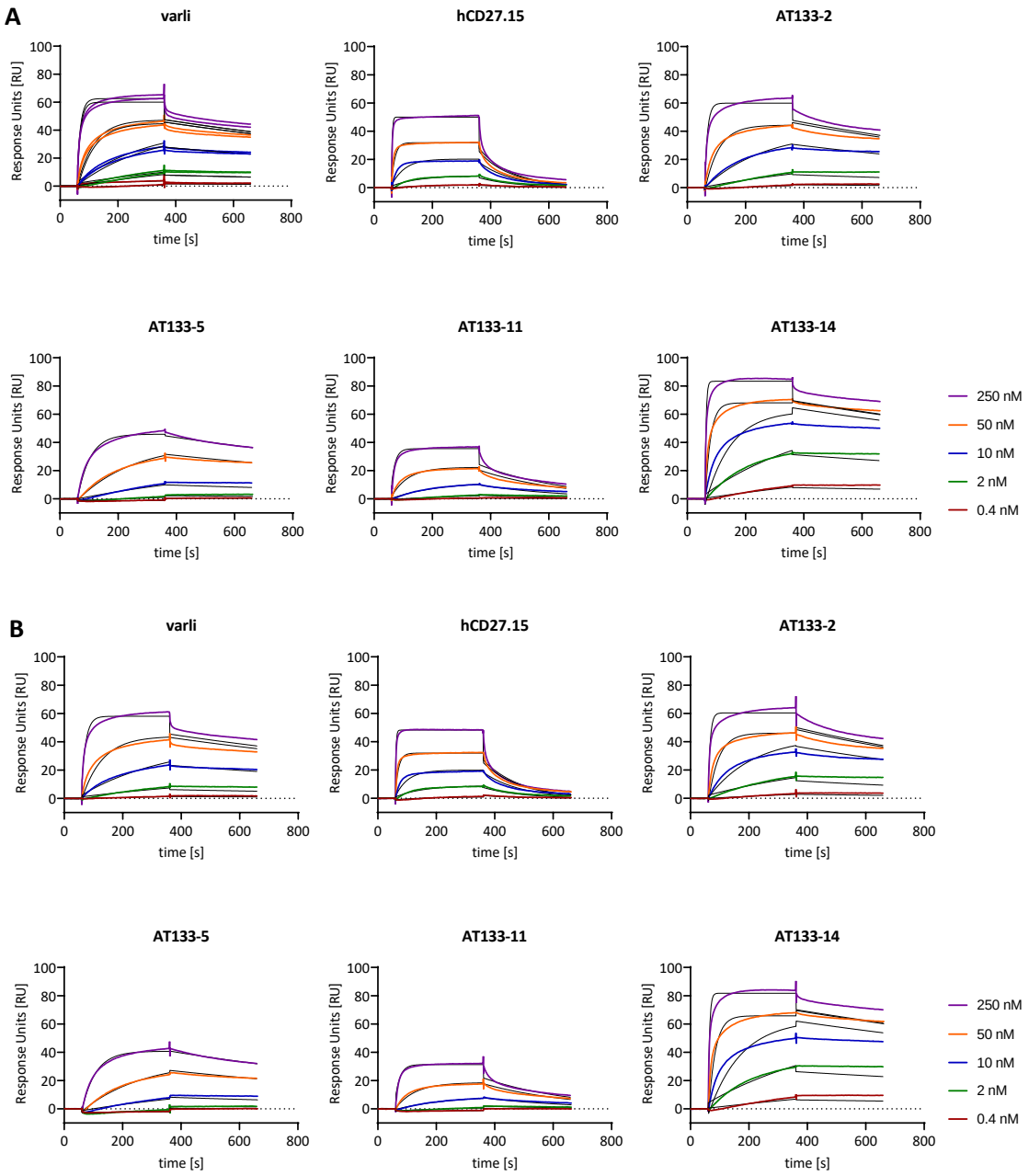

Figure A.2| SPR analysis of anti-hCD27 mAbs at 100 RU. A, B: Anti-hCD27 h1 (A) and anti-hCD27 h2 (B) mAbs were diluted to 0.4, 2, 10, 50 and 250 nM and binding curves were achieved by plotting the RU over time. His-tagged hCD27 was immobilised at 100 RU. A 1:1 binding fitting was applied (black line) (n=1).

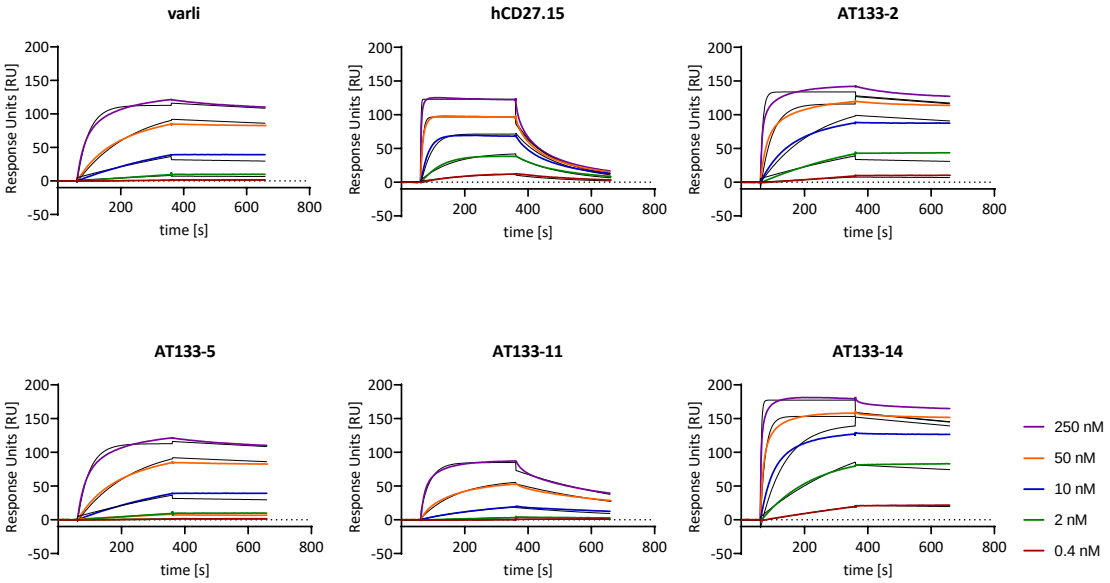

Figure A.3| SPR analysis of anti-hCD27 h1 mAbs at 180 RU. Anti-hCD27 h1 mAbs were diluted to 0.4, 2, 10, 50 and 250 nM and binding curves were achieved by plotting the RU over time. His-tagged hCD27 was immobilised at 180 RU. A 1:1 binding fitting was applied (black line) (n=1).

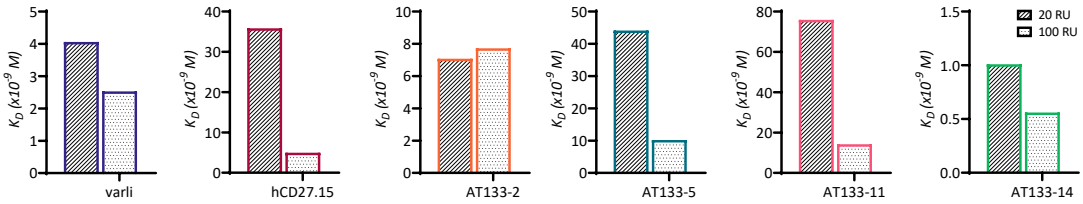

Figure A.4| Impact of hCD27 receptor density on the binding affinity of anti-hCD27 h2 mAbs. Comparison of K_D of anti-hCD27 h2 mAbs at hCD27 ligand densities of 20, 100 or 180 RU (n=1 for 20, 100 and 180 RU, respectively).

A.5 Alanine scanning mutagenesis

Table A.3| Calculated ratios of alanine scanning mutagenesis of consecutive amino acids. Ratios were calculated by dividing the percentage of anti-hCD27 mAb-binding with the percentage of the highest anti-hCD27 mAb-binding per mutant.

CRD1							
	AT133-2	AT133-5	AT133-11	CD27.15	varli	hCD70 Fc	AT133-14
T34/P35	0.93	0.91	0.91	0.82	0.87	0.79	1.00
P37/K38	0.96	0.91	0.88	0.88	0.94	0.92	1.00
S39/P40	0.98	0.97	0.87	0.89	0.98	0.93	1.00
E41/R42	1.00	0.93	0.76	0.86	0.91	0.80	0.92
H43/Y44	0.00	0.00	0.00	0.00	0.00	0.00	1.00
W45/Q47	0.90	0.00	0.00	0.97	0.98	0.93	1.00
G48/K49	1.00	0.00	0.00	0.89	0.62	0.86	1.00
L50/Q53	0.92	0.94	0.65	0.74	0.97	0.85	1.00
M54/E56	0.05	0.10	0.00	0.01	0.13	0.02	1.00
P57/G58	0.95	0.96	0.80	0.42	0.99	0.87	1.00
T59/F60	0.00	0.00	0.00	0.00	0.00	0.00	1.00
L61/V62	0.00	0.01	0.00	0.00	0.00	0.00	1.00
K63/D64	0.87	1.00	0.27	0.00	0.98	0.67	0.96
D66/Q67	0.87	0.94	0.92	0.50	1.00	0.88	0.84
H68/R69	0.00	0.35	0.00	0.87	1.00	0.89	0.99
K70/Q73	0.36	0.98	0.98	0.33	1.00	0.93	0.95
D75/P76	0.97	0.93	0.75	0.00	1.00	0.88	0.77
CRD2							
	AT133-2	AT133-5	AT133-11	CD27.15	varli	hCD70 Fc	AT133-14
I78/P79	0.96	1.00	0.85	0.80	0.80	0.89	1.00
G80/V81	0.03	0.10	0.01	0.02	0.06	0.00	1.00
S82/F83	0.01	0.08	0.01	0.00	0.00	0.09	1.00
S84/P85	0.98	0.99	0.94	0.93	0.92	0.92	1.00
D86/H87	0.91	0.95	0.85	1.00	0.92	0.80	0.83
H88/T89	0.97	0.95	0.83	0.94	0.93	0.91	1.00
R90/P91	0.93	1.00	0.79	0.96	0.88	0.10	0.88
H92/E94	0.87	0.95	0.85	1.00	0.90	0.04	0.87
S95/R97	0.81	1.00	0.82	0.81	0.10	0.50	0.92
H98/N100	0.90	1.00	0.84	1.00	0.60	0.86	0.97
S101/G102	0.85	0.94	0.97	1.00	0.47	0.96	0.94

CRD1							
L103/L104	0.77	0.83	0.85	0.79	1.00	0.86	0.81
V105/R106	1.00	0.94	0.55	0.87	0.90	0.89	0.98
N107/T109	0.10	0.17	0.03	0.12	0.18	0.15	1.00
I110/T111	0.75	1.00	0.74	0.09	0.89	0.68	0.67
N113/E115	0.00	0.02	0.00	0.00	0.01	0.07	1.00
CRD3							
	AT133-2	AT133-5	AT133-11	CD27.15	varli	hCD70 Fc	AT133-14
R119/N120	1.00	0.94	0.92	0.88	0.20	0.74	0.94
G121/W122	0.94	1.00	0.90	0.91	0.01	0.69	0.86
Q123/R125	1.00	1.00	0.89	0.98	0.94	0.64	0.99
D126/K127	0.46	0.92	0.65	1.00	0.96	0.38	0.05

Table A.4| Calculated ratios of alanine scanning mutagenesis with individually mutated amino acids. Ratios were calculated by dividing the percentage of anti-hCD27-binding with the percentage of the anti-highest hCD27-binding per mutant.

CRD1							
	AT133-2	AT133-5	AT133-11	hCD27.15	Varli	hCD70 Fc	AT133-14
W45	0.95	0.13	0.01	1.00	0.90	0.96	0.97
Q47	0.95	0.58	0.05	1.00	0.94	0.95	0.98
G48	0.99	1.00	0.10	0.98	0.96	0.92	0.92
K49	1.00	0.44	0.06	0.90	0.96	0.91	0.64
K63	0.89	0.92	0.82	0.24	1.00	0.60	1.00
D64	0.86	0.94	0.90	0.86	0.83	0.84	1.00
H68	0.43	0.73	0.86	0.95	0.96	0.88	1.00
R69	0.32	0.74	0.85	1.00	1.00	0.87	0.95
D75	0.98	0.99	0.82	0.42	1.00	0.84	1.00
P76	0.97	1.00	0.93	0.98	1.00	0.97	0.90
CRD2							
	AT133-2	AT133-5	AT133-11	hCD27.15	Varli	hCD70 Fc	AT133-14
R90	0.98	1.00	0.97	0.92	0.89	0.21	0.94
P91	0.90	0.95	0.89	0.95	1.00	0.81	1.00
H92	0.95	1.00	0.92	0.95	0.79	0.15	0.98
E94	0.88	1.00	0.81	0.91	0.78	0.31	0.89
S95	0.92	0.89	0.90	0.90	0.87	0.92	1.00
R97	0.82	1.00	0.86	0.98	0.24	0.75	0.96
I110	0.99	0.94	0.88	0.75	0.88	0.97	0.88
T111	0.94	1.00	0.85	0.96	0.84	0.86	0.85

Appendix B

B.1 hCD27 receptor constructs for stable transfections

Table B.1| Sequences of hCD27 constructs for stable transfections. The table lists the sequences for thehCD27 WT and hCD27 R214 STOP construct which is lacking the intracellular signalling domain, as well as the construct of the hCD27/GFP fusion protein.

hCD27	ATPAPKSCPERHYWAQGKLCCQMCEPGTFLVKDCDQHRKAAQCDPCIPGVSFSPDHHTRPHCESCRHC NSGLLVRNCTITANAECACRNGWQCRDKECTECDPLPNPSLTARSSQALSPHPQPTHLPYVSEMLEART AGHMQTLADFRQLPARTLSTHWPPQRSLCSSDFIRILVIFSGMFLVFTLAGALFLHQRRKYRSNKGESPVE PAEPCRYSCPREEEGSTIPIQEDYRKPEPACSP
hCD27 R214 STOP	ATPAPKSCPERHYWAQGKLCCQMCEPGTFLVKDCDQHRKAAQCDPCIPGVSFSPDHHTRPHCESCRHC NSGLLVRNCTITANAECACRNGWQCRDKECTECDPLPNPSLTARSSQALSPHPQPTHLPYVSEMLEART AGHMQTLADFRQLPARTLSTHWPPQRSLCSSDFIRILVIFSGMFLVFTLAGALFLHQ
hCD27/ GFP	ATPAPKSCPERHYWAQGKLCCQMCEPGTFLVKDCDQHRKAAQCDPCIPGVSFSPDHHTRPHCESCRHC NSGLLVRNCTITANAECACRNGWQCRDKECTECDPLPNPSLTARSSQALSPHPQPTHLPYVSEMLEART AGHMQTLADFRQLPARTLSTHWPPQRSLCSSDFIRILVIFSGMFLVFTLAGALFLHQRRKYRSNKGESPVE PAEPCRYSCPREEEGSTIPIQEDYRKPEPACSPDPPVMVSKGAELFTGIVPILIELNGDVNGHKFSVSGEGE GDATYGKLTLKFICTTGKLPVPWPTLVTTLSYGVQCFSRYPDHMKQHDFFKSAMPEGYIQERTIFFEDDG NYKSRAEVKFEGDTLVNRIELTGTDFKEDGNILGNKMEYNYNAHNVYIMTDKAKNGIKVNFKIRHNIEDG SVQLADHYQQNTPIGDGPVLLPDNHYLSTQSALSKDPNEKRDHMIYFGFVTAAAITHGMDELYK

B.2 Expression of hFcγRIIb on CHO cells and human immune cell subsets

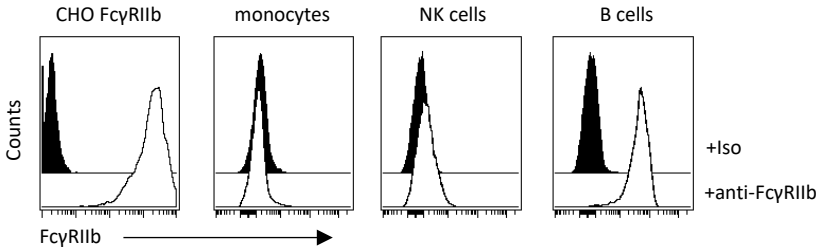

Figure B.1| FcγRIIb expression on FcγRIIb transfected CHO cells and immune cell subsets. The histogram plots show the FcγRIIb expression on FcγRIIb transfected CHO cells and PBMC-derived monocytes, NK cells and B cells. Plots are representative of n=2-3 experimental repeats.

B.3 Clustering of hCD27 upon anti-hCD27 mAb binding after 30 minutes, 2 and 24 hours

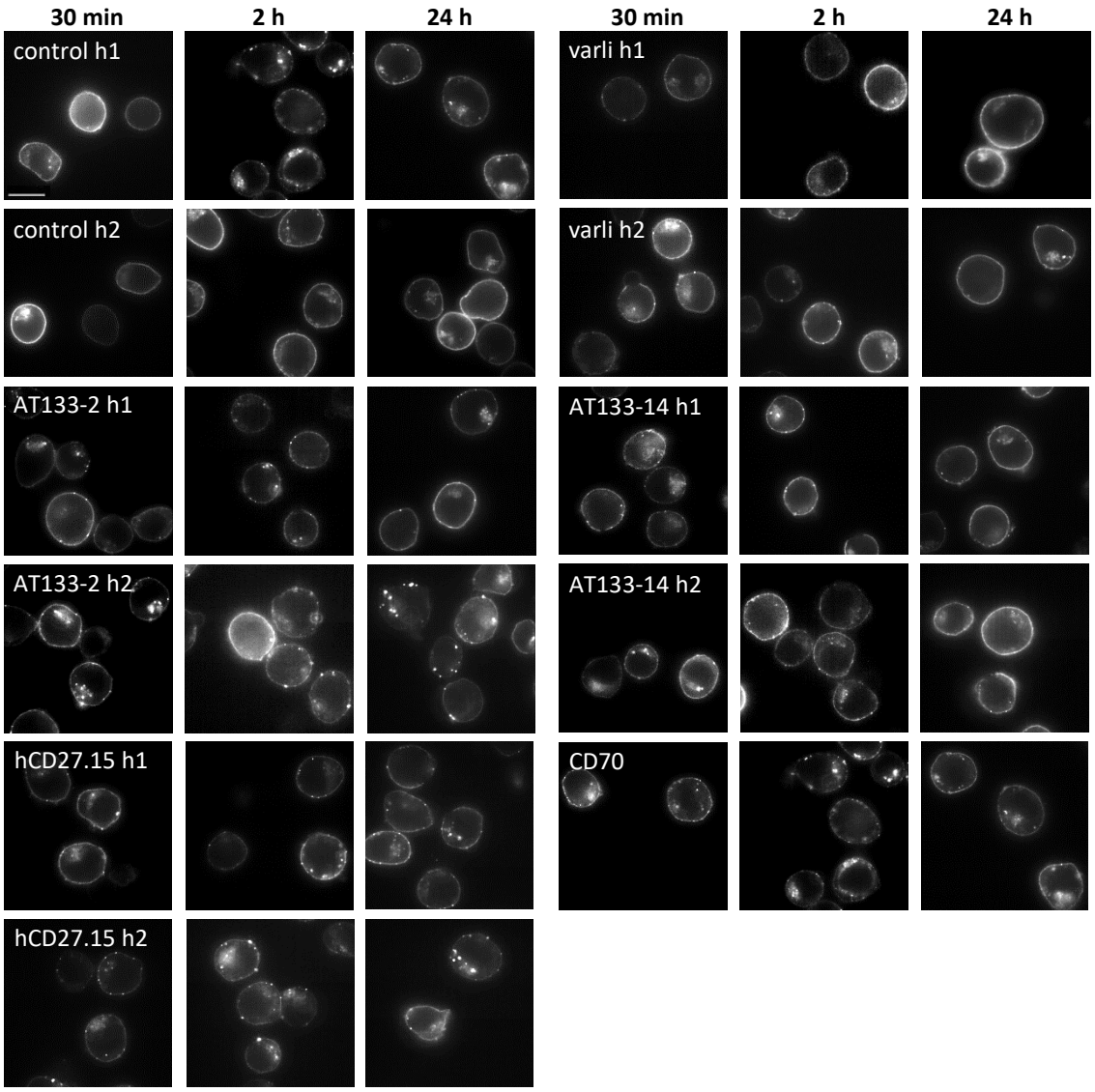

Figure B.2| Confocal microscopy of hCD27 receptor clustering upon hCD27 stimulation. hCD27/GFP Jurkat cells were incubated with 10 µg/ml of the h1 and h2 isotype of AT133-2, hCD27.15, varli or AT133-14 or CD70 h1 as well as with the respective controls. Cells were acquired on an ONI Nanoimager in confocal mode (100x lens). Displayed are representative images of receptor clustering after 30 minutes, 2 and 24 hour stimulation with either hCD27 h1 or h2 mAb. Scale bar represents 10 µm.

B.4 Co-localisation of hCD27:anti-hCD27 mAb complexes with lysosomes

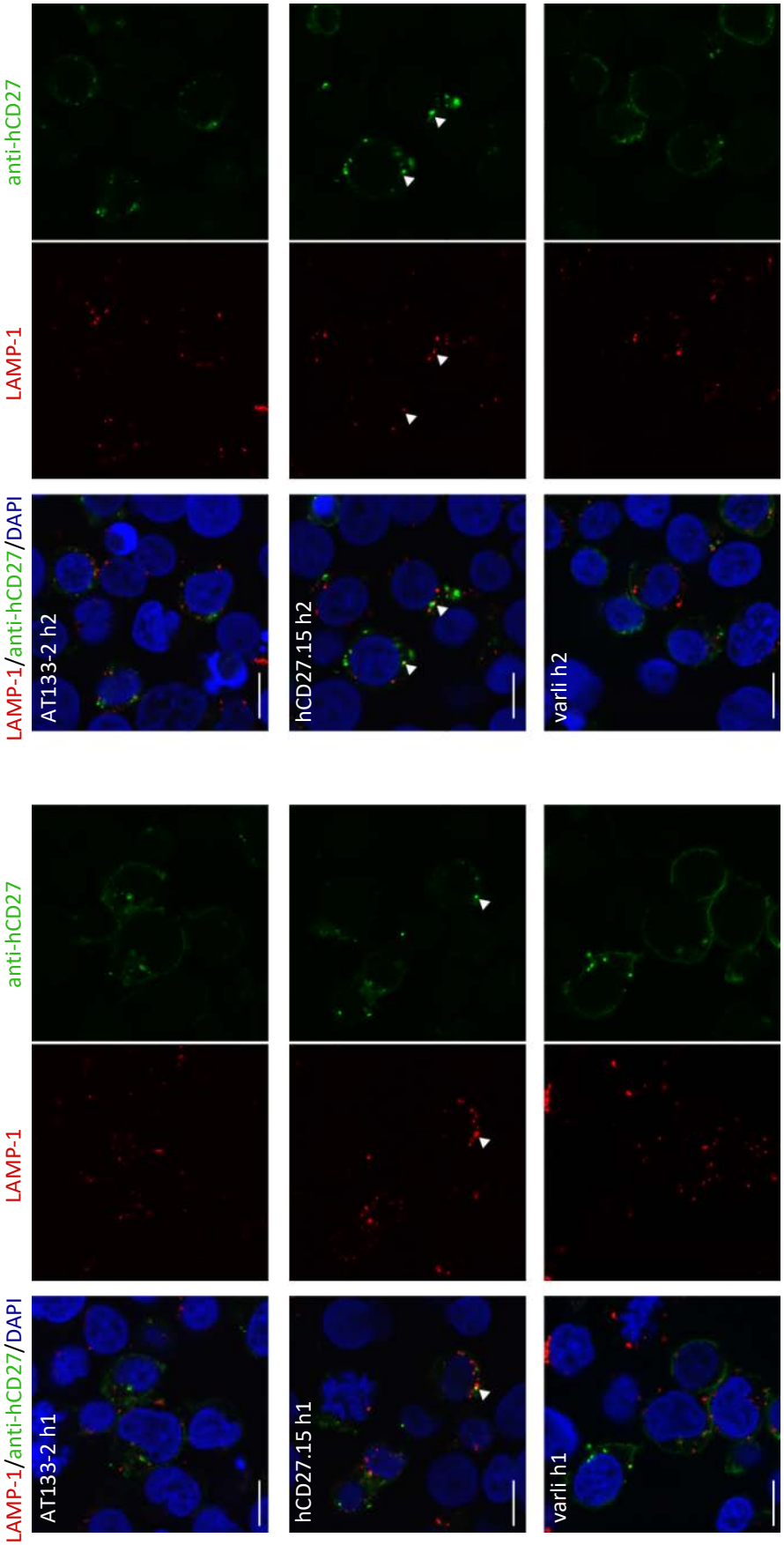

Figure B.3| Assessment of co-localisation of anti-hCD27 mAbs with lysosomes by confocal microscopy. Jurkat cells expressing hCD27 Jurkat cells were incubated with the indicated Alexa488-labelled anti-hCD27 h1/h2 mAbs. After 2 hours, cells were stained with a primary antibody to detect LAMP-1 and following with a secondary fluorochrome conjugated antibody (Alexa 647) to detect anti-LAMP-1 binding. Shown are representative images for the 2 hour incubation time point. DAPI was used to visualise cell nuclei (blue) and anti-LAMP1 for lysosomes (red). Binding of anti-hCD27 mAbs to hCD27 is indicated in green. White arrows indicate co-localisation of LAMP-1 and anti-hCD27 mAb staining. The scale bar represents 10 µm. Images were analysed using Adobe Photoshop CS6 software and adjusted for brightness.

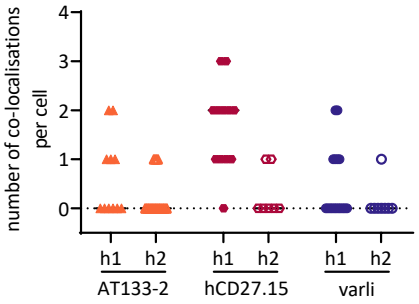

Figure B.4| Quantification of co-localisation of hCD27:anti-hCD27 mAb complexes with lysosomes after 6 hours incubation. The number of co-localisations of hCD27:anti-hCD27 mAb complexes with LAMP-1-stained lysosomes visualised by confocal microscopy (Figure 4.11) was manually counted using Adobe Photoshop CS6 software. The hCD27 Jurkat cells utilised heterogeneously express hCD27. Therefore only cells that appeared $CD27^+$ (Alexa488) were taken into consideration. Per condition the following number of cells was counted: AT133-2 h1: 11, AT133-2 h2: 15, hCD27.15 h1: 11, hCD27.15 h2: 7, varli h1: 17, varli h2: 8.

Appendix C

C.1 Sequences of the hCD38 construct for stable transfections

AQLCLGVSILVLILVVVLAVVVPRWRQQWSGPGTTKRFPETVLARCVKYTEIHPEMRHVDCQSVWDAFKGAFISKHPCNIT
EEDYQPLMKLGTQTVPCNKILLWSRIKDLAHQFTQVQRDMFTLEDTLLGYLADDLTWCGEFNTSKINYQSCPDWRKDCSN
NPVSVFWKTVSRRFAEAACDVVHVMLNGSRSKIFDKNSTFGSVEVHNLQPEKVQTLEAWVIHGGREDSRDLCQDPTIKELE
SIISKRNIQFSCKNIYRPDKFLQCVKNPEDSSCTSEI

C.2 Phenotyping of mCD38 on murine immune cell subsets

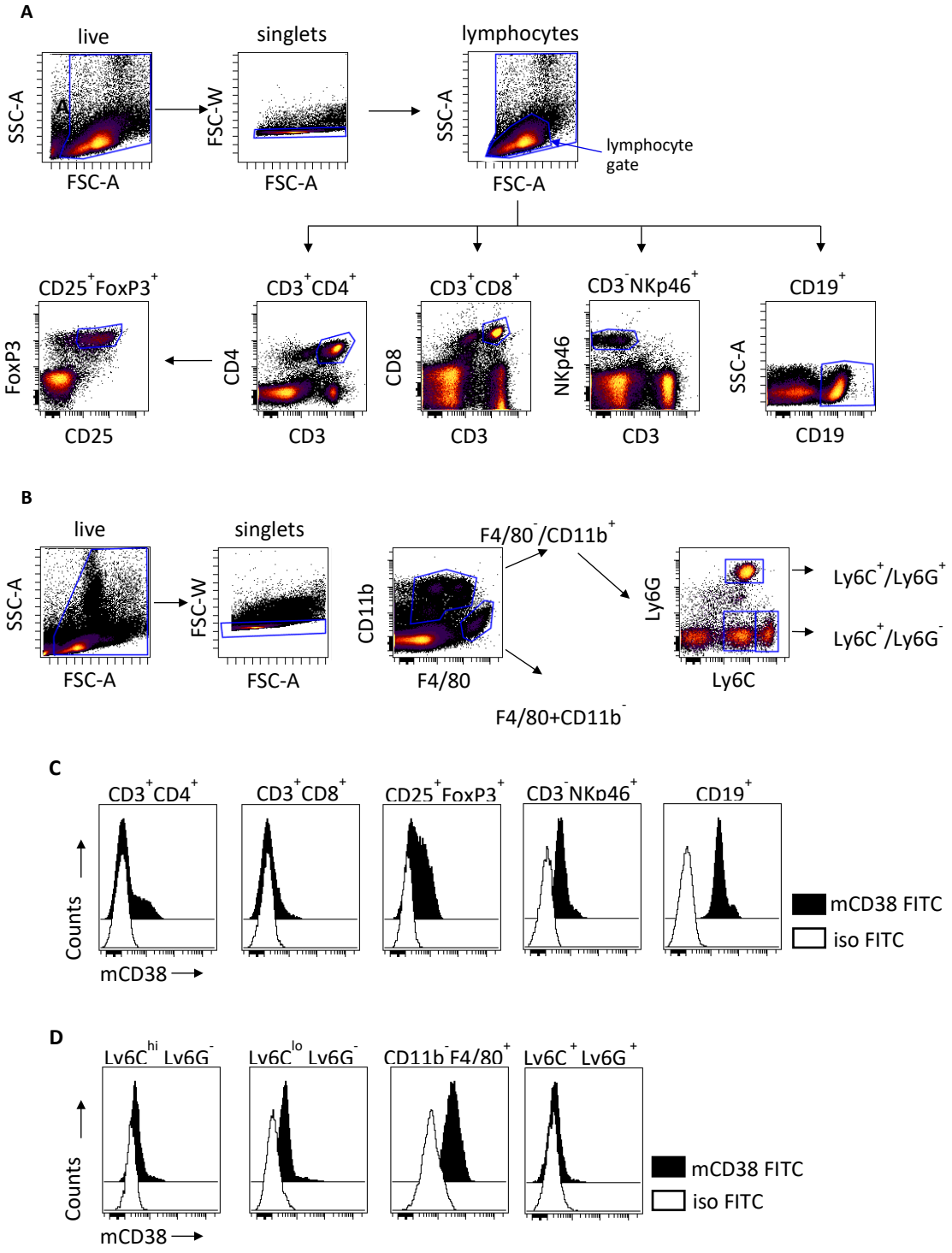

Figure C.1| Expression of mCD38 on murine splenocytes. Splenocytes were stained with fluorochrome-conjugated mAbs to determine the mCD38 expression on lymphoid and myeloid immune cell subsets by flow cytometry. **A**: Gating strategy for $CD3^+CD4^+$, $CD3^+CD8^+$ and $CD25^+FoxP3^+$ T cells, $NKp46^+$ NK cells and $CD19^+$ B cells were identified. **B**: Gating strategy for classical ($L6C^{hi}Ly6G^-$) and non-classical ($Ly6C^{lo}Ly6G^-$) monocytes, macrophages ($CD11b^-F4/80^+$) and neutrophils ($Ly6C^+Ly6G^+$). **C**, **D**: Histograms show the MFI of mCD38 on the indicated lymphoid and myeloid immune cells subsets. Filled histograms show splenocytes stained with anti-mCD38 and clear histograms show splenocytes stained with the respective isotype control (n=1).

C.3 Cross-reactivity of daratumumab with mCD38

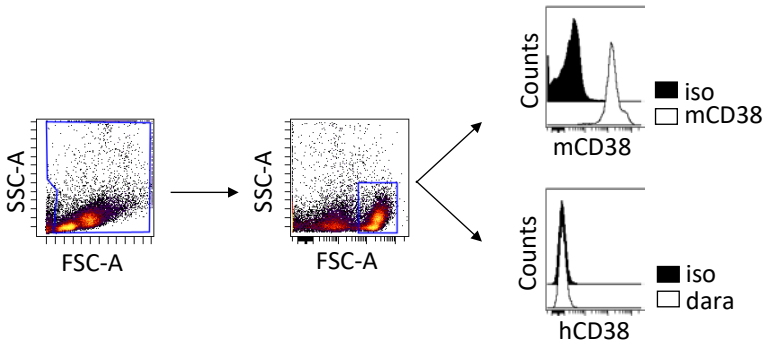

Figure C.2| Cross-reactivity of daratumumab with mCD38. Peripheral blood was obtained from WT BALB/c mice. The mCD38 expression on $CD19^+$ B cells was determined using a fluorochrome anti-mCD38 mAb, whereas the hCD38 expression was determined with daratumumab (dara) and a secondary fluorochrome-conjugated anti-hFc. Shown is the gating strategy for $CD19^+$ B cells and histograms depict the expression of mCD38 or hCD38 on murine $CD19^+$ B cells. .

C.4 Expression of hCD27 and hCD38 on Daudi cells

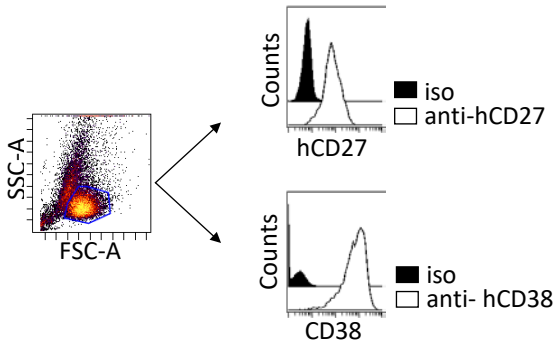

Figure C.3| Expression of hCD27 and hCD38 on Daudi cells. Daudi cells were stained with a fluorochrome-conjugated hCD27 or hCD38-specific mAb and the expression was determined by flow cytometry. Cells were initially gated on live Daudi cells and the hCD27 or hCD38 expression displayed in histogram plots.

C.5 Assessment of Daudi cell proliferation by CFSE dilution

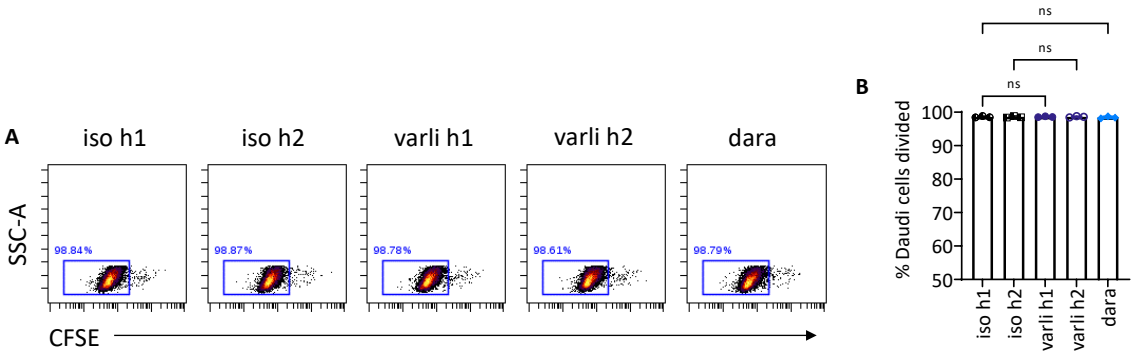

Figure C.4|Assessment of Daudi cell proliferation upon hCD27 mAb or daratumumab stimulation by CFSE dilution. A: CFSE-labelled Daudi cells ($1x10^5$) were incubated for 3 days with 10 µg/ml varli h1, varli h2 or daratumumab (dara) or the irrelevant isotype controls. Proliferation of the tumour cell line was assessed by examining the CFSE dilution via flow cytometry. Representative dotplots of the CFSE dilution upon the indicated mAb treatments. The gate indicates divided Daudi cells. **B**: Graph shows the percentage of $Ki67^+$ Daudi cells (n=3). Data were assessed using one-way ANOVA with Tukey's test; ns: $p > 0.05$.

References

1. Vogelstein B, Papadopoulos N, Velculescu VE, Zhou S, Diaz LA, Jr., Kinzler KW. Cancer genome landscapes. *Science*. 2013;339(6127):1546-1558.

2. Hanahan D, Weinberg RA. Hallmarks of cancer: the next generation. *Cell*. 2011;144(5):646-674.

3. Hanahan D, Weinberg RA. The hallmarks of cancer. *Cell*. 2000;100(1):57-70.

4. Burnet F. The concept of immunological surveillance. In: RS S (ed.) *Immunological Aspects of Neoplasia. Prog Tumor Res.* Basel: Karger Publishers; 1970 pp 1-27.

5. Dunn GP, Bruce AT, Ikeda H, Old LJ, Schreiber RD. Cancer immunoediting: from immunosurveillance to tumor escape. *Nat. Immunol.* 2002;3(11):991-998.

6. Galon J, Costes A, Sanchez-Cabo F, Kirilovsky A, Mlecnik B, Lagorce-Pagès C, et al. Type, density, and location of immune cells within human colorectal tumors predict clinical outcome. *Science*. 2006;313(5795):1960-1964.

7. Fridman WH, Pagès F, Sautès-Fridman C, Galon J. The immune contexture in human tumours: impact on clinical outcome. *Nat. Rev. Cancer*. 2012;12(4):298-306.

8. Zúñiga-Pflücker JC. T-cell development made simple. *Nat. Rev. Immunol.* 2004;4(1):67-72.

9. Godfrey DI, Kennedy J, Suda T, Zlotnik A. A developmental pathway involving four phenotypically and functionally distinct subsets of CD3-CD4-CD8- triple-negative adult mouse thymocytes defined by CD44 and CD25 expression. *J. Immunol.* 1993;150(10):4244-4252.

10. Murphy KM, Weaver C. *Janeway's Immunobiology*: Garland Science/Taylor & Francis Group, LLC; 2016.

11. Owen JA, Punt J, Stranford SA. *Kuby immunology*: WH Freeman New York; 2013.

12. Blum JS, Wearsch PA, Cresswell P. Pathways of antigen processing. *Annu. Rev. Immunol.* 2013;31:443-473.

13. Reeves E, James E. Antigen processing and immune regulation in the response to tumours. *Immunology*. 2017;150(1):16-24.

14. Koopmann J-O, Post M, Neefjes JJ, Hämmerling GJ, Momburg F. Translocation of long peptides by transporters associated with antigen processing (TAP). *Eur. J. Immunol.* 1996;26(8):1720-1728.

15. Saric T, Chang SC, Hattori A, York IA, Markant S, Rock KL, et al. An IFN-gamma-induced aminopeptidase in the ER, ERAP1, trims precursors to MHC class I-presented peptides. *Nat. Immunol.* 2002;3(12):1169-1176.

16. Chicz RM, Urban RG, Lane WS, Gorga JC, Stern LJ, Vignali DA, et al. Predominant naturally processed peptides bound to HLA-DR1 are derived from MHC-related molecules and are heterogeneous in size. *Nature*. 1992;358(6389):764-768.

17. Rudensky Y, Preston-Hurlburt P, Hong SC, Barlow A, Janeway CA, Jr. Sequence analysis of peptides bound to MHC class II molecules. *Nature*. 1991;353(6345):622-627.

18. Bevan MJ. Minor H antigens introduced on H-2 different stimulating cells cross-react at the cytotoxic T cell level during in vivo priming. *J. Immunol.* 1976;117(6):2233-2238.

19. Lin M-L, Zhan Y, Villadangos JA, Lew AM. The cell biology of cross-presentation and the role of dendritic cell subsets. *Immunol. Cell Biol.* 2008;86(4):353-362.

20. Joffre OP, Segura E, Savina A, Amigorena S. Cross-presentation by dendritic cells. *Nat. Rev. Immunol.* 2012;12(8):557-569.

21. Van Mierlo GJ, Boonman ZF, Dumortier HM, den Boer AT, Fransen MF, Nouta J, et al. Activation of dendritic cells that cross-present tumor-derived antigen licenses CD8+ CTL to cause tumor eradication. *J. Immunol.* 2004;173(11):6753-6759.

22. Gaud G, Lesourne R, Love PE. Regulatory mechanisms in T cell receptor signalling. *Nat. Rev. Immunol.* 2018;18(8):485-497.

23. Brownlie RJ, Zamoyska R. T cell receptor signalling networks: branched, diversified and bounded. *Nat. Rev. Immunol.* 2013;13(4):257-269.

24. Smith-Garvin JE, Koretzky GA, Jordan MS. T cell activation. *Annu. Rev. Immunol.* 2009;27:591-619.

25. Oh-Hora M, Rao A. Calcium signaling in lymphocytes. *Curr. Opin. Immunol.* 2008;20(3):250-258.

26. Macian F. NFAT proteins: key regulators of T-cell development and function. *Nat. Rev. Immunol.* 2005;5(6):472-484.

27. Sun S-C. The non-canonical NF-κB pathway in immunity and inflammation. *Nat. Rev. Immunol.* 2017;17(9):545-558.

28. Chen L, Flies DB. Molecular mechanisms of T cell co-stimulation and co-inhibition. *Nat. Rev. Immunol.* 2013;13(4):227-242.

29. Simpson TR, Quezada SA, Allison JP. Regulation of CD4 T cell activation and effector function by inducible costimulator (ICOS). *Curr. Opin. Immunol.* 2010;22(3):326-332.

30. Selby MJ, Engelhardt JJ, Quigley M, Henning KA, Chen T, Srinivasan M, et al. Anti-CTLA-4 antibodies of IgG2a isotype enhance antitumor activity through reduction of intratumoral regulatory T cells. *Cancer Immunol. Res.* 2013;1(1):32-42.

31. Kohrt HE, Tumeh PC, Benson D, Bhardwaj N, Brody J, Formenti S, et al. Immunodynamics: a cancer immunotherapy trials network review of immune monitoring in immuno-oncology clinical trials. *J Immunother Cancer*. 2016;4(1):15.

32. French RR, Taraban VY, Crowther GR, Rowley TF, Gray JC, Johnson PW, et al. Eradication of lymphoma by CD8 T cells following anti-CD40 monoclonal antibody therapy is critically dependent on CD27 costimulation. *Blood*. 2007;109(11):4810-4815.

33. Vonderheide RH, Glennie MJ. Agonistic CD40 antibodies and cancer therapy. *Clin. Cancer Res.* 2013;19(5):1035-1043.

34. Ramakrishna V, Sundarapandiyan K, Zhao B, Bylesjo M, Marsh HC, Keler T. Characterization of the human T cell response to in vitro CD27 costimulation with varlilumab. *J. Immunother. Cancer*. 2015;3(1):37.

35. Vanamee ÉS, Faustman DL. Structural principles of tumor necrosis factor superfamily signaling. *Sci Signal*. 2018;11(511):eaao4910.

36. Bodmer J-L, Schneider P, Tschopp J. The molecular architecture of the TNF superfamily. *Trends Biochem. Sci.* 2002;27(1):19-26.

37. Liu W, Maben Z, Wang C, Lindquist KC, Li M, Rayannavar V, et al. Structural delineation and phase-dependent activation of the co-stimulatory CD27: CD70 complex. *J. Biol. Chem.* 2021;297(4):101102.

38. Teplyakov A, Obmolova G, Malia TJ, Gilliland GL. Crystal structure of CD27 in complex with a neutralizing noncompeting antibody. *Acta Crystallogr. F:Struct. Biol. Commun.* 2017;73(5):294-299.

39. An H-J, Kim YJ, Song DH, Park BS, Kim HM, Lee JD, et al. Crystallographic and mutational analysis of the CD40-CD154 complex and its implications for receptor activation. *J. Biol. Chem.* 2011;286(13):11226-11235.

40. Nocentini G, Giunchi L, Ronchetti S, Krausz LT, Bartoli A, Moraca R, et al. A new member of the tumor necrosis factor/nerve growth factor receptor family inhibits T cell receptor-induced apoptosis. *Proc. Natl. Acad. Sci. U. S. A.* 1997;94(12):6216-6221.

41. Compaan DM, Hymowitz SG. The crystal structure of the costimulatory OX40-OX40L complex. *Structure*. 2006;14(8):1321-1330.

42. Bitra A, Doukov T, Croft M, Zajonc DM. Crystal structures of the human 4-1BB receptor bound to its ligand 4-1BBL reveal covalent receptor dimerization as a potential signaling amplifier. *J. Biol. Chem.* 2018;293(26):9958-9969.

43. Gilbreth RN, Oganesyan VY, Amdouni H, Novarra S, Grinberg L, Barnes A, et al. Crystal structure of the human 4-1BB/4-1BBL complex. *J. Biol. Chem.* 2018;293(25):9880-9891.

44. Arch RH, Gedrich RW, Thompson CB. Tumor necrosis factor receptor-associated factors (TRAFs)--a family of adapter proteins that regulates life and death. *Genes Dev.* 1998;12(18):2821-2830.

45. Mosmann TR, Cherwinski H, Bond MW, Giedlin MA, Coffman RL. Two types of murine helper T cell clone. I. Definition according to profiles of lymphokine activities and secreted proteins. *J. Immunol.* 1986;136(7):2348-2357.

46. Crome S, Wang A, Levings M. Translational mini-review series on Th17 cells: function and regulation of human T helper 17 cells in health and disease. *Clin. Exp. Immunol.* 2010;159(2):109-119.

47. Jonuleit H, Schmitt E. The regulatory T cell family: distinct subsets and their interrelations. *J. Immunol.* 2003;171(12):6323-6327.

48. Zhang N, Bevan MJ. CD8+ T cells: foot soldiers of the immune system. *Immunity*. 2011;35(2):161-168.

49. Voskoboinik I, Whisstock JC, Trapani JA. Perforin and granzymes: function, dysfunction and human pathology. *Nat. Rev. Immunol.* 2015;15(6):388-400.

50. Thiery J, Keefe D, Boulant S, Boucrot E, Walch M, Martinvalet D, et al. Perforin pores in the endosomal membrane trigger the release of endocytosed granzyme B into the cytosol of target cells. *Nat. Immunol.* 2011;12(8):770-777.

51. Lopez JA, Susanto O, Jenkins MR, Lukoyanova N, Sutton VR, Law RH, et al. Perforin forms transient pores on the target cell plasma membrane to facilitate rapid access of granzymes during killer cell attack. *Blood, The Journal of the American Society of Hematology*. 2013;121(14):2659-2668.

52. Lieberman J. The ABCs of granule-mediated cytotoxicity: new weapons in the arsenal. *Nat. Rev. Immunol.* 2003;3(5):361-370.

53. Martinvalet D, Zhu P, Lieberman J. Granzyme A induces caspase-independent mitochondrial damage, a required first step for apoptosis. *Immunity*. 2005;22(3):355-370.

54. Trapani JA, Sutton VR. Granzyme B: pro-apoptotic, antiviral and antitumor functions. *Curr. Opin. Immunol.* 2003;15(5):533-543.

55. Williams MA, Bevan MJ. Effector and memory CTL differentiation. *Annu. Rev. Immunol.* 2007;25:171-192.

56. Mueller SN, Mackay LK. Tissue-resident memory T cells: local specialists in immune defence. *Nat. Rev. Immunol.* 2016;16(2):79-89.

57. Abele R, Tampé R. The ABCs of immunology: structure and function of TAP, the transporter associated with antigen processing. *Physiology (Bethesda)*. 2004;19:216-224.

58. Blanc C, Hans S, Tran T, Granier C, Saldman A, Anson M, et al. Targeting Resident Memory T Cells for Cancer Immunotherapy. *Front. Immunol.* 2018;9.

59. Van Lier R, Borst J, Vroom TM, Klein H, Van Mourik P, Zeijlemaker WP, et al. Tissue distribution and biochemical and functional properties of Tp55 (CD27), a novel T cell differentiation antigen. *J. Immunol.* 1987;139(5):1589-1596.

60. Loenen W, Gravestein LA, Beumer S, Melief C, Hagemeijer A, Borst J. Genomic organization and chromosomal localization of the human CD27 gene. *J. Immunol.* 1992;149(12):3937-3943.

61. Gravestein LA, Blom B, Nolten LA, de Vries E, Horst GVD, Ossendorp F, et al. Cloning and expression of murine CD27: comparison with 4-1BB, another lymphocyte-specific member of the nerve growth factor receptor family. *Eur. J. Immunol.* 1993;23(4):943-950.

62. Martorell J, Rojo I, Vilella R, Martinez-Caceres E, Vives J. CD27 induction on thymocytes. *J. Immunol.* 1990;145(5):1356-1363.

63. Appay V, Dunbar PR, Callan M, Klenerman P, Gillespie GM, Papagno L, et al. Memory CD8+ T cells vary in differentiation phenotype in different persistent virus infections. *Nat. Med.* 2002;8(4):379-385.

64. Kuijpers TW, Vossen MT, Gent M-R, Davin J-C, Roos MT, Wertheim-van Dillen PM, et al. Frequencies of circulating cytolytic, CD45RA+ CD27−, CD8+ T lymphocytes depend on infection with CMV. *J. Immunol.* 2003;170(8):4342-4348.

65. Hintzen R, De Jong R, Lens S, Brouwer M, Baars P, Van Lier R. Regulation of CD27 expression on subsets of mature T-lymphocytes. *J. Immunol.* 1993;151(5):2426-2435.

66. Koch S, Larbi A, Derhovanessian E, Özcelik D, Naumova E, Pawelec G. Multiparameter flow cytometric analysis of CD4 and CD8 T cell subsets in young and old people. *Immun. Ageing*. 2008;5(1):1-12.

67. Arroyo Hornero R, Georgiadis C, Hua P, Trzupek D, He L-Z, Qasim W, et al. CD70 expression determines the therapeutic efficacy of expanded human regulatory T cells. *Commun Biol*. 2020;3(1):375.

68. Jung J, Choe J, Li L, Choi YS. Regulation of CD27 expression in the course of germinal center B cell differentiation: the pivotal role of IL-10. *Eur. J. Immunol.* 2000;30(8):2437-2443.

69. Sims GP, Ettinger R, Shirota Y, Yarboro CH, Illei GG, Lipsky PE. Identification and characterization of circulating human transitional B cells. *Blood*. 2005;105(11):4390-4398.

70. Maurer D, Holter W, Majdic O, Fischer GF, Knapp W. CD27 expression by a distinct subpopulation of human B lymphocytes. *Eur. J. Immunol.* 1990;20(12):2679-2684.

71. Vossen MT, Matmati M, Hertoghs KM, Baars PA, Gent M-R, Leclercq G, et al. CD27 defines phenotypically and functionally different human NK cell subsets. *J. Immunol.* 2008;180(6):3739-3745.

72. Schürch C, Riether C, Matter MS, Tzankov A, Ochsenbein AF. CD27 signaling on chronic myelogenous leukemia stem cells activates Wnt target genes and promotes disease progression. *J. Clin. Investig.* 2012;122(2):624-638.

73. Riether C, Schürch CM, Bührer ED, Hinterbrandner M, Huguenin A-L, Hoepner S, et al. CD70/CD27 signaling promotes blast stemness and is a viable therapeutic target in acute myeloid leukemia. *J. Exp. Med.* 2017;214(2):359-380.

74. Riether C, Schürch CM, Flury C, Hinterbrandner M, Drück L, Huguenin AL, et al. Tyrosine kinase inhibitor-induced CD70 expression mediates drug resistance in leukemia stem cells by activating Wnt signaling. *Sci. Transl. Med.* 2015;7(298):298ra119.

75. Vazquez SE, Inlay MA, Serwold T. CD201 and CD27 identify hematopoietic stem and progenitor cells across multiple murine strains independently of Kit and Sca-1. *Exp. Hematol.* 2015;43(7):578-585.

76. Wiesmann A, Phillips RL, Mojica M, Pierce LJ, Searles AE, Spangrude GJ, et al. Expression of CD27 on murine hematopoietic stem and progenitor cells. *Immunity*. 2000;12(2):193-199.

77. Gravestein LA, Nieland JD, Kruisbeek AM, Borst J. Novel mAbs reveal potent co-stimulatory activity of murine CD27. *Int. Immunol.* 1995;7(4):551-557.

78. Baars PA, Sierro S, Arens R, Tesselaar K, Hooibrink B, Klenerman P, et al. Properties of murine CD8+ CD27–T cells. *Eur. J. Immunol.* 2005;35(11):3131-3141.

79. Wherry EJ, Teichgräber V, Becker TC, Masopust D, Kaech SM, Antia R, et al. Lineage relationship and protective immunity of memory CD8 T cell subsets. *Nat. Immunol.* 2003;4(3):225-234.

80. Hayakawa Y, Smyth MJ. CD27 dissects mature NK cells into two subsets with distinct responsiveness and migratory capacity. *J. Immunol.* 2006;176(3):1517-1524.

81. Xiao Y, Hendriks J, Langerak P, Jacobs H, Borst J. CD27 is acquired by primed B cells at the centroblast stage and promotes germinal center formation. *J. Immunol.* 2004;172(12):7432-7441.

82. Hintzen R, De Jong R, Hack C, Chamuleau M, De Vries E, Ten Berge I, et al. A soluble form of the human T cell differentiation antigen CD27 is released after triggering of the TCR/CD3 complex. *J. Immunol.* 1991;147(1):29-35.

83. Van Oers M, Pals S, Evers L, Van der Schoot C, Koopman G, Bonfrer J, et al. Expression and release of CD27 in human B-cell malignancies. *Blood*. 1993;82(11):3430-3436.

84. Kok M, Bonfrer JM, Korse CM, de Jong D, Kersten MJ. Serum soluble CD27, but not thymidine kinase, is an independent prognostic factor for outcome in indolent non-Hodgkin's lymphoma. *Tumour Biol.* 2003;24(1):53-60.

85. Taraban VY, Rowley TF, Al-Shamkhani A. Cutting edge: a critical role for CD70 in CD8 T cell priming by CD40-licensed APCs. *J. Immunol.* 2004;173(11):6542-6546.

86. Krause P, Bruckner M, Uermösi C, Singer E, Groettrup M, Legler DF. Prostaglandin E2 enhances T-cell proliferation by inducing the costimulatory molecules OX40L, CD70, and 4-1BBL on dendritic cells. *Blood*. 2009;113(11):2451-2460.

87. Huang J, Wang QJ, Yang S, Li YF, El-Gamil M, Rosenberg SA, et al. Irradiation enhances human T-cell function by upregulating CD70 expression on antigen-presenting cells in vitro. *J. Immunother.* 2011;34(4):327-335.

88. Lens SMA, De Jong R, Hooibrink B, Koopman G, Pals ST, van Oers MHJ, et al. Phenotype and function of human B cells expressing CD70 (CD27 ligand). *Eur. J. Immunol.* 1996;26(12):2964-2971.

89. Tesselaar K, Xiao Y, Arens R, van Schijndel GM, Schuurhuis DH, Mebius RE, et al. Expression of the murine CD27 ligand CD70 in vitro and in vivo. *J. Immunol.* 2003;170(1):33-40.

90. Ramakrishnan P, Wang W, Wallach D. Receptor-specific signaling for both the alternative and the canonical NF-kappaB activation pathways by NF-kappaB-inducing kinase. *Immunity*. 2004;21(4):477-489.

91. Yamamoto H, Kishimoto T, Minamoto S. NF-κB activation in CD27 signaling: involvement of TNF receptor-associated factors in its signaling and identification of functional region of CD27. *J. Immunol.* 1998;161(9):4753-4759.

92. Gravestein LA, Amsen D, Boes M, Calvo CR, Kruisbeek AM, Borst J. The TNF receptor family member CD27 signals to Jun N-terminal kinase via Traf-2. *Eur. J. Immunol.* 1998;28(7):2208-2216.

93. Akiba H, Nakano H, Nishinaka S, Shindo M, Kobata T, Atsuta M, et al. CD27, a member of the tumor necrosis factor receptor superfamily, activates NF-κB and stress-activated protein kinase/c-Jun N-terminal kinase via TRAF2, TRAF5, and NF-κB-inducing kinase. *J. Biol. Chem.* 1998;273(21):13353-13358.

94. Liao G, Zhang M, Harhaj EW, Sun SC. Regulation of the NF-kappaB-inducing kinase by tumor necrosis factor receptor-associated factor 3-induced degradation. *J. Biol. Chem.* 2004;279(25):26243-26250.

95. de Jong R, Loenen W, Brouwer M, van Emmerik L, de Vries E, Borst J, et al. Regulation of expression of CD27, a T cell-specific member of a novel family of membrane receptors. *J. Immunol.* 1991;146(8):2488-2494.

96. Vitale LA, He L-Z, Thomas LJ, Widger J, Weidlick J, Crocker A, et al. Development of a human monoclonal antibody for potential therapy of CD27-expressing lymphoma and leukemia. *Clin. Cancer Res.* 2012;18(14):3812-3821.

97. Goodwin RG, Alderson MR, Smith CA, Armitage RJ, VandenBos T, Jerzy R, et al. Molecular and biological characterization of a ligand for CD27 defines a new family of cytokines with homology to tumor necrosis factor. *Cell*. 1993;73(3):447-456.

98. Rowley TF, Al-Shamkhani A. Stimulation by soluble CD70 promotes strong primary and secondary CD8+ cytotoxic T cell responses in vivo. *J. Immunol.* 2004;172(10):6039-6046.

99. Hendriks J, Gravestein LA, Tesselaar K, van Lier RA, Schumacher TN, Borst J. CD27 is required for generation and long-term maintenance of T cell immunity. *Nat. Immunol.* 2000;1(5):433-440.

100. Hendriks J, Xiao Y, Borst J. CD27 promotes survival of activated T cells and complements CD28 in generation and establishment of the effector T cell pool. *J. Exp. Med.* 2003;198(9):1369-1380.

101. Dolfi DV, Boesteanu AC, Petrovas C, Xia D, Butz EA, Katsikis PD. Late signals from CD27 prevent Fas-dependent apoptosis of primary CD8+ T cells. *J. Immunol.* 2008;180(5):2912-2921.

102. Peperzak V, Veraar EA, Keller AM, Xiao Y, Borst J. The Pim kinase pathway contributes to survival signaling in primed CD8+ T cells upon CD27 costimulation. *J. Immunol.* 2010;185(11):6670-6678.

103. Van Oosterwijk MF, Juwana H, Arens R, Tesselaar K, Van Oers MH, Eldering E, et al. CD27–CD70 interactions sensitise naive CD4+ T cells for IL-12-induced Th1 cell development. *Int. Immunol.* 2007;19(6):713-718.

104. Peperzak V, Veraar EA, Xiao Y, Bąbała N, Thiadens K, Brugmans M, et al. CD8+ T cells produce the chemokine CXCL10 in response to CD27/CD70 costimulation to promote generation of the CD8+ effector T cell pool. *J. Immunol.* 2013;191(6):3025-3036.

105. Janssen EM, Lemmens EE, Wolfe T, Christen U, von Herrath MG, Schoenberger SP. CD4+ T cells are required for secondary expansion and memory in CD8+ T lymphocytes. *Nature*. 2003;421(6925):852-856.

106. Schildknecht A, Miescher I, Yagita H, van den Broek M. Priming of CD8+ T cell responses by pathogens typically depends on CD70-mediated interactions with dendritic cells. *Eur. J. Immunol.* 2007;37(3):716-728.

107. Ridge JP, Di Rosa F, Matzinger P. A conditioned dendritic cell can be a temporal bridge between a CD4+ T-helper and a T-killer cell. *Nature*. 1998;393(6684):474-478.

108. Borst J, Hendriks J, Xiao Y. CD27 and CD70 in T cell and B cell activation. *Curr. Opin. Immunol.* 2005;17(3):275-281.

109. Alkhairy OK, Perez-Becker R, Driessen GJ, Abolhassani H, Van Montfrans J, Borte S, et al. Novel mutations in TNFRSF7/CD27: Clinical, immunologic, and genetic characterization of human CD27 deficiency. *J. Allergy Clin. Immunol.* 2015;136(3):703-712. e710.

110. Salzer E, Daschkey S, Choo S, Gombert M, Santos-Valente E, Ginzel S, et al. Combined immunodeficiency with life-threatening EBV-associated lymphoproliferative disorder in patients lacking functional CD27. *Haematologica*. 2013;98(3):473.

111. Seidel MG. CD27: a new player in the field of common variable immunodeficiency and EBV-associated lymphoproliferative disorder? *J. Allergy Clin. Immunol.* 2012;129(4):1175.

112. Van Montfrans JM, Hoepelman AI, Otto S, van Gijn M, van de Corput L, de Weger RA, et al. CD27 deficiency is associated with combined immunodeficiency and persistent symptomatic EBV viremia. *J. Allergy Clin. Immunol.* 2012;129(3):787-793. e786.

113. Abolhassani H, Edwards ES, Ikinciogullari A, Jing H, Borte S, Buggert M, et al. Combined immunodeficiency and Epstein-Barr virus-induced B cell malignancy in humans with inherited CD70 deficiency. *J. Exp. Med.* 2017;214(1):91-106.

114. Caorsi R, Rusmini M, Volpi S, Chiesa S, Pastorino C, Sementa AR, et al. CD70 Deficiency due to a Novel Mutation in a Patient with Severe Chronic EBV Infection Presenting As a Periodic Fever. *Front. Immunol.* 2018;8.

115. Izawa K, Martin E, Soudais C, Bruneau J, Boutboul D, Rodriguez R, et al. Inherited CD70 deficiency in humans reveals a critical role for the CD70-CD27 pathway in immunity to Epstein-Barr virus infection. *J. Exp. Med.* 2017;214(1):73-89.

116. Riether C, Pabst T, Höpner S, Bacher U, Hinterbrandner M, Banz Y, et al. Targeting CD70 with cusatuzumab eliminates acute myeloid leukemia stem cells in patients treated with hypomethylating agents. *Nat. Med.* 2020;26(9):1459-1467.

117. Coiffier B, Lepage E, Brière J, Herbrecht R, Tilly H, Bouabdallah R, et al. CHOP Chemotherapy plus Rituximab Compared with CHOP Alone in Elderly Patients with Diffuse Large-B-Cell Lymphoma. *N. Engl. J. Med.* 2002;346(4):235-242.

118. Walboomers JM, Jacobs MV, Manos MM, Bosch FX, Kummer JA, Shah KV, et al. Human papillomavirus is a necessary cause of invasive cervical cancer worldwide. *J. Pathol.* 1999;189(1):12-19.

119. Schiller JT, Castellsagué X, Garland SM. A review of clinical trials of human papillomavirus prophylactic vaccines. *Vaccine*. 2012;30:F123-138.

120. Houot R, Levy R. Vaccines for lymphomas: idiotype vaccines and beyond. *Blood Rev.* 2009;23(3):137-142.

121. Freedman A, Neelapu SS, Nichols C, Robertson MJ, Djulbegovic B, Winter JN, et al. Placebo-controlled phase III trial of patient-specific immunotherapy with mitumprotimut-T and granulocyte-macrophage colony-stimulating factor after rituximab in patients with follicular lymphoma. *J. Clin. Oncol.* 2009;27(18):3036.

122. Levy R, Robertson M, Ganjoo K, Leonard J, Vose J, Denney D. Abstract LB-204: Results of a Phase 3 trial evaluating safety and efficacy of specific immunotherapy, recombinant idiotype (Id) conjugated to KLH (Id-KLH) with GM-CSF, compared to non-specific immunotherapy, KLH with GM-CSF, in patients with follicular non-Hodgkin's lymph. *Cancer Res.* 2008;68(9_suppl):LB-204.

123. Lopes A, Vandermeulen G, Préat V. Cancer DNA vaccines: current preclinical and clinical developments and future perspectives. *J. Exp. Clin. Cancer Res.* 2019;38(1):146.

124. Rice J, Elliott T, Buchan S, Stevenson FK. DNA fusion vaccine designed to induce cytotoxic T cell responses against defined peptide motifs: implications for cancer vaccines. *J. Immunol.* 2001;167(3):1558-1565.

125. Rice J, Ottensmeier CH, Stevenson FK. DNA vaccines: precision tools for activating effective immunity against cancer. *Nat. Rev. Cancer*. 2008;8(2):108-120.

126. Cheever MA, Higano CS. PROVENGE (Sipuleucel-T) in prostate cancer: the first FDA-approved therapeutic cancer vaccine. *Clin. Cancer Res.* 2011;17(11):3520-3526.

127. Kantoff PW, Higano CS, Shore ND, Berger ER, Small EJ, Penson DF, et al. Sipuleucel-T immunotherapy for castration-resistant prostate cancer. *N. Engl. J. Med.* 2010;363(5):411-422.

128. Rosenberg SA, Restifo NP, Yang JC, Morgan RA, Dudley ME. Adoptive cell transfer: a clinical path to effective cancer immunotherapy. *Nat. Rev. Cancer*. 2008;8:299.

129. Hinrichs CS, Rosenberg SA. Exploiting the curative potential of adoptive T-cell therapy for cancer. *Immunol. Rev.* 2014;257(1):56-71.

130. Fesnak AD, June CH, Levine BL. Engineered T cells: the promise and challenges of cancer immunotherapy. *Nat. Rev. Cancer*. 2016;16:566.

131. Gill S, June CH. Going viral: chimeric antigen receptor T-cell therapy for hematological malignancies. *Immunol. Rev.* 2015;263(1):68-89.

132. Geresu MA, Sultan AF, Ahmed SK, Kassa GM. Immunotherapy against cancer: A comprehensive review. *J. Cancer Res. Exp. Oncol.* 2016;8(2):15-25.

133. Reichert JM. Marketed therapeutic antibodies compendium. *MAbs*. 2012;4(3):413-415.

134. Bachmann MF, Kündig TM, Hengartner H, Zinkernagel RM. Regulation of IgG antibody titers by the amount persisting of immune-complexed antigen. *Eur. J. Immunol.* 1994;24(10):2567-2570.

135. Chaplin DD. Overview of the immune response. *J. Allergy Clin. Immunol.* 2010;125(2):S3-S23.

136. Kuehl WM, Bergsagel PL. Multiple myeloma: evolving genetic events and host interactions. *Nat. Rev. Cancer*. 2002;2(3):175-187.

137. Kretschmer A, Schwanbeck R, Valerius T, Rosner T. Antibody Isotypes for Tumor Immunotherapy. *Transfus. Med. Hemother.* 2017;44(5):320-326.

138. Leusen JH. IgA as therapeutic antibody. *Mol. Immunol.* 2015;68(1):35-39.

139. Karagiannis SN, Josephs DH, Bax HJ, Spicer JF. Therapeutic IgE Antibodies: Harnessing a Macrophage-Mediated Immune Surveillance Mechanism against Cancer. *Cancer Res.* 2017;77(11):2779-2783.

140. Pan Q, Hammarström L. Molecular basis of IgG subclass deficiency. *Immunol. Rev.* 2000;178:99-110.

141. Vidarsson G, Dekkers G, Rispens T. IgG subclasses and allotypes: from structure to effector functions. *Front. Immunol.* 2014;5:520.

142. Schroeder Jr HW, Cavacini L. Structure and function of immunoglobulins. *J. Allergy Clin. Immunol.* 2010;125(2):S41-S52.

143. Warmerdam P, Van de Winkel J, Gosselin EJ, Capel P. Molecular basis for a polymorphism of human Fc gamma receptor II (CD32). *J. Exp. Med.* 1990;172(1):19-25.

144. Ravetch JV, Perussia B. Alternative membrane forms of Fc gamma RIII (CD16) on human natural killer cells and neutrophils. Cell type-specific expression of two genes that differ in single nucleotide substitutions. *J. Exp. Med.* 1989;170(2):481-497.

145. Ory PA, Clark MR, Kwoh EE, Clarkson SB, Goldstein IM. Sequences of complementary DNAs that encode the NA1 and NA2 forms of Fc receptor III on human neutrophils. *J. Clin. Invest.* 1989;84(5):1688-1691.

146. FcNimmerjahn F, Ravetch JV. Fc-receptors as regulators of immunity. *Adv. Immunol.* 2007;96:179-204.

147. Rosales C, Uribe-Querol E. Fc receptors: cell activators of antibody functions. *Adv. Biosci. Biotechnol.* 2013;4(04):21.

148. Maxwell KF, Powell MS, Hulett MD, Barton PA, McKenzie IF, Garrett TP, et al. Crystal structure of the human leukocyte Fc receptor, Fc gammaRIIa. *Nat. Struct. Biol.* 1999;6(5):437-442.

149. Nimmerjahn F, Ravetch JV. Fcgamma receptors as regulators of immune responses. *Nat. Rev. Immunol.* 2008;8(1):34-47.

150. Beum PV, Lindorfer MA, Taylor RP. Within peripheral blood mononuclear cells, antibody-dependent cellular cytotoxicity of rituximab-opsonized Daudi cells is promoted by NK cells and inhibited by monocytes due to shaving. *J. Immunol.* 2008;181(4):2916-2924.

151. Cullen S, Martin S. Mechanisms of granule-dependent killing. *Cell Death Differ.* 2008;15(2):251-262.

152. García-García E, Rosales C. Signal transduction during Fc receptor-mediated phagocytosis. *J. Leukoc. Biol.* 2002;72(6):1092-1108.

153. Kiyoshi M, Caaveiro JM, Kawai T, Tashiro S, Ide T, Asaoka Y, et al. Structural basis for binding of human IgG1 to its high-affinity human receptor FcγRI. *Nat Commun*. 2015;6(1):1-11.

154. Lu J, Ellsworth JL, Hamacher N, Oak SW, Sun PD. Crystal structure of Fcγ receptor I and its implication in high affinity γ-immunoglobulin binding. *J. Biol. Chem.* 2011;286(47):40608-40613.

155. Bruhns P, Iannascoli B, England P, Mancardi DA, Fernandez N, Jorieux S, et al. Specificity and affinity of human Fcgamma receptors and their polymorphic variants for human IgG subclasses. *Blood*. 2009;113(16):3716-3725.

156. Gillis C, Gouel-Chéron A, Jönsson F, Bruhns P. Contribution of Human FcγRs to Disease with Evidence from Human Polymorphisms and Transgenic Animal Studies. *Front. Immunol.* 2014;5(254).

157. Meknache N, Jönsson F, Laurent J, Guinnepain M-T, Daëron M. Human basophils express the glycosylphosphatidylinositol-anchored low-affinity IgG receptor FcγRIIIB (CD16B). *J. Immunol.* 2009;182(4):2542-2550.

158. Li X, Wu J, Ptacek T, Redden DT, Brown EE, Alarcón GS, et al. Allelic-dependent expression of an activating Fc receptor on B cells enhances humoral immune responses. *Sci. Transl. Med.* 2013;5(216):216ra175.

159. Nimmerjahn F, Ravetch JV. Fc-receptors as regulators of immunity. *Adv. Immunol.* 2007;96:179-204.

160. Beers SA, Glennie MJ, White AL. Influence of immunoglobulin isotype on therapeutic antibody function. *Blood*. 2016;127(9):1097-1101.

161. Nimmerjahn F, Bruhns P, Horiuchi K, Ravetch JV. FcgammaRIV: a novel FcR with distinct IgG subclass specificity. *Immunity*. 2005;23(1):41-51.

162. Li F, Ravetch JV. Inhibitory Fcγ receptor engagement drives adjuvant and anti-tumor activities of agonistic CD40 antibodies. *Science*. 2011;333(6045):1030-1034.

163. White AL, Chan HC, French RR, Willoughby J, Mockridge CI, Roghanian A, et al. Conformation of the human immunoglobulin G2 hinge imparts superagonistic properties to immunostimulatory anticancer antibodies. *Cancer Cell*. 2015;27(1):138-148.

164. Chu SY, Vostiar I, Karki S, Moore GL, Lazar GA, Pong E, et al. Inhibition of B cell receptor-mediated activation of primary human B cells by coengagement of CD19 and FcgammaRIIb with Fc-engineered antibodies. *Mol. Immunol.* 2008;45(15):3926-3933.

165. Dahan R, Barnhart BC, Li F, Yamniuk AP, Korman AJ, Ravetch JV. Therapeutic activity of agonistic, human anti-CD40 monoclonal antibodies requires selective fcgammar engagement. *Cancer Cell*. 2016;29(6):820-831.

166. Mimoto F, Katada H, Kadono S, Igawa T, Kuramochi T, Muraoka M, et al. Engineered antibody Fc variant with selectively enhanced FcγRIIb binding over both FcγRIIaR131 and FcγRIIaH131. *Protein Eng. Des. Sel.* 2013;26(10):589-598.

167. Smith P, DiLillo DJ, Bournazos S, Li F, Ravetch JV. Mouse model recapitulating human Fcγ receptor structural and functional diversity. *Proc. Natl. Acad. Sci. USA*. 2012;109(16):6181-6186.

168. Liu YD, Chen X, Zhang-van Enk J, Plant M, Dillon TM, Flynn GC. Human IgG2 antibody disulfide rearrangement in vivo. *J. Biol. Chem.* 2008;283(43):29266-29272.

169. Yu X, Chan HTC, Orr CM, Dadas O, Booth SG, Dahal LN, et al. Complex interplay between epitope specificity and isotype dictates the biological activity of anti-human CD40 antibodies. *Cancer Cell*. 2018;33(4):664-675 e664.

170. Cleary KLS, Chan HTC, James S, Glennie MJ, Cragg MS. Antibody distance from the cell membrane regulates antibody effector mechanisms. *J. Immunol.* 2017;198(10):3999-4011.

171. Carvalho S, Levi-Schaffer F, Sela M, Yarden Y. Immunotherapy of cancer: from monoclonal to oligoclonal cocktails of anti-cancer antibodies: IUPHAR Review 18. *Br. J. Pharmacol.* 2016;173(9):1407-1424.

172. McLaughlin P, Grillo-López AJ, Link BK, Levy R, Czuczman MS, Williams ME, et al. Rituximab chimeric anti-CD20 monoclonal antibody therapy for relapsed indolent lymphoma: half of patients respond to a four-dose treatment program. *J. Clin. Oncol.* 1998;16(8):2825-2833.

173. Lim SH, Vaughan AT, Ashton-Key M, Williams EL, Dixon SV, Chan HT, et al. Fc gamma receptor IIb on target B cells promotes rituximab internalization and reduces clinical efficacy. *Blood*. 2011;118(9):2530-2540.

174. Reinherz EL, Kung PC, Goldstein G, Levey RH, Schlossman SF. Discrete stages of human intrathymic differentiation: analysis of normal thymocytes and leukemic lymphoblasts of T-cell lineage. *Proceedings of the National Academy of Sciences*. 1980;77(3):1588-1592.

175. Mehta K, Shahid U, Malavasi F. Human CD38, a cell-surface protein with multiple functions. *FASEB J.* 1996;10(12):1408-1417.

176. Deaglio S, Morra M, Mallone R, Ausiello CM, Prager E, Garbarino G, et al. Human CD38 (ADP-ribosyl cyclase) is a counter-receptor of CD31, an Ig superfamily member. *J. Immunol.* 1998;160(1):395-402.

177. De Santanna A, Merlo A, Pesce C, Grossi CE, Tenca C, Zarcone D, et al. Death of T cell precursors in the human thymus: a role for CD38. *Int. Immunol.* 2003;15(9):1105-1116.

178. Dianzani U, Funaro A, DiFranco D, Garbarino G, Bragardo M, Redoglia V, et al. Interaction between endothelium and CD4+ CD45RA+ lymphocytes. Role of the human CD38 molecule. *J. Immunol.* 1994;153(3):952-959.

179. Musso T, Deaglio S, Franco L, Calosso L, Badolato R, Garbarino G, et al. CD38 expression and functional activities are up-regulated by IFN-γ on human monocytes and monocytic cell lines. *J. Leukoc. Biol.* 2001;69(4):605-612.

180. Fedele G, Frasca L, Palazzo R, Ferrero E, Malavasi F, Ausiello CM. CD38 is expressed on human mature monocyte-derived dendritic cells and is functionally involved in CD83 expression and IL-12 induction. *Eur. J. Immunol.* 2004;34(5):1342-1350.

181. Ortaldo J, Sharrow S, Timonen T, Herberman R. Determination of surface antigens on highly purified human NK cells by flow cytometry with monoclonal antibodies. *J. Immunol.* 1981;127(6):2401-2409.

182. Malavasi F, Deaglio S, Funaro A, Ferrero E, Horenstein AL, Ortolan E, et al. Evolution and function of the ADP ribosyl cyclase/CD38 gene family in physiology and pathology. *Physiol. Rev.* 2008;88(3):841-886.

183. Costa F, Toscani D, Chillemi A, Quarona V, Bolzoni M, Marchica V, et al. Expression of CD38 in myeloma bone niche: a rational basis for the use of anti-CD38 immunotherapy to inhibit osteoclast formation. *Oncotarget*. 2017;8(34):56598.

184. Lonial S, Weiss BM, Usmani SZ, Singhal S, Chari A, Bahlis NJ, et al. Daratumumab monotherapy in patients with treatment-refractory multiple myeloma (SIRIUS): an open-label, randomised, phase 2 trial. *The Lancet*. 2016;387(10027):1551-1560.

185. de Weers M, Tai YT, van der Veer MS, Bakker JM, Vink T, Jacobs DC, et al. Daratumumab, a novel therapeutic human CD38 monoclonal antibody, induces killing of multiple myeloma and other hematological tumors. *J. Immunol.* 2011;186(3):1840-1848.

186. Overdijk MB, Jansen JM, Nederend M, van Bueren JJL, Groen RW, Parren PW, et al. The therapeutic CD38 monoclonal antibody daratumumab induces programmed cell death via Fcγ receptor–mediated cross-linking. *J. Immunol.* 2016;197(3):807-813.

187. Overdijk MB, Verploegen S, Bogels M, van Egmond M, Lammerts van Bueren JJ, Mutis T, et al. Antibody-mediated phagocytosis contributes to the anti-tumor activity of the therapeutic antibody daratumumab in lymphoma and multiple myeloma. *MAbs*. 2015;7(2):311-321.

188. Usmani SZ, Weiss BM, Plesner T, Bahlis NJ, Belch A, Lonial S, et al. Clinical efficacy of daratumumab monotherapy in patients with heavily pretreated relapsed or refractory multiple myeloma. *Blood*. 2016;128(1):37-44.

189. Lokhorst HM, Plesner T, Laubach JP, Nahi H, Gimsing P, Hansson M, et al. Targeting CD38 with daratumumab monotherapy in multiple myeloma. *N. Engl. J. Med.* 2015;373(13):1207-1219.

190. Deckert J, Wetzel MC, Bartle LM, Skaletskaya A, Goldmacher VS, Vallee F, et al. SAR650984, a novel humanized CD38-targeting antibody, demonstrates potent antitumor activity in models of multiple myeloma and other CD38+ hematologic malignancies. *Clin. Cancer Res.* 2014;20(17):4574-4583.

191. Martin TG, Hsu K, Strickland SA, Glenn MJ, Mikhael J, Charpentier E. A phase I trial of SAR650984, a CD38 monoclonal antibody, in relapsed or refractory multiple myeloma. [Abstract]. *J. Clin. Oncol.* 2014;32(15_suppl):8532-8532.

192. Boxhammer R, Weirather J, Steidl S, Endell J. MOR202, a human anti-CD38 monoclonal antibody, mediates potent tumoricidal activity in vivo and shows synergistic efficacy in combination with different antineoplastic compounds [Abstract]. *Blood*. 2015;126(23):3015.

193. Endell J, Boxhammer R, Wurzenberger C, Ness D, Steidl S. The activity of MOR202, a fully human anti-CD38 antibody, is complemented by ADCP and is synergistically enhanced by lenalidomide in vitro and in vivo. [Abstract]. *Blood*. 2012;120(21):4018.

194. Raab MS, Engelhardt M, Blank A, Goldschmidt H, Agis H, Blau IW, et al. MOR202, a novel anti-CD38 monoclonal antibody, in patients with relapsed or refractory multiple myeloma: a first-in-human, multicentre, phase 1-2a trial. *Lancet Haematol*. 2020;7(5):e381-e394.

195. Smithson G, Zalevsky J, Korver W, Roepcke S, Dahl M, Zhao L, et al. TAK-079 is a high affinity monoclonal antibody that effectively mediates CD38+ cell depletion: Am Assoc Immnol, 2017.

196. Wang X, Dahl M, Nguyen D, Jenks S, Cashman K, Lee F, et al. The anti-CD38 monoclonal antibody TAK-079 depletes antibody secreting cells from normal and SLE patients. *Arthritis Rheumatol.* 2016;68(suppl_10).

197. Roepcke S, Plock N, Yuan J, Fedyk ER, Lahu G, Zhao L, et al. Pharmacokinetics and pharmacodynamics of the cytolytic anti-CD38 human monoclonal antibody TAK-079 in monkey - model assisted preparation for the first in human trial. *Pharmacol Res Perspect*. 2018;6(3):e00402.

198. Krishnan AY, Patel KK, Hari P, Jagannath S, Niesvizky R, Silbermann RW, et al. A phase Ib study of TAK-079, an investigational anti-CD38 monoclonal antibody (mAb) in patients with relapsed/ refractory multiple myeloma (RRMM): Preliminary results. *J. Clin. Oncol.* 2020;38(15_suppl):8539-8539.

199. Lipson EJ, Drake CG. Ipilimumab: an anti-CTLA-4 antibody for metastatic melanoma. *Clin. Cancer Res.* 2011;17(22):6958-6962.

200. Vargas FA, Furness AJ, Litchfield K, Joshi K, Rosenthal R, Ghorani E, et al. Fc effector function contributes to the activity of human anti-CTLA-4 antibodies. *Cancer Cell*. 2018;33(4):649-663.e644.

201. Hodi FS, O'day SJ, McDermott DF, Weber RW, Sosman JA, Haanen JB, et al. Improved survival with ipilimumab in patients with metastatic melanoma. *N. Engl. J. Med.* 2010;363(8):711-723.

202. Robert C, Thomas L, Bondarenko I, O'day S, Weber J, Garbe C, et al. Ipilimumab plus dacarbazine for previously untreated metastatic melanoma. *N. Engl. J. Med.* 2011;364(26):2517-2526.

203. Dong H, Strome SE, Salomao DR, Tamura H, Hirano F, Flies DB, et al. Tumor-associated B7-H1 promotes T-cell apoptosis: a potential mechanism of immune evasion. *Nat. Med.* 2002;8(8):793.

204. Gong J, Chehrazi-Raffle A, Reddi S, Salgia R. Development of PD-1 and PD-L1 inhibitors as a form of cancer immunotherapy: a comprehensive review of registration trials and future considerations. *J. ImmunoTher. Cancer*. 2018;6(1):1-18.

205. Larkin J, Chiarion-Sileni V, Gonzalez R, Grob JJ, Cowey CL, Lao CD, et al. Combined nivolumab and ipilimumab or monotherapy in untreated melanoma. *N. Engl. J. Med.* 2015;373(1):23-34.

206. Yap TA, Burris HA, Kummar S, Falchook GS, Pachynski RK, LoRusso P, et al. ICONIC: Biologic and clinical activity of first in class ICOS agonist antibody JTX-2011 +/- nivolumab (nivo) in patients (pts) with advanced cancers. *J. Clin. Oncol.* 2018;36(15_suppl):3000-3000.

207. Yap TA, Gainor JF, Callahan MK, Falchook GS, Pachynski RK, LoRusso P, et al. Improved progression-free and overall survival (PFS/OS) in patients (pts) with emergence of JTX-2011 associated biomarker (ICOS high CD4 T cells) on the ICONIC trial [abstract]. *Cancer Res.* 2019;79(13_Supplement):CT189.

208. Hansen A, Bauer T, Moreno V, Maio M, Groenland S, Martin-Liberal J, et al. First in Human Study with GSK3359609, Inducible T cell Co-stimulator Receptor Agonist in Patients with Advanced, Solid Tumors: Preliminary Results from INDUCE-1. *Ann. Oncol.* 2018;29(iii404).

209. Lin C-C, Naing A, Patel MR, III HAB, Curigliano G, Thistlethwaite F, et al. KY1044 to target the ICOS pathways inducing intratumoral Treg depletion and agonism of effector T cells: Preliminary pharmacodynamic markers from a phase 1/2 multicenter trial. *J. Clin. Oncol.* 2021;39(15_suppl):2626-2626.

210. Patel MR, Naing A, III HAB, Lin C-C, Curigliano G, Thistlethwaite F, et al. A phase 1/2 open-label study of KY1044, an anti-ICOS antibody with dual mechanism of action, as single agent and in combination with atezolizumab, in adult patients with advanced malignancies. *J. Clin. Oncol.* 2021;39(15_suppl):2624-2624.

211. Curti BD, Kovacsovics-Bankowski M, Morris N, Walker E, Chisholm L, Floyd K, et al. OX40 is a potent immune-stimulating target in late-stage cancer patients. *Cancer Res.* 2013;73(24):7189-7198.

212. Duhen R, Ballesteros-Merino C, Frye AK, Tran E, Rajamanickam V, Chang SC, et al. Neoadjuvant anti-OX40 (MEDI6469) therapy in patients with head and neck squamous cell carcinoma activates and expands antigen-specific tumor-infiltrating T cells. *Nat Commun*. 2021;12(1):1047.

213. Diab A, Hamid O, Thompson JA, Ros W, Eskens F, Doi T, et al. A Phase I, Open-Label, Dose-Escalation Study of the OX40 Agonist Ivuxolimab in Patients with Locally Advanced or Metastatic Cancers. *Clin. Cancer Res.* 2022;28(1):71-83.

214. Hamid O, Thompson JA, Diab A, Ros W, Eskens F, Bermingham C, et al. First in human (FIH) study of an OX40 agonist monoclonal antibody (mAb) PF-04518600 (PF-8600) in adult patients (pts) with select advanced solid tumors: Preliminary safety and pharmacokinetic (PK)/pharmacodynamic results. *J. Clin. Oncol.* 2016;34(15_suppl):3079-3079.

215. Glisson B, Leidner R, Ferris R, Powderly J, Rizvi N, Keam B, et al. Safety and clinical activity of MEDI0562, a humanized OX40 agonist monoclonal antibody, in adult patients with advanced solid tumors. *Ann. Oncol.* 2018;29:viii410.

216. Glisson B, Leidner R, Ferris R, Powderly J, Rizvi N, Norton J, et al. Phase 1 study of MEDI0562, a humanized OX40 agonist monoclonal antibody (mAb), in adult patients (pts) with advanced solid tumors. *Ann. Oncol.* 2016;27:vi361.

217. Glisson BS, Leidner RS, Ferris RL, Powderly J, Rizvi NA, Keam B, et al. Safety and Clinical Activity of MEDI0562, a Humanized OX40 Agonist Monoclonal Antibody, in Adult Patients with Advanced Solid Tumors. *Clin. Cancer Res.* 2020;26(20):5358-5367.

218. Hansen AR, Infante JR, McArthur G, Gordon MS, Lesokhin AM, Stayner A-L, et al. A first-in-human phase I dose escalation study of the OX40 agonist MOXR0916 in patients with refractory solid tumors. *Cancer Res.* 2016;76(14_Supplement):CT097.

219. Gutierrez M, Moreno V, Heinhuis KM, Olszanski AJ, Spreafico A, Ong M, et al. OX40 agonist BMS-986178 alone or in combination with nivolumab and/or ipilimumab in patients with advanced solid tumors. *Clin. Cancer Res.* 2021;27(2):460-472.

220. Wang R, Feng Y, Hilt E, Yuan X, Gao C, Shao X, et al. From bench to bedside: Exploring OX40 receptor modulation in a phase 1/2a study of the OX40 costimulatory agonist BMS-986178 ± nivolumab (NIVO) or ipilimumab (IPI) in patients with advanced solid tumors. *Cancer Res.* 2018;78(13_Supplement):LB-127.

221. Moiseyenko A, Muggia F, Condamine T, Pulini J, Janik JE, Cho DC. Sequential therapy with INCAGN01949 followed by ipilimumab and nivolumab in two patients with advanced ovarian carcinoma. *Gynecol. Oncol. Rep.* 2020;34:100655.

222. Postel-Vinay S, Lam VK, Ros W, Bauer TM, Hansen AR, Cho DC, et al. A first-in-human phase I study of the OX40 agonist GSK3174998 (GSK998) +/- pembrolizumab in patients (Pts) with selected advanced solid tumors (ENGAGE-1). *Cancer Res.* 2020;80(16_Supplement):CT150.

223. Piha-Paul SA, Geva R, Tan TJ, Lim DW, Hierro C, Doi T, et al. First-in-human phase I/Ib open-label dose-escalation study of GWN323 (anti-GITR) as a single agent and in combination with spartalizumab (anti-PD-1) in patients with advanced solid tumors and lymphomas. *J. for Immunother. Cancer*. 2021;9(8):e002863.

224. Zappasodi R, Sirard C, Li Y, Budhu S, Abu-Akeel M, Liu C, et al. Rational design of anti-GITR-based combination immunotherapy. *Nat. Med.* 2019;25(5):759-766.

225. Papadopoulos KP, Autio K, Golan T, Dobrenkov K, Chartash E, Chen Q, et al. Phase I Study of MK-4166, an Anti-human Glucocorticoid-Induced TNF Receptor Antibody, Alone or with Pembrolizumab in Advanced Solid Tumors. *Clin. Cancer Res.* 2021;27(7):1904-1911.

226. Geva R, Voskoboynik M, Dobrenkov K, Mayawala K, Gwo J, Wnek R, et al. First-in-human phase 1 study of MK-1248, an anti-glucocorticoid-induced tumor necrosis factor receptor agonist monoclonal antibody, as monotherapy or with pembrolizumab in patients with advanced solid tumors. *Cancer*. 2020;126(22):4926-4935.

227. Tran B, Carvajal RD, Marabelle A, Patel SP, LoRusso PM, Rasmussen E, et al. Dose escalation results from a first-in-human, phase 1 study of glucocorticoid-induced TNF receptor-related protein agonist AMG 228 in patients with advanced solid tumors. *J Immunother Cancer*. 2018;6(1):93.

228. Heinhuis KM, Carlino M, Joerger M, Di Nicola M, Meniawy T, Rottey S, et al. Safety, Tolerability, and Potential Clinical Activity of a Glucocorticoid-Induced TNF Receptor–Related Protein Agonist Alone or in Combination With Nivolumab for Patients With Advanced Solid Tumors: A Phase 1/2a Dose-Escalation and Cohort-Expansion Clinical Trial. *JAMA Oncology*. 2020;6(1):100-107.

229. Zhang L. Identification of a predictive biomarker and two pharmacodynamic biomarkers to ADG106 treatment, a novel anti-CD137 agonist antibody, in phase I clinical trials. *J. Clin. Oncol.* 2021;39(15_suppl):e14505-e14505.

230. Zhang L, Zhao H, Ma Y, Zheng X, Jiang J, Zhang Y, et al. A phase I, dose-escalation study of ADG106, a fully human anti-CD137 agonistic antibody, in subjects with advanced solid tumors or relapsed/refractory non-Hodgkin lymphoma. *J. Clin. Oncol.* 2020;38(15_suppl):3105-3105.

231. Zhao H, Zheng S, Liu G, Ma Y, She K, Chen M, et al. 43P Assessment of biomarker kinetics for ADG106 (anti-CD137 agonist) as monotherapy or combined with toripalimab. *Ann. Oncol.* 2021;32:S1389-S1390.

232. Ullenhag GJ, Yachnin J, Carneiro A, Schultz L, Ellmark P, Enell Smith K, et al. A first-in-human, multicenter, open-label, phase 1 study of ATOR-1017, a 4-1BB antibody, in patients with advanced solid malignancies. *J. Clin. Oncol.* 2021;39(15_suppl):2646-2646.

233. Segal NH, He AR, Doi T, Levy R, Bhatia S, Pishvaian MJ, et al. Phase I Study of Single-Agent Utomilumab (PF-05082566), a 4-1BB/CD137 Agonist, in Patients with Advanced Cancer. *Clin. Cancer Res.* 2018;24(8):1816-1823.

234. Sznol M, Hodi FS, Margolin K, McDermott DF, Ernstoff MS, Kirkwood JM, et al. Phase I study of BMS-663513, a fully human anti-CD137 agonist monoclonal antibody, in patients (pts) with advanced cancer (CA). *J. Clin. Oncol.* 2008;26(15_suppl):3007-3007.

235. Tolcher AW, Carvajal RD, El-Khoueiry AB, Feliu WO, Zang H, Ancukiewicz M, et al. Initial findings of the first-in-human phase I study of AGEN2373, a conditionally active CD137 agonist antibody, in patients (pts) with advanced solid tumors. *J. Clin. Oncol.* 2021;39(15_suppl):2634-2634.

236. Ansell SM, Flinn I, Taylor MH, Sikic BI, Brody J, Nemunaitis J, et al. Safety and activity of varlilumab, a novel and first-in-class agonist anti-CD27 antibody, for hematologic malignancies. *Blood adv.* 2020;4(9):1917-1926.

237. Burris HA, Infante JR, Ansell SM, Nemunaitis JJ, Weiss GR, Villalobos VM, et al. Safety and activity of varlilumab, a novel and first-in-class agonist anti-CD27 antibody, in patients with advanced solid tumors. *J. Clin. Oncol.* 2017;35(18):2028-2036.

238. Shapira-Frommer R, van Dongen MG, Dobrenkov K, Chartash E, Liu F, Li C, et al. O83 Phase 1 study of an anti-CD27 agonist as monotherapy and in combination with pembrolizumab in patients with advanced solid tumors. *J. ImmunoTher. Cancer*. 2020;8.

239. Roberts DJ, Franklin NA, Kingeter LM, Yagita H, Tutt AL, Glennie MJ, et al. Control of established melanoma by CD27 stimulation is associated with enhanced effector function and persistence, and reduced PD-1 expression, of tumor infiltrating CD8+ T cells. *J. Immunother.* 2010;33(8):769-779.

240. Sakanishi T, Yagita H. Anti-tumor effects of depleting and non-depleting anti-CD27 monoclonal antibodies in immune-competent mice. *Biochem. Biophys. Res. Commun.* 2010;393(4):829-835.

241. He L-Z, Prostak N, Thomas LJ, Vitale L, Weidlick J, Crocker A, et al. Agonist anti-human CD27 monoclonal antibody induces T cell activation and tumor immunity in human CD27–transgenic mice. *J. Immunol.* 2013;191(8):4174-4183.

242. Wasiuk A, Testa J, Weidlick J, Sisson C, Vitale L, Widger J, et al. CD27-mediated regulatory T cell depletion and effector T cell costimulation both contribute to antitumor efficacy. *J. Immunol.* 2017;199(12):4110-4123.

243. Turaj AH, Hussain K, Cox KL, Rose-Zerilli MJJ, Testa J, Dahal LN, et al. Antibody tumor targeting is enhanced by CD27 agonists through myeloid recruitment. *Cancer Cell*. 2017;32(6):777-791 e776.

244. Vitale LA, He LZ, Thomas LJ, Wasiuk A, O'Neill T, Widger J, et al. Development of CDX-527: a bispecific antibody combining PD-1 blockade and CD27 costimulation for cancer immunotherapy. *Cancer Immunol. Immunother.* 2020;69(10):2125-2137.

245. Sanborn RE, Pishvaian MJ, Callahan MK, Weise AM, Sikic BI, Rahma OE, et al. Anti-CD27 agonist antibody varlilumab (varli) with nivolumab (nivo) for colorectal (CRC) and ovarian (OVA) cancer: Phase (Ph) 1/2 clinical trial results. *J. Clin. Oncol.* 2018;36(15_suppl):3001-3001.

246. Reardon D, Kaley T, Iwamoto F, Baehring J, Subramaniam D, Rawls T, et al. ATIM-23. Anti-CD27 agonist antibody varlilumab in combination with nivolumab for recurrent glioblastoma (rGBM): phase 2 clinical trial results. *Neuro Oncol.* 2018;20(Suppl 6):vi6.

247. Lim SH, Linton KM, Collins GP, Dhondt J, Caddy J, Rossiter L, et al. RIVA – a phase IIa study of rituximab and varlilumab in relapsed or refractory B-cell malignancies: study protocol for a randomized controlled trial. *Trials*. 2018;19(1):619.

248. Aduro, Biotech. *Aduro Biotech Announces Milestone Achieved under Merck Collaboration for Initiation of Phase 2 Trial of Anti-CD27 Agonist MK-5890 in Non-Small Cell Lung Cancer*. https://www.globenewswire.com/news-release/2020/02/06/1981453/0/en/Aduro-Biotech-Announces-Milestone-Achieved-under-Merck-Collaboration-for-Initiation-of-Phase-2-Trial-of-Anti-CD27-Agonist-MK-5890-in-Non-Small-Cell-Lung-Cancer.html (accessed 07/04/2022).

249. Sanborn RE, Bordoni RE, Fleming GF, Khasraw M, Hawthorne T, Thomas LJ, et al. A phase 1 dose-escalation study of a PD-L1xCD27 bispecific antibody CDX-527 in patients with advanced malignancies. *J. Clin. Oncol.* 2021;39(15_suppl):2585-2585.

250. Biosciences S. NF-κB/Jurkat/GFP™ NF-κB/Jurkat/GFP Transcriptional Reporter Cell Line - User Manual, 2007.

251. Kim KJ, Kanellopoulos-Langevin C, Merwin RM, Sachs DH, Asofsky R. Establishment and characterization of BALB/c lymphoma lines with B cell properties. *J. Immunol.* 1979;122(2):549-554.

252. Tutt AL, James S, Laversin SA, Tipton TR, Ashton-Key M, French RR, et al. Development and characterization of monoclonal antibodies specific for mouse and human Fcγ receptors. *J. Immunol.* 2015;195(11):5503-5516.

253. Klein E, Klein G, Nadkarni JS, Nadkarni JJ, Wigzell H, Clifford P. Surface IgM-kappa specificity on a Burkitt lymphoma cell in vivo and in derived culture lines. *Cancer Res.* 1968;28(7):1300-1310.

254. DeNOVIX. CellDrop User Guide, 2020.

255. Keler T, Marsh HC, He L, Vitale LA, Thomas LJ.*Antibodies that bind human CD27 and uses thereof*. US9169325B2 (Patent) 2015.

256. Van Eenennaam H, Mulder WR, Borst JG, Veraar AME, Vink PMF.*Agonistic antibody to CD27*. US9527916B2 (Patent) 2016.

257. Köhler G, Milstein C. Continuous cultures of fused cells secreting antibody of predefined specificity. *Nature*. 1975;256(5517):495-497.

258. Kotecha N, Krutzik PO, Irish JM. Web-based analysis and publication of flow cytometry experiments. *Crurr. Protoc. Cytom.* 2010;53(Chapter10):10.17.

259. Zimmermann B, Hahnefeld C, Herberg FW. Applications of biomolecular interaction analysis in drug development. *Targets*. 2002;1(2):66-73.

260. Sanchez AB, Nguyen T, Dema-Ala R, Kummel AC, Kipps TJ, Messmer BT. A general process for the development of peptide-based immunoassays for monoclonal antibodies. *Cancer Chemother. Pharmacol.* 2010;66(5):919-925.

261. Ai W, Li H, Song N, Li L, Chen H. Optimal method to stimulate cytokine production and its use in immunotoxicity assessment. *Int. J. Environ. Res. Public Health*. 2013;10(9):3834-3842.

262. Hussain K, Hargreaves CE, Roghanian A, Oldham RJ, Chan HTC, Mockridge CI, et al. Upregulation of FcγRIIb on monocytes is necessary to promote the superagonist activity of TGN1412. *Blood*. 2015;125(1):102-110.

263. Foltz CJ, Ullman-Cullere M. Guidelines for assessing the health and condition of mice. *Lab Animal*. 1999;28(5).

264. French RR, Chan HC, Tutt AL, Glennie MJ. CD40 antibody evokes a cytotoxic T-cell response that eradicates lymphoma and bypasses T-cell help. *Nat. Med.* 1999;5(5):548-553.

265. Zhang P, Tu GH, Wei J, Santiago P, Larrabee LR, Liao-Chan S, et al. Ligand-blocking and membrane-proximal domain targeting anti-OX40 antibodies mediate potent T cell-stimulatory and anti-tumor activity. *Cell Rep.* 2019;27(11):3117-3123 e3115.

266. Cunningham BC, Wells JA. High-resolution epitope mapping of hGH-receptor interactions by alanine-scanning mutagenesis. *Science*. 1989;244(4908):1081-1085.

267. Schuck P, Zhao H. The role of mass transport limitation and surface heterogeneity in the biophysical characterization of macromolecular binding processes by SPR biosensing. In: Mol NJ, Fischer MJE (eds.) *Surface Plasmon Resonance: Methods and Protocols*. Totowa, NJ: Springer; 2010 pp15-54.

268. Hadzhieva M, Pashov AD, Kaveri S, Lacroix-Desmazes S, Mouquet H, Dimitrov JD. Impact of Antigen Density on the Binding Mechanism of IgG Antibodies. *Sci. Rep.* 2017;7(1):3767.

269. Velders MP, van Rhijn CM, Oskam E, Fleuren GJ, Warnaar SO, Litvinov SV. The impact of antigen density and antibody affinity on antibody-dependent cellular cytotoxicity: relevance for immunotherapy of carcinomas. *Br. J. Cancer*. 1998;78(4):478-483.

270. Niederfellner G, Lammens A, Mundigl O, Georges G, Schaefer W, Schwaiger M, et al. Epitope characterization and crystal structure of GA101 provide insights into the molecular basis for type I/II distinction of CD20 antibodies. *Blood*. 2011;118:358-367.

271. Segal NH, Logan TF, Hodi FS, McDermott D, Melero I, Hamid O, et al. Results from an integrated safety analysis of urelumab, an agonist anti-CD137 monoclonal antibody. *Clin. Cancer Res.* 2017;23(8):1929-1936.

272. Chin SM, Kimberlin CR, Roe-Zurz Z, Zhang P, Xu A, Liao-Chan S, et al. Structure of the 4-1BB/4-1BBL complex and distinct binding and functional properties of utomilumab and urelumab. *Nat Commun*. 2018;9(1):1-13.

273. Buchan SL, Dou L, Remer M, Booth SG, Dunn SN, Lai C, et al. Antibodies to costimulatory receptor 4-1BB enhance anti-tumor immunity via T regulatory cell depletion and promotion of CD8 T cell effector function. *Immunity*. 2018;49(5):958-970.e957.

274. Griffiths J, Hussain K, Smith HL, Sanders T, Cox K, Semmrich M, et al. Domain binding and isotype dictate the activity of anti-human OX40 antibodies. *J. ImmunoTher. Cancer*. 2020;8(2):e001557.

275. White AL, Beers SA, Cragg MS. FcgammaRIIB as a key determinant of agonistic antibody efficacy. *Curr. Top. Microbiol. Immunol.* 2014;382:355-372.

276. White AL, Chan HT, Roghanian A, French RR, Mockridge CI, Tutt AL, et al. Interaction with FcgammaRIIB is critical for the agonistic activity of anti-CD40 monoclonal antibody. *J. Immunol.* 2011;187(4):1754-1763.

277. Yu X, Chan HC, Fisher H, Penfold CA, Kim J, Inzhelevskaya T, et al. Isotype switching converts anti-CD40 antagonism to agonism to elicit potent antitumor activity. *Cancer Cell*. 2020;37(6):850-866.e857.

278. Zhang D, Goldberg MV, Chiu ML. Fc engineering approaches to enhance the agonism and effector functions of an anti-OX40 antibody. *J. Biol. Chem.* 2016;291(53):27134-27146.

279. Li F, Ravetch JV. Antitumor activities of agonistic anti-TNFR antibodies require differential FcgammaRIIB coengagement in vivo. *Proc. Natl. Acad. Sci. U. S. A.* 2013;110(48):19501-19506.

280. Ritchie M, Tchistiakova L, Scott N. Implications of receptor-mediated endocytosis and intracellular trafficking dynamics in the development of antibody drug conjugates. *MAbs*. 2013;5(1):13-21.

281. Mane SM, Marzella L, Bainton DF, Holt VK, Cha Y, Hildreth JE, et al. Purification and characterization of human lysosomal membrane glycoproteins. *Arch. Biochem. Biophys.* 1989;268(1):360-378.

282. Stewart R, Hammond SA, Oberst M, Wilkinson RW. The role of Fc gamma receptors in the activity of immunomodulatory antibodies for cancer. *J Immunother Cancer*. 2014;2(1):29.

283. Clynes RA, Towers TL, Presta LG, Ravetch JV. Inhibitory Fc receptors modulate in vivo cytoxicity against tumor targets. *Nat. Med.* 2000;6(4):443-446.

284. Bruhns P. Properties of mouse and human IgG receptors and their contribution to disease models. *Blood*. 2012;119(24):5640-5649.

285. Yu X, James S, Felce JH, Kellermayer B, Johnston DA, Chan HC, et al. TNF receptor agonists induce distinct receptor clusters to mediate differential agonistic activity. *Commun. Biol.* 2021;4(1):1-15.

286. Wajant H. Principles of antibody-mediated TNF receptor activation. *Cell Death Differ.* 2015;22(11):1727-1741.

287. Martinez-Forero I, Azpilikueta A, Bolaños-Mateo E, Nistal-Villan E, Palazon A, Teijeira A, et al. T cell costimulation with Anti-CD137 monoclonal antibodies is mediated by K63–Polyubiquitin-Dependent signals from endosomes. *J. Immunol.* 2013;190(12):6694-6706.

288. Chen DS, Mellman I. Oncology meets immunology: the cancer-immunity cycle. *Immunity*. 2013;39(1):1-10.

289. Larkin J, Chiarion-Sileni V, Gonzalez R, Grob J-J, Rutkowski P, Lao CD, et al. Five-Year Survival with Combined Nivolumab and Ipilimumab in Advanced Melanoma. *N. Engl. J. Med.* 2019;381(16):1535-1546.

290. Heckel F, Turaj AH, Fisher H, Chan H, Marshall MJ, Dadas O, et al. Agonistic CD27 antibody potency is determined by epitope-dependent receptor clustering augmented through Fc-engineering. *Commun. Biol.* 2022;5(1):1-15.

291. Cancer-Research-UK. *Myeloma incidence statistics*. https://www.cancerresearchuk.org/health-professional/cancer-statistics/statistics-by-cancer-type/myeloma/incidence (accessed 07/04/2022).

292. Fairfield H, Falank C, Avery L, Reagan MR. Multiple myeloma in the marrow: pathogenesis and treatments. *Ann. N. Y. Acad. Sci.* 2016;1364(1):32.

293. Bosma GC, Custer RP, Bosma MJ. A severe combined immunodeficiency mutation in the mouse. *Nature*. 1983;301(5900):527-530.

294. Ito M, Hiramatsu H, Kobayashi K, Suzue K, Kawahata M, Hioki K, et al. NOD/SCID/γ c null mouse: an excellent recipient mouse model for engraftment of human cells. *Blood*. 2002;100(9):3175-3182.

295. Mosier DE, Gulizia RJ, Baird SM, Wilson DB. Transfer of a functional human immune system to mice with severe combined immunodeficiency. *Nature*. 1988;335(6187):256-259.

296. Vafa O, Gilliland GL, Brezski RJ, Strake B, Wilkinson T, Lacy ER, et al. An engineered Fc variant of an IgG eliminates all immune effector functions via structural perturbations. *Methods*. 2014;65(1):114-126.

297. Ye C, Yang H, Cheng M, Shultz LD, Greiner DL, Brehm MA, et al. A rapid, sensitive, and reproducible in vivo PBMC humanized murine model for determining therapeutic-related cytokine release syndrome. *FASEB J.* 2020;34(9):12963-12975.

298. Auffray C, Sieweke MH, Geissmann F. Blood monocytes: development, heterogeneity, and relationship with dendritic cells. *Annu. Rev. Immunol.* 2009;27:669-692.

299. Passlick B, Flieger D, Ziegler-Heitbrock HW. Identification and characterization of a novel monocyte subpopulation in human peripheral blood. *Blood*. 1989;74(7):2527-2534.

300. Heidenreich S, Schmidt M, August C, Cullen P, Rademaekers A, Pauels H-G. Regulation of human monocyte apoptosis by the CD14 molecule. *J. Immunol.* 1997;159(7):3178-3188.

301. Zanoni I, Granucci F. Role of CD14 in host protection against infections and in metabolism regulation. *Front. Cell. Infect. Microbiol.* 2013;3:32.

302. Ziegler-Heitbrock L, Ancuta P, Crowe S, Dalod M, Grau V, Hart DN, et al. Nomenclature of monocytes and dendritic cells in blood. *Blood*. 2010;116(16):e74-80.

303. Fleischer J, Soeth E, Reiling N, Grage-Griebenow E, FLAD HD, Ernst M. Differential expression and function of CD80 (B7-1) and CD86 (B7-2) on human peripheral blood monocytes. *Immunology*. 1996;89(4):592-598.

304. Patel VK, Williams H, Li SC, Fletcher JP, Medbury HJ. Monocyte inflammatory profile is specific for individuals and associated with altered blood lipid levels. *Atherosclerosis*. 2017;263:15-23.

305. Mukherjee R, Barman PK, Thatoi PK, Tripathy R, Das BK, Ravindran B. Non-classical monocytes display inflammatory features: validation in sepsis and systemic lupus erythematous. *Sci. Rep.* 2015;5:13886.

306. Wong KL, Tai JJ-Y, Wong W-C, Han H, Sem X, Yeap W-H, et al. Gene expression profiling reveals the defining features of the classical, intermediate, and nonclassical human monocyte subsets. *Blood*. 2011;118(5):e16-e31.

307. Zawada AM, Rogacev KS, Rotter B, Winter P, Marell R-R, Fliser D, et al. SuperSAGE evidence for CD14++CD16+ monocytes as a third monocyte subset. *Blood*. 2011;118(12):e50-e61.

308. Cros J, Cagnard N, Woollard K, Patey N, Zhang S-Y, Senechal B, et al. Human CD14dim monocytes patrol and sense nucleic acids and viruses via TLR7 and TLR8 receptors. *Immunity*. 2010;33(3):375-386.

309. Kapellos TS, Bonaguro L, Gemünd I, Reusch N, Saglam A, Hinkley ER, et al. Human monocyte subsets and phenotypes in major chronic inflammatory diseases. *Front. Immunol.* 2019:2035.

310. Sampath P, Moideen K, Ranganathan UD, Bethunaickan R. Monocyte Subsets: Phenotypes and Function in Tuberculosis Infection. *Front. Immunol.* 2018;9:1726.

311. Yang J, Zhang L, Yu C, Yang XF, Wang H. Monocyte and macrophage differentiation: circulation inflammatory monocyte as biomarker for inflammatory diseases. *Biomark Res*. 2014;2(1):1.

312. Stoeckius M, Hafemeister C, Stephenson W, Houck-Loomis B, Chattopadhyay PK, Swerdlow H, et al. Simultaneous epitope and transcriptome measurement in single cells. *Nat. Methods*. 2017;14(9):865-868.

313. Jin S, Guerrero-Juarez CF, Zhang L, Chang I, Ramos R, Kuan C-H, et al. Inference and analysis of cell-cell communication using CellChat. *Nat Commun*. 2021;12(1):1088.

314. Cruikshank WW, Kornfeld H, Center DM. Interleukin-16. *J. Leukoc. Biol.* 2000;67(6):757-766.

315. Elssner A, Doseff AI, Duncan M, Kotur M, Wewers MD. IL-16 Is Constitutively Present in Peripheral Blood Monocytes and Spontaneously Released During Apoptosis. *J. Immunol.* 2004;172(12):7721-7725.

316. Cruikshank WW, Berman JS, Theodore AC, Bernardo J, Center DM. Lymphokine activation of T4+ T lymphocytes and monocytes. *J. Immunol.* 1987;138(11):3817-3823.

317. Liu Y, Cruikshank WW, O'Loughlin T, O'Reilly P, Center DM, Kornfeld H. Identification of a CD4 domain required for interleukin-16 binding and lymphocyte activation. *J. Biol. Chem.* 1999;274(33):23387-23395.

318. Parada NA, Cruikshank WW, Danis HL, Ryan TC, Center DM. IL-16- and other CD4 ligand-induced migration is dependent upon protein kinase C. *Cell. Immunol.* 1996;168(1):100-106.

319. Calandra T, Bernhagen J, Mitchell RA, Bucala R. The macrophage is an important and previously unrecognized source of macrophage migration inhibitory factor. *J. Exp. Med.* 1994;179(6):1895-1902.

320. Leng L, Metz CN, Fang Y, Xu J, Donnelly S, Baugh J, et al. MIF Signal Transduction Initiated by Binding to CD74. *J. Exp. Med.* 2003;197(11):1467-1476.

321. Shi X, Leng L, Wang T, Wang W, Du X, Li J, et al. CD44 is the signaling component of the macrophage migration inhibitory factor-CD74 receptor complex. *Immunity*. 2006;25(4):595-606.

322. Bernhagen J, Krohn R, Lue H, Gregory JL, Zernecke A, Koenen RR, et al. MIF is a noncognate ligand of CXC chemokine receptors in inflammatory and atherogenic cell recruitment. *Nat. Med.* 2007;13(5):587-596.

323. Alampour-Rajabi S, El Bounkari O, Rot A, Müller-Newen G, Bachelerie F, Gawaz M, et al. MIF interacts with CXCR7 to promote receptor internalization, ERK1/2 and ZAP-70 signaling, and lymphocyte chemotaxis. *FASEB J.* 2015;29(11):4497-4511.

324. Fan H, Hall P, Santos LL, Gregory JL, Fingerle-Rowson G, Bucala R, et al. Macrophage Migration Inhibitory Factor and CD74 Regulate Macrophage Chemotactic Responses via MAPK and Rho GTPase. *J. Immunol.* 2011;186(8):4915-4924.

325. Gregory JL, Leech MT, David JR, Yang YH, Dacumos A, Hickey MJ. Reduced leukocyte-endothelial cell interactions in the inflamed microcirculation of macrophage migration inhibitory factor-deficient mice. *Arthritis Rheum.* 2004;50(9):3023-3034.

326. Aeberli D, Yang Y, Mansell A, Santos L, Leech M, Morand EF. Endogenous macrophage migration inhibitory factor modulates glucocorticoid sensitivity in macrophages via effects on MAP kinase phosphatase-1 and p38 MAP kinase. *FEBS Lett.* 2006;580(3):974-981.

327. Lue H, Thiele M, Franz J, Dahl E, Speckgens S, Leng L, et al. Macrophage migration inhibitory factor (MIF) promotes cell survival by activation of the Akt pathway and role for CSN5/JAB1 in the control of autocrine MIF activity. *Oncogene*. 2007;26(35):5046-5059.

328. Hudson JD, Shoaibi MA, Maestro R, Carnero A, Hannon GJ, Beach DH. A proinflammatory cytokine inhibits p53 tumor suppressor activity. *J. Exp. Med.* 1999;190(10):1375-1382.

329. Beyer M, Mallmann MR, Xue J, Staratschek-Jox A, Vorholt D, Krebs W, et al. High-resolution transcriptome of human macrophages. *PLoS One*. 2012;7(9):e45466.

330. Ohradanova-Repic A, Machacek C, Fischer MB, Stockinger H. Differentiation of human monocytes and derived subsets of macrophages and dendritic cells by the HLDA10 monoclonal antibody panel. *Clin Transl Immunology*. 2016;5(1):e55.

331. Ziegler-Heitbrock HL, Fingerle G, Ströbel M, Schraut W, Stelter F, Schütt C, et al. The novel subset of CD14+/CD16+ blood monocytes exhibits features of tissue macrophages. *Eur. J. Immunol.* 1993;23(9):2053-2058.

332. Le Naour F, Hohenkirk L, Grolleau A, Misek DE, Lescure P, Geiger JD, et al. Profiling changes in gene expression during differentiation and maturation of monocyte-derived dendritic cells using both oligonucleotide microarrays and proteomics. *J. Biol. Chem.* 2001;276(21):17920-17931.

333. Mathy NL, Scheuer W, Lanzendörfer M, Honold K, Ambrosius D, Norley S, et al. Interleukin-16 stimulates the expression and production of pro-inflammatory cytokines by human monocytes. *Immunology*. 2000;100(1):63-69.

334. Bach J-P, Deuster O, Balzer-Geldsetzer M, Meyer B, Dodel R, Bacher M. The role of macrophage inhibitory factor in tumorigenesis and central nervous system tumors. *Cancer*. 2009;115(10):2031-2040.

335. Yaddanapudi K, Putty K, Rendon BE, Lamont GJ, Faughn JD, Satoskar A, et al. Control of tumor-associated macrophage alternative activation by macrophage migration inhibitory factor. *J. Immunol.* 2013;190(6):2984-2993.

336. Mullard A. FDA approves 100th monoclonal antibody product. *Nat. Rev. Drug Discov.* 2021;20(7):491-495.

337. Kaplon H, Chenoweth A, Crescioli S, Reichert JM. Antibodies to watch in 2022. *MAbs*. 2022;14(1):2014296.

338. Suntharalingam G, Perry MR, Ward S, Brett SJ, Castello-Cortes A, Brunner MD, et al. Cytokine storm in a phase 1 trial of the anti-CD28 monoclonal antibody TGN1412. *N. Engl. J. Med.* 2006;355(10):1018-1028.

339. Chodorge M, Zuger S, Stirnimann C, Briand C, Jermutus L, Grutter MG, et al. A series of Fas receptor agonist antibodies that demonstrate an inverse correlation between affinity and potency. *Cell Death Differ.* 2012;19(7):1187-1195.

340. Carrascosa LC, van Beek AA, de Ruiter V, Doukas M, Wei J, Fisher TS, et al. FcγRIIB engagement drives agonistic activity of Fc-engineered αOX40 antibody to stimulate human tumor-infiltrating T cells. *J Immunother Cancer*. 2020;8(2).

341. Qi X, Li F, Wu Y, Cheng C, Han P, Wang J, et al. Optimization of 4-1BB antibody for cancer immunotherapy by balancing agonistic strength with FcγR affinity. *Nat Commun*. 2019;10(1):2141.

342. Zhang D, Armstrong AA, Tam SH, McCarthy SG, Luo J, Gilliland GL, et al. Functional optimization of agonistic antibodies to OX40 receptor with novel Fc mutations to promote antibody multimerization. *MAbs*. 2017;9(7):1129-1142.

343. Liu X, Zhao Y, Shi H, Zhang Y, Yin X, Liu M, et al. Human immunoglobulin G hinge regulates agonistic anti-CD40 immunostimulatory and antitumour activities through biophysical flexibility. *Nat Commun*. 2019;10(1):4206.

344. Clair EWS. The calm after the cytokine storm: lessons from the TGN1412 trial. *The Journal of clinical investigation*. 2008;118(4):1344-1347.

345. Chester C, Sanmamed MF, Wang J, Melero I. Immunotherapy targeting 4-1BB: mechanistic rationale, clinical results, and future strategies. *Blood*. 2018;131(1):49-57.

346. Mikami N, Sakaguchi S. CD 28 signals the differential control of regulatory T cells and effector T cells. *Eur. J. Immunol.* 2014;44(4):955-957.